2nd

NASA TECHNICAL TRANSLATION NASA TT F 15,391

A PROCEDURE FOR THE DIRECT NUMERICAL SIMULATION OF TURBULENT FLOWS IN PLATE AND ANNULAR CHANNELS AND ITS APPLICATION IN THE DEVELOPMENT OF TURBULENCE MODELS

U. Schumann

Translation of "Ein Verfahren zur direkten numerischen Simulation turbulenter Strömungen in Platten — und Ringspaltkanälen und über seine Anwendung zur Untersuchung von Turbulenzmodellen", Dissertation, University of Karlsruhe, Karlsruhe, and Report KFK, Kernforschungszentrum Karlsruhe, 1973, pp. 1-249.

NATIONAL AERONAUTICS AND SPACE ADMINISTRATION
WASHINGTON, D. C. 20546 APRIL 1974

N74-21927

NASA-TT-F-15391) A PROCEDURE FOR THE DIRECT NUMERICAL SIMULATION OF TURBULENT FLOWS IN PLATE AND ANNULAR CHANNELS AND ITS APPLICATION IN (Scientific Translation Service) 321 p HC $14.50 CSCL 20D G3/12 Unclas 37276

STANDARD TITLE PAGE

1. Report No.	2. Government Accession No.	3. Recipient's Catalog No.
NASA TT F 15,391		

4. Title and Subtitle	5. Report Date
A PROCEDURE FOR THE DIRECT NUMERICAL SIMULATION OF TURBULENT FLOWS IN PLATE AND ANNULAR CHANNELS AND ITS APPLICATION IN THE DEVELOPMENT OF TURBULENCE MODELS	April, 1974
	6. Performing Organization Code

7. Author(s)	8. Performing Organization Report No.
U. Schumann	10. Work Unit No.
	11. Contract or Grant No. NASw-2483

9. Performing Organization Name and Address	13. Type of Report and Period Covered
SCITRAN Box 5456 Santa Barbara, CA 93108	Translation

12. Sponsoring Agency Name and Address	14. Sponsoring Agency Code
National Aeronautics and Space Administration Washington, D.C. 20546	

15. Supplementary Notes

Translation of "Ein Verfahren zur direkten numerischen Simulation turbulenter Strömungen in Platten - und Ringspaltkanälen und über seine Anwendung zur Untersuchung von Turbulenzmodellen", Dissertation, University of Karlsruhe, Karlsruhe, and Report KFK, Kernforschungszentrum Karlsruhe, 1973, pp. 1-249.

16. Abstract A numerical difference scheme is described to simulate three-dimensional, time-dependent, turbulent flows of incompressible fluids at high Reynolds numbers in a plate channel and in concentric annuli.

The Navier-Stokes equations averaged over grid volumes are integrated. A novel model has been developed which takes into account strongly inhomogeneous turbulence and grid volumes of unequal side lengths.

Stability criteria are established for this method and for similar difference schemes. For computation of the pressure field the appropriate Poisson's equation is solved by Fast Fourier Transform.

The procedure implemented in the TRUBIT-1 program is used to simulate turbulent flows in a plate channel and an annulus radius ratio of 5:1. The numerical results are in good agreement with experimental values. Especially the velocity profile and the mean velocity fluctuations are computed with significantly better accuracy than in earlier, direct simulations.

The energy - length-scale model and the pressure-velocity gradient correlations are used as examples to show that the method may be used successfully to evaluate the parameters of turbulence models.

17. Key Words (Selected by Author(s))	18. Distribution Statement
	Unclassified - Unlimited

19. Security Classif. (of this report)	20. Security Classif. (of this page)	21. No. of Pages	22. Price
Unclassified	Unclassified	227	

SUMMARY

A numerical difference scheme is described to simulate three-dimensional, time-dependent, turbulent flows of incompressible fluids at high Reynolds numbers in a plate channel and in concentric annular channels.

Starting from the results of Deardorff, the Navier-Stokes equations, averaged over grid volumes, are integrated. For a description of the subgrid scale motion a novel model has been developed which takes into account strongly inhomogeneous turbulence and grid volumes of unequal side lengths. The premises used in the model are described and discussed.

Stability criteria are established for this method and for similar difference schemes. For computation of the pressure field the appropriate Poisson's equation is solved accurately, except for rounding errors, by Fast Fourier Transform.

The procedure implemented in the TURBIT-1 program is used to simulate turbulent flows in a plate channel and annulus with radius ratio of 5:1. For both types of flow different cases are realized with a maximum number of grid volumes of 65536. Already for rather small grid volume numbers the numerical results are in good agreement with experimental values. Especially the velocity profile and the mean velocity fluctuations are computed with

significantly better accuracy than in earlier, direct simulations.

The energy — length-scale model and the pressure-velocity gradient correlations are used as examples to show that the method may be used successfully to evaluate the parameters of turbulence models.

Earlier results are reviewed and proposals for future research are made.

LISTING OF OFTEN-USED SYMBOLS

1) General Characterization of an Arbitrary Variable y

$\langle y \rangle$	Average over time or over ensemble
$\bar{y}$	Average value over a space limited volume
y'	Deviation from average value
$^{V}\langle y \rangle$	Average value over total flow volume
$^{P}\langle y \rangle$	Average value over the planes with periodic boundary conditions $(x_1\text{-}x_2; x\text{-}\varphi)$; "Period average value"
y''	Deviation from period average value
$^{V}\bar{y}$	Average value over a mesh volume
$^{i}\bar{y}$	Average value over a mesh area with normal parallel to the x_i coordinate ("i-surface")
$^{x}\bar{y}, {}^{\varphi}\bar{y}, {}^{r}\bar{y}$	Average value over the x-, φ- or r-surface of a mesh
$\tilde{y}^{i}$	Arithmetic average value over adjacent values in the x_i direction in the grid (same weight)
$\bar{y}^{x}, \bar{y}^{\varphi}, \bar{y}^{r}$	Same as $\bar{y}^{i}$ for the x-, φ-, r-direction
$\tilde{\bar{y}}^{i}, \tilde{\bar{y}}^{x}, \tilde{\bar{y}}^{\varphi}, \tilde{\bar{y}}^{r}$	Same as $\bar{y}^{i}, \bar{y}^{x}, \bar{y}^{\varphi}, \bar{y}^{r}$ with unequal weights for considering non-equidistant meshes according to (6-1)
$\frac{\partial y}{\partial x}$	Partial derivative of y with respect to x
$\delta_x y$	Central difference quotient of y: $\frac{y(x+\frac{\Delta x}{2}) - y(x-\frac{\Delta x}{2})}{\Delta x}$

$\overline{\delta}_x y$	Difference quotient according to (6-2)
$\delta_x^* y$	Difference quotient according to (6-20)
y_i	(As a rule) component in x_i direction ($i=1,2,3$) /168
y_x, y_φ, y_r	Components in the x-, φ-, r direction
$\underline{y}$	Vector
$\underline{\underline{y}}$	Matrix
y_m	Average value
y_{max}	Maximum value
y_{min}	Minimum value
y_w	Wall value
$\tilde{y}$	(for velocities:) Velocity value at new time step when pressure is ignored.
$\hat{y}$	Dimensioned variable
y_o	Reference quantity

2) Summation Convention

Sums from one to three are taken over pairs of unknown subscripts on the lower right:

$$y_{ii} = \sum_{i=1}^{3} y_{ii} \quad ; \quad y_i^2 \equiv \sum_{i=1}^{3} y_i^2$$

The same indices take on corresponding values when located at another position (upper left or upper right).

No sums are taken over indices on the lower right, if they are in square brackets

$$y_{[i][j]} \neq \sum_{i=1}^{3} y_{ii}$$

3) Symbols

$a_1, a_2, \ldots, a_8$	Turbulence model constants (Chapter 2)
A_w	Constants in (2-8)
$c_1, c_2, \ldots, c_{11}; c_\mu$	Fine structure model constants (Chapter 5)
$d_1, d_2, \ldots, d_5$	(A2 - 32)
D	Wall distance
$D_{ij} =$	$\frac{\partial u_i}{\partial x_j} + \frac{\partial u_j}{\partial x_i}$ Deformation velocity
$_kD^2$	Time average of the difference form of the square of the deformation velocity (according to 4-23 to 26)
D^2	Undetermined form of $_kD^2$
$D1, D2, \ldots, D5$	Fortran program according to Appendix 2
$D1N, D2N, \ldots, D5N$	Fortran program according to Appendix 2
$D11, \ldots, D14$	Fortran program according to Appendix 2
$\underline{e}_i$	Unit vector in x_i direction
E	Kinetic energy
$\sqrt{E'}$	Kinetic energy of the fluctuation motion within the mesh
$E(k)$	Three-dimensional, average, scalar energy spectrum (Appendix 1)
$E_1(k_1)$	One-dimensional energy spectrum (Appendix 1)

$E_{ij}(\underline{k})$	Tensorial energy spectrum (Appendix 1)	/170
$E_{11}(k_1)$	$= E_{11}(k_1 \cdot \underline{e}_1)$	
$E_{22}(k_1)$	$= E_{22}(k_1 \cdot \underline{e}_1)$	
$E_{33}(k_1)$	$= E_{33}(k_1 \cdot \underline{e}_1)$	
$E2, E3, En$	Function according to Chapter A2.2	
E_1, E_2	Constants for considering the wall roughnesses in (7-8), E_1 for the wall at R1,E2 for r=R2.	
f_1, f_2, f_3	Factors according to (4-38-40)	
F	Area	
j_F	j-area; mesh area, whose normal is parallel to the x_j coordinate	
$F(\tau)$	Longitudinal correlation (A1-5)	
FED	(4-27)	
FED1	Fortran program according to Appendix 2	
$G(\tau)$	Transverse correlation (A1-6)	
$\underline{\underline{G}}$	Amplification matrix (A6-15)	
h	Average mesh edge length (5-6)	
h_1, h_2, h_3	Relative mesh edge lengths $h_i = \Delta x_i / h$	
H_1, H_2, H_3	Mesh edge lengths	
i	Subscript (often with respect to the x_1 direction	
$i = \sqrt{-1}$	Imaginary unit	/171
IM	Number of meshes in the x_1 direction	
j	Subscript (often with respect to x_2 direction)	
J	Number of meshes in the x_2 direction	
k	Subscript (often with respect to x_3 direction)	

k	Scalar wave number
k_1	Scalar wave number with respect to x_1 direction
$\underline{k}$	Wave number vector
k	Karman constant (0.4)
k_p	Rotta constant (A1-48)
$K(\underline{1})$	Weighting function (4-13)
KM	Number of meshes in x_3 direction
m	Subscript with respect to x_1 direction
l	Turbulence ball diameter
L	Correlation length (2-5,6,7)
L_{iso}	Diameter of the region with local isotropy (Chapter 4.1)
m	Subscript with respect to x_2 direction
n	Subscript with respect to x_3 direction or for characterizing the time step /172
no, n1, n2	Various time steps of the differencing procedure; see Chapter 6.2.1.
N	Number of time steps over which averaging is carried out according to Chapter 6.2.1.
p	Pressure
P_x	Average axial pressure gradient
r	Radius coordinate
Re	Reynolds number (1-13)
Re_m	Reynolds number (1-14)
R1	Radius of inner cylinder
R2	Radius of outer cylinder

R_n	Residual term
R_{ij}	Two-point correlation (A1-1) between velocity fluctuations
R_{ψ_1,ψ_2}	Two-point correlation between arbitrary variables
s	Coordinate
t	Time
u	Axial velocity component (Figure 1)
$\underline{u}$	Velocity vector
u_1, u_2, u_3	See Figure 1
v_x, v_y, v_z	See Figure 1
v	Azimuthal velocity component (Figure 1)
V	A volume
w	Radial velocity component (Figure 1) /173
$\underline{x}$	Position vector
x_1, x_2, x_3	Position vector (Figure 1)
x	Axial coordinate (Figure 1)
X_1, X_2	Period length for plate in the x_1 or x_2 direction, respectively.
X	Period length in x direction for annulus
y	Azimuthal coordinate (Figure 1)

y	An undetermined quantity
z	Radial coordinate (Figure 1)
α	Kolmogorov constant (4-4)
δ_{ij}	Kronecker-Delta
Δ	Interval
Γ	Gamma function
ε	Dissipation (1-16)
η	Kolmogorov length (A1-33)
ϑ	Dirac function
λ	Eigenvalue
μ	Turbulent velocity of fine structure
$^{i}\mu$	Locally isotropic part of fine structure-viscosity
$^{p}\mu$	Inhomogeneous part of fine structure-viscosity
μ^{+}	$= \mu+\nu$
ν	Kinematic molecular viscosity
$\underline{\xi}$	Displacement vector
ϱ	Density /174
$\sigma_1, \sigma_2, \sigma_3$	Correction factors (5-14,15, 5-82)
τ	Integration variable
φ	Volume correlation (4-20)
$\emptyset$	Period length in azimuthal direction for annulus
x	Auxiliary potential (Chapter 6.2.2)
x_1, x_2	Undetermined turbulent fields (Chapter 4.2)
ω	Rotational velocity, rotation

A PROCEDURE FOR THE DIRECT NUMERICAL SIMULATION OF TURBULENT FLOWS IN PLATE AND ANNULAR CHANNELS AND ITS APPLICATION IN THE DEVELOPMENT OF TURBULENCE MODELS*

Ulrich Schumann **

1. INTRODUCTION /1***

1.1. Turbulence

Turbulent flow fields [53, 89, 115, 120] are characterized by their irregular structure. The velocity at a position fluctuates greatly and in an irregular way. Turbulence is a flow state which usually comes about when the ratio of the inertia forces and the viscosity forces inside of the fluid characterized by a Reynolds number exceeds a critical value. Below this critical Reynolds number there is a laminar flow field. For large Reynolds numbers, the flow is unstable, i.e. two flow states which differ by an arbitrarily small amount diverge in time so much that after some time they no longer have as much in common as two arbitrarily selected flow states. This instability is the reason for the existence of turbulent flows. Because of the large velocity fluctuations, the exchange of momentum and

---

* Accepted dissertation presented to the Mechanical Engineer Faculty of the Univ. of Karlsruhe (TH)

** Nuclear Research Center, Karlsruhe, Report KFK 1854, Institute for Reactor Development, Nuclear Research Association mbH.

*** Numbers in the margin indicate pagination of original foreign text.

scalar variables such as enthalpy and mixing components is greatly intensified over the molecular exchange which takes place in laminar flows. The quantitative description of turbulent flows is therefore important for many regions. In practice, usually one must depend on experiments. This is especially true for complicated geometries, such as for example the flow around local blocking units in reactor fuel elements [75] as well as in channel flows, for example [88].

The results of such experiments were first approximated by simple formulas, with which it was possible to perform interpolation within the measurement range. The Blasius law [120] for the representation of the dependence of tube friction coefficient on Reynolds number is a typical example of this. By considering the basic equations, at the present time turbulence models are being established with which it is possible to carry extrapolations to ranges for which no measurements are yet available. Chapter 2 reports on such turbulence models. It becomes clear that these models must be supported by expensive experimental work. /2

An old dream of flow research scientists is to theoretically solve the Navier-Stokes equation, which is assumed to be valid for the description of turbulent flows (see Chapter 1.3). At the present time, this is not possible under general conditions, especially because of the great deal of effort required to describe the nonsteady flow fields. Even for "one-dimensional" geometries (for example tube), these are always three-dimensional functions of location. As the capacity of electronic computers is enlarged, we believe that this problem will be brought closer to a solution. For example, it was Deardorff [29] who simulated the turbulent flow between two plates. In the present paper we continue this work. This further development is in the following areas:

- Improvement of the theoretical fundamentals
- Simulation of flows in plate channels as well as in an annulus channel
- Application of methods for determining turbulence model constants.

In addition to flows in closed channels (for example, in a reactor fuel element), the numerical description of turbulent flows is also of interest in meteorology [6|4]. Much basic work has been performed in this connection. The application of numerical methods for simulating turbulent flows within the framework of reactor technology will be important in the description of local meteorological processes in the vicinity of nuclear power plants [129].

1.2. Geometry, Boundary Conditions, Material Constants, Reference Variables /3

In this paper we will consider channel flows, which are problems usually considered in reactor technology. Because of their simplicity, we consider the annulus channel and the plate channel in order to reduce the numerical effort and because there exist experimental results for comparison. According to Figure 1, the annulus considered is "infinite" in the axial direction and is determined by the separation of the walls, $\hat{D}$ as well as the ratio $\hat{R}2/\hat{R}1$ of the radii of the outer and inner walls. The plate channel which is extended to "infinity" in two directions is found by the limiting transition

$$\hat{R}2/\hat{R}1 \rightarrow 1 \quad , \quad \hat{R}2 - \hat{R}1 = \hat{D} = \text{const}$$

These geometries can be described using relatively simple Cartesian coordinates

$$\underline{\hat{x}} \equiv \left\{ \hat{x}_1, \hat{x}_2, \hat{x}_3 \right\}_{kart.} \equiv \left\{ \hat{x}, \hat{y}, \hat{z} \right\}_{kart.}$$

or cylindrical coordinates

$$\hat{\underline{x}} \equiv \{\hat{x}_1, \hat{x}_2, \hat{x}_3\}_{zyl.} \equiv \{\hat{x}, \hat{\varphi}, \hat{r}\}_{zyl.}$$

where

$$\hat{y} = \hat{r} \cdot \cos\hat{\varphi}\,; \quad \hat{z} = \hat{r} \cdot \sin\hat{\varphi}$$

More complicated geometries are described in Chapter 11.2.
The flow under consideration is assumed to be a steady (turbulent) flow in the x direction in the statistical sense*, which is produced by forced convection because of a specified pressure gradient

$$\hat{P}_x = -\frac{\partial}{\partial \hat{x}} \langle \hat{p} \rangle \qquad (1\text{-}1)$$

or a corresponding axial field force per unit of volume.

The average velocity is not a dependent variable, but depends on $\hat{P}_x$ instead. As a reference variable $\hat{u}_o$ for the velocity, we will not use the average or maximum velocity but instead the velocity which can be derived from the pressure gradient

$$\hat{u}_o \equiv \sqrt{\frac{\hat{P}_x \hat{D}}{2\hat{\varrho}}} \qquad (1\text{-}2)$$

Equilibrium of forces results in the following average value of the shear stress $\langle \hat{\tau}_w \rangle$ at the walls:

$$\langle \hat{\tau}_w \rangle = \frac{\hat{P}_x \cdot \hat{D}}{2} \qquad (1\text{-}3)$$

and therefore we also have

$$\hat{u}_o = \sqrt{\frac{\langle \hat{\tau}_w \rangle}{\hat{\varrho}}} \qquad (1\text{-}4)$$

---

* i.e. average values < > taken over time or the ensemble.

This velocity is called the "shear stress velocity" [120, P. 542]./4

The following dimensioned reference variables are

Symbol	Meaning	Dimension (i.e.)
$\hat{D}$	Distance between walls	m
$\hat{t}_o \equiv \hat{D}/\hat{u}_o$	Characteristic time	s
$\hat{p}_o \equiv \hat{p}_x \cdot \hat{D}$	Pressure	$\frac{kg}{m\ s^2}$
$\hat{\varrho}_o$	Specific density	$\frac{kg}{m^3}$
$\hat{\nu}_o$	Characteristic kinematic molecular viscosity	$\frac{m^2}{s}$

The fluid is assumed to be incompressible and the density $\hat{\varrho}$ is independent of location and time. The average viscosity is assumed to be $\hat{\nu}_o$; the viscosity $\hat{\nu}$ can be a function of position and time. We will impose the wall adhesion condition

$$\hat{\underline{u}}\,|_{\text{wall}} = 0 \qquad (1\text{-}5)$$

as a boundary condition. In addition, the flow field in the axial direction is assumed to be constant in the statistical sense.

1.3. Basic Equations

The basic equations are the conservation equations for mass and momentum. Using the reference variables defined in Chapter 1.2, we have the following equations [53] which go back to Navier [86] and Stokes [117]:

Assumptions:

- Incompressible fluid
- Constant densities
- Newtonian fluid (i.e. linear, isotropic) material law for the shear stress as a function of the deformation rates, no moment stresses
- Fluid can be described as a continuum
- No field forces except the average pressure gradient $\hat{P}_x$
- Euler frame of reference

Cartesian coordinates:

Mass conservation (continuity equation): $$\frac{\partial u_i}{\partial x_i} = 0 \quad *) \qquad (1\text{-}6)$$

- Momentum conservation /5

$$\underbrace{\frac{\partial u_i}{\partial t}}_{I} + \underbrace{\frac{\partial}{\partial x_j}(u_i u_j)}_{II} = -\underbrace{\frac{\partial p}{\partial x_i}}_{III} + \underbrace{\frac{\partial}{\partial x_j}\left(\nu\left(\frac{\partial u_i}{\partial x_j} + \frac{\partial u_j}{\partial x_i}\right)\right)}_{IV} + \underbrace{\delta_{1i}\, P_x}_{V}, \quad i=1,2,3 \qquad (1\text{-}7)$$

Cylindrical coordinates:

- Mass conservation (continuity equation)

$$\frac{\partial v_x}{\partial x} + \frac{\partial v_\varphi}{r\partial \varphi} + \frac{1}{r}\frac{\partial}{\partial r}(r v_r) = 0 \qquad (1\text{-}8)$$

- Momentum conservation

$$\underbrace{\frac{\partial v_x}{\partial t}}_{I} + \underbrace{\frac{\partial}{\partial x}(v_x^2) + \frac{1}{r}\frac{\partial}{\partial \varphi}(v_\varphi v_x) + \frac{1}{r}\frac{\partial}{\partial r}(r v_r v_x)}_{II} = -\underbrace{\frac{\partial p}{\partial x}}_{III} + \underbrace{P_x}_{V}$$
$$+ \underbrace{\left[\frac{\partial}{\partial x}\left\{2\nu\frac{\partial v_x}{\partial x}\right\} + \frac{\partial}{r\partial \varphi}\left\{\nu\left(\frac{\partial v_x}{r\partial \varphi} + \frac{\partial v_\varphi}{\partial x}\right)\right\} + \frac{1}{r}\frac{\partial}{\partial r}\left\{\nu r\left(\frac{\partial v_x}{\partial r} + \frac{\partial v_r}{\partial x}\right)\right\}\right]}_{IV}; \qquad (1\text{-}9)$$

$$\underbrace{\frac{\partial v_\varphi}{\partial t}}_{I} + \underbrace{\frac{\partial}{\partial x}(v_x v_\varphi) + \frac{1}{r}\frac{\partial}{\partial \varphi}(v_\varphi^2) + \frac{1}{r}\frac{\partial}{\partial r}(r v_r v_\varphi) + \frac{v_r v_\varphi}{r}}_{II} = -\underbrace{\frac{\partial p}{r\partial \varphi}}_{III}$$

* The summation convention holds. Terms with repeated subscripts [not in brackets] are summed from 1 to 3.

$$+\underbrace{\left[\frac{\partial}{\partial x}\left\{\nu\left(\frac{\partial v_\varphi}{\partial x}+\frac{\partial v_x}{r\partial\varphi}\right)\right\}+\frac{\partial}{r\partial\varphi}\left\{2\nu\left(\frac{\partial v_\varphi}{r\partial\varphi}+\frac{v_r}{r}\right)\right\}+\frac{1}{r}\frac{\partial}{\partial r}\left\{\nu r\left(\frac{\partial}{\partial r}\left(\frac{v_\varphi}{r}\right)+\frac{\partial v_r}{r\partial\varphi}\right)\right\}+\frac{\nu}{r}\left\{r\frac{\partial}{\partial r}\left(\frac{v_\varphi}{r}\right)+\frac{\partial v_r}{r\partial\varphi}\right\}\right]}_{IV};$$

$$\underbrace{\frac{\partial v_r}{\partial t}}_{I}+\underbrace{\frac{\partial}{\partial x}(v_x v_r)+\frac{1}{r}\frac{\partial}{\partial\varphi}(v_\varphi v_r)+\frac{1}{r}\frac{\partial}{\partial r}(r v_r^2)-\frac{v_\varphi^2}{r}}_{II}=\underbrace{-\frac{\partial}{\partial r}p}_{III}$$

$$+\underbrace{\left[\frac{\partial}{\partial x}\left\{\nu\left(\frac{\partial v_r}{\partial x}+\frac{\partial v_x}{\partial r}\right)\right\}+\frac{\partial}{r\partial\varphi}\left\{\nu\left(r\frac{\partial}{\partial r}\left(\frac{v_\varphi}{r}\right)+\frac{\partial v_r}{r\partial\varphi}\right)\right\}+\frac{\partial}{r\partial r}\left\{\nu r 2\frac{\partial v_r}{\partial r}\right\}-\frac{2\nu}{r}\left\{\frac{\partial v_\varphi}{r\partial\varphi}+\frac{v_r}{r}\right\}\right]}_{IV}. \qquad (1\text{-}9)\ \text{(Cont'd)}$$

Here we have defined:

$$\underline{u} = \{u_1, u_2, u_3\}_{kart.} = \{v_x, v_\varphi, v_r\}_{zyl.} = \hat{\underline{u}} / \hat{u}_0$$

$$\underline{x} = \{x_1, x_2, x_3\}_{kart.} = \{x, \varphi, r\}_{zyl.} = \hat{\underline{x}} / \hat{D}$$

$$p = (\hat{p}/\hat{\varrho}) / (\hat{p}_0/\hat{\varrho}_0)$$

$$t = \hat{t} / \hat{t}_0$$

$$P_x = (\hat{P}_x \cdot \hat{D}) / (\hat{\varrho}\,\hat{u}_0^2) = 2$$

$$\nu = \frac{\hat{\nu}}{\hat{u}_0 \hat{D}} \equiv \frac{1}{Re}$$

The terms have the following meaning:

I : Local acceleration

II : "Convection terms", difference between momentum flowing into and out of a differential volume element.

III : Pressure fluctuation gradient

IV : "Diffusion terms", the momentum supplied per unit of volume by molecular transport (negative, therefore momentum sink)

/6

V : $P_x = 2$, average pressure gradient in the x direction or force per unit of volume (position and usually time-dependent) (momentum-source)

The terms $\frac{v_r v_\varphi}{r}$ and $-\frac{v_\varphi^2}{r}$ in the convection terms of the v_φ- and v_r-components are called the Coriolis or centrifugal accelerations.

Sometimes other notations are used for the convection or diffusion terms, which are sometimes more advantageous. We will only give them for Cartesian coordinates:

$$\frac{\partial}{\partial x_j}(u_i u_j) = u_j \frac{\partial u_i}{\partial x_j} \quad \text{(because of 1-6)} \tag{1-10}$$

The left form is called the conservative form, because its integral over the entire volume is zero (see Chapter A5.4).

$$\frac{\partial}{\partial x_j}\left(\nu\left(\frac{\partial u_i}{\partial x_j} + \frac{\partial u_j}{\partial x_i}\right)\right) = \nu \frac{\partial^2 u_i}{\partial x_j^2} + \frac{\partial \nu}{\partial x_j}\left(\frac{\partial u_i}{\partial x_j} + \frac{\partial u_j}{\partial x_i}\right) \tag{1-11}$$

$$= \nu \frac{\partial}{\partial x_j}\left(\frac{\partial u_i}{\partial x_j} - \frac{\partial u_j}{\partial x_i}\right) + \frac{\partial \nu}{\partial x_j}\left(\frac{\partial u_i}{\partial x_j} + \frac{\partial u_j}{\partial x_i}\right) \tag{1-12}$$

(In the second equation, the first term only contains mixed derivatives. This can be used to formulate simplified boundary conditions.)

One should consider that $\frac{1}{\nu}$ corresponds to a Reynolds number Re

$$Re = \hat{u}_0 \vec{D} / \hat{\nu}, \tag{1-13}$$

which, however, is not an independent variable (see Chapter 1.2.). The Reynolds numbers Re_m of Re_{max} formulated with the average velocity $v_{\langle \hat{u} \rangle}$, and the maximum velocity $\langle \hat{u} \rangle_{max}$, respectively,

are found as

$$Re_m = \frac{v_{\langle u \rangle}}{v_0} Re \frac{\vec{v}}{\vec{v}_0}$$
$$Re_{max} = \frac{\langle u \rangle_{max}}{v_0} Re \frac{\vec{v}}{\vec{v}_0} \qquad (1\text{-}14)$$

In the following we will refer to Re_m when we speak of Reynolds numbers.

1.4. Derived Basic Equations

Further equations can be derived from the momentum and mass conservation equations and the wall adhesion condition by carrying out purely mathematical operations. In this paper, we will require such equations for the kinetic energy per unit of mass $E = \frac{1}{2} u_i^2$ and the pressure per unit of mass p.

1.4.1. Conservation Equations of Kinetic Energy /7

By forming the scalar product of a velocity vector and its partial time derivative, whereby the latter is specified by the momentum conservation equation, we find a conservation equation for the kinetic energy of a fluid:

Cartesian: $E \equiv \frac{1}{2} u_i^2$

$$\frac{\partial E}{\partial t} + u_j \frac{\partial E}{\partial x_j} = - \frac{\partial (u_i p)}{\partial x_i} + \frac{\partial}{\partial x_j} \left(\nu \left(\frac{\partial E}{\partial x_j} + \frac{\partial (u_i u_j)}{\partial x_i} \right) \right) + u_i P_x - \varepsilon \qquad (1\text{-}15)$$

where

$$\varepsilon \equiv \nu \frac{\partial u_i}{\partial x_j} \left(\frac{\partial u_i}{\partial x_j} + \frac{\partial u_j}{\partial x_i} \right) = \nu \frac{1}{2} \left(\frac{\partial u_i}{\partial x_j} + \frac{\partial u_j}{\partial x_i} \right)^2 \qquad (1\text{-}16)$$

is the dissipation, i.e. the energy converted into heat per unit of time and unit of volume by the work of the viscosity forces. The equation itself does not contain any new physical information, but the dissipation can be identified from the first theorem of thermodynamics [7, 53, 120].

The corresponding equation in cylindrical coordinates is given as follows where $E \equiv \frac{1}{2}(v_x^2+v_\varphi^2+v_r^2)$.

$$\begin{aligned}
&\frac{\partial E}{\partial t} + \frac{\partial}{\partial x}(v_x E) + \frac{\partial}{r\partial\varphi}(v_\varphi E) + \frac{1}{r}\frac{\partial}{\partial r}(r v_r E) = v_x \cdot P_x \\
&+\frac{\partial}{\partial x}\left\{\nu\left(\frac{\partial}{\partial x}E + \frac{\partial}{\partial x}(v_x^2) + \frac{\partial}{r\partial\varphi}(v_x v_\varphi) + \frac{1}{r}\frac{\partial}{\partial r}(r v_x v_r)\right)\right\} \\
&+\frac{\partial}{r\partial\varphi}\left\{\nu\left(\frac{\partial}{r\partial\varphi}E + \frac{\partial}{\partial x}(v_x v_\varphi) + \frac{\partial}{r\partial\varphi}(v_\varphi^2) + \frac{1}{r}\frac{\partial}{\partial r}(r v_\varphi v_r)\right)\right\} \\
&+\frac{1}{r}\frac{\partial}{\partial r}\left\{\nu\left(r\frac{\partial E}{\partial r} + \frac{\partial}{\partial x}(v_r v_x) + \frac{\partial}{r\partial\varphi}(v_r v_\varphi) + \frac{1}{r}\frac{\partial}{\partial r}(r v_r^2)\right)\right\} - \varepsilon
\end{aligned} \tag{1-17}$$

The dissipation ε is given by:

$$\begin{aligned}
\varepsilon = \nu\Bigg\{ & 2\left(\frac{\partial v_x}{\partial x}\right)^2 + 2\left(\frac{\partial v_\varphi}{r\partial\varphi} + \frac{v_r}{r}\right)^2 + 2\left(\frac{\partial v_r}{\partial r}\right)^2 \\
& + \left(\frac{\partial v_x}{r\partial\varphi} + \frac{\partial v_\varphi}{\partial x}\right)^2 + \left(\frac{\partial v_r}{\partial x} + \frac{\partial v_x}{\partial r}\right)^2 + \left(r\frac{\partial}{\partial r}\left(\frac{v_\varphi}{r}\right) + \frac{\partial v_r}{r\partial\varphi}\right)^2\Bigg\}
\end{aligned} \tag{1-18}$$

Because of (1-5), we have the following wall condition

$$E/_{\text{Wall}} = 0$$

1.4.2. Equation for Determining Pressure (Poisson Equation)

/8

If we form the divergence of the acceleration vector given by the momentum conservation equation (1-7,9), then because of the continuity equation $\frac{\partial}{\partial x_i}\frac{\partial u_i}{\partial t} = 0$ we have the following:

In cartesian coordinates:

$$\frac{\partial^2 p}{\partial x_i^2} = q_{kart.} \tag{1-19}$$

$$q_{kart.} = -\frac{\partial^2}{\partial x_i \partial x_j}(u_i u_j) + \frac{\partial}{\partial x_i}\left\{\frac{\partial \nu}{\partial x_j}\left(\frac{\partial u_i}{\partial x_j} + \frac{\partial u_j}{\partial x_i}\right)\right\} \tag{1-20}$$

or in cylindrical coordinates

$$\frac{\partial^2 p}{\partial x^2} + \frac{1}{r^2}\frac{\partial^2 p}{\partial \varphi^2} + \frac{1}{r}\frac{\partial}{\partial r}\left(r\frac{\partial p}{\partial r}\right) = q_{zyl.} \qquad (1\text{-}21)$$

where $q|_{zyl}$ is the expression corresponding to $q|_{kart.}$ for which we will not give the details.

From (1-5) and (1-7) we find the following wall condition:

$$\frac{\partial p}{\partial x_j} = \frac{\partial}{\partial x_j}\left(\nu\left(\frac{\partial u_j}{\partial x_j} + \frac{\partial u_j}{\partial x_j}\right)\right)\Big|_{Wall} \qquad (1\text{-}22)$$

This is an elliptical, partial differential equation of the Poisson equation type with a Neumann (inhomogeneous) boundary condition which must be satisfied at all times. This equation characterizes the importance of the incompressibility condition and of the pressure, because it causes a disturbance in the velocity field to propagate in the flow space with "infinite speed of sound".

1.5. Principles of Numerical Simulation of Turbulent Flows

1.5.1. Direct and Model Simulation

There are two principally different directions in the numerical simulation of turbulent flows.

One method (used in this paper) consists of the direct integration of the basic equations according to Chapter 1.3. Models are only used for certain deficiencies associated with the solution, which are called fine structure models or correction models. The limited solution is always caused by the limited computer capacity, as will be discussed in the following. The direct simulation methods are characterized by the fact

that the fine structure models contained in them and the other errors go to zero when the resolution is increased in very powerful computers. Three-dimensional, nonsteady flow fields are always simulated. In the second method, first the exact basic equations are approximated by model equations, and their model character does not disappear when the resolution is increased arbitrarily. Usually these are model equations for describing time averages or ensemble averages of flow fields [12]. In Chapter 2| we will discuss the principles and problems of such models. /9

In the following we will give a summary of the numerical method of direct simulation. Since true turbulent flow fields have only been calculated by Deardorff [29, 30, 31, 33], this summary will also include methods of simulating laminar flows.

1.5.2. Methods of Numerical Simulation

The natural method of directly using the basic equations given in Chapter 1.3 and then making them discrete and transforming them into a difference method suitable for computer simulation is neither the only method nor the first used method. In addition to this type of simulation of the so-called "primitive variables", the velocity components u_i and the pressure p, first a rotation potential form was used. Recently, the basic equations were expanded into eigen functions, using the Galerkin method. A summary of the various methods is given in [58, 43, 44]. In the simulation of the primitive variables, a problem arises in the consideration of the incompressibility condition and therefore a problem associated with the pressure. For the first time Harlow-Welch [54] carried out this method (only for laminar flows in two dimensions). Starting with initial conditions, which satisfy the continuity equation, the pressure is determined at any time using a difference formulation of

Equations (1-19, 21) in such a way that the time derivative of the velocity components satisfies the continuity equation. The same method was used by Williams [149] and Deardorff [29] in three dimensions. In this case, a correction according to Hirt-Harlow [56] was introduced so that small deviations of the initial values from the incompressibility condition do not gradually increase. The simplification of this process was suggested by Chorin [21], and for example Amsden-Harlow [3]. The pressure was not /10
calculated directly, but instead an equivalent auxiliary potential ψ the magnitude of which was determined in such a way that the incompressibility condition is maintained for arbitrary initial conditions. This method will also be used in this paper and will be explained in Chapter 6.2.2. Other papers in which the primitive variables were integrated are, for example, [27, 42, 62, 63, 94].

The problems with the pressure do not occur in the rotation potential form of the basic equations. For this purpose, the rotation ω_i is formed for the basic equations

$$\omega_i \equiv \varepsilon_{ijk} \frac{\partial u_j}{\partial x_k} \quad ; \; i=1,2,3 \tag{1-23}$$

where ε_{ijk} = 0 in case two subscripts are the same
= 1 in case the subscripts are cyclical
= -1 in case the subscripts are anticyclical

The pressure drops off because of

$$\varepsilon_{ijk} \frac{\partial^2 p}{\partial x_k \partial x_j} \equiv 0 \tag{1-24}$$

The velocities are calculated from a vector potential ψ_j

$$u_i \equiv \varepsilon_{ijk} \frac{\partial \psi_j}{\partial x_k} \quad ; \; i=1,2,3 \; , \tag{1-25}$$

so that $\partial u_i / \partial x_i \equiv 0$.

From (1-23) and (1-25) we find the following equations for determining the vector potential

$$\omega_i = -\frac{\partial^2 \psi_i}{\partial x_k^2} \quad ; \; i=1,2,3 \qquad (1\text{-}26)$$

Instead of a Poisson equation for the pressure, it is necessary to solve three Poisson equations in three dimensions at every time step. In addition, the solutions ψ_i and w_i are not so simple to interpret as are u_i, p; this has an effect on the formulation of boundary conditions. This method used by Aziz-Hellums [2] and Schönauer [121] for laminar flows is not being recommended in recent papers [44]. This is not true for two-dimensional flows. Here only one component of rotation is different from zero and therefore only one Poisson equation must be solved. This method has proven itself many times [40, 41, 44, 49, 78, 83], but a three-dimensional representation is required for the simulation of turbulent flows. (See for example Chapter A1.2.2 as well as [81, 83]).

Over the last three years, the Galerkin method was developed further, especially by Orszag [94, 95, 96, 97]. The velocity field $\underline{u}(\underline{x},t)$ with respect to position $\underline{x}$ is expanded into eigen functions, for example:

$$\underline{u}(\underline{x},t) = \sum_{\underline{k}} \underline{v}(\underline{k},t) \exp\left(\sqrt{-1}\, \underline{k}\cdot\underline{x}\right) \qquad (1\text{-}27)$$

where only a finite number of discrete wave number vector elements $\underline{k}$ are numerically considered. The advantages of the /11 method are the following [96]:

a) The derivatives of the velocity field can be determined without any truncation error.

b) For the same storage capacity, 8 (two in each direction) times as many wave number components can be simulated in three dimensions as can be done using a difference method. This is because

in a spatially discrete mesh network containing KM meshes, only a maximum of $\frac{KM}{2}$ wave numbers can be represented in one direction.

c) The aliasing problem (see Chapter A5.3) can be avoided.

Advantage a) is not very important [33],(see Chapter A5.2.1.) The disadvantages of the method are the following:

a) Nonlinear terms, such as for example the convection terms or nonlinear viscosities can only be calculated in real space. For this, the fields $\underline{v}(\underline{k},t)$ must be transformed into the real field $\underline{u}(\underline{x},t)$, whereupon the nonlinear terms are calculated and then a retransformation is carried out. This transformation costs a lot of computer time, and only the fast Fourier transformation, FFT [19,20] limits this time to within acceptable limits.

b) The eigen function development is only possible for simple geometries (plate, sphere, cylinder) [94,97]. However, complicated geometries can be mapped into manageable and simpler geometries using suitable conformal mappings.

c) The methods and the corresponding programs are more complex. This method is not to be recommended in spite of its elegance [44, 95].

Finally, we should mention the finite element method (F.E.M.), which was applied to flow problems,by Crastan-Devos [24] for example. Crastan showed that even if a variational principle does not exist, which has not yet been found for the general Navier-Stokes equation, it is possible to apply the (F.E.M.). The advantage of the (F.E.M.) is in the simplified description of complicated geometries and boundary conditions. However, this method leads to large systems of equations which are very nonlinear

for turbulent flow. The finite element method has only proven itself for linear flow problems. /12

In this paper we will therefore use the method of simulating the "primitive variables" mentioned first.

1.5.3. The Method of Deardorff

Deardorff [28, 29] simulated the nonsteady, three-dimensional and turbulent flow between two parallel plates. He considers a section of the plate flow having a length of $X_1 = 3$ in the flow direction, with $X_2 = 0.7$ in the azimuth direction (perpendicular to the flow direction, parallel to the plates), as well as the complete plate cross section in the radial direction (perpendicular to the plates) with D = 1. The flow volume is divided into equidistant measures having the edge lengths

$$\Delta x = 3/24 = 0.125, \quad \Delta y = 7/14 = 0.05, \quad \Delta z = 1/20 = 0.05 \qquad (1\text{-}28)$$

that is, into 24·14·20 = 6720 meshes.

The fine structure of turbulence (see Chapter 5.1) is considered by means of models, such as developed by Lilly [80, 81, 32]. The agreement of the average results with the measurements of Laufer [76, 77] is average. For example, the average velocity profile deviates by up to 50% from the measured values. The agreement with the measurements of Comte-Bellot [18] at higher Reynolds numbers is slightly better. These errors can partially be traced to the small numbers of meshes, as well as to errors in the fine structure model and the boundary conditions, as we will show in this paper. Deardorff's fine structure model, strictly speaking, is suited for meshes having equal sidelength, in contrast to (1-28). It is now possible to transfer the fine structure model to cylindrical coordinates.

The evaluation of the results resulted in information on the structure of a flow. For example, it was possible to determine that the "turbulence balls" have different dimensions depending on the velocity component in the axial direction. In the papers [27, 30, 33] the temperature field considered as a positive quantity was also integrated, and the stability of the atmosphere flow was investigated with suitable boundary conditions. The mesh network consisted of a maximum of 40*40*20 meshes in this case. No evaluations were carried out for testing or improving the turbulence models, as we will do in this paper.

The most important result of Deardorff's work is the proof that the direct numerical simulation of turbulent flows is possible at high Reynolds numbers and that a fine structure model can be used which is independent of specific experimental support.

1.6. Resolution Capacity and Requirement for Fine Structure Models

/13/

1.6.1. Physically Required Resolution for Direct Simulation of Turbulent Flows

Up to a few years ago, it was doubted that it would be possible to carry out a direct numerical simulation of turbulent flows [23, 35, 121]. The requirements for a complete numerical simulation are found as follows:

Emmons [35] estimates that about 10^{10} meshes will be required for describing the fine structure of a turbulent tube flow at a Reynolds number of about 5,000. The computation time using modern computers is estimated at 100 years. The order of magnitude of the lengths which must still be resolved

is derived from the wall roughness magnitude, which brings about a change in the pressure loss amounting to 10% compared with that for a smooth wall. In addition, the amount of effort increases with increasing Reynolds number.

A similar estimation can be made as follows: a direct and complete simulation must at least include the laminar sublayer. A measure of the mesh edge length required for this is therefore Δz, the thickness of the laminar sublayer. In general, the following formula is used [120, P. 553]

$$\Delta z = 5 \frac{\nu}{\beta \hat{u}_0} \tag{1-29}$$

Using the definition of $\hat{u}_0$ and the resistance coefficient λ

$$\lambda \equiv \frac{2 \left(-\langle \partial \hat{p} / \partial \hat{x} \rangle\right) \delta}{\hat{\rho}\ {}^{V}\langle \hat{u} \rangle^2} \tag{1-30}$$

we find

$$\hat{u}_0 = \left(\frac{1}{8} \lambda\ {}^{V}\langle \hat{u} \rangle^2 \right)^{1/2} \tag{1-31}$$

and therefore

$$\Delta z = \frac{5 \cdot \sqrt{8}}{\sqrt{\lambda}\ Re_m} \tag{1-32}$$

If the Blasius resistance law [120, P. 553] is substituted for λ for tubes at Reynolds numbers which are not too high

$$\lambda = 0.3164\ Re_m^{-1/4} \tag{1-33}$$

then we find

$$\Delta z \approx 25\ Re_m^{-7/8} \tag{1-34}$$

and therefore, for example, for $Re = 10^5$, according to Figure 2

$$\Delta z \approx 10^{-3}$$

Consequently, KM $\approx 10^3$ meshes would be required in the radial direction or 10^9 meshes in the three dimensions. /14

If a special "wall law" model is applied for the wall layer, it would be interesting to determine the resolution Δz which would be required in the turbulent core flow. A measure for the required length is the Kolmogorov length η, as will be discussed in Chapter A1.2. For locally isotropic turbulence, we use the turbulence ball diameter to characterize the flow for which the inertia force and the viscosity force make an equal contribution to the disintegration of the ball:

$$\hat{\eta} = \left(\hat{\nu}^3 / \langle \hat{\varepsilon} \rangle\right)^{1/4} \tag{1-35}$$

If the energy conservation Equation (1-15) is averaged over the entire flow volume, we find

$$V \langle \hat{\varepsilon} \rangle = \frac{V}{\hat{s}} \langle \hat{u} \rangle \left(-\langle \partial \hat{p} / \partial \hat{x} \rangle\right) \approx \langle \hat{\varepsilon} \rangle \tag{1-36}$$

Because of $\langle \partial \hat{p} / \partial \hat{x} \rangle = 2 \hat{\rho} \hat{u}_0^2 / \hat{D}$ we then find

$$\Delta z = \frac{\hat{\eta}}{\hat{D}} = \left(\frac{4}{\lambda Re_m^2}\right)^{1/4} \tag{1-37}$$

and with (1-33)

$$\Delta z = 1.9 \, Re_m^{-11/16} \tag{1-38}$$

For Re = 10^5 we would also have the following according to Figure 2

$$\Delta z \approx 10^{-3}$$

Therefore we obtain the same results, which is interesting.

We would expect that such a large number of meshes could not be handled on a modern computer. The following section will show this.

1.6.2. Possible Resolution and Final Conclusion

If KM is the number of meshes in one direction, then the required core storage increases according to KM^3 for isotropic resolution. If we consider the fact that about nine variable values (3 velocity components, and one energy and divergence value each at 3 different times, that is 15, and only nine at any time if suitable programming is used) must be stored, then we find that 4 bytes are required per storage location and per value, according to Figure 3. The core storage available on the IBM 370/165 in Karlsruhe to the users is 2000 K byte (1K=1024) at the present time. This means that problems with KM ≈ 40 /15 can be calculated with core storage as a maximum. If suitable dynamic data management is used, so that at any time only one value is in core storage per mesh point and the rest is on background storage units, then it is possible to process problems with up to KM ≈ 80.

However, the computation time restriction is even greater. In order to simulate a three-dimensional unit of time, a computation time is required which increases in proportion to KM^4 because the permissible time step is proportional to KM^{-1} (see Chapter 6.3.2). For a mesh network of 16x16x16 meshes, and for a time step of $\Delta t \approx 5 \cdot 10^{-3}$ on the IBM 370/165, the approximate calculation time is 3 seconds. This means that the computation time per dimensionless time unit is about 10 minutes. This means we have the computation time dependence on KM as shown in Figure 4. In order to obtain a statistically steady solution 2-3 dimensionless time units are required. This value obtained from experience [33]

is confirmed if we consider the "break in time" T_e, the time during which the inlet length is passed by the flow in a tube, that is

$$T_e = \frac{L_e}{\nu / \langle u_1 \rangle} \tag{1-39}$$

According to Latzko [48, P. 233] the following applies for tubes:

$$L_e = 0.693 \, (Re_m)^{1/4} \tag{1-40}$$

where $\nu / \langle u_1 \rangle \approx 30$ (order of magnitude [18]

therefore

$$T_e \approx 0.023 \, Re_m^{1/4} \tag{1-41}$$

For $Re_m \approx 10^8$ we find $T_e \approx 2.3$

If we assume that commutation times of about 10 hours are acceptable, we find that the maximum usable mesh number is KM $\approx$ 40. This is probably the order of magnitude of the upper limit which can be reached today.

More as a footnote we would like to state that the computation times required for KM $\approx$ 1000 in one direction, according to Chapter 1.6.1, can be realized in 20-30 years with a reasonable amount of effort. We can make this estimation if we extrapolate the computer improvements which have taken place over the last 20 years. The computer speed increases by a factor of 10 every 6 years and the core storage capacity increases by a factor of 10 every 5 years [71]. Of course, some reservations must be made about exponential extrapolation.

We therefore have the following results: for a complete direct simulation of turbulent flows, a mesh network with about $(1000)^3$ meshes is required, already at moderate Reynolds numbers /16

($RE_m \approx 10^5$). Based on the computer capacity of today, only mesh networks of the order of $(40)^3$ can be processed today, i.e. the resolution which can be achieved is not sufficient to resolve the turbulent structure with characteristic lengths of less than $\frac{1}{40}$. Therefore, better models are required for this "fine structure".

1.7. The Purpose of this Paper

The overall purpose of this paper is to develop methods for the direct numerical simulation of turbulent flows at high Reynolds numbers. The results of the numerical simulation will be used for the following purposes:

a) To improve our knowledge of processes in turbulent flows
b) To determine characteristic features of turbulence which cannot be measured
c) To test the validity of turbulence models for flow fields averaged over time or over the ensemble. To determine empirically determined variables and to suggest improvements.

We do not intend to develop direct simulation methods for practical design problems in technology. Instead we wish to support the only practical turbulence models. We would like to emphasize the fine structure model. This will be done independent of any selected geometry, should be independent of experimental support and should be valid for all variable mesh sizes.

2. STATISTICAL TURBULENCE MODELS

In this chapter we will discuss the details of turbulence models, their problems and the direct numerical simulation

of turbulent flow fields using these models. In particular, we will discuss the problem of the "universal" applicability of turbulence models. The turbulence models discussed are not new. However, we believe that the discussion will be helpful for the understanding of turbulent flows. In addition, we will define the turbulence model variables determined during an evaluation.

/17

2.1. Requirements for Turbulence Models and Purpose of Model Theories

Turbulence is a random process [89]. It is not desirable and not possible to describe all of the details of this process. As a rule, we are only interested in certain statistical average values, such as for example those of the velocity values, pressures, or their products. Therefore, it is not appropriate to solve the unsteady differential equations and determine the solution. Instead, the differential equations themselves are averaged first. If we form the time average, (characterized by the < >) of the momentum conservation Equations (1-7), we find equations which contain more unknowns than equations:

$$\left\langle \frac{\partial u_i}{\partial t} \right\rangle + \frac{\partial}{\partial x_j}\left(\langle u_i \rangle \cdot \langle u_j \rangle \right) = -\frac{\partial}{\partial x_i}\langle p \rangle + \frac{\partial}{\partial x_j}\left(\nu \left(\frac{\partial \langle u_i \rangle}{\partial x_j} + \frac{\partial \langle u_j \rangle}{\partial x_i} \right) - \langle u_i' u_j' \rangle \right) \quad (2\text{-}1)$$

Additional unknowns are the following correlations named after Reynolds [107]

$$\langle u_i' u_j' \rangle \equiv \left\langle \left(u_i - \langle u_i \rangle \right) \cdot \left(u_j - \langle u_j \rangle \right) \right\rangle , \quad (2\text{-}2)$$

which have the dimensions of a stress per unit of mass, and which are therefore called Reynolds stresses. It is possible to establish differential equations for these unknowns [12, 115]. However, these contain a large number of unknowns which are triple correlations of the type $\langle u_i' u_j' u_k' \rangle$ and $\langle u_i' p' \rangle$, respectively. In this way we do not obtain as many equations as unknowns for a finite number of equations. A truncation must be carried out

in some way, and the other unknown quantities must be calculated using suitable approximations from the known variables. In this case one refers to "closure problems". The set of equations obtained with these approximations is called the turbulence model.

In the following we will describe a few turbulence models and discuss the large number of suggestions put forth in this area. Summaries can be found in [53, 59, 91, 115, 127]. In the formulas, we will restrict ourselves to one-dimensional, Cartesian problems, and x will be the flow direction axis. z is the perpendicular axis to x, measured from a limiting wall, where we have $\langle u \rangle = \langle u_1 \rangle (z)$. It is the general goal of turbulence theoreticians to find a "universal" turbulence model which satisfies the following requirements:

- It is valid in as many cases as possible (for various geometries, boundary conditions, types of turbulence production, etc.) without changing the model or without any model constants, so that extrapolations into new areas can be made without any new experiments,
- On the other hand it should be simple enough that it can be used in practice with a justifiable amount of effort.

/18

In the following we will discuss the existence of such a "universal" turbulence model in connection with a few special models.

2.2. The Prandtl Mixing Length Model

According to what was said above, in one-dimensional flows only one component of the Reynolds stresses is different from zero. Let us assume that it is

$$\langle u_1' u_3' \rangle \equiv \langle u' w' \rangle \qquad (2\text{-}3)$$

ω' is the fluctuation component perpendicular to the wall (Figure 1). The simplest model for this is the Prandtl mixing length model [98]. Using a Boussinesq model [5], in which the following expression is assumed for the molecular stresses,

$$\langle u'w' \rangle = - \nu_{turb} \frac{\partial \langle u \rangle}{\partial z}, \tag{2-4}$$

in analogy to the Newtonian stress law Prandtl determined the apparent turbulent viscosity ν_{turb} based on the idea of motion based on the individual turbulence balls (in analogy to the kinetic gas theory) over a distance of one free path length L (the mixing length) as follows

$$\nu_{turb} = L^2 \left| \frac{\partial \langle u \rangle}{\partial z} \right|. \tag{2-5}$$

It is difficult to determine the mixing length L. In the vicinity of the wall we find [120]

$$L = k \cdot z \tag{2-6}$$

with the Kármán constant $k \approx 0.4$ and for a large distance from the wall

$$L \approx 0.1 \cdot D, \tag{2-7}$$

where D is a characteristic geometric length. Van Driest [25] then gave a formula for L which makes it possible to calculate $\langle u'w' \rangle$ into the laminar sublayer. This was generalized by Pantankar-Spalding to variable shear stresses τ [104]:

$$L = k z \left[1 - \exp \left\{ -z \cdot Re \, \tau^{1/2} / A_w \right\} \right] \tag{2-8}$$

The constant A_w considers the wall roughness τ as the dimensionless shear stress at the location z, which is determined from a force equilibrium in the plate flow.

/19

The Prandtl mixing length model has proven itself in many cases, especially in boundary layer flows. For example, see [104]. One obtains erroneous results using this model in the following cases:

a) Equation (2-4) leads to contradictions in the center of a channel flow, if the location of zero shear stress $\langle u'w' \rangle = 0$ is not the same as the position of maximum velocity ($\frac{\partial \langle u \rangle}{\partial z} = 0$) because of a non-symmetric geometry, for example annulus, or because of differences in the wall roughnesses [90].

b) Equation (2-5) can produce large errors if it is assumed that the turbulent exchange coefficients are proportional to ν_{turb} for scalar quantities such as temperature or concentration (which is done often [49, 104]).

c) The quantities ν_{turb} and $\left|\frac{\partial \langle u \rangle}{\partial z}\right|$ are only proportional with with a time lag for nonsteady flows or flows which are substantially accelerated by varying cross sections.

d) In the case of complicated channel cross sections, it becomes difficult to determine L in a suitable way; in addition the real exchange coefficients have an isotropic character; for example see [8].

e) For recirculating flows [49], such as behind ribs or blockages [75], the model fails completely.

f) The model also usually fails for secondary flows and other convective mixing effects.

From this, some people infer that it is not possible to have a universally valid turbulence model. Most researchers in this area attempt to expand the range of validity of the turbulence models by considering other variables and approximations to the exact equations which are valid for this case and which can be derived from the basic equations.

In fact, a universally valid model probably does not exist, unless the Navier-Stokes equations themselves are used. However, just like the Prandtl model can be looked upon as universally valid at least for simple channel flows and in many cases, we can expect that a model which extracts somewhat more information from the exact equations will have "universal" validity in many cases.

2.3. Energy Model According to Prandtl /20

Prandtl also suggested [99] such an improved turbulence model. He set:

$$\langle u'w' \rangle = - a_1 \sqrt{\langle E' \rangle}\, L \frac{\partial \langle u \rangle}{\partial z} \qquad (2\text{-}9)$$

The exact time-average kinetic energy $\langle E' \rangle \equiv \frac{1}{2}\langle (u_i - \langle u_i \rangle)^2 \rangle$ of the fluctuation velocities, which is required here, satisfies the following equation which is derived from (1-15) by time averaging (with ν = const)

$$0 = \underbrace{\frac{\partial}{\partial z}\left[\nu \frac{\partial \langle E' \rangle}{\partial z} - \underline{\langle w'E' \rangle - \langle w'p' \rangle} \right]}_{\text{Diffusion}} \underbrace{- \langle u'w' \rangle \frac{\partial \langle u \rangle}{\partial z}}_{\text{Production}} \underbrace{- \nu \underline{\left\langle \left(\frac{\partial u_i'}{\partial x_i} \right)^2 \right\rangle}}_{\text{Dissipation}} \qquad (2\text{-}10)$$

Approximations for the underlined and unknown correlations can be introduced from a dimensional analysis or with simple models. Therefore we obtain the following model equation [115]:

$$0 = \underbrace{\frac{\partial}{\partial z}\left[\nu \frac{\partial \langle \varepsilon' \rangle}{\partial z} - a_3 \sqrt{\langle \varepsilon' \rangle} \cdot L \frac{\partial \langle \varepsilon' \rangle}{\partial z}\right]}_{\text{Diffusion}} - \underbrace{\langle u'w' \rangle \frac{\partial \langle u \rangle}{\partial z}}_{\text{Production}} - \underbrace{a_2 \frac{\langle \varepsilon' \rangle^{3/2}}{L}}_{\text{Dissipation}} \quad (2\text{-}11)$$

The model consisting of Equations (2-6), (2-9) and (2-11) contains the Karman constant k as well as three constants a_1, a_2, a_3 which are determined from experiment (see Chapter 2.6).

This model is especially advantageous where the Prandtl mixing length model fails because of restrictions b) and c) mentioned in Chapter 2.2. Nevertheless, the calculation of the length scale L is probelematical and it is computed according to Chapter 2.2 as a first approximation. This is a considerable disadvantage for recirculating flows, as the paper of Runchal and Spalding [116] clearly shows. These authors use the model given above to calculate the flow field (and from it the temperature field) after a sudden tube expansion. The calculated streamlines are impressive. However, when one reads that the field of length values L was determined using complicated algebraic equations containing four empirical constants such that the velocity field agreed with the corresponding measurements, one is disappointed. The temperature field calculations are the only ones that are of any value. Consequently, it is necessary to have models for the length L, which are obtained from approximations of exact equations.

2.4 Length Models According to Rotta /21

As mentioned above, for an example, it is necessary to know the characteristic lengths L for turbulent exchange processes in a description of any turbulence models. Such a statement is typical for turbulence problems. Incompressible flows are characterized by the fact that perturbations at one location

are transmitted to the entire flow field through the action of the pressure field (see Chapter 1.4.2). This becomes clear if we consider the general solution of the Poisson Equation (1-19) for pressure [134] (for ν = const):

$$p(\underline{x}) = \iiint_V \frac{\partial^2}{\partial x_i \partial x_j} (u_i u_j)(\underline{x}') \frac{dV(\underline{x}')}{|\underline{x}' - \underline{x}|} \qquad (2\text{-}12)$$

Turbulence variables, which consider the spatial structure of the flow, also represent statements on correlations between variables at various points in location-time space [53, 115], in addition to length scales. This is also true for correlation spectra at a location as a function of the time frequency f or as a function of the three-dimensional wave number vector $\underline{k}$ [132, 53, 116] (see Chapter 4.2.2). This is also true for the derived variables, such as, for example the average frequency [68, 127].

In order to have a model equation for a length L, it is first necessary to give a suitable mathematical definition of this length L. The mixing length model is not sufficient to define a theorem according to the exact equations. Rotta [108, 115] gave the following definition for one-dimensional flows:

$$L(z) \equiv \frac{3}{\varepsilon} \int_0^D \frac{\langle u_i'(z) u_i'(r) \rangle}{\frac{1}{2} \langle (u_i'(z))^2 \rangle} \, dr \qquad (2\text{-}13)$$

According to the following sketch, this length is the integral of the correlation coefficient

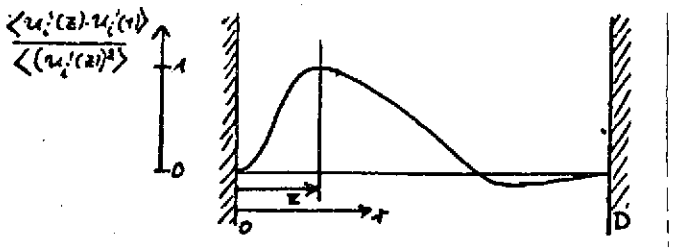

(The negative course for $r \gg z$, is a consequence of the continuity equation). The quantity L defined in this way can be interpreted as the average diameter of turbulence balls. If the time derivative of the integral given above is formed and if we substitute the momentum exchange equations for $\frac{\partial u_i'}{\partial t}$, we obtain an equation for determining L [109, 114, 115]. The following equation presentation shows the exact equation on the top and the approximation adjusted by Rotta [114, 115] on the bottom

/22

$$0 = -\frac{3}{16}\left\{\frac{\partial \langle u\rangle}{\partial z}\int_0^D \langle w'(z)u'(\tau)\rangle\, d\tau + \int_0^D \frac{\partial \langle u(\tau)\rangle}{\partial \tau}\langle u'(z)w'(\tau)\rangle\, d\tau\right\}$$

$$0 = -\langle u'w'\rangle\left(a_4 L\frac{\partial\langle u\rangle}{\partial z} + a_5 L^2\frac{\partial^3\langle u\rangle}{\partial z^3}\right)$$

Production

$$+\frac{3}{16}\int_0^D \frac{\partial}{\partial r_k}\left\langle u_i'(z)u_k'(z)u_i'(\tau)\right\rangle d\tau + \nu\frac{3}{8}\int_0^D \frac{\partial^2\langle u_i'(z)u_i'(\tau)\rangle}{\partial r_k^2}\, d\tau$$

$$-a_2\cdot a_6\langle\varepsilon'\rangle^{3/2}$$

Sink

$$-\frac{\partial}{\partial z}\left\{\frac{3}{16}\int_0^D\left[\langle u_i'(z)w'(z)u_i'(\tau)\rangle + \langle p'(z)w'(\tau)\rangle + \langle p'(\tau)w'(z)\rangle\right]d\tau - \nu\frac{\partial}{\partial z}\left(\langle\varepsilon'\rangle L\right)\right\}$$

$$+\frac{\partial}{\partial z}\left\{a_7\langle\varepsilon'\rangle^{\frac{1}{2}}L\left[L\frac{\partial\langle\varepsilon'\rangle}{\partial z} + a_8\langle\varepsilon'\rangle\frac{\partial L}{\partial z}\right] + \nu\frac{\partial}{\partial z}\left(\langle\varepsilon'\rangle\cdot L\right)\right\}$$

Diffusion

Dimensional analysis can be used to obtain the approximate equations (especially for the sink term and the pressure velocity correlations). Also analytical methods must be used. The approximation of the production term is based on a Taylor series development of the integrals. Additional terms of the type $L^n \frac{\partial^n \langle u \rangle}{\partial z^n}$, n=5,7,... are conceivable. Up to the present, only the first term was considered ($a_5 = 0$), as will be reported on later on. This together with Equations (2-9), (2-11) represents a model which makes it possible to calculate $\langle v \rangle$, $\langle \varepsilon \rangle$, and L based on the so-called transport equations and $\langle u'w' \rangle$ based on an algebraic relationship. Numerical methods for solving this and similar equations are given in [49, 104]. This model contains 8 constants a_i. When using an additional transport equation for $\langle u'w' \rangle$ according to Rotta [114], 13 constants are required. The main problem of turbulence model theory then consists of determining these constants in a suitable way.

2.5. Methods for Determining the Model Constants

Three main ways can be used to determine the constants, for example a_1 to a_8:

a) Consideration of limiting cases in which many terms can be ignored, (such as the immediate vicinity of the wall where the Prandtl mixing length model is valid) or homogeneous turbulence (where all terms of the transport equations for L vanish). /23

b) Integration of the differential equation with selected values of the constants and variation of the constants, so that the integral results agree with as many experimental results as possible "target values" in the sense of a least square fit.

c) Direct determination of the constants by measuring the terms which occur in the defining equations; for example

$$a_2 \equiv \frac{\nu \langle (\partial u_i'/\partial x_j)^2 \rangle}{\langle \varepsilon' \rangle^{3/2}/L} \qquad (2\text{-}15)$$

Method a) makes it possible to determine only a few constants. Method b) has been used by Ng-Spalding [91]. For plate flow, tube flow, plate boundary layer flow and free jet flow they used measured values of the following type as target values

$$(\langle u \rangle_{max} - \nu \langle u \rangle)$$

for plate and tube flows.

Method c) would be the most exact one. It will be possible to determine whether the "constants" are indeed independent of location and flow geometry and whether the model is therefore universally valid. However, the measurement technique fails here in almost all cases. The measurement of complicated correlations of velocity derivatives, pressures and their integrals over space is almost impossible. Perhaps the energy dissipation is an exception, which is required in (2-15). The space derivatives are usually determined by measuring time derivatives and recalculating using the Taylor hypotheses [134]

$$x \approx \langle u \rangle \cdot t \qquad (2\text{-}16)$$

(for discussion of these problems see [115, P. 148]), also local isotropic conditions are assumed (see Chapter 4).

Therefore, one of the goals of this paper is to numerically determine the terms contained in the definition equations according to numerical simulation of position-dependent and time-dependent flow fields, in order to determine the constants.

2.6. Data for the Constant Values, the Influence of the Uncertainties in the Constants and Their Numerical Determination

/24

Table 1 shows the constant values given by various authors. It is difficult to make comparisons because the length L has been defined in various ways, which according to (2-9) is expressed in particular by the value of the constant a_1. We can see the following:

a) No agreement exists regarding the values
b) No data is given for the second development coefficient a_5 of the length-product term ($a_5=0$).
c) It was found that the constants are not universally valid. Rodi-Spalding [113] had to use constants for a turbulent free jet emerging from a round or rectangular nozzle which differ by almost a factor of two; Ng-Spalding [91] used a position function for a_6.

It is very important to establish the variations of the model equation solutions which are obtained when the constants are varied. In other words, what are the effects of the uncertainties in the values of the individual constants. Ng-Spalding [91] varied their constants by 5% each to investigate this question and calculated how much the integral values used as target values varied. On the average we find the variations given in Table 2. The constants are sorted according to the magnitude of the target value change brought about by their variation. We can see the following:

a) It is more important to determine the constants exactly which are contained in the source and sink terms than those in the diffusion terms.

b) It is very important to have the correct model for the length-production term. This means that additional terms should also be considered.

In particular, item b) represents an important justification for an experiment to determine the constants from numerically simulated flow fields. A numerical method which on the one hand does require models for the fine structure cannot produce any particularly usable results for terms which are greatly influenced by this fine structure, such as, for example the energy-dissipation term and the diffusion terms. On the other hand, we can expect that those terms can be calculated in a realistic manner which are primarily determined by the resolved coarse structure. Among these we have the length-production term and the time-average Reynolds stress $\langle u'w' \rangle$. In this paper we will make a particular effort to determine the constants a_1, a_4 and a_5.

/25

3. BASIC EQUATIONS AVERAGED OVER MESH VOLUMES

In this chapter we will average the conservation equations for mass and momentum over the mesh volume, in order to prepare ourselves for the differencing method and the fine structure model for direct simulation. In addition, we will derive a conservation equation for the kinetic energy of the fluctuation velocities contained within the mesh. The chapter contains purely formal derivations and therefore no approximations which must be given a physical justification. The method is new, and

in contrast to earlier work, it is possible to build exact difference approximations and fine structure models. At the conclusion of this chapter, we will give a summary of the basic ideas in the following chapters.

3.1. Justification and Definition of Mesh Averaging

In order to build up a differencing method, the flow space is divided into as many regularly arranged meshes as possible. For each mesh, one of the field values being integrated is stored. In addition to the spatial division, the time axis is also divided into a finite number of time intervals Δt and for each time interval one each of the field values is stored at all space locations. Then the differentials of the field values are approximated by differencing field values at the various adjacent meshes. One arrives at such differencing approximations by either a Taylor series expansion and truncation of the series after a few terms, or by formal integration of the differential equations over a space-time mesh with subsequent approximation of the non-analytic integral terms.

The Taylor series development can be truncated after a few, for example, after n, terms [13]

$$f(x) = \sum_{i=0}^{n} \frac{1}{n!} f^{(n)}(0)\, x^n \qquad (3\text{-}1)$$

If the residual term

$$R_n(x) = \frac{x^{n+1}}{(n+1)!} f^{(n+1)}(\theta \cdot x) \quad , \quad 0 < \theta < 1 \qquad (3\text{-}2)$$

can be ignored for very irregular turbulent flow fields, it is not possible to simply assume that the product $x^{n+1} f^{(n+1)}$ will remain sufficiently small for small x, because the derivatives $f^{(n+1)}$ can increase greatly with increasing n. Therefore, the second method must be used for turbulent flows. Approximations are also required in this case. They only assume that the higher

derivatives of the field values averaged over mesh volumes (that is, smoothed field values) are sufficiently small. /26
The effect of the irregular fine structure within the meshes is also represented in the averaged equations. The so-called Reynolds stresses show this. These terms cannot be obtained for Taylor series expansions.

Therefore, we will first use the method of Lilly [80, 81] and Deardorff [29]. In the averaging, that is, in the integration over the mesh volume and subsequent division by the mesh volume, these authors did not take into account that some of the integration can be done analytically. Therefore, they have to assume that

$$\frac{1}{\Delta x}\int_{x-\frac{\Delta x}{2}}^{x+\frac{\Delta x}{2}}\frac{\partial u}{\partial x}\,dx \approx \frac{\partial}{\partial x}\,\frac{1}{\Delta x}\int_{x-\frac{\Delta x}{2}}^{x+\frac{\Delta x}{2}} u\,dx\,, \qquad (3\text{-}3)$$

which is, of course, correct. It would be correct to assume that

$$\frac{1}{\Delta x}\int_{x-\frac{\Delta x}{2}}^{x+\frac{\Delta x}{2}}\frac{\partial u}{\partial x}\,dx = \frac{u(x+\frac{\Delta x}{2})-u(x-\frac{\Delta x}{2})}{\Delta x} \equiv \delta_x u(x) \qquad (3\text{-}4)$$

Consequently, the field values considered in the differencing method have been falsely identified as volume average values. It is more correct to say that they are area average values. The same difference formulas for the averaged field values can be formally obtained from the above (for equidistant mesh networks). However, this leads to a different definition and approximation of the Reynolds stresses which describe the fine structure. Also the boundary conditions for the different formulas are different. This will become clear in the following sections.

First let us explain the mesh network used and the average values used. The mesh network is determined by a field (not necessarily equidistant of surfaces x_i=const. and t=const.). A mesh with the indices l, m, n, p is made up of the following

space-time element:

$$V_{l,m,n,p} \equiv \left\{ (x_1, x_2, x_3, t);\ \begin{array}{l} x_1|_{l-\frac{1}{2}} \le x_1 \le x_1|_{l+\frac{1}{2}} \\ x_2|_{m-\frac{1}{2}} \le x_2 \le x_2|_{m+\frac{1}{2}} \\ x_3|_{n-\frac{1}{2}} \le x_3 \le x_3|_{n+\frac{1}{2}} \\ t|_{p-\frac{1}{2}} \le t \le t|_{p+\frac{1}{2}} \end{array} \right\} \qquad (3\text{-}5)$$

where the coordinates $x_1/_{l+\frac{1}{2}}$ $x_2/_{m+\frac{1}{2}}$, $x_3/_{n+\frac{1}{2}}$, $t/_{p+\frac{1}{2}}$ increase monotonically with the indices, and in addition we have, for example

$$1 >> \Delta x_{1_l} \equiv x_1|_{l+\frac{1}{2}} - x_1|_{l-\frac{1}{2}} > 0$$
$$1 >> \Delta t_p \equiv t|_{p+\frac{1}{2}} - t|_{p-\frac{1}{2}} > 0$$

/27

The averaging of a variable y in a volume V' (which at the same time equals the mesh volume as well as a space-time region which is displaced with respect to the mesh volume) is defined as

$$\overline{y}^{V'} \equiv \frac{1}{V'} \iiint_{V'} y \, dV' \qquad (3\text{-}6)$$

If the volume V' is equal to $V_{l,m,n,p}$, we have:

Cartesian:

$$\overline{y}^{V}\Big|_{l,m,n,p} \equiv \frac{1}{\Delta x_1|_l \cdot \Delta x_2|_m \cdot \Delta x_3|_n \cdot \Delta t|_p} \int_{t|_{p-\frac{1}{2}}}^{t|_{p+\frac{1}{2}}} \int_{x_3|_{n-\frac{1}{2}}}^{x_3|_{n+\frac{1}{2}}} \int_{x_2|_{m-\frac{1}{2}}}^{x_2|_{m+\frac{1}{2}}} \int_{x_1|_{l-\frac{1}{2}}}^{x_1|_{l+\frac{1}{2}}} y(x_1', x_2', x_3', t') \, dx_1' dx_2' dx_3' dt' \qquad (3\text{-}7)$$

Cylindrical:

$$\overline{y}^{V}\Big|_{l,m,n,p} \equiv \frac{1}{\Delta x_l \cdot \Delta \varphi_m \, \Delta r_n \, r_n \, \Delta t_p} \int_{t|_{p-\frac{1}{2}}}^{t|_{p+\frac{1}{2}}} \int_{r|_{n-\frac{1}{2}}}^{r|_{n+\frac{1}{2}}} \int_{\varphi_{m-\frac{1}{2}}}^{\varphi_{m+\frac{1}{2}}} \int_{x|_{l-\frac{1}{2}}}^{x|_{l+\frac{1}{2}}} y(x', \varphi', r', t') \, dx \cdot r \, d\varphi \, dr \, dt \qquad (3\text{-}8)$$

$$r|_n = \frac{1}{2}\left(r|_{n+\frac{1}{2}} + r|_{n-\frac{1}{2}}\right)$$

3.2. Continuity Equation (Mass Conservation)

First we will consider cartesian coordinates. The exact differential equation

$$\frac{\partial u_i}{\partial x_i} = 0 \qquad (1\text{-}6)$$

is to be averaged over V. We obtain:

$$\overline{\frac{\partial u_i}{\partial x_i}}^{V} = 0 = \frac{1}{\Delta x_1 \Delta x_2 \Delta x_3 \Delta t} \int_{t}^{} \int_{x_3}^{} \int_{x_2}^{} \int_{x_1}^{} \frac{\partial u_i}{\partial x_i} \, dx_1' dx_2' dx_3' dt' \qquad (3\text{-}9)$$

If we consider the fact that each of the three sum terms of the integrand is formally integrated with respect to one of the coordinates (the x_i coordinate) we obtain differences of two terms in which it is only necessary to integrate over two space variables and time, that is over a mesh area segment and a time interval. This region defined in space-time space is called "area" in the following. In order to simplify the notation, we will call these area averages $\overline{{}^{i}y}$, for example

$$\overline{{}^{1}y}\Big|_{l+\frac{1}{2},m,n,p} \equiv \frac{1}{\Delta x_2|_m \, \Delta x_3|_n \, \Delta t|_p} \int_{t|_{p-\frac{1}{2}}}^{t|_{p+\frac{1}{2}}} \int_{x_3|_{n-\frac{1}{2}}}^{x_3|_{n+\frac{1}{2}}} \int_{x_2|_{m-\frac{1}{2}}}^{x_2|_{m+\frac{1}{2}}} y(x_1|_{l+\frac{1}{2}}, x_2', x_3', t') \, dx_2' dx_3' dt'$$

and we will call the differences which occur $\delta_{x_i} y$, where, for example

$$\delta_{x_1} y|_{l,m,n,p} \equiv \frac{1}{\Delta x_1|_l} \left(y_{l+\frac{1}{2},m,n,p} - y_{l-\frac{1}{2},m,n,p} \right)$$

Then the averaging gives,

$$\overline{\frac{\partial u_i}{\partial x_i}}^{V}\Big|_{l,m,n,p} = \delta_{x_i} \overline{{}^{i}u_i}\Big|_{l,m,n,p} \, . \qquad (3\text{-}10)$$

/ 28

This equation is exact and has a formal correspondence with the Gauss integral theorem [13]:

$$\int_{V} \operatorname{div} \underline{u} \, dV = \oint_{F} \underline{u} \cdot d\underline{F}$$

In a similar way, we find the following for cylindrical coordinates (starting with (1-8))

$$\delta_x \overline{{}^{x}v_x} + \frac{1}{r_n} \delta_\varphi \overline{{}^{\varphi}v_\varphi} + \frac{1}{r_n} \delta_r \left(r \overline{{}^{r}v_r} \right) = 0\Big|_{l,m,n,p} \qquad (3\text{-}11)$$

where, for example

$$\overline{v_x}\Big|_{l+\frac{1}{2},m,n,p} \equiv \frac{1}{\Delta r_n \, r_n \cdot \Delta\varphi_m \, \Delta t_p} \int_{r_{n-\frac{1}{2}}}^{r_{n+\frac{1}{2}}} \int_{\varphi_{m-\frac{1}{2}}}^{\varphi_{m+\frac{1}{2}}} \int_{t_{p-\frac{1}{2}}}^{t_{p+\frac{1}{2}}} v_x\left(x_{|l+\frac{1}{2}}, \varphi', r', t'\right) d\varphi' \, r' \, dr' \, dt' \Big| \tag{3-12}$$

and the difference quotients $\delta_x, \delta_\varphi, \delta_r|$ are defined according to the cartesian $\delta_{x_i}|$.

We will repeat the result: At least the continuity equation can exactly be replaced by difference formulas, if the velocity average values which occur are defined as average values of velocities over a mesh area segment (as well as over a time interval Δt), the normal of which is parallel with the velocity component vector.

Since these area average values are taken over a different area segment of the mesh, depending on the velocity components, a so-called "staggered grid" [29, 30, 33, 42, 54, 62, 96, 141], is used, i.e. an "overlapping grid" in which the velocity values to be stored are assigned to various locations depending on the direction. Figure 5 shows the grid used. This grid has up to the present not been used in the literature for formation of area average values. It has only been justified because of the simplicity and accuracy of the truncation errors of the resulting difference formulas [33, 96].

3.3. Averaged Momentum Conservation Laws

We will now derive the average momentum conservation laws which are similar to the average continuity equation. Because of the complicated nature of these equations, we cannot expect such a simple and elegant result here. However, we will show how a different notation can be found using a formal method which is very close to the differential equations. We will also show

where approximations will have to be made.

/29

Depending on the equation component, a volume is averaged according to the staggered grid which contains the reference surface of the average surface value of the velocity component under consideration in approximately its center. The following sketch shows this V_l for the component 1 of the momentum equations in cartesian coordinates:

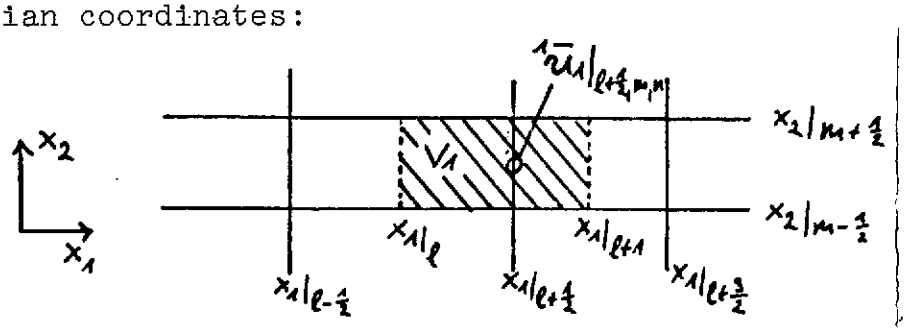

$$x_1|_l \equiv \frac{1}{2}\left(x_1|_{l-\frac{1}{2}} + x_1|_{l+\frac{1}{2}}\right) \tag{3-12}$$

The limitation of the volume V_1 in x_1 direction is selected between the coordinate surfaces $x_1|_{l+\frac{1}{2}} = \text{const}$, because in this case the error of the difference approximations required later on becomes the smallest. If the momentum conservation equations are averaged over such volumes V_i, and if formal integrations are carried out wherever possible, we find the following:*

Cartesian:

$$V_i \frac{\partial \overline{u_i}}{\partial t} = -\delta_{x_j}\overline{(u_i u_j)^j} - \delta_{x_i}\overline{p^i} + \delta_{x_j}\left[\overline{\nu\left(\frac{\partial u_i}{\partial x_j} + \frac{\partial u_j}{\partial x_i}\right)^j}\right] + \delta_{1i}\, p_x \tag{3-14}$$

* Instead of integrating the differential conservation theorems over volumes, one could start with integral conservation theorems. It seems that the procedure used here is simpler when curvilinear coordinates are considered.

Cylindrical:

$$
\begin{aligned}
&\overline{V_x}\,\overline{\frac{\partial v_x}{\partial t}} + \delta_x\,\overline{v_x^2}^{\,x} + \frac{1}{\tau_n}\,\delta_\varphi\,\overline{(v_\varphi v_x)}^{\,\varphi} + \frac{1}{\tau_n}\,\delta_r\,\overline{(\tau v_r v_x)}^{\,r} = -\,\delta_x\,\overline{p}^{\,x} + P_x \\
&+ \delta_x\left\{\nu 2\,\frac{\partial v_x}{\partial x}\right\} + \frac{1}{\tau}\,\delta_\varphi\left\{\nu\left(\frac{\partial v_x}{\tau\partial\varphi} + \frac{\partial v_\varphi}{\partial x}\right)\right\} + \frac{1}{\tau}\,\delta_r\left\{\tau\,\nu\left(\frac{\partial v_x}{\partial r} + \frac{\partial v_r}{\partial x}\right)\right\}; \\
&\overline{V_\varphi}\,\overline{\frac{\partial v_\varphi}{\partial t}} + \delta_x\,\overline{(v_x v_\varphi)}^{\,x} + \frac{1}{\tau}\,\delta_\varphi\,\overline{(v_\varphi^2)}^{\,\varphi} + \frac{1}{\tau}\,\delta_r\,\overline{(\tau v_r v_\varphi)}^{\,r} + \overline{\frac{1}{\tau}\,(v_r v_\varphi)}^{\,V_\varphi} = -\,\frac{1}{\tau}\,\delta_\varphi\,\overline{p}^{\,\varphi} \\
&+ \delta_x\left\{\nu\left(\frac{\partial v_\varphi}{\partial x} + \frac{\partial v_x}{\tau\partial\varphi}\right)\right\} + \frac{1}{\tau}\,\delta_\varphi\left\{2\nu\left(\frac{\partial v_\varphi}{\tau\partial\varphi} + \frac{v_r}{\tau}\right)\right\} + \frac{1}{\tau}\,\delta_r\left\{\tau\,\nu\left(\tau\frac{\partial}{\partial r}\left(\frac{v_\varphi}{\tau}\right) + \frac{\partial v_r}{\tau\partial\varphi}\right)\right\} \qquad (3\text{-}15) \\
&+ \overline{\left\{\frac{\nu}{\tau}\left(\tau\frac{\partial}{\partial r}\left(\frac{v_\varphi}{\tau}\right) + \frac{\partial v_r}{\tau\partial\varphi}\right)\right\}}^{\,V_\varphi}; \\
&\overline{V_r}\,\overline{\frac{\partial v_r}{\partial t}} + \delta_x\,\overline{(v_x v_r)}^{\,x} + \frac{1}{\overline{\tau}}\,\delta_\varphi\,\overline{(v_\varphi v_r)}^{\,\varphi} + \frac{1}{\overline{\tau}}\,\delta_r\,\overline{(\tau v_r^2)}^{\,r} - \overline{\frac{v_\varphi^2}{\tau}}^{\,V_r} = -\,\delta_r\,\overline{p}^{\,r} \\
&+ \delta_x\left\{\nu\left(\frac{\partial v_r}{\partial x} + \frac{\partial v_x}{\partial r}\right)\right\} + \frac{1}{\overline{\tau}}\,\delta_\varphi\left\{\nu\left(\tau\frac{\partial}{\partial r}\left(\frac{v_\varphi}{\tau}\right) + \frac{\partial v_r}{\tau\partial\varphi}\right)\right\} + \frac{1}{\overline{\tau}}\,\delta_r\left\{2\nu\tau\,\frac{\partial v_r}{\partial r}\right\} \\
&- 2\,\overline{\frac{\nu}{\tau}\left\{\frac{\partial v_\varphi}{\tau\partial\varphi} + \frac{v_r}{\tau}\right\}}^{\,V_r}.
\end{aligned}
$$

Here

$$
\overline{\tau}\Big|_{n+\frac{1}{2}} \equiv \frac{1}{2}\,(\tau_{n+1} + \tau_n) \equiv \frac{1}{4}\,(\tau_{n-\frac{1}{2}} + 2\tau_{n+\frac{1}{2}} + \tau_{n+\frac{3}{2}}) \qquad (3\text{-}16)
$$

/ 30

is the average value of the radius in the volume Vr.

Area average values of velocity products occur in the convection terms. (Volume average values occur in the Coriolis and centrifugal acceleration terms). We may formally make a division into average values and fluctuation variables as follows:

$$
{}^{j}\overline{(u_i u_j)} = {}^{j}\overline{u_i}\;{}^{j}\overline{u_j} + {}^{j}\overline{(u_i - {}^{j}\overline{u_i})\,(u_j - {}^{j}\overline{u_j})} \qquad (3\text{-}18)
$$

If we define the fluctuation variable u_i' to be the local deviation

of the velocity from its (area-) average value,*

$$u_i' \equiv u_i - \overline{u_i}^j \qquad (3\text{-}19)$$

then we obtain

$$\overline{(u_i u_j)}^j = \overline{u_i}^j \overline{u_j}^j + \overline{u_i' u_j'}^j \qquad (3\text{-}20)$$

We find that terms occur also here which can be called Reynolds stresses [107], just like what occurred in the time averaging according to Chapter 2.1. In contrast to the Reynolds stresses which occur when time averaging is formed, these vanish when the diameter of the volume goes to zero because in this case u_i' also goes to zero.

We will thus repeat the results again: Many terms of the momentum conservation equations can be formally integrated for volume averaging and then can be transformed into difference form. Correlations occur among the fluctuation velocities referring to area average values (and sometimes volume average values) which are of the Reynolds stress type. However, they become zero when the volume element diameter goes to zero. In addition to these Reynolds stresses, there are numerous velocity average values, which do not agree with those stored in the grid, as well as terms with derivatives (however, only first derivatives). This means that more unknowns than equations exist and these unknowns must be calculated from the known velocity average values using approximations.

The approximations will be introduced in Chapters 5 and 6. In order to provide approximations for the Reynolds stresses,

* The notation $u_i'^j \equiv u_i - \overline{u_i}^j$ would be ambiguous; this complicated notation is not used because it is always clear what is meant.

it is first necessary to formulate the conservation equation of the kinetic energy averaged over the volume. / 31

3.4. Average Conservation Equations of Kinetic Energy

In the following we will derive a conservation equation for the kinetic energy of the fluctuation velocities within a mesh volume, that is for

$$\overline{E'}^{V} \equiv \frac{1}{2}\overline{(u_i - \overline{u_i}^{V})^2}^{V} = \frac{1}{2}\left(\overline{u_i^2}^{V} - (\overline{u_i}^{V})^2\right)$$

We obtain this conservation equation by formulating the time derivative

$$\overline{\frac{\partial E'}{\partial t}}^{V} = \left(\frac{1}{2}\overline{\frac{\partial u_i^2}{\partial t}}^{V} - \overline{u_i}^{V}\,\overline{\frac{\partial u_i}{\partial t}}^{V}\right)$$

We formulate the volume average value using Equations (1-7) and (1-9) respectively and then subtract the scalar product of the velocity vector $\overline{u_i}^{V}$ and $\overline{\frac{\partial u_i}{\partial t}}^{V}$ using Equations (3-14) and (3-15), respectively.

Just like in Chapters 3.2 and 3.3, we obtain the following for cartesian coordinates:

$$\overline{\frac{\partial u_i^2/2}{\partial t}}^{V} = \overline{\frac{\partial}{\partial t}E}^{V} = -\delta_{x_j}\overline{(u_j E)}^{j} - \delta_{x_i}\overline{(u_i p)}^{i} + \delta_{x_j}\overline{\left(\nu\left(\frac{\partial E}{\partial x_j} + \frac{\partial (u_i u_j)}{\partial x_i}\right)\right)}^{j} - \overline{\varepsilon}^{V} + \overline{u_i}^{V} P_x \qquad (3\text{-}21)$$

If we introduce the following as fluctuation variables according to (3-19)

$$u_j' \equiv u_j - \overline{u_j}^{j} \;;\quad p' \equiv p - \overline{p}^{j} \;;\quad \nu' \equiv \nu - \overline{\nu}^{j} \qquad (3\text{-}22)$$

where the bar refers to the averaging process, and

$$\overline{E}^{j} \equiv \frac{1}{2}\left(\overline{u_i}^{j}\right)^2 \;;\quad \overline{E'}^{j} \equiv \frac{1}{2}\overline{(u_i - \overline{u_i}^{j})^2}^{j} \qquad (3\text{-}23)$$

we find:

$$\overline{\frac{\partial E}{\partial t}} = -\delta_{x_j}\left(\overline{E}^{j}\overline{u_j}^{j} + \overline{u_j}^{j}\overline{E'}^{j} + \frac{1}{2}\overline{u_i'^2 u_j'}^{j}\right) - \delta_{x_j}\left(\overline{u_i}^{i}\overline{u_i' u_j'}^{j}\right)$$
$$- \delta_{x_i}\left(\overline{u_i}^{i}\overline{p}^{i}\right) - \delta_{x_i}\left(\overline{p' u_i'}^{i}\right) + \overline{u_1}^{v} P_x - \overline{\varepsilon}^{v}$$
$$+ \delta_{x_j}\left(\overline{\nu}^{j}\left(\frac{\partial \overline{E}^{j}}{\partial x_j} + \frac{\partial \overline{E'}^{j}}{\partial x_j} + \overline{\frac{\partial (u_i u_j)}{\partial x_i}}^{j}\right)\right)$$
$$+ \delta_{x_j}\left(\overline{\nu'\left(\frac{\partial E}{\partial x_j} + \frac{\partial (u_i u_j)}{\partial x_i}\right)'}^{j}\right)$$

/32

On the other hand, the scalar product $\overline{u_i}^{v} \cdot \overline{\frac{\partial u_i}{\partial t}}^{v}$ is

$$\overline{u_i}^{v}\overline{\frac{\partial u_i}{\partial t}}^{v} = -\overline{u_i}^{v}\delta_{x_j}\left(\overline{u_i}^{i}\overline{u_j}^{i} + u_i' u_j'\right) - \overline{u_i}^{v}\delta_{x_i}\overline{p}^{i} + \overline{u_1}^{v} P_x$$
$$+ \overline{u_i}^{v}\delta_{x_j}\left[\overline{\nu}^{j}\left(\overline{\frac{\partial u_i}{\partial x_j}}^{j} + \overline{\frac{\partial u_j}{\partial x_i}}^{j}\right) + \overline{\nu'\left(\frac{\partial u_i}{\partial x_j} + \frac{\partial u_j}{\partial x_i}\right)'}^{j}\right] \qquad (3\text{-}25)$$

If we introduce the following arithmetic averaging operation:

$$\overline{y}^{\wedge} \equiv \frac{1}{2}\left(y\left(x_1 + \frac{\Delta x_1}{2}, x_2, x_3\right) + y\left(x_1 - \frac{\Delta x_1}{2}, x_2, x_3\right)\right), \qquad (3\text{-}26)$$

and if we introduce the identities

$$\delta_{x_i}(ab) \equiv \overline{a}^{i}\delta_{x_i} b + \overline{b}^{i}\delta_{x_i} a, \qquad (3\text{-}27)$$
$$\frac{1}{2}\delta_{x_i}(a^2) = \overline{a}^{i}\delta_{x_i} a, \qquad (3\text{-}28)$$

and we assume the following approximation*:

$$\overline{{}^{V}u_i} \approx \overline{{}^{i}u_i}, \tag{3-29}$$

we can write:

$$\begin{aligned}
&\overline{{}^{V}u_i}\,\overline{\frac{\partial {}^{V}u_i}{\partial t}} = -\delta_{x_j}\left(\overline{{}^{i}E}\,\overline{{}^{i}u_j} + \overline{{}^{i}u_i}\,\overline{{}^{i}u_i'u_j'}\right) + \overline{{}^{i}u_i'u_j'}^{\,j}\,\delta_{x_j}\,\overline{{}^{i}u_i} - \delta_{x_i}\left(\overline{{}^{i}u_i}\,\overline{{}^{i}p}\right) + \overline{{}^{V}u_i}\,p_x \\
&- \delta_{x_j}\left(\overline{{}^{i}\nu}\left(\frac{\partial \overline{{}^{i}E}}{\partial x_j} + \overline{{}^{j}u_i}\,\frac{\partial \overline{{}^{j}u_j}}{\partial x_i}\right) - \overline{{}^{V}\nu}\left(\delta_{x_j}\,\overline{{}^{j}u_i}\left(\delta_{x_j}\,\overline{{}^{i}u_i} + \delta_{x_i}\,\overline{{}^{i}u_j}\right)\right)\right. \\
&\left. - \overline{{}^{V}u_i}\,\delta_{x_j}\left(\overline{{}^{j}\nu'\left(\frac{\partial u_i}{\partial x_j} + \frac{\partial u_j}{\partial x_i}\right)'}\right)\right.
\end{aligned} \tag{3-30}$$

If we now subtract the result from the Equation (3-24), we find the desired equation

$$\begin{aligned}
&\underbrace{\overline{{}^{V}\frac{\partial E'}{\partial t}}}_{I} = \underbrace{-\delta_{x_j}\left(\overline{{}^{i}u_j}\,\overline{{}^{i}E'}\right)}_{II} - \underbrace{\overline{{}^{j}u_i'u_j'}^{\,j}\,\delta_{x_j}\,\overline{{}^{i}u_i}}_{III} \\
&+ \underbrace{\delta_{x_j}\left\{\overline{{}^{i}\nu}\,\frac{\partial \overline{{}^{i}E'}}{\partial x_j} + \overline{{}^{j}u_i\frac{\partial u_j}{\partial x_i}} - \overline{{}^{i}u_i}\,\overline{\frac{\partial {}^{j}u_j}{\partial x_i}} - \overline{{}^{j}u_j'E'} - \overline{{}^{j}u_j'p'}\right\}}_{IV\,a} \\
&+ \underbrace{\delta_{x_j}\left\{\overline{{}^{j}\nu'\left(\frac{\partial E}{\partial x_j} + \frac{\partial (u_iu_j)}{\partial x_i}\right)'} - \overline{{}^{i}u_i}\,\overline{{}^{j}\nu'\left(\frac{\partial u_i}{\partial x_j} + \frac{\partial u_j}{\partial x_i}\right)'}\right\}}_{IV\,b} \\
&\underbrace{-\overline{{}^{V}\varepsilon}}_{V\,a} + \underbrace{\overline{{}^{V}\nu}\left\{\delta_{x_j}\,\overline{{}^{i}u_i}\left(\delta_{x_j}\,\overline{{}^{i}u_i} + \delta_{x_i}\,\overline{{}^{i}u_j}\right)\right\}}_{V\,b}
\end{aligned} \tag{3-31}$$

The terms have the following meaning:

I Time change of the average fluctuation energy.

II Convection of the fluctuation energy.

III Production terms; work of the Reynolds stresses

IV Diffusion terms; the term IVb can be ignored as a rule,

---

* According to the mean volume theorem of integral calculus we have $\overline{{}^{V}u_i} = \overline{{}^{i}u_i}(\underline{\xi})$, where $\underline{\xi}$ is a point in the volume V.

because the viscosity fluctuations are apparently not correlated with the other terms.

V. Dissipation of the fluctuation energy. /33

Va: Total Dissipation

Vb: Dissipation due to average velocity

3.5. Summary of the Basic Ideas for Formulating a Closed System of Equations

In this section we will describe the models which will be used to formulate a closed system of difference equations, so as to clarify the following chapters. We will only consider cartesian coordinates.

Equation (3-14) with the division of the convective terms according to Equation (3-20) contains two types of unknowns, which must be calculated from the variables stored in the grid: on the one hand there are quantities such as for example $^{j}\bar{u}_{i}$, which must be approximately calculated from adjacent mesh values (for example, from adjacent values of $^{i}\bar{u}_{i}$) using linear relationships (algebraic average values). On the other hand, there are the fine structure Reynolds stresses $^{j}\overline{u'_{i}u'_{j}}$, which must be calculated using nonlinear approximations from the average velocity field $^{i}\bar{u}_{i}$ as well as from the kinetic energy of the fine structure within a mesh $\overline{v_{E'}}$. Chapter 6 will discuss the linear approximations, which are simple in nature. The main problem and most of the development in this paper will be the discussion of the modeling of the nonlinear fine structure Reynolds stresses. In the following we will give a brief description of the principles used in the model, which are discussed in detail in Chapters 4 and 5, as well as in the Appendices 1 -3.

A trial solution is used for the fine structure Reynolds stresses, which have the form of a Boussinesq trial solution:

$$ {}^{j}\overline{u_i' u_j'} = -{}^{j}\mu \left(\partial_{x_j} {}^{i}\bar{u}_i + \partial_{x_i} {}^{i}\bar{u}_j \right) + \frac{1}{3} \delta_{ij} {}^{\ell}\overline{u_\ell' u_\ell'} \qquad (3\text{-}32) $$

Here ${}^{j}\mu$ is the turbulent viscosity which must still be determined. The subscript points to the fact that the viscosity will differ depending on the size and shape of the area considered over which the averaging is carried out.

The Boussinesq trial solution assumes that the shear stress and the velocity deformation vanish at the same time. As discussed in Chapter 2.2, this condition is not always satisfied for the time average flow field. The reasons for this are the effects of the walls and the geometry which are deterministic in nature. /34

The analogy between the Boussinesq trial solution and the molecular Newtonian shear stress trial solution assumes that the turbulent exchange process as well as the molecular momentum transport process are purely statistical in nature. This assumption is probably more applicable for the fine structure than for the coarse structure. Therefore the assumption seems valid. The Boussinesq trial solution accordingly represents an approximation, because strictly speaking the Reynold stresses must be determined by integration of a corresponding conservation equation (which is in the form of a partial differential equation). The most significant error in such an approximation is probably the fact that the Reynolds stresses in the approximation are more closely coupled with the actual coarse structure of the velocity field as represented by the grid, than the exact equations state. In order to consider this effect at least partially, the viscosity ${}^{j}\mu$ is not calculated using an algebraic relationship from the velocity field average over the mesh area

(as is done for the Prandtl mixing length model, Equation (2-5) and also as Deardorff (see Chapter 5.1) has done.) Instead, it is calculated as follows:

$$\overset{j}{\mu} = c \left(\overset{j}{\overline{E'}} \cdot \overset{j}{F} \right)^{1/2} \qquad (3\text{-}33)$$

from the kinetic energy of the fine structure, for which a transport equation corresponding to (3-31) is also integrated at the same time. $\overset{j}{\overline{E'}}$ is the kinetic energy within the mesh area under consideration, and its magnitude is $\overset{j}{F}$. This trial solution has an even more detailed physical basis. Here we will simply state that it has the correct dimensions and seems plausible.

The problem is now to determine the constant c. We will attempt to find a method of determining it which is as independent of experiments as possible. Since we cannot do this entirely, we require that the experimental support is independent of the geometry under consideration, so that models derived from this can also be transferred to other problem areas.

We obtain an equation for the determination of the constant c by substituting the trial solution (3-32, 33) in the conservation equation for kinetic energy (3-31), in which the fine structure Reynolds stresses occur in the product term. We now assume that the turbulent flow under consideration is steady in the statistical sense. This means that the time derivative of the energy $\overset{V}{E'}$ vanishes when we take the time average. /35
The convective and diffusion terms also vanish for the additional averaging over the entire flow volume, because no kinetic energy is transferred through the walls. It only remains to find the difference between the production and the dissipation. This net balance results in the equation for determining the constant c (shown in the following for $\nu \ll 1$):

$$c = \frac{\langle \varepsilon \rangle}{\left\langle \left({}^{j}\bar{E}^{i}\,{}^{j}F\right)^{1/2} \overline{\left(\delta_{x_j}{}^{i}\bar{u}_i + \delta_{x_i}{}^{j}\bar{u}_j\right)^{j}}\, \delta_{x_j}{}^{j}\bar{u}_i \right\rangle} \qquad (3\text{-}34)$$

We can approximately transform this equation as follows:

$$c = \frac{\langle \varepsilon \rangle}{\gamma \langle {}^{j}\bar{E}^{i}\,{}^{j}F \rangle^{1/2} \left\langle \overline{\left(\delta_{x_j}{}^{i}\bar{u}_i + \delta_{x_i}{}^{j}\bar{u}_j\right)^{j}}\, \delta_{x_j}{}^{j}\bar{u}_i \right\rangle} \qquad (3\text{-}35)$$

(3-36)

Using the theory of isotropic turbulence and after the experimental determination of the individual "constants" (the Kolmogorov constant α), it is possible to establish a quantitative relationship between the terms occurring in the denominator of this equation and the average dissipation $\langle \varepsilon \rangle$. Finally, the latter can be cancelled. The terms which must be calculated are the time average of the kinetic energy of the fluctuation motion in a mesh area as well as the time average of a difference form involving the square of the deformation rate D_{ij}^2, which is defined by the following differential quotient:

$$D_{ij}^2 = 2\left(\frac{\partial u_i}{\partial x_j} + \frac{\partial u_j}{\partial x_i}\right)\frac{\partial u_j}{\partial x_i} = \left(\frac{\partial u_i}{\partial x_j} + \frac{\partial u_j}{\partial x_i}\right)^2 \qquad (3\text{-}37)$$

These terms are also called correlations and will be calculated in Chapter 4 and Appendix 2. Correlations are related to relatively complicated integrals using a purely mathematical method. In addition to the geometric factors, only the correlations between the velocity components at two points occur. These so-called two point correlations can be calculated for isotropic, incompressible turbulence using kinematic relationships, if the energy spectrum of the velocity fluctuations is known. Physical models exist for the energy spectrum which lead to the statement

that this spectrum has a universal form under some conditions (this is known as the Kolmogorov spectrum) and in which only one experimental constant occurs. From measurements of this constant under various conditions, one is left to the conclusion that this is a universal constant. This means that the correlations which occur in (3-35) and therefore the constant c can be quantitatively determined. In the present paper, we have continued the development of the mathematical part of this computation procedure used in earlier methods, so that we again did not use meshes with the same side lengths. Instead, we used the actual difference formulas. / 36

It may now be argued that the theory of isotropic turbulence cannot be applied here, because the turbulent channel flow under consideration here is very anisotropic and inhomogeneous. Here we must apply the concept of local isotropy, as will be discussed in Chapter 4.1. Nevertheless, trial solution (3-32) basically contradicts the assumption of isotropic turbulence because in true isotropic turbulence all components of the Reynolds stress tensor ${}^{j}\overline{u_i' u_j'}$ must vanish for $i \neq j$ when the time average is taken. Because of the fact that the time average of the velocity gradient $\langle \delta_{x_3} {}^{1}\tilde{u}_1 \rangle$ is not zero, the trial solution (3-32) gives values which are different from zero for $i,j = 1,3$. For this reason, in Chapter 5.2 we will develop a concept according to which the fine structure Reynolds stresses is divided into its time average (or period average values, see below) and the deviations from it:

$$ {}^{j}\overline{u_i' u_j'} = \underbrace{\langle {}^{j}\overline{u_i' u_j'} \rangle}_{\text{I}} + \underbrace{\left({}^{j}\overline{u_i' u_j'} - \langle {}^{j}\overline{u_i' u_j'} \rangle \right)}_{\text{II}} \qquad (3\text{-}38) $$

The theory of isotropic turbulence is only applied for sum term II (the "locally isotropic part"). A special model will be applied to sum term I ("inhomogeneous part"). This model is characterized by the fact that it becomes the Prandtl mixing length model for the

limiting case of very large meshes. For the other limiting case, in which the meshes are very small, the Reynolds stresses become zero.

In order not to be restricted to steady turbulent flows in a statistical sense by using the time averages, when the division is made according to (3-38), we will not use the actual time averages but so-called period average values. The period average value is the average value taken over those planes in the flow channel in which the statistical properties of the flow field are constant. According to Figure 1, these are the x_1-x_2 for the plate and the $x - \varphi$ planes for the annulus. The term "period average value" was selected because periodic boundary conditions are prescribed (Chapter 7.1) in the numerical model at the limits of these planes. /37

The model for the inhomogeneous part can also be determined quantitatively, but not as elegantly as the model for the locally isotropic part. Since the inhomogeneous part is only very important in the vicinity of the wall, where the average velocity profile has large gradients, simple assumptions can be used here. In any case, this division represents a significant advance over earlier models, in which local isotropic conditions had to be assumed even in the immediate vicinity of the wall. This is especially evident because the numerical results (Chapter 10) correspond better to the measured values even for a relatively large mesh, than do the numerical results of Deardorff [29].

The details of these models will be presented in the following chapters.

4. LOCAL ISOTROPIC TURBULENCE AND CORRELATIONS OF SPACE-AVERAGE FIELD VARIABLES

We will establish some fundamentals for the quantitative determination of the fine structure model using the theory of isotropic turbulence. In order to apply this theory, it must only be valid for local isotropic turbulence. In the following we will define local isotropic conditions and we will determine the range of existence by evaluating the corresponding experimental results. Then two methods of calculating the correlations of two space-average field variables will be presented (i.e. time averages of products). The details of the theory of isotropic turbulence are contained in Appendix 1 and the calculation of correlations is presented in Appendix 2.

4.1. Local Isotropic Conditions

4.1.1. Definition and Justification

A turbulent flow field is called "isotropic" if the statistical averages of arbitrary variables which can be derived from the velocity field and the pressure field (for example $\langle u_i u_j \rangle$), are invariant with respect to rotation and translation of the coordinate system. It is called "homogeneous" if these averages are only invariant with respect to translations [6, 53, 115, 134].

Channel flows are neither isotropic nor homogeneous. Nevertheless, many results of the theory of isotropic turbulence can be applied, if there is local isotropy or local homogeneity. The concept of "local isotropy" was introduced by Kolmogorov [67]. The author, Deissler [26], for example, speaks of "local homogeneity". In this paper we will use the following definitions

for these terms:

A turbulent flow field $\underline{u}(\underline{x},t)$ is locally isotropic in the vicinity having the diameter L_{iso} of a location $\underline{x}_o$, if

$$\left(\underline{u}(\underline{x},t) - \langle \underline{u} \rangle (\underline{x}) \right) - \left(\underline{u}(\underline{x}_o,t) - \langle \underline{u} \rangle (\underline{x}_o) \right) \quad (4\text{-}1)$$

is isotropic for $|\underline{x} - \underline{x}_o| \leq \frac{1}{2} L_{iso}$ except for deviations which can be ignored.

A similar requirement is that the Fourier transform

$$\underline{v}(\underline{k},t) = \iiint_{\underline{x}} \underline{u}(\underline{x},t) \exp\{\sqrt{-1}\,(\underline{x}-\underline{x}_o)\cdot\underline{k}\}\, dV(\underline{x}) \quad (4\text{-}2)$$

is invariant for $|\underline{k}| \geq 1/L_{iso}$ with respect to rotation and translation of the wave number coordinate system. This definition is well adapted for the experimental determination of L_{iso}. / 39

Local homogeneous conditions are therefore defined in a similar way, by the requirement for invariance with respect to translations alone. Local isotropic conditions can be shown to exist in channel flows as follows. Channel flows are anisotropic in their macroscopic structure because of the anisotropic boundary conditions and the momentum sources (average pressure gradient only acts in one direction). The "turbulence balls" which are produced because of the macroscopically unstable flow have a relatively large diameter, which is only slightly smaller than the characteristic length of the channel geometry. Since for large Reynolds numbers, the dissipation of the turbulent energy only becomes effective for very small "turbulence ball" diameters, the large turbulence balls must decay into smaller ones because of the influence of the inertia forces. The pressure-velocity correlations bring about an energy exchange between the velocity fluctuations in various directions, as Rotta [108] has shown,

so that the motion of the turbulence balls becomes more isotropic as the diameter is reduced. This is the physical reason for the existence of local isotropic conditions.

4.1.2. Results of the Theory of Isotropic Turbulence

The following two results are important for the quantitative determination of the fine structure model, and these results are from the theory of isotropic turbulence. Appendix 1 contains a detailed presentation.

a) The two-point correlations $R_{ij} \equiv \langle u_i(\underline{x} - \frac{1}{2}\underline{r}) \cdot u_j(\underline{x} + \frac{1}{2}\underline{r}) \rangle$ which only depend on $\underline{r}$ for isotropic turbulence ($R_{ij}(\underline{x}, \underline{r}) = R_{ij}(\underline{r})$), can be calculated using relationships which are entirely kinematic in nature (i.e., they can be derived from the isotropic condition and the continuity equation), if the three-dimensional scalar spectrum E(k) (defined in Appendix 1) is known; k is a scalar wave number (Dimension: 1/length).

b) For the wave number range (inertial subrange) determined by inertia forces

$$\frac{1}{L_0} < k < \frac{1}{\eta} \qquad (4\text{-}3)$$

we can give a generally valid law for the energy spectrum, which is called the Kolmogorov spectrum:

$$E(k) = \alpha \langle \varepsilon \rangle^{2/3} k^{-5/3} \qquad (4\text{-}4)$$

α Kolmogorov constant ($\alpha \approx 1.5$, see Table 3)
k scalar wave number (Dimension: 1/length
$\langle \varepsilon \rangle$ average energy dissipation
L_0 macroscopic length scale
$\eta = (\nu^3/\langle \varepsilon \rangle)^{1/4}$ Kolmogorov length

/ 40

Using the relationships discussed under a), we can derive the following from the Kolmogorov spectrum (see Appendix 1):

$$R_{[i][i]}(\underline{r}) - R_{[i][i]}(\underline{0}) = -\frac{18}{55}\Gamma(\tfrac{1}{3})\alpha\langle\varepsilon\rangle^{2/3} r^{2/3}\left(1 - \frac{r_{[i]}^2}{4r^2}\right) \quad (4\text{-}5)$$

$$R_{ij}(\underline{r}) = -\frac{18}{55}\Gamma(\tfrac{1}{3})\alpha\langle\varepsilon\rangle^{2/3}\frac{r_i r_j}{4r^{4/3}}\,; \; i \neq j \quad (4\text{-}6)$$

where $r = (r_i r_i)^{1/2} = |\underline{r}|$

for $\eta < r < L_0$.

These correlations can also be calculated for other spectra such as for example the Pao spectrum valid for $k \gtrsim \frac{1}{\eta}$ (see Appendix 1). The Kolmogorov spectrum is advantageous here, because it leads to analytical expressions for R_{ij}.

In order for these results to be applicable for the quantitative determination of the fine structure model, that is, to determine the local structure within the difference meshes having the average edge length h, the following conditions must be satisfied:

a) The length L_{iso} and L_o must at least be as large as h. The Kolmogorov length η must be substantially smaller than h.

b) α must be a known universal constant.

In Appendix 1 we give the experimental proof for the fact that these conditions are satisfied. It therefore follows that:

For $\frac{1}{300} \leq h \leq \frac{1}{30}$ and Reynolds number $Re_m \gtrsim 10^5$, the results given above can be applied. The constant α can be assumed to be given by the following formula based on many measurements (also in a channel flow) and because of theoretical estimates, to within an error of about ±5%

$$\alpha = 1.5$$

/41

4.2. Methods for Calculating Space Correlations

4.2.1. Definition and Assumption

In the following sections we will present two methods for calculating correlations of the following type

$$R(\psi_1, \psi_2, V_1, V_2, \underline{\xi}) \equiv \langle \overline{\psi_1}^{V_1}(\underline{x}) \cdot \overline{\psi_2}^{V_2}(\underline{x}+\underline{\xi}) \rangle \qquad (4\text{-}7)$$

Here ψ_1 and ψ_2 are two turbulent fields (velocities, pressures or their derivatives). V_1, V_2 are space volumes used for averaging, which can be one, two or three-dimensional. Their centers are specified by $\underline{x}$ or $\underline{x}$ or $\underline{\xi}$, respectively. The averaging operations are linear and are defined by integrals of the following type

$$\overline{\psi_1}^{V_1}(\underline{x}) \equiv \frac{1}{V_1} \int\cdots\int_{V_1} \psi_1(\underline{x}+\underline{Y})\, dV(\underline{Y}) \qquad (4\text{-}8)$$

As an example, the time average of the kinetic energy within a mesh volume V is:

$$\overline{E}^{V} = \frac{1}{2} \sum_{i=1}^{3} R(u_i, u_i, V, V, 0)$$

It is assumed that ψ_1 and ψ_2 are locally isotropic within a region whose diameter is given by the maximum separation between

the points contained in the averaging volume V_1 and the volume V_2. In addition, we assume that the fields ψ_1 and ψ_2 are homogeneous such that $R(\psi_1, \psi_2, V_1, V_2, \underline{\xi})$ does not depend on the position vector $\underline{x}$.

4.2.2. Method of Direct Integration

According to definitions (4-7, 8) we have:

$$R(\psi_1,\psi_2,V_1,V_2,\underline{\xi}) = \left\langle \left(\frac{1}{V_1}\int_{V_1}\psi_1(\underline{y})\,dV(\underline{y})\right)\cdot\left(\frac{1}{V_2}\int_{V_2}\psi_2(\underline{z}+\underline{\xi})\,dV(\underline{z})\right)\right\rangle \quad (4\text{-}9)$$

Different integration variables were used for the two integrations. Therefore we have the following transformation:

$$R(\psi_1,\psi_2,V_1,V_2,\underline{\xi}) = \left\langle \frac{1}{V_1\cdot V_2}\int_{V_1}\int_{V_2}\psi_1(\underline{y})\cdot\psi_2(\underline{z}+\underline{\xi})\,dV(\underline{y})\,dV(\underline{z})\right\rangle \quad (4\text{-}10)$$

The time averaging < > as well as the space averaging are linear operations, so that they can be exchanged:

$$R(\psi_1,\psi_2,V_1,V_2,\underline{\xi}) = \frac{1}{V_1\cdot V_2}\int_{V_1}\int_{V_2} R_{\psi_1,\psi_2}(\underline{y}-\underline{z}-\underline{\xi})\,dV(\underline{y})\,dV(\underline{z}) \quad (4\text{-}11)$$

where

$$R_{\psi_1,\psi_2}(\underline{r}) = \langle \psi_1(\underline{x})\cdot\psi_2(\underline{x}+\underline{r})\rangle . \quad (4\text{-}12)$$

/ 42

For example, for $\psi_1 \equiv u_1$, $\psi_2 \equiv u_1$, $R_{\psi_1,\psi_2}(\underline{r}) \equiv R_{11}(\underline{r})$, where R_{11} is given by (4-5). Using this method, Lilly calculated the correlations $\frac{1}{2}\langle \overline{u_i'^2}\rangle$ for $V_1=V_2=V=h^3$, $\underline{\xi}=\underline{0}$ [80]. The disadvantage of this method is that six-fold integrals must be (numerically) evaluated for the three-dimensional volumes. This is very laborious. In the following section we will demonstrate that the number of independent integration variables can be cut in half, as shown in [136]. This means that the computation times for numerical evaluation of the integrals can be reduced from hours

to seconds.

4.2.3. Volume Correlation Method

The space averages can be defined as follows according to [136]

$$\overline{\psi_1} = \iiint_{\infty} K_1(\underline{s})\,\psi_1(\underline{s})\,dV(\underline{s}), \qquad (4\text{-}13)$$

where

$$\iiint_{\infty} K_1(\underline{s})\,dV(\underline{s}) = 1\ . \qquad (4\text{-}14)$$

$K_1(\underline{s})$ is a (normalized) weighting function. The only condition it must satisfy is at $|\underline{s}|\to\infty$ it must go to zero such that the integral given above will exist. In order for the average value defined in this way to agree with (4-8), apparently we must have

$$K_1(\underline{s}) = \begin{cases} 0 & \underline{s} \notin V_1 \\ 1/V_1 & \underline{s} \in V_1 \end{cases}, \qquad (4\text{-}15)$$

where the range V_1 is defined such that

$$|s_i| \le \tfrac{1}{2} H_i \quad ; \quad i = 1,2,3\ . \qquad (4\text{-}16)$$

In addition to the simple weighting functions, it is possible to define average values having weights which vary continuously in space, using this concept. The corresponding correlations can then be calculated. This is important in the evaluation of measurements using the laser Doppler method [15], where $K(\underline{s})$ corresponds to the light intensity distribution.

If $K_2(\underline{s})$ is defined in a way similar to $K_1(\underline{s})$, we have:

$$R(\psi_1,\psi_2,V_1,V_2,\underline{\xi}) = \left\langle \iiint_{\infty} K_1(\underline{y})\,\psi_1(\underline{y})\,dV(\underline{y}) \right\rangle \cdot \qquad (4\text{-}17)$$

$$\left\langle \iiint_{\infty} K_2(\underline{z})\,\psi_2(\underline{z}+\underline{\xi})\,dV(\underline{z}) \right\rangle$$

After exchanging the (linear) averaging operations /43
we find:

$$R(\psi_1,\psi_2,V_1,V_2,\underline{\xi}) = \iiint_{\infty}\iiint_{\infty} K_1(\underline{y})\,K_2(\underline{z})\,R_{\psi_1,\psi_2}(\underline{y}-\underline{z}-\underline{\xi})\,dV(\underline{y})\,dV(\underline{z}) \quad (4\text{-}18)$$

where R_{ψ_1,ψ_2} according to (4-12).

Using the substitution $\underline{x}=\underline{z}-\underline{y}$, $dV(\underline{x})=dV(\underline{z})$, we find:

$$R(\psi_1,\psi_2,V_1,V_2,\underline{\xi}) = \iiint_{\infty}\iiint_{\infty} K_1(\underline{y})\,K_2(\underline{x}+\underline{y})\,R_{\psi_1,\psi_2}(\underline{x}-\underline{\xi})\,dV(\underline{y})\,dV(\underline{x}) \quad (4\text{-}19)$$

Here $R_{\psi_1\psi_2}$ is independent of $\underline{y}$ and it is possible to extract a partial integral, the so-called volume correlation $\varphi_{12}(\underline{x})$:

$$\varphi_{12}(\underline{x}) \equiv \iiint_{\infty} K_1(\underline{y})\,K_2(\underline{x}+\underline{y})\,dV(\underline{y})$$

and we have:

$$R(\psi_1,\psi_2,V_1,V_2,\underline{\xi}) = \iiint_{\infty} \varphi_{12}(\underline{x})\,R_{\psi_1,\psi_2}(\underline{x}-\underline{\xi})\,dV(\underline{x}) \quad (4\text{-}21)$$

$\varphi_{12}(\underline{x})$ depends only on the geometry and the relative orientation as a function dependent on the volumes V_1 and V_2. Often this can be calculated analytically. This means that only one integral must be (numerically) evaluated, in which it is necessary to integrate over one-half as many independent integration variables as was the case for (4-11). In Section 2 we will calculate the volume correlations which apply for rectangular volumes.

4.3. Results

In the following we will give the results for a few special correlations, which follow from the preceding sections.

It is assumed that $u_i(\underline{x},t)$ is a turbulent velocity field, which is locally isotropic in regions having the diameter L_{iso} where $L_{iso} \approx 3\,\Delta x_{max}$ holds (Δx_{max}: maximum of the mesh edge length Δx_1, Δx_2, Δx_3). The energy spectrum E(k) is assumed to be the same

as the Kolmogorov spectrum (4-4), so that the correlations $R_{ij}(r)$ apply for $|r| < L_{iso}$ according to (4-5,6). The grid is assumed to be cartesian and equidistant, but the mesh edge lengths Δx_i are not all the same. The time increment Δt is negligibly small.

Using the methods of Chapter 4.2, we calculate the following variables:

a) $$\langle {}^{n}\overline{E'} \rangle \equiv \left\langle \frac{1}{\prod_{i=1}^{n} \Delta x_i} \int_{-\frac{\Delta x_1}{2}}^{\Delta x_1/2} \cdots \int_{-\frac{\Delta x_n}{2}}^{\Delta x_n/2} \frac{1}{2} \left[u_i(x_1, x_2, x_3, t) - \langle u_i \rangle \right]^2 dx_1 \ldots dx_n \right\rangle \quad (4\text{-}22)$$

b) $$ {}_1D^2 \equiv \left\langle \delta_{x_j} {}^{j}\overline{u_i} \left(\delta_{x_j} {}^{j}\overline{u_i} + \delta_{x_i} {}^{i}\overline{u_j} \right) \right\rangle \quad (4\text{-}23)$$

$$ {}_2D^2 \equiv \left\langle \delta_{x_j} {}^{j}\overline{u_i} \; \overline{\left(\delta_{x_j} {}^{i}\overline{u_i} + \delta_{x_i} {}^{j}\overline{u_j} \right)}^{j} \right\rangle \quad (4\text{-}24)$$

$$ {}_3D^2 \equiv \frac{1}{2} \left\langle \overline{\left(\delta_{x_i} {}^{j}\overline{u_j} + \delta_{x_j} {}^{i}\overline{u_i} \right)^2}^{j} \right\rangle (1 - \delta_{[i][j]}) + 2 \left\langle \left(\delta_{x_j} {}^{i}\overline{u_i} \right)^2 \right\rangle \delta_{[i][j]} \quad (4\text{-}25)$$

$$ {}_4D^2 \equiv \frac{1}{2} \left\langle \overline{\left(\delta_{x_i} {}^{j}\overline{u_j} + \delta_{x_j} {}^{i}\overline{u_i} \right)^2}^{j} \right\rangle - \frac{1}{2} \left\langle \left(\overline{\delta_{x_i} {}^{j}\overline{u_j} + \delta_{x_j} {}^{i}\overline{u_i}}^{j} \right)^2 \right\rangle \quad (4\text{-}26)$$

c) $$FED \equiv \left(\langle {}^{j}\overline{E'} \rangle \cdot {}^{j}F \right)^{1/2} \left\langle \overline{\left(\delta_{x_i} {}^{j}\overline{u_j} + \delta_{x_j} {}^{i}\overline{u_i} \right)}^{j} \delta_{x_i} {}^{i}\overline{u_j} \right\rangle \quad (4\text{-}27)$$

Remark to a). $\langle {}^{n}\overline{E'} \rangle$ is the generalization of the volume average value of the kinetic energy of the fluctuation motion, extended to n-dimensional volumes. We have the special cases

$$\langle {}^{1}\overline{E'} \rangle \equiv \langle {}^{1/3}\overline{E'} \rangle \; , \quad \langle {}^{3}\overline{E'} \rangle \equiv \langle {}^{1/2}\overline{E'} \rangle$$

Remarks to b). The quantities ${}_kD^2$, k = 1,2,3,4 are various forms of the average square of the deformation rate, given in different form. The notation was discussed in Chapter 3. The term $\left\langle \overline{\frac{\partial u_i}{\partial x_j}} \cdot \left(\overline{\frac{\partial u_i}{\partial x_j}} + \overline{\frac{\partial u_j}{\partial x_i}} \right) \right\rangle$ calculated by Lilly [80] for $\Delta x_1 = \Delta x_2 = \Delta x_3 = h$ is identical to D^2. The approximation $\left\langle \overline{\partial u_2/\partial x_1} \cdot \overline{\partial u_1/\partial x_2} \right\rangle = \left\langle \overline{\partial u_1/\partial x_1} \cdot \overline{\partial u_2/\partial x_2} \right\rangle$ used by Lilly and the difficult calculation methods are avoided here.

Remarks to c). The term FED corresponds to the average energy dissipation used for the approximation FED. ${}^jF$ here is the contribution of the mesh surface, the normal of which is parallel to the coordinate x_j; for example ${}^1F = \Delta x_2 \cdot \Delta x_3$.

The details of the calculation are given in Appendix 1. The results cannot be presented analytically, because the integrals which occur must be evaluated numerically. Using the Fortran Subprograms (E2, E3, D11, D12, D13, D14, FED1 described in Appendix 2), we find

/45

$$\left\langle \overline{E'}^{V_1} \right\rangle = f_1 \cdot \langle \varepsilon \rangle^{2/3} \Delta x_1^{2/3} \cdot 0.45 \qquad (4\text{-}28)$$

$$\left\langle \overline{E'}^{V_2} \right\rangle = f_1 \langle \varepsilon \rangle^{2/3} h_2^{2/3} \; E2\left(\frac{\Delta x_1}{h_2}, \frac{\Delta x_2}{h_2}\right) \qquad (4\text{-}29)$$

$$h_2 = (\Delta x_1 \cdot \Delta x_2)^{1/2} \qquad (4\text{-}30)$$

$$\left\langle \overline{E'}^{V_3} \right\rangle = f_1 \langle \varepsilon \rangle^{2/3} h^{2/3} \; E3\left(\frac{\Delta x_1}{h}, \frac{\Delta x_2}{h}, \frac{\Delta x_3}{h}\right) \qquad (4\text{-}31)$$

$${}_1D^2 = f_2 \langle \varepsilon \rangle^{2/3} h^{-4/3} \; D11(\Delta x_1/h, \Delta x_2/h, \Delta x_3/h) \qquad (4\text{-}32)$$

$${}_2D^2 = f_2 \langle \varepsilon \rangle^{2/3} h^{-4/3} \; D12(\Delta x_1/h, \Delta x_2/h, \Delta x_3/h) \qquad (4\text{-}33)$$

$$ {}_3D^2 = f_2 \langle \varepsilon \rangle^{2/3} h^{-4/3} D13(\Delta x_1/h, \Delta x_2/h, \Delta x_3/h) \quad (4\text{-}34) $$

$$ {}_4D^2 = f_2 \langle \varepsilon \rangle^{2/3} h^{-4/3} D14(\Delta x_1/h, \Delta x_2/h, \Delta x_3/h) \quad (4\text{-}35) $$

$$ FED = f_3 \langle \varepsilon \rangle FED1(\Delta x_1/h, \Delta x_2/h, \Delta x_3/h) \quad (4\text{-}36) $$

$$ h = (\Delta x_1 \cdot \Delta x_2 \cdot \Delta x_3)^{1/3} \quad (4\text{-}37) $$

$$ f_1 = \alpha \, \Gamma(\tfrac{1}{3}) \, 9/20 = 1.8083 \quad (4\text{-}38) $$

$$ f_2 = \alpha \, \Gamma(\tfrac{1}{3}) \, 18/55 = 1.3151 \quad (4\text{-}39) $$

$$ f_3 = \left[(\alpha \, \Gamma(\tfrac{1}{3}))^3 \cdot 729/15125 \right]^{1/2} = 1.7685 \quad (4\text{-}40) $$

$$ (\alpha = 1.5, \; \Gamma(\tfrac{1}{3}) = 2.67894) $$

For special values of the edge lengths $\Delta x_1, \Delta x_2, \Delta x_3$, the numerical evaluation of the integrals gives the following:

	$\Delta x_1 : \Delta x_2 : \Delta x_3$ = 1 : 1 : 1	$\Delta x_1 : \Delta x_2 : \Delta x_3$ = 0.125:0.05:0.05
E 3	0.746	0.825
D 11	6.13	6.85
D 12	6.73	7.35
D 13	3.88	3.90
D 14	0.984	1.32
FED1	5.30	5.39

(4-41)

as well as

$$E2(1,1) = 0.6293 \qquad (4\text{-}42)$$

$$E2(0.125/h_2, 0.05/h_2) = 0.6821 \qquad h_2=(0.125\cdot 0.05)^{1/2} \qquad (4\text{-}43)$$

Comparison: Lilly [80] gave the following results:

$$E3\ (1,1,1) = 0.761 \qquad (4\text{-}44)$$

$$D11(1,1,1) = 7.66 \qquad (4\text{-}45)$$

The small deviations between (4-44) and the value of 0.746 can be explained from (4-41) because of numerical inaccuracies, which are understandable when evaluating six-fold integrals numerically. The deviation of (4-45) from the value of 6.13 according to (4-41) can be attributed to Lilly's erroneous assumption that $\langle \overline{\partial u_2/\partial x_1} \cdot \overline{\partial u_1/\partial x_2} \rangle = \langle \overline{\partial u_1/\partial x_1} \cdot \overline{\partial u_2/\partial x_2} \rangle$.

We have the following general results: assuming local isotropic conditions and for known correlations $R_{ij}(\underline{r}) = \langle u_i(\underline{x}-\frac{1}{2}\underline{r}) u_j(\underline{x}+\frac{1}{2}\underline{r}) \rangle$ we can calculate time average products of arbitrary space average velocities, using a purely formal procedure.

In the next chapter we will calculate a few such special correlations. We will use the correlations (4-5, 6) which follow from the Kolmogorov spectrum (4-4).

Without changing the method, the variables of interest can also be calculated for arbitrary spectra. However, if the Kolmogorov spectrum is assumed, R_{ij} can be calculated analytically, so that one additional numerical integration can be dropped.

5. FINE STRUCTURE MODEL

/47

In this chapter we will give a justification for the approximation for the area values of products of the area average values referred to the fluctuation velocities, which are called Reynolds stresses and which occur during the averaging process of the momentum equation. In Cartesian coordinates, we must approximate the following terms:

$$\overline{u_i' u_j'} \quad ; \quad i,j = 1,2,3 \,,$$

in cylindrical coordinates these are:

$$\begin{array}{lll} \overline{v_x'^2} & \overline{v_\varphi' v_x'} & \overline{v_r' v_x'} \\ \overline{v_x' v_\varphi'} & \overline{v_\varphi'^2} & \overline{v_r' v_\varphi'} \\ \overline{v_x' v_r'} & \overline{v_\varphi' v_r'} & \overline{v_r'^2} \end{array} ,$$

as well as the apparent stresses which are brought about because of volume averaging of the Coriolis and centrifugal acceleration.

$$v_\varphi \overline{v_r' v_\varphi'} \qquad v_r \overline{v_\varphi'^2}$$

First we will determine the correlations which occur in Cartesian coordinates. The terms which are valid for cylindrical coordinates are then determined by simple analogies. First of all we will investigate the trial solutions used by Deardorff [29,33]. We will demonstrate a few of the deficiencies which will be avoided in the new model.

5.1. Boussinesq Trial Solution for Volume Reynolds Stresses, according to Smagorinsky, Lilly and Deardorff

5.1.1. Summary and Definition of the Trial Solution

In Chapter 2 we discussed the fact that the Boussinesq trial solution is suitable only for steady boundary layer flows when applied to the Reynolds surface which occurred during the time averaging process. It can be assumed that the unsteady Reynolds stresses, which are produced in the averaging over small volumes or areas, respectively, are more appropriately modeled by a Boussinesq trial solution * because they have a smaller order of magnitude. Lilly [81] described some of his experiences with this in his older papers. These are two-dimensional simulations, and because of this they do not result in the expected quasi-random and turbulent flow fields. The two-dimensional simulation of /48
the turbulent momentum transport and heat transport gave rather good results according to Deardorff [27]. This may be due to the fact that the temperature field represents an additional degree of freedom here, which makes it possible for random fields to be produced. Leith [82] has suggested a special model which is suitable for two-dimensional turbulence. The Boussinesq trial solution for the Reynolds stresses caused by the turbulent fine structure was first used by Smagorinsky [118] for the simulation of large space atmospheric circulation. Lilly [80, 81] followed the ideas of Smagorinsky and suggested the following trial solution:

$$\overline{u_i' u_j'} = -\mu \overline{D_{ij}} + \frac{1}{3} \delta_{ij} \overline{u_\ell' u_\ell'} \qquad (5\text{-}1)$$

with the deformation velocity

$$D_{ij} = \frac{\partial u_i}{\partial x_j} + \frac{\partial u_j}{\partial x_i} \qquad (5\text{-}2)$$

and the turbulent viscosity

$$\mu = (c_s h)^2 \left[\frac{1}{2} \left(\overline{D_{ij}} \right)^2 \right]^{1/2} \qquad (5\text{-}3)$$

---

* This statement was already discussed in Chapter 3.5.

where c_1 is determined, as discussed in Appendix 3.

We must consider the fact that, in contrast to the derivations discussed in Chapter 3, Smagorinsky, Lilly and Deardorff considered the following Reynolds stresses averaged over mesh volumes V (Edges Δx_i)

$$\overline{u_i' u_j'}^V \equiv \overline{u_i u_j}^V - \overline{u_i}^V \cdot \overline{u_j}^V \qquad (5\text{-}4)$$

No averaging over the time interval Δt is included here. Lilly [80, 81] justifies the trial solution given above only for meshes with equal side lengths

$$h \equiv \Delta x_1 = \Delta x_2 = \Delta x_3 \qquad (5\text{-}5)$$

Deardorff [29] transferred these derivations through meshes which did not have equal sides (1-28) and assumed that the characteristic mesh length h is given by

$$h = (\Delta x_1 \cdot \Delta x_2 \cdot \Delta x_3)^{1/3} \qquad (5\text{-}6)$$

The methods used by Smagorinsky [118] and Lilly [80, 81] for calculating c_1 are shown in Appendix 3, as well as their results and the expected values of Deardorff [29, 33]. In addition, the calculation of c_1 using the methods discussed here is described.

5.1.2. Simplifications, Deficiencies and Contradictions of the Theories Advanced So Far

The fine structure model as developed by Lilly and applied by Deardorff is based on the following assumptions: /49

a) Locally isotropic (homogeneous) turbulence
b) The Kolmogorov spectrum is valid

c) Use of a Boussinesq trial solution instead of integrating the conservation equations for $\overline{u_i' u_j'}$

d) $\overline{u_i' u_j'}$ is calculated in a deterministic way from the average velocity field, even though we only have a statistical relationship [43].

e) Use of a conservation equation for $\overline{E'}$, which is derived using another averaging operation than is used for averaging the momentum equations. (See Chapter A 3.2.1)

f) $\left\langle \left(\overline{D_{ij}}^{2} \right)^{3/2} \right\rangle \approx \left\langle \overline{D_{ij}}^{2} \right\rangle^{3/2}$ (Equation (A3-15)

g) $\langle \varepsilon' \rangle \approx \langle \varepsilon \rangle$, Equation (A3-16)

h) Re>>> 1 (molecular viscosity is ignored in the momentum conservation equations by Deardorff).

i) A theory exists only for mass volumes having equal side lengths.

j) Lilly's assumption of difference formulas for calculating $\overline{D}_{ij}$ (A3-29) does not correspond to the difference formulas used by Deardorff.

k) It is erroneously assumed that the same difference formulas are valid for both factors in (A3-14); different formulas according to (A3-44) should be used.

The model used by Deardorff [29] has the following deficiencies and contradictions:

a) $\overline{u_i' u_j'}$ is completely correlated in time with the velocity field, even though the development of these

Reynolds stresses is a dynamic process (more precisely, described by the unsteady conservation Equation [115]). Therefore, the magnitude of $\overline{u_i' u_j'}$ only increases with a time delay, if the square of the deformation velocity increases.

b) The assumption (5-6) for h cannot apply, because according to it, for example $\Delta x_1 \to 0$ it also follows that $h \to 0$, whereas we have $\lim_{\Delta x_1 \to 0} \overline{u_i' u_j'} = \overline{u_i' u_j'} \neq 0$. /50

c) $\overline{u_i' u_j'}$ is isotropic, even though an anisotropic grid is used.

d) When the difference formulas (A3-33) are used for calculating $(\overline{D}_{ij})^2$, then the turbulent viscosity μ will also be positive according to (5-3) if the flow is laminar, where $\mu = 0$ should apply.

e) The fact that $\langle \overline{u_i' u_j'} \rangle \neq 0$ contradicts the assumption of locally isotropic turbulence, where all $\langle \overline{u_i' u_j'} \rangle = 0$ for $i \neq j$.

f) For $\Delta x_1 \to \infty$ and $\Delta x_2 \to \infty$ (for example), we have $\mu \to \infty$. In other words the model contradicts experience for these limiting cases. Therefore it is questionable whether the model is sufficiently accurate for finite Δx_i.

g) The Kolmogorov spectrum must also apply in the prevailing theory for very small wavelengths $k \ll \frac{\pi}{h}$ because $\langle \overline{D}_{ij}^2 \rangle$ is obtained according to (A3-20) from an intregal over $k^2 \cdot E(k)$ over all wave numbers smaller than $\frac{\pi}{h}$. Even though the error will be small because of the factor k^2, we nevertheless see a weakness of the theory.

h) The concept of modeling of volume correlations $\overline{u_i' u_j'}^V$ is erroneous in principle; according to Chapter 3, area average values must be approximated.

In the following chapters we will derive an improved fine structure model, which will avoid all of these weaknesses and most of the assumptions. Only assumptions a) to d) are required for establishing the improved model, but later on their effects can be partially decreased.

5.2. Improved Fine Structure Model in Cartesian Coordinates

5.2.1. Requirements for the Fine Structure Model and Separation into Locally Isotropic and Inhomogeneous Parts

The channel flows under discussion are expressly inhomogeneous and anisotropic turbulent flows. According to Appendix 1, /51
the assumption of local isotropy can be looked upon as being valid for sufficiently high mesh numbers (KM>30). Nevertheless it is desirable to have a model which will still be valid for inhomogeneous flows, if the mesh number limits cannot be exceeded sufficiently. Such a model must satisfy the following boundary conditions.

a) The contribution of the Reynolds stresses $\langle \overline{u_i' u_j'}^j \rangle_1$ calculated based on the assumption of locally isotropic turbulence must as a consequence satisfy the following condition which is characteristic for this assumption

$$\langle \overline{u_i' u_j'}^j \rangle = 0 \qquad i,j = 1,2,3 \; ; \; i \neq j \tag{5-7}$$

b) Considering the inhomogeneity ($\langle u_1(x_3)\rangle \neq$ const) for the entire model we must have

$$\langle {}^{j}\overline{u_1' u_3'} \rangle \neq 0 \quad , j = 1,3 \tag{5-8}$$

c) The turbulence model used should agree with experience in the limiting case of very large meshes because it then becomes the simpler and well known model. For example it should be transformed into the Prandtl mixing length model.

$$\lim_{\substack{\Delta x_1 \to \infty \\ \Delta x_3 \to \infty}} \langle {}^{3}\overline{u_1' u_3'} \rangle = - L^2 \left| \frac{\partial \langle u_1 \rangle}{\partial x_3} \right| \cdot \frac{\partial \langle u_1 \rangle}{\partial x_3} \tag{5-9}$$

where L is given by (2-8).

d) For the opposite limiting case $\Delta x_k \to 0 \; (k=1,2,3)$, of course we should have $\langle {}^{j}\overline{u_i' u_j'} \rangle \to 0$. (5-10)

e) For $y \to \infty$, i.e. for laminar flow, ${}^{j}\overline{u_i' u_j'}$ should vanish.

In order to establish the fine structure model according to these requirements, the turbulent flow field is divided into

$$u_i \equiv u_i'' + {}^{P}\langle u_i \rangle \; ; \quad p \equiv p'' + {}^{P}\langle p \rangle \tag{5-11}$$

where ${}^{P}\langle y \rangle$ is the "period average value" of y:

$${}^{P}\langle y \rangle \equiv \lim_{\substack{X_1 \to \infty \\ X_2 \to \infty}} \frac{1}{X_1 \cdot X_2} \int_0^{X_1} \int_0^{X_2} y(x_1, x_2, x_3, t)\, dx_1\, dx_2 = {}^{P}\langle y \rangle (x_3, t) \tag{5-12}$$

/52

The Reynold stresses are divided up in a similar way (5-13)

$${}^{j}\overline{u_i' u_j'} \equiv \left({}^{j}\overline{u_i' u_j'} \right)'' + {}^{P}\langle ({}^{j}\overline{u_i' u_j'}) \rangle$$

The assumptions connected with local isotropy are only invoked when the model for $(\overline{u_i' u_j'})''$ is established. Therefore $(\overline{u_i' u_j'})''$ are called the "locally isotropic" Reynolds stresses. The residual terms $\overline{\langle u_i' u_j' \rangle}$ are called the "inhomogeneous" Reynolds stresses. In the following we will first derive a model for calculating the locally isotropic part and then derive a model for the inhomogeneous part.

5.2.2. Model for Locally Isotropic Part of the Reynolds Stresses

In this section we will derive a model for $(\overline{u_i' u_j'})''$ according to (5-13).

5.2.2.1. Assumptions for the Determination of $(\overline{u_i' u_j'})''$

The following assumptions are made for deriving the locally isotropic fine structure model. Some of them will be restricted completely in Chapter 5.2.2.5.

a) The turbulence is assumed to be locally isotropic over a region with a diameter of approximately 3 mesh edge lengths h (see definition in Chapter 4.1).

b) The turbulence has an energy spectrum E(k), which is given by the Kolmogorov spectrum (4-4) for wave numbers $k > \frac{1}{2}\frac{\pi}{h}$.

c) The Reynolds stresses can be described using an appropriate trial solution similar to the Boussinesq trial solution for the Reynolds stresses which occur during the time averaging. This trial solution will be justified in Chapter 5.2.2.3.

d) The Reynolds stresses can be determined deterministically from the average velocity field and the kinetic energy of the fluctuation motion. (See Chapter 5.2.2.5.3).

e) Since triple correlations cannot be calculated with the present theory *, we will assume the following approximations:

$$\left\langle \left({}^{i}F\,{}^{s}\overline{E'}\right)^{1/2} \left(\overline{\delta_{x_i}\,{}^{i}\overline{u_j} + \delta_{x_j}\,{}^{i}\overline{u_i}}^{\,j} \right) \delta_{x_j}\,{}^{i}\overline{u_i} \right\rangle = \sigma_1 \cdot \left\langle {}^{i}F\,{}^{s}\overline{E'}\right\rangle^{1/2} \left\langle \left(\overline{\delta_{x_i}\,{}^{i}\overline{u_j} + \delta_{x_j}\,{}^{i}\overline{u_i}}^{\,j} \right) \delta_{x_j}\,{}^{i}\overline{u_i} \right\rangle \quad (5\text{-}14)$$

$$\left\langle \left({}^{v}\overline{E'}\right)^{3/2} \right\rangle = \sigma_2 \left\langle {}^{v}\overline{E'} \right\rangle^{3/2} \quad (5\text{-}15)$$

/53

where

$$\sigma_1 \approx 1 \;,\; \sigma_2 \approx 1 \quad (5\text{-}16)$$ **)

(see Chapter 5.2.2.5.3).

f) The grid is assumed to be equidistant and Cartesian, but the mesh edge lengths Δx_i all do not have to be equal.

g) The averaging over Δt can be ignored (see Chapter 5.2.2.5.1).

5.2.2.2. Basic Equation for Locally Isotropic Turbulence

In this section we will show that the local fluctuation field for locally isotropic turbulence essentially obeys the same basic equations as does the entire flow field, and that there are no additional terms which have to be considered which would describe

---

* If additional experiments are not considered.

** As for the validity of these approximations, see Chapter 10.4.6.

the interaction between the fluctuation field and the total flow field.

We will divide the fields u_i and p into the periodic average values ${}^{P}\langle u_i \rangle$, ${}^{P}\langle p \rangle$ and the fluctuations u_i'', p" according to (5-11). Then we will form the periodic average value of the mass and momentum conservation equations and we obtain:

$$\frac{\partial}{\partial x_i}\,{}^{P}\langle u_i \rangle = 0 \qquad (5\text{-}17)$$

$$\frac{\partial}{\partial t}{}^{P}\langle u_i \rangle + \frac{\partial}{\partial x_j}\left({}^{P}\langle u_i \rangle \cdot {}^{P}\langle u_j \rangle\right) + \frac{\partial}{\partial x_j}\left({}^{P}\langle u_i'' u_j'' \rangle\right) = -\frac{\partial}{\partial x_j}{}^{P}\langle p \rangle + \frac{\partial}{\partial x_j}\left(\nu\left[\frac{\partial}{\partial x_j}{}^{P}\langle u_i \rangle + \frac{\partial}{\partial x_i}{}^{P}\langle u_j \rangle\right]\right) + P_x \qquad (5\text{-}18)$$

If we subtract these average equations from the initial equations we find

$$\frac{\partial}{\partial x_i}\,u_i'' = 0 \qquad (5\text{-}19)$$

$$\frac{\partial}{\partial t}u_i'' + \frac{\partial}{\partial x_j}(u_i'' u_j'') = -\frac{\partial}{\partial x_j}p'' + \frac{\partial}{\partial x_j}\left[\nu\left(\frac{\partial}{\partial x_j}u_i'' + \frac{\partial}{\partial x_i}u_j''\right)\right] + \frac{\partial}{\partial x_j}{}^{P}\langle u_i'' u_j'' \rangle - u_j''\frac{\partial\,{}^{P}\langle u_i \rangle}{\partial x_j} - {}^{P}\langle u_j \rangle\frac{\partial u_i''}{\partial x_j} \qquad (5\text{-}20)$$

Because of the assumption of local isotropy, it is possible to ignore the following variables in regions having the diameter L_{iso} [103]: /54

$$\frac{\partial}{\partial x_j}\left({}^{P}\langle u_i'' u_j'' \rangle\right) \approx 0\,; \qquad \frac{\partial}{\partial x_j}{}^{P}\langle u_i \rangle \approx 0 \qquad (5\text{-}21)$$

If in addition the observer is moving at the velocity ${}^{P}\langle u_j \rangle$, then the last term in (5-20) can be ignored. This assumption is permissible because it only affects the boundary conditions (see Chapter 7.2), which are inconsequential within the region of local isotropy. This is why the conservation equations for momentum and mass of the fluctuation field u_i'', p" reduce to the basic equations (with $P_x = 0$). Consequently, all of the derived relationships, especially the conservation equation for

$\nu_{E'}$ (3-31) are valid, if u_i,p is replaced everywhere by u_i",p" and we set $P_x=0$.

In the following subchapters of this section 5.2.2, we will write u_i,p in place of u_i", p".

5.2.2.3. Justification of the Improved Boussinesq Trial Solution

5.2.2.3.1. Model Concept and Trial Solution

In Chapter 3.3 we showed that by averaging the momentum conservation equations, area average values of velocity fluctuation products $\overline{u_i' u_j'}$ are found instead of volume average values. In this section we will discuss the model for which a Boussinesq trial solution can be defined in a suitable way. For this we will consider in particular $\overline{u_1' u_2'}$ with the notations of the following sketch

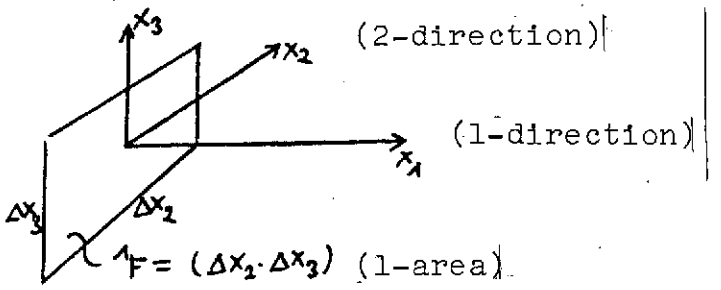

The terms $\overline{u_1' u_2'}$ apparently were produced by averaging of $u_1 \cdot u_2$. The product $u_1 \cdot u_2$ on the one hand describes the convective transport of momentum (per unit of mass) in the 1-direction because of convection in the 2-direction, and at the same time, the momentum in the 2-direction because of convection in the 1-direction. The first point of view is applicable for the 1-component of the momentum conservation equations and the second point of view is valid for the 2-component. The area

average value of $u_1 \cdot u_2$ over the 1-area, that is $\overline{{}^1u_1 u_2}$, only occurs in the second equation component according to (3-14). The product of the fluctuation velocities averaged over the 1-area /55

$$\overline{{}^1u_1' u_2'} \equiv \overline{{}^1u_1 u_2} - \overline{{}^1u_1}\,\overline{{}^1u_2} \qquad (5\text{-}22)$$

is therefore the convective transport of the second momentum component in the 1-direction because of the fluctuation motion. $\overline{{}^1u_1' u_2'}$ is therefore to be interpreted as the Reynolds stresses which apply at the 1-area (per unit of mass) in the 2-direction. Only the momentum transport produced by the fluctuation motion has to be considered here because $\overline{{}^1u_1}\,\overline{{}^1u_2}$ is explicitly described by the average equations.

This part of the convective momentum transport can be looked upon as the momentum transport due to small turbulence balls. These turbulence balls must be so small that their motion does not have any contribution to the average velocities, because their motion otherwise would be described by the average velocity fields and would be described by the average equations. The cross-sectional area of the turbulence balls must therefore be small so that at least two approximately equally large turbulence balls having opposing fluctuation direction will have room in the 1-area; Their diameter ${}^1\ell$ therefore satisfies the condition

$$({}^1\ell)^2 \lessapprox \tfrac{1}{2}\,{}^1F \qquad (5\text{-}23)$$

On the other hand, ${}^1\ell^2 \propto {}^1F$ does not hold, because the fraction of kinetic energy of the turbulence balls increases greatly with decreasing diameter according to assumption b (Kolmogorov spectrum). The momentum magnitude transported by these turbulence balls can be assumed to be proportional to $({}^1\ell)^n$ where n is an

exponent which must be determined.

According to the interpretation given above of the meaning of $\overline{u_1' u_2'}$, we must ask ourselves what are the contributions of the motions of turbulence balls in the 1 and 2-directions to the convection of the second momentum component. Any motion of the balls in the 1-direction results in a momentum transport in the 2-direction, which in the first approximation is proportional to the gradient of the velocity u_2 in the 1-direction. This is made clear by the following sketch:

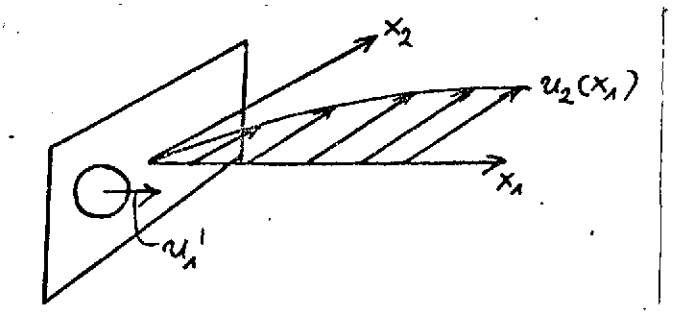

/56

Any motion of the ball with a positive u_1' results in a negative momentum transport with a positive gradient $\partial u_2/\partial x_1$ and therefore

$$\overline{u_1' u_2'} \sim - \ell^n \, |u_1'| \, \partial u_2/\partial x_1 \,, \qquad (5\text{-}24)$$

with a positive proportionality factor. Any motion of the small turbulence balls in the 2-direction at u_2' results in a momentum transport in the 2-direction, which again in the first approximation is proportional to the gradient of the velocity u_1 in the 2-direction, and the same sign convections as used above apply:

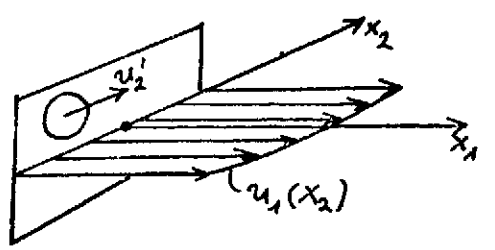

$$\overline{u_1'u_2'} \sim - \ell^n \, |u_2'| \, \partial u_1/\partial x_2 \qquad (5\text{-}25)$$

According to assumption a) (local isotropy) we may set:

$$|u_1'| \sim |u_2'| \sim \left(\overline{E'}\right)^{1/2} \equiv \left[\frac{1}{2}\left(\overline{u_i^2} - \overline{u_i}^2\right)\right]^{1/2} \qquad (5\text{-}26)$$

If the contributions of the fluctuation components are selected and if the unknown gradients are replaced by the corresponding difference quotients and if we consider that we must have

$$\overline{u_1'u_2'} = \overline{u_2'u_1'}, \qquad (5\text{-}27)$$

it follows that:

$$\overline{u_1'u_2'} = - c_2 \, (F)^{1/2} \left(\overline{E'}\right)^{1/2} \left(\delta_{x_1} \overline{u_2} + \delta_{x_2} \overline{u_1}\right). \qquad (5\text{-}28)$$

Here we have set the undetermined exponent n equal to one, because then the proportionality factor c_2 is a dimensionless positive constant. When generalized to other subscripts, we have:

$$\overline{u_i'u_j'} = - c_2 \, (F \, \overline{E'})^{1/2} \left(\delta_{x_i} \overline{u_j} + \delta_{x_j} \overline{u_i}\right) + \frac{1}{3} \delta_{ij} \overline{u_\ell'u_\ell'} \qquad (5\text{-}29)$$

The last sum term was added according to [53, p. 21], in order to have a positive contribution of $\delta_{ij} \cdot \overline{u_i'u_j'}$, in spite of the fact that

$$\delta_{ij} \left(\delta_{x_i} \overline{u_j} + \delta_{x_j} \overline{u_i}\right) = 2 \, \delta_{x_i} \overline{u_i} = 0 \qquad (5\text{-}30)$$

The analogy to the Newton material law becomes clear if we define /57
the "turbulent kinematic viscosity" as follows:

$$\mu \equiv c_2 \, (F \, \overline{E'})^{1/2} \qquad (5\text{-}31)$$

5.2.2.3.2. Calculation of the Constant c_2

An equation for determining the constant c_2 is obtained by substituting the trial solution (5-29) into the conservation equation for the kinetic energy of the fluctuation velocities within a volume element (3-31):

$$\frac{\partial \overline{{}^{\nu}E'}}{\partial t} = - \overline{{}^{j}u_i' u_j'}\, \delta_{x_j} \overline{{}^{i}u_i} - \overline{{}^{\nu}\varepsilon'} - \text{Conv.} + \text{Diff}, \tag{5-32}$$

where

$$\overline{{}^{\nu}\varepsilon'} \equiv \overline{{}^{\nu}\varepsilon} - \nu \left[\delta_{x_j} \overline{{}^{i}u_i} \left(\delta_{x_j} \overline{{}^{i}u_i} + \delta_{x_i} \overline{{}^{i}u_j} \right) \right] \tag{5-33}$$

and Conv. or Diff. are the abbreviations for the terms II and IV of Equation (3-31) which are not of interest here. Equation (5-29) is substituted for $\overline{{}^{j}u_i' u_j'}$. The additional term $\frac{1}{3}\delta_{ij}\, \overline{{}^{k}u_i' u_i'}$ vanishes because of (5-30). If we take the time average, then we find the following for stationary turbulence:

$$\left\langle \frac{\partial \overline{{}^{\nu}E'}}{\partial t} \right\rangle = 0 = \left\langle c_2 \left(\overline{{}^{i}F\, {}^{i}E'} \right)^{1/2} \cdot \overline{\left(\delta_{x_i} \overline{{}^{i}u_j} + \delta_{x_j} \overline{{}^{i}u_i} \right)^{j}}\, \delta_{x_j} \overline{{}^{i}u_i} \right\rangle - \left\langle \overline{{}^{\nu}\varepsilon'} \right\rangle - \langle \text{Conv.} \rangle + \langle \text{Diff} \rangle . \tag{5-34}$$

The two last sum terms vanish because of the assumption of homogeneous turbulence. They therefore also vanish for a channel flow, if in addition to the time averaging we also average over the entire channel, because the kinetic energy and its gradient vanish at the wall. Therefore we have the following equation for determining c_2:

$$c_2 = \frac{\left\langle \overline{{}^{\nu}\varepsilon'} \right\rangle}{\left\langle \left(\overline{{}^{i}F\, {}^{i}E'} \right)^{1/2} \overline{\left(\delta_{x_i} \overline{{}^{i}u_j} + \delta_{x_j} \overline{{}^{i}u_i} \right)^{j}}\, \delta_{x_j} \overline{{}^{i}u_i} \right\rangle} \tag{5-35}$$

The evaluation of the denominator can only be performed if we set:

$$\left\langle \left(\overline{{}^{i}F\, {}^{i}E'} \right)^{1/2} \left(\delta_{x_i} \overline{{}^{i}u_j} + \delta_{x_j} \overline{{}^{i}u_i} \right) \delta_{x_j} \overline{{}^{i}u_i} \right\rangle \equiv \sigma_1 \left\langle \overline{{}^{i}F\, {}^{i}E'} \right\rangle^{1/2} \cdot \left\langle \overline{\left(\delta_{x_i} \overline{{}^{i}u_j} + \delta_{x_j} \overline{{}^{i}u_i} \right)^{j}}\, \delta_{x_j} \overline{{}^{i}u_i} \right\rangle \tag{5-36}$$

According to assumption e) we have set $\sigma_1 = 1$. This assumption is necessary because with the present theory, the correlation of triple velocities which occur cannot be calculated. In contrast to the assumption used by Deardorff (A3-15), with only a small degree of error we can assume that $({}^{j}\tilde{E}')^{1/2}$ is only slightly correlated with the square of the deformation but because of /58

$$\langle ({}^{j}\tilde{E}')^{1/2} \rangle \quad > \quad \langle {}^{j}\tilde{E}' \rangle^{1/2} \tag{5-37}$$

we should have $\sigma_1 > 1$.

Thus c_2 follows from

$$c_2 = \frac{\langle \varepsilon \rangle - \nu \langle (\delta_{x_j} {}^{i}\tilde{u}_i + \delta_{x_i} {}^{i}\tilde{u}_j) \cdot \delta_{x_j} {}^{i}\tilde{u}_i \rangle}{\sigma_1 \langle {}^{j}F {}^{j}\tilde{E}' \rangle^{1/2} \langle \overline{(\delta_x {}^{i}\tilde{u}_j + \delta_{x_j} {}^{i}\tilde{u}_i)^2} \, \delta_{x_j} {}^{i}\tilde{u}_i \rangle} \tag{5-38}$$

Considering the results of Chapter 4.3 (4-32) and (4-36) we find:

$$c_2 = \frac{1 - c_\nu}{\sigma_1 \cdot f_3 \cdot FED1(\Delta x_1/h, \Delta x_2/h, \Delta x_3/h)} \tag{5-39}$$

where $h = (\Delta x_1 \cdot \Delta x_2 \cdot \Delta x_3)^{1/3}$

$$c_\nu = \left(\frac{\nu^3}{h^4 \langle \varepsilon \rangle}\right)^{1/3} f_2 \; D11(\Delta x_1/h, \Delta x_2/h, \Delta x_3/h) \tag{5-40}$$

For $\alpha = 1{,}5$, $\sigma_1 = 1$ we find the following numerical results:

$\Delta x_1 : \Delta x_2 : \Delta x_3 = 1:1:1$	$\Delta x_1 : \Delta x_2 : \Delta x_3 = 0.125 : 0.05 : 0.05$
$c_2 = \left(1 - 7.78 \left(\frac{\nu^3}{h^4 \langle \varepsilon \rangle}\right)^{1/3}\right) 0.1431$	$\left(1 - 8.70 \left(\frac{\nu^3}{h^4 \langle \varepsilon \rangle}\right)^{1/3}\right) 0.1409$

(5-41)

For very high Reynolds numbers, the correction term c_ν can be ignored. For finite Reynolds numbers, c_ν as well as h and $\langle \varepsilon \rangle$ are independent of position. Because of the small order of magnitude, $\langle \varepsilon \rangle$ can be approximated as follows without a large error (see 1-36)):

$$\langle \varepsilon \rangle \approx {}^{\nu}\langle \varepsilon \rangle = 2 \, {}^{\nu}\langle u_1 \rangle \tag{5-42}$$

and therefore

$$c_\nu = \left(\frac{\nu^3}{h^4 \cdot 2 \sqrt{u_1}}\right)^{1/3} f_2\, D_{11}\left(\Delta x_1/h, \Delta x_2/h, \Delta x_3/h\right) \qquad (5\text{-}43)$$

5.2.2.4. Calculation of the Kinetic Energy $\sqrt{E'}$ / 59

Starting with the exact Equation (3-31) (in which, according to Chapter 5.2.2.2., u_i and u_i'' appear), we assume the following approximate equation:

$$\underbrace{\frac{\partial \sqrt{E'}}{\partial t}}_{I} = -\underbrace{\delta_{x_j}\left({}^{j}\overline{u_j}\ {}^{j}c_5\ \sqrt{E'}\right)}_{II} + \underbrace{P}_{III} + \underbrace{\delta_{x_j}\left[\left(\nu + {}^{j}c_6\left({}^{j}F\sqrt{E'}\right)^{1/2}\right)\delta_{x_j}\sqrt{E'}\right]}_{IV} - \underbrace{S}_{V} \qquad (5\text{-}44)$$

The Roman Numerals I to V here refer to the terms as in Chapter 3.4. We assume the following for P and S, the production and sink terms:

$$P = c_4\, h\, D^2\, \left(\sqrt{E'}\right)^{1/2} \qquad (5\text{-}45)$$

$$S = c_3 \left(\sqrt{E'}\right)^{3/2}/h \; - \; \nu\, c_8\, D^2 \qquad (5\text{-}46)$$

D^2 is a difference approximation for the square of the deformation velocity D_{ij}^2,

$$D_{ij}^2 = \tfrac{1}{2}\left(\frac{\partial u_i}{\partial x_j} + \frac{\partial u_j}{\partial x_i}\right)^2, \qquad (5\text{-}47)$$

and its exact form is to be discussed later on.

By comparing the approximation and the exact equation, we find the following equations for determining the constants c_3, c_4, ${}^{j}c_5$, c_8:

$$c_3 \equiv \frac{\langle \varepsilon \rangle \cdot h}{\left\langle \left(\sqrt{E'}\right)^{3/2} \right\rangle} \qquad (5\text{-}48)$$

$$c_4 \equiv \frac{\left\langle -{}^{j}\overline{u_i' u_j'}\ \delta_{x_j}\, {}^{j}\overline{u_i} \right\rangle}{h \left\langle \left(\sqrt{E'}\right)^{1/2} D^2 \right\rangle} \qquad (5\text{-}49)$$

$${}^{j}c_5 \equiv \left\langle {}^{j}\overline{E'} \right\rangle \Big/ \left\langle \sqrt{E'} \right\rangle \qquad (5\text{-}50)$$

$$c_8 = \frac{\langle \delta_{x_j} {}^i\bar{u}_i \, (\delta_{x_j} {}^i\bar{u}_i + \delta_{x_i} {}^i\bar{u}_j) \rangle}{\langle D^2 \rangle} \qquad (5\text{-}51)$$

Such an equation cannot be given for determining the constant ${}^j c_6$. It would be of no value because the correlations which occur in it could not be calculated because their time averages vanish. Since here the energy always occurs as an area average, we also set

$${}^j c_6 = {}^j c_5 \cdot c_7 \qquad (5\text{-}52)$$

The constant c_7 cannot be determined from the theory. Its value should lie in the following range, as does the value for the time average kinetic energy (constant a_3 in Table 1)

$$0 < c_7 \leq 1$$

According to Chapter 2.6, the constants in the energy diffusion terms do not play an important role. The value

$$c_7 = 0.3 \qquad (5.53)$$

has proven itself in practical calculations (see Chapter 10). /60
In order to calculate ${}^j\overline{u_i' u_j'}$ in Equation (5-49), the trial solution (5-29) is substituted

$$c_4 = \frac{c_2 \langle ({}^j F \, {}^j\bar{E}')^{1/2} \, (\overline{\delta_{x_i} {}^j\bar{u}_j + \delta_{x_j} {}^i\bar{u}_i})^j \, \delta_{x_j} {}^i\bar{u}_i \rangle}{h \langle ({}^v\bar{E}')^{1/2} \, D^2 \rangle} \qquad (5\text{-}54)$$

In the equations for c_3 and c_4 only triple correlations occur, which cannot be calculated with the present theory. Therefore, according to assumption e), we make the following simplifications:

$$c_3 = \frac{\langle \varepsilon \rangle \cdot h}{\alpha_2 \langle {}^v\bar{E}' \rangle^{3/2} \cdot} \qquad (5\text{-}55)$$

$$c_4 = \frac{\langle {}^{j}F\,{}^{j}\bar{E}^{1}\rangle^{1/2}\left\langle \left(\delta_{x_i}{}^{j}\bar{u}_j + \delta_{x_j}{}^{i}\bar{u}_i\right)\delta_{x_j}{}^{j}\bar{u}_i\right\rangle}{h\,\langle (\bar{E}^{1})\rangle^{1/2}\langle D^2\rangle} c_2 \qquad (5\text{-}56)$$

A correction (σ-factor) is not necessary for c_4, because approximately the same error occurs in the numerator as well as the denominator.

Two difference forms have been suggested for D^2: *

$$\text{a)}\quad D^2 = {}_3D^2 \equiv \frac{1}{2}\,\overline{\overline{\left(\delta_{x_i}{}^{j}\bar{u}_j + \delta_{x_j}{}^{i}\bar{u}_i\right)^2}}^{ij}\left(1-\delta_{[i]j[i]}\right) + 2\left(\delta_{x_j}{}^{i}\bar{u}_i\right)^2\delta_{[i]j[i]} \qquad (5\text{-}57)$$

This formula corresponds to the formula derived by Deardorff (Equation A3-36). It has the disadvantage that for the quantitative determination of $\langle {}_3D^2\rangle$, we have an integral of the form

$$\int_0^{\pi/h} k^2 E(k)\,dk$$

just like in Chapter A3.2.2. This means that it is necessary to integrate over small wavelengths, and E(k) does not agree with the assumed Kolmogorov spectrum.

However, if we subtract a term corresponding to the square of the deformation velocity from ${}_3D^2$, which is formed from differences over twice as many mesh distances and which is therefore determined by an integral having the form

$$\int_0^{\frac{1}{2}\pi/h} k^2 E(k)\,dk$$

then one can avoid the integration over the wave numbers $k<\frac{1}{2}\pi/h$. In this case the assumption b) mentioned in Chapter 5.2.2.1. is sufficient. Such a formula is the following:

/61

$$\text{b)}\quad D^2 = {}_4D^2 \equiv \frac{1}{2}\,\overline{\overline{\left(\delta_{x_j}{}^{i}\bar{u}_i + \delta_{x_i}{}^{j}\bar{u}_j\right)^2}}^{ij} - \frac{1}{2}\left(\overline{\overline{\delta_{x_j}{}^{i}\bar{u}_i + \delta_{x_i}{}^{j}\bar{u}_j}}^{ij}\right)^2 \qquad (5\text{-}58)$$

---

* See Appendix 7

Another advantage of this formula (it would also be valuable in (5-3)) is the fact that the kinetic fluctuation energy is uncoupled more from processes which occur at small wave numbers just like in physics. However, the large numerical effort is one disadvantage of this formula. The ratio $\langle {}_4D^2\rangle/\langle {}_3D^2\rangle$ can be estimated as follows:

$$\frac{\langle {}_4D^2\rangle}{\langle {}_3D^2\rangle} = \frac{\int_{\frac{\pi}{4}}^{\pi/4} k^2 E(k)\,dk}{\int_0^{\pi/4} k^2 E(k)\,dk} \qquad (5\text{-}59)$$

and therefore with $E(k) = \alpha \langle \varepsilon \rangle^{2/3} k^{-5/3}$ we have:

$$\langle {}_4D^2\rangle/\langle {}_3D^2\rangle = 1 - \left(\tfrac{1}{2}\right)^{4/3} \approx 0.602 \qquad (5\text{-}60)$$

According to Appendix 2, for $\Delta x_1 : \Delta x_2 : \Delta x_3 = 1:1:1$ the exact calculation gives:

$$\langle {}_4D^2\rangle / \langle {}_3D^2\rangle = 0.237 \qquad (5\text{-}61)$$

This shows that the approximation given in Chapter A3.2.2 can lead to large errors.

Using results of Chapter 4.3, these constants can be quantitatively determined as follows:

$$C_3 = \frac{1}{\sigma_2 \cdot [f_1 \cdot E_3(\Delta x_1/4, \Delta x_2/4, \Delta x_3/4)]^{1/2}} \qquad (5\text{-}62)$$

$$C_4 = \frac{C_3 \; FED1(\Delta x_1/4, \Delta x_2/4, \Delta x_3/4)}{[E_3(\Delta x_1/4, \Delta x_2/4, \Delta x_3/4)]^{3/2} \cdot D1k(\Delta x_1/4, \Delta x_2/4, \Delta x_3/4)} \qquad (5\text{-}63)$$

$k = 3$ for ${}_3D^2$

$k = 4$ for ${}_4D^2$

$$^jC_5 = \frac{E_2(\Delta x_m, \Delta x_n)}{E_3(\Delta x_1, \Delta x_2, \Delta x_3)} \quad m \neq n \neq j \qquad (5\text{-}64)$$

$$ {}^{j}c_6 = {}^{j}c_5 \cdot c_7 \quad ; \quad c_7 \approx 0.3 \qquad (5\text{-}65) $$

$$ c_8 = \frac{D11\,(\Delta x_1/h, \Delta x_2/h, \Delta x_3/h)}{D1k\,(\Delta x_1/h, \Delta x_2/h, \Delta x_3/h)} \qquad (5\text{-}66) $$

/62

$k = 3$ for ${}_3D^2$

$k = 4$ for ${}_4D^2$

We obtain the following numerical values for $\alpha = 1.5\,,\ \vartheta_1 = \vartheta_2 = 1$:

c	k	$\Delta x_1 : \Delta x_2 : \Delta x_3 = 1:1:1$	$\Delta x_1 : \Delta x_2 : \Delta x_3 = .125 : 0.05 : 0.05$
c_3		1.022	0.884
c_4	3	$1.6301 \cdot c_2$	$1.57 \cdot c_2$
c_4	4	$6.87 \cdot c_2$	$4.80 \cdot c_2$
${}^1c_5$		0.8283	0.6135
${}^2c_5$		0.8283	0.9147
${}^3c_5$		0.8283	0.9147
c_8	3	1.573	1.747
c_8	4	6.63	5.344

(5.67)

For known $\overline{{}^{\nu}E'}$, the values of the area average values $\overline{{}^{j}E'}$ required in (5-29), are calculated from

$$\overline{{}^{j}E'} = {}^{j}c_S \cdot \overline{{}^{\nu}E'} \tag{5-68}$$

We obtain the following from the time average of the turbulent viscosity ${}^{j}\mu$:

$$\begin{aligned} \langle {}^{j}\mu \rangle &= c_2 \langle ({}^{j}F \, \overline{{}^{j}E'})^{1/2} \rangle \\ &\approx c_2 \, {}^{j}F^{1/2} \langle \overline{{}^{\nu}E'} \rangle^{1/2} \\ &\sim h^{4/3} \langle \varepsilon \rangle^{1/3} \quad \text{(because of 4-29)} \end{aligned} \tag{5-69}$$

i.e., the turbulent viscosity obtained from this model goes to zero faster than the mesh constant h for given dissipation (corresponding to the applied pressure).

It can also be seen that for the meshes used by Deardorff [29], the turbulent viscosities have the following ratios:

$${}^{1}\mu : {}^{2}\mu : {}^{3}\mu = ({}^{1}c_S \, {}^{1}F)^{1/2} : ({}^{2}c_S \, {}^{2}F)^{1/2} : ({}^{3}c_S \, {}^{3}F)^{1/2} = 1 : 1.93 : 1.93 \tag{5-70}$$

and therefore, we have expressed anisotropy, which has not yet been considered in papers up to the present.

5.2.2.5 Correction Factors

In order to limit the effects of assumptions e), g) in Chapter 5.2.2.1, corrections will be introduced. Correction factors are suggested for assumptions b), d). /63

5.2.2.5.1. Consideration of the Time Averaging over Δ t (Assumption g)

In Chapter 3.1, averaging operations are defined as an average over mesh areas or mesh volumes, as well as over a time interval Δt. This is required because for the time integration we set

$$\frac{\partial u}{\partial t} \approx \delta_t u_i$$

which is obtained by a formal averaging over Δt. In this Chapter 5 we have not yet considered the fact that the Reynolds stresses ${}^j\overline{u_i' u_j'}$ contain averages over Δt as well as over the j-area. This will be considered by means of the following correction factor ${}^j c_g$:

$${}^j c_g \equiv \left[\langle {}^{\Delta t} \overline{E'} \rangle / \langle {}^j \overline{E'} \rangle \right]^{1/2} \qquad (5\text{-}71)$$

This means that the complete trial solution is as follows:

$${}^j\overline{u_i' u_j'} = - {}^j c_g \, c_2 \left({}^j F \, {}^j \overline{E'} \right)^{1/2} \left(\delta_{x_i} {}^j\overline{u_j} + \delta_{x_j} {}^i\overline{u_i} \right) + \frac{1}{3} \delta_{ij} \, {}^l\overline{u_l' u_l'} \qquad (5\text{-}72)$$

In order to determine ${}^j c_g$ according to the Taylor hypothesis [132, 115], it is assumed that the time axis can be transformed into a space coordinate according to $x_1 = t \cdot \langle u_1 \rangle$. Therefore, $\langle {}^{\Delta t} \overline{E'} \rangle$ must be determined for the three-dimensional volume with the edge lengths $\Delta t \langle u_1 \rangle, \Delta x_m, \Delta x_n \; (m \neq n \neq j)$. From the results of Chapter 4 we find

$${}^j c_g = \left[\frac{E3(\Delta t \langle u_1 \rangle, \Delta x_m, \Delta x_n)}{E2(\Delta x_m, \Delta x_n)} \right]^{1/2} . \qquad (5\text{-}73)$$

For the problem calculated by Deardorff [29] with

$$\Delta x_1 = 0.125,\ \Delta x_2 = 0.05,\ \Delta x_3 = 0.05,\ \Delta t = 0.003,\ \langle u_1 \rangle = 28$$

we find:

$$^1c_q = 1.18\ ,\ ^2c_q = 1.09\ ,\ ^3c_q = 1.09 \qquad (5\text{-}74)$$

The effect of time averaging is therefore not negligible, and becomes more important the greater the ratio $\Delta t/(^jF)^{1/2}$.

/64

The correction factor therefore brings about a small reduction in the anisotropy of j_μ according to (5-70).

5.2.2.5.2. Consideration of the Deviations of the True Energy Spectrum from the Kolmogorov Spectrum (Assumption b)

According to (A3-20) and (A3-37) deviations of the true spectrum at wave numbers $k < \pi/h$ bring about errors in the calculated mean squares of the deformation velocities, as well as errors in the calculated average kinetic energies for $k > \pi/h$. In the first case, one would have to apply correction factors having the form

$$c_d = \frac{\int_0^{\pi/h} k^2 E(k)\,dk}{\int_0^{\pi/h} k^2 E_k(k)\,dk} \qquad (5\text{-}75)$$

and in the second case they would have to be

$$c_e = \frac{\int_{\pi/h}^{\infty} E(k)\,dk}{\int_{\pi/h}^{\infty} E_k(k)\,dk} \qquad (5\text{-}76)$$

where $E_k(k)$ is the Kolmogorov spectrum according to (4-4). Possible generalized forms of E(k), which for $k \ll \pi/h$ become the asymptote k^4 according to (A1-37) and for $k \gg \pi/h$ they become Pao spectrum E_p (A1-34), or as follows:

$$E(k) = \left(1 - e^{-(Lk)^{4+5/3}}\right) E_p(k) \qquad (5\text{-}77)$$

or

$$E(k) = \frac{(Lk)^{4+5/3}}{1 + (Lk)^{4+5/3}} E_p(k). \qquad (5\text{-}78)$$

L is a length to be determined experimentally. Since no data about it are known, the corrections will not be investigated for $k < \pi/4$ *.

In the following we will estimate above which Reynolds numbers it is necessary to consider the Pao spectrum. From (5-76, A1-34) it follows that:

$$c_e = \exp\left[-\frac{3}{2}\alpha \nu \langle\varepsilon\rangle^{1/3} \left(\frac{\pi}{4}\right)^{4/3}\right] \qquad (5\text{-}79)$$

If according to (1-36) we set $\langle\varepsilon\rangle = 2\nu\langle u_1\rangle$, and if we set $\nu\langle u_1\rangle \approx 26$, $\alpha = 0.05$ according to [18] (corresponding to the minimum Δx_1 for Deardorff [29]) it follows that

$$c_e \approx \exp\left[-\nu/6.66\cdot10^{-3}\right] \approx 1 - \frac{\nu}{6.66\cdot10^{-3}} \quad \text{for } \nu \ll 10^{-3}. \qquad (5\text{-}80)$$

In order for this correction factor c_e to have an influence which is smaller than 1% in the calculation of the kinetic energy, we must have /65

$$\nu < 7\cdot10^{-5} \qquad (5\text{-}81)$$

Because of (1-14) the Reynolds number Re_m must therefore be greater than $3\cdot10^5$. In other words, the turbulence model used

* Figure 22 shows that the Kolmogorov spectrum already applies for the coarse structure. Therefore it seems justified to ignore these correction factors.

which assumes the existence of the Kolmogorov spectrum, applies for $Re_m \gtrsim 10^5$. For Reynolds numbers, smaller than 10^5, the Pao spectrum must be considered. This assumption agrees with the results of Chapter 4.1.2.

5.2.2.5.3. Consideration of the Random Nature (Assumption d)

As mentioned by Fox-Lilly [43], the model described up to the present is a deterministic model according to assumption d) (Chapter 5.2.2.1). The fine structure model used can only agree with reality on a statistical average basis, because true turbulence is random in nature. Effects such as the time span over which the prediction of the turbulent motion is possible for given initial conditions at discrete points within a prescribed statistical error [85] can therefore not be investigated. In order to artificially introduce a random effect into the model, one could in addition introduce a factor in (5-29) using a random generator and having an average value of one. The problem here consists of determining the fluctuation with possible correlations to the viscosities μ_j in adjacent meshes. Up to the present, the problem has not been investigated and could not be solved within this paper either. However, by means of an additional integration of the energy equation, the model used here contains an additional degree of freedom, so that it could be assumed that the "deterministic degree" is reduced somewhat. In this connection, we should also mention the question of the effects of averaging the kinetic energies $\sqrt{E'}$ over four meshes, in order to find the relevant value at the corner point of the four meshes. This is required for calculating the viscosity μ_j at this location. The model does not answer the question either.

5.2.2.5.4. Consideration of the Numerically Determined Constants (Assumption e)

According to Assumption e) (Chapter 5.2.2.1), the constants σ_1, σ_2 up to the present have been assumed to be equal to one. This assumption can be restricted afterwards by determining the values of the constants defined by (5-14, 15) from the numerical solution. After approximating ${}^{j}\bar{E}'$ by ${}^{v}\bar{E}'$ and approximation of the squares of the deformation velocity which occur in the definitions by (5-57), σ_1 and σ_2 were calculated. In addition, according to the Deardorff model, the correction factor to be introduced (see Section A 3.5) was determined /66

$$\sigma_3 = \langle \left(\tfrac{1}{2}\, {}^{v}\bar{D}_{ij}^{\,2}\right)^{3/2} \rangle \,/\, \langle \tfrac{1}{2}\, {}^{v}\bar{D}_{ij}^{\,2} \rangle^{3/2} \qquad (5\text{-}82)$$

The results will be reported on in Chapter 10.4.6.

5.2.3. Model for the Inhomogeneous Part of the Fine Structure and Summary

5.2.3.1. Model for the Inhomogeneous Part*

In this section, the trial solution for ${}^{p}\langle {}^{j}\overline{u_i' u_j'} \rangle$ must be explained. For the channel flow under consideration we have

$$ {}^{p}\langle {}^{j}\overline{u_i' u_j'} \rangle = 0 \quad \text{for} \quad i,j \neq 1,3 \qquad \text{or} \qquad (5\text{-}83)$$

In addition we have

$$\delta_{x_1}\, {}^{p}\langle {}^{1}\overline{u_1' u_3'} \rangle = 0 \qquad (5\text{-}84)$$

---

* According to definitions in Chapter 5.2.1.

Therefore, only a model is required for $^{p}\langle {}^{3}\overline{u_1' u_3'} \rangle$. For this purpose we will use a Boussinesq trial solution according to Chapter 5.2.2.3.1.:

$$^{p}\langle {}^{3}\overline{u_1' u_3'} \rangle = - {}^{p}\mu \, \delta_{x_3} \, {}^{p}\langle u_1 \rangle \tag{5-85}$$

The turbulent viscosity $^{p}\mu$ is calculated according to the Prandtl mixing length model

$$^{p}\mu = {}^{p}L^2 \, | \delta_{x_3} \, {}^{p}\langle u_1 \rangle | \tag{5-86}$$

with

$$^{p}L^2 = \min \left(c_{10} \cdot {}^{2}F_1 \, L^2 \right) \tag{5-87}$$

and L according to the generalization of the formula of van Driest [2-8]:

$$L = k \cdot z' \left[1 - \exp \{ - z' \, Re' \, \tau^{1/2} / A_w \} \right] \tag{5-88}$$

The generalization consists here in the use of

$$Re' = \max \left(\frac{1}{\nu} - Re_{Crit} , 0 \right) \tag{5-89}$$

where Re_{Crit} is the critical Reynolds number Re below which the flow is laminar:

$$Re_{Crit} = Re_{m,Crit} / {}^{v}\langle u_1 \rangle \qquad Re_{m,Crit} \approx 2100 \tag{5-90}$$

/67

Therefore $^{p}\langle {}^{3}\overline{u_1' u_3'} \rangle$ satisfies the requirements b, c, d, e according to Chapter 5.2.1, because

b) $\langle {}^{p}\langle {}^{3}\overline{u_1' u_3'} \rangle \rangle + \langle ({}^{3}\overline{u_1' u_3'})^{*} \rangle = \langle {}^{p}\langle {}^{3}\overline{u_1' u_3'} \rangle \rangle \neq 0$

c) $\lim_{\substack{\Delta x_1 \to \infty \\ \Delta x_2 \to \infty}} \left(\langle {}^3\overline{u_1' u_3'} \rangle \right) = - L^2 \left| \partial_{x_3} \langle u_1 \rangle \right| \partial_{x_3} \langle u_1 \rangle |$

because L according to (5-88)

d) $\lim_{\substack{\Delta x_1 \to 0 \\ \Delta x_3 \to 0}} \left({}^P\langle {}^3\overline{u_1' u_3'} \rangle + ({}^3\overline{u_1' u_3'})'' \right) = 0$ |

because (5-88)

e) ${}^P\langle u_1' u_3' \rangle + \langle (u_1' u_3')'' \rangle = 0$ | for $\frac{1}{\nu} < Re_{krit}$ | because (5-88,89)

The only constant which had to be determined is c_{10}. This constant, according to (5-87) is apparently determined by the fact that for $c_{10} \cdot {}^3F = L^2$ we have

$${}^P\langle u_1' u_3' \rangle = {}^P\langle {}^3\overline{u_1' u_3'} \rangle \quad \text{or} \quad ({}^3\overline{u_1' u_3'})'' = 0$$

In other words, if the mesh area ${}^3F$ is equal to L^2/c_{10}, the entire convective momentum transport occurs within the fine structure. The mesh area F must then be large enough so that there is no correlation between the velocities at extremely situated points of the surface. From the measurements of Comte-Bellot [18], the area ${}^3F$ in the middle of a channel in the flow direction must approximately have the length 1.6 and the length 0.8 (dimensionless) in the azimuth direction. If according to (2-7) we assume the value of 0.1 for L, it follows that

$$c_{10} = \frac{L^2}{{}^3F} \approx 0.01 \qquad (5\text{-}91)$$

Of course this estimation is very inaccurate. However, there is no other more accurate determination method available, and we will therefore use this value in calculations. The constant can

easily be changed because it is an input variable for the program used. The value given above has been found to be satisfactory (see Chapter 10). In order to obtain the total kinetic energy contained in the fine structure, for evaluation purposes of the kinetic energy calculated according to (5-44), it is necessary to add a part which corresponds to this inhomogeneous shear stress contribution. /68

According to (2-9) we set

$$ {}^{p}\langle \overline{\varepsilon'} \rangle = \frac{1}{a_1^2} \; {}^{p}L^2 \; \left(\delta_{x_3} {}^{p}\langle u_1 \rangle \right)^2 \qquad (5\text{-}92) $$

where $a_1=1$ according to [91, 113] (see Table 1). This approximation also seems somewhat daring but its error is inconsequential for the numerical integration and during the evaluation can also be tolerated because of

$$ L^2 < 0.01 \, {}^{3}F \lesssim 10^{-4} $$

5.2.3.2. Summary of the Locally Isotropic and Inhomogeneous Parts

If we add the locally isotropic part and the inhomogeneous part, we find the following results

$$ \begin{aligned} {}^{j}\overline{u_i' u_j'} = & -{}^{j}\mu \left(\delta_{x_j} \left({}^{i}\overline{u_i} - {}^{p}\langle {}^{i}\overline{u_i} \rangle \right) + \delta_{x_i} \left({}^{j}\overline{u_j} - \langle {}^{j}\overline{u_j} \rangle \right) \right) \\ & - {}^{p}\mu \, \delta_{x_3} {}^{p}\langle u_1 \rangle \delta_{i1} \delta_{j3} + \langle \overline{u_1' u_3'} \rangle \delta_{i3} \delta_{j1} \\ & + \tfrac{1}{3} \delta_{ij} \, {}^{e}\overline{u_e' u_e'} \end{aligned} \qquad (5\text{-}93) $$

where ${}^{j}\mu$ given by (5-31) and ${}^{p}\mu$ is given by (5-86); the values of ${}^{p}\langle \overline{u_1' u_3'} \rangle$ and ${}^{e}\overline{u_e' u_e'}$ are not important for the integration. Because of ${}^{p}\langle u_2 \rangle \approx {}^{p}\langle u_3 \rangle = 0$ we can also write

$$ {}^{j}\overline{u_i' u_j'} = -{}^{j}\mu \left(\delta_{x_i} {}^{j}\overline{u_j} + \delta_{x_j} {}^{i}\overline{u_i} \right) + \tfrac{1}{3} \delta_{ij} \, \overline{u_e' u_e'} \quad ; \; i,j \neq 1,3 ; \; i,j \neq 3,1. \qquad (5.94) $$

$$ {}^{3}\overline{u_i' u_3'} = -{}^{3}\mu \left(\delta_{x_1} {}^{3}\bar{u}_3 + \delta_{x_3} {}^{1}\bar{u}_1 \right) + \left({}^{P}\mu - {}^{3}\mu \right) \delta_{x_3} {}^{P}\langle u_1 \rangle \qquad (i,j = 1,3) \tag{5-95} $$

5.2.4. Invariance Properties of the Trial Solution

In order for turbulence models not to contradict the basic equations, we must satisfy the following invariance requirements [34].

1) The modeled terms must have the same tensor and symmetry properties as the original term;
2) They must have the correct dimensions;
3) They must be invariant with respect to the Galileo transformation (displacement of the coordinate system).

Equation (5-93) satisfies (Requirement 1), because there is a second order tensor on both sides which is symmetric with respect to the subscripts. The second requirement is apparently also satisfied. Since only velocity differences occur on the right side, the third requirement is also satisfied. This invariance property makes it possible to carry out a transfer to cylindrical coordinates, if the corresponding components of the deformation velocities are substituted on the right side. /69

At first glance, it may appear questionable whether the inequality

$$ {}^{i}\overline{u_i' u_j'} \neq {}^{j}\overline{u_i' u_j'} $$

is permissible. The following will show that this is indeed the case:

We form the time average $\langle u_i u_j \rangle$ of $u_i . u_j$ and then take the average over an i or a j-area:

$$\overline{{}^{i}\langle u_i u_j \rangle} = \langle \overline{{}^{i}u_i u_j} \rangle = \langle {}^{i}\bar{u}_i \cdot {}^{i}\bar{u}_j \rangle + \langle \overline{{}^{i}u_i' u_j'} \rangle$$
$$\overline{{}^{j}\langle u_i u_j \rangle} = \langle \overline{{}^{j}u_i u_j} \rangle = \langle {}^{j}\bar{u}_i \cdot {}^{j}\bar{u}_j \rangle + \langle \overline{{}^{j}u_i' u_j'} \rangle$$

For homogeneous turbulence we have:

$$\overline{{}^{i}\langle u_i u_j \rangle} = \overline{{}^{j}\langle u_i u_j \rangle}$$

If the diameter of the i-surface now goes to zero and the diameter of the j-surface goes to infinity, we have

$$\langle {}^{i}\bar{u}_i \, {}^{i}\bar{u}_j \rangle = \langle \overline{{}^{i}u_i u_j} \rangle = \langle u_i u_j \rangle$$

and

$$\langle {}^{j}\bar{u}_i \, {}^{j}\bar{u}_j \rangle = 0$$

Consequently we have $\langle \overline{{}^{i}u_i' u_j'} \rangle = 0 \neq \langle \overline{{}^{j}u_i' u_j'} \rangle = \langle u_i u_j \rangle$

On the other hand, using the Boltzmann axiom [119], the limit transition to infinitesimal measures requires that

$$\langle \overline{{}^{i}u_i u_j} \rangle = \langle \overline{{}^{j}u_i u_j} \rangle \qquad (\Delta x_k \to 0,\ k = 1,2,3),$$

because then both terms go to zero.

Therefore, the model used here satisfies the required invariance conditions.

5.2.5. Transfer to Cylindrical Coordinates and Non-Equidistant Meshes /70

5.2.5.1. Reynolds Stresses

In cylindrical coordinates, the formulas for the Reynolds stresses averaged over the areas are given by the same formulas as for Cartesian coordinates, if the tensor of the deformation velocities $\bar{D}_{ij} \equiv \delta_{x_i} \bar{v}_j + \delta_{x_j} \bar{v}_i$ is replaced by the corresponding one for cylindrical coordinates [53]:

$$\bar{D}_{ij} = \begin{pmatrix} 2\delta_x {}^{x}\bar{v}_x & \frac{1}{r}\delta_\varphi {}^{x}\bar{v}_x + \delta_x {}^{\varphi}\bar{v}_\varphi & \delta_r {}^{x}\bar{v}_x + \delta_x {}^{r}\bar{v}_r \\ \delta_x v_\varphi + \frac{1}{r}\delta_\varphi {}^{x}\bar{v}_x & 2\left(\frac{1}{r}\delta_\varphi v_\varphi + \frac{\overline{{}^{r}v_r}}{r}\right) & +\delta_r\left(\frac{{}^{\varphi}\bar{v}_\varphi}{r}\right) + \frac{1}{r}\delta_\varphi {}^{r}\bar{v}_r \\ \delta_x {}^{r}\bar{v}_r + \delta_r {}^{x}\bar{v}_x & \frac{1}{r}\delta_\varphi {}^{r}\bar{v}_r + r\delta_r\left(\frac{{}^{\varphi}\bar{v}_\varphi}{r}\right) & 2\delta_r {}^{r}\bar{v}_r \end{pmatrix} \quad (5\text{-}96)$$

We will substitute the following for the two terms $\overline{{}^{v}v_r' v_\varphi'}$, $\overline{{}^{v}v_\varphi'^2}$:

$$\overline{{}^{v}v_r' v_\varphi'} = -{}^{v}\mu \left[r\delta_r\left(\frac{{}^{\varphi}\bar{v}_\varphi}{r}\right) + \frac{1}{r}\delta_\varphi {}^{r}\bar{v}_r \right], \quad (5\text{-}97)$$

$$\overline{{}^{v}v_\varphi'^2} = -{}^{v}\mu \; 2\left(\frac{1}{r}\delta_\varphi {}^{\varphi}\bar{v}_\varphi + \frac{{}^{r}\bar{v}_r}{r}\right), \quad (5\text{-}98)$$

where

$${}^{v}\mu = c_2 \, {}^{v}\overline{E'} \cdot h \, . \quad (5\text{-}99)$$

The deformation velocity which determines the inhomogeneous part is

$$\delta_r {}^{p}\langle {}^{x}\bar{v}_x \rangle .$$

The constant c_2 is calculated just like for the Cartesian mesh using the edge lengths $\Delta x, r\Delta\varphi, \Delta r$:

5.2.5.2. Energy Calculation

The following equation is used to calculate the kinetic energy ${}^{v}\overline{E'}$:

$$\frac{\partial \overline{E'}^{\nu}}{\partial t} = -\delta_x \left(\overline{\upsilon}_x^{x} c_s^{x} \overline{E'}^{\nu} \right) - \frac{1}{r} \delta_\varphi \left(\overline{\upsilon}_\varphi^{\varphi} c_s^{\varphi} \overline{E'}^{\nu} \right) - \frac{1}{r} \delta_r \left(r \overline{\upsilon}_r^{r} c_s^{r} \overline{E'}^{\nu} \right)$$
$$+ P + \delta_x \left[\left(\nu + {}^{x}c_c \left({}^{x}F \overline{E'}^{\nu} \right)^{n} \right) \delta_x \overline{E'}^{\nu} \right]$$
$$+ \frac{1}{r} \delta_\varphi \left[\left(\nu + {}^{\varphi}c_c \left({}^{\varphi}F \overline{E'}^{\nu} \right)^{n} \right) \frac{1}{r} \delta_\varphi \overline{E'}^{\nu} \right]$$
$$+ \frac{1}{r} \delta_r \left[r \left(\nu + {}^{r}c_c \left({}^{r}F \overline{E'}^{\nu} \right)^{n} \delta_r \overline{E'}^{\nu} \right] \right] - S \qquad (5\text{-}100)$$

/71

P, S are calculated using appropriate formulas for D^2, just like in the case of Cartesian coordinates using Equation 5-96) *. The constants and areas are characterized by the subscripts x, φ, r and are calculated just like for a corresponding Cartesian mesh with the edges $\Delta x, r\Delta\varphi, \Delta r$ and the subscripts 1, 2, 3 are used instead of x, φ, r.

5.2.5.3. Transition to Non-Equidistant Meshes

Slightly modified difference formulas are used for non-equidistant meshes, and this will be discussed in the following chapter. The calculation of the constants is done according to the methods derived for Cartesian, equidistant meshes. The characteristic mesh edge lengths used are the average edge lengths which apply with respect to the center of the mesh under consideration. This is permissible if the mesh edge lengths vary only slightly.

---

* See Appendix 7

6. DIFFERENCE METHODS

According to the preceding chapter, the nonlinear terms remain undetermined during the integration of the basic equations over the mesh volumes according to Chapter 3. They are approximated by a fine structure model. Now we must also approximate the undetermined linear quantities. The result is a close system of different formulas which can be integrated for suitable boundary and initial conditions using a numerical method.

6.1. Linear Difference Approximation

Two types of linear quantities must be approximated:

a) Area and volume average values of velocities and pressures which do not agree with the variables already stored with the grid;

b) Partial derivatives of velocities (only first derivatives) and we have two types:

b 1) $\overline{\frac{\partial u_1}{\partial x_1}}^1$ (Derivative perpenducular to the averaging area)

b 2) $\overline{\frac{\partial u_1}{\partial x_2}}^1$ (Derivative parallel to the averaging area)

The quantities given by a) are approximated by arithmetic averaging of adjacent variables known in the grid. Non-equidistant meshes are considered as well as the variation of the mesh sizes with radius using appropriate weighting factors in the case of cylindrical coordinates. The notation used is

defined by

$$\tilde{y}^x = \left[\Delta x_+ \cdot y\left(x + \tfrac{1}{2}\Delta x_+\right) + \Delta x_- y\left(x - \tfrac{1}{2}\Delta x_-\right)\right] \qquad (6\text{-}1)$$

The quantity b1) can be approximated without any truncation error of order Δx^2 without any problems by means of

$$\overline{\frac{\partial u_1}{\partial x_1}} \approx \delta_{x_1} \overline{u}_{1/1}$$

because the derivative according to (3-13) is approximated by the point half-way between two mesh surfaces. /73

As far as b2) is concerned, according to the following sketch, the derivative of a function y(x) must be determined at a point $x_{1/2}$, and only the average values within the adjacent intervals of y are known.

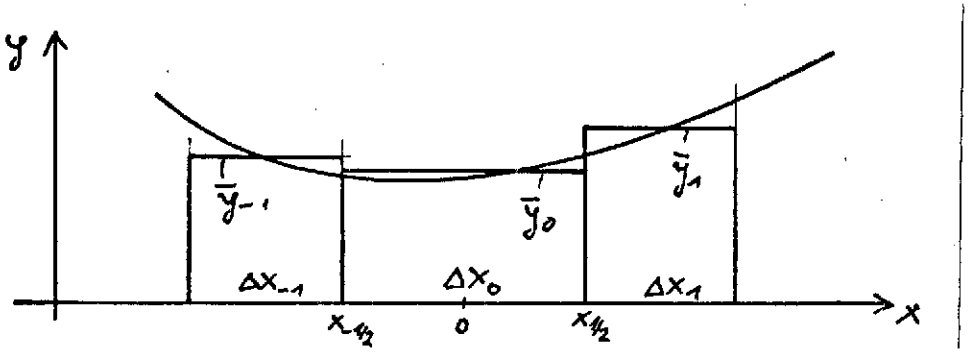

If we now consider a Taylor series expansion and according to the stationary laminar solution if we assume that y(x) is given by a parabola having the form

$$y = a\,x^2 + bx + c$$

as a first approximation (coordinate origin x in the center of the central mesh) then the coefficients a, b, c can be calculated for given $\bar{y}_{-1}, \bar{y}_0, \bar{y}_1$ as well as the derivatives $\partial y/\partial x(x_{1/2})$. The asymmetric form of y_{-1} is selected and not for y_2 because the derivative is always calculated in pairs for $x_{1/2}$ and

$x_{-1/2}$. We then obtain the following difference approximation:

$$\frac{\partial y}{\partial x}(x_{1/2}) = \bar{\delta}_x y(x_{1/2}) \equiv a_1 \bar{y}_1 + a_2 \bar{y}_0 + a_3 \bar{y}_{-1} \qquad (6\text{-}2)$$

where

$$a_1 = (6\,\Delta x_{-1}\cdot\Delta x_0 + 2\,\Delta x_{-1}^2 + 4\Delta x_0^2)/d$$
$$a_2 = (-6\,\Delta x_{-1}\,\Delta x_0 - \Delta x_0^2 + 2\Delta x_1^2 - 2\Delta x_{-1}^2)/d$$
$$a_3 = (2\,\Delta x_0^2 - 2\Delta x_1^2)/d$$
$$d = (\Delta x_{-1}+\Delta x_0)(\Delta x_0+\Delta x_{+1})(\Delta x_{-1}+\Delta x_0+\Delta x_{+1})$$

For equidistant meshes, $\Delta x_{-1}=\Delta x_0=\Delta x_1=\Delta x$ we have $a_1=\frac{1}{\Delta x}$, $a_2=-\frac{1}{\Delta x}$, $a_3=0$ i.e., these developments only apply for nonequidistant meshes; however, they are important here. The author does not know of any similar developments from the literature.

6.2. Difference Formulas

/ 74

Considering the "one-dimensional" geometries used, nonequidistant meshes are only appropriate in the radial direction. This will be considered in the following formulas. The difference formulas are only given for cylindrical coordinates. The corresponding formulas for Cartesian coordinates are found by substituting the value 1 for the radii r in terms in which r does not occur in both the numerator and denominator as a pair. In terms where the radius r occurs more frequently in the denominator than in the numerator, r is set equal to zero (corresponding to the limit transition $r\to\infty$).

The velocities which occur are area averages; the averaging bar is therefore omitted in the following. The symbol p refers to the apparent turbulent pressure fluctuations:

$$p = {}^{i}\bar{p} + \frac{1}{3}\,{}^{i}\overline{u_i' u_i'} \quad ; \; i = 1,2,3 \tag{6-3}$$

6.2.1. Difference Formulas for Momentum

The difference formulas for momentum are:

$$\left[\overline{\delta_t v_x}^{t} + \delta_x\left(\overline{v_x}^{x}\,\overline{v_x}^{x}\right) + \frac{1}{\tau}\delta_\varphi\left(\overline{v_\varphi}^{x}\,\overline{v_x}^{\varphi}\right) + \frac{1}{\tau}\delta_r\left(\overline{\tau v_x}^{r}\,\overline{v_r}^{x}\right)\right]^{n1} = \left[-\delta_x p\right]^{n2} + P_x$$
$$+\left[\delta_x\left\{{}^{x}\mu^{*}\left(2\delta_x v_x\right)\right\} + \frac{1}{\tau}\delta_\varphi\left\{{}^{\varphi}\mu^{*}\left(\frac{1}{\tau}\delta_\varphi v_x + \delta_x v_\varphi\right)\right\} + \frac{1}{\tau}\delta_r\left\{{}^{r}\mu\left(\overline{\delta}_r v_x + \delta_x v_r\right)\right\}\right.$$
$$\left. + \frac{1}{\tau}\delta_r\left\{\tau\left({}^{p}\mu^{*} - {}^{r}\mu\right)\overline{\delta}_r\,{}^{p}\langle v_x\rangle\right\}\right]^{no}$$

$$\left[\overline{\delta_t v_\varphi}^{t} + \delta_x\left(\overline{v_x}^{\varphi}\,\overline{v_\varphi}^{x}\right) + \frac{1}{\tau}\delta_\varphi\left(\overline{v_\varphi}^{\varphi}\,\overline{v_\varphi}^{\varphi}\right) + \frac{1}{\tau}\delta_r\left(\overline{\tau v_\varphi}^{r}\,\overline{v_r}^{\varphi}\right) + \overline{\frac{v_\varphi}{\tau^2}\,\overline{v_r\tau}^{r}}^{\varphi}\right]^{n1}$$
$$= \left[-\frac{1}{\tau}\delta_\varphi p\right]^{n2} + \left[\delta_x\left\{{}^{x}\mu^{*}\left(\delta_x v_\varphi + \frac{1}{\tau}\delta_\varphi v_x\right)\right\} + \frac{1}{\tau}\delta_\varphi\left\{2\,{}^{\varphi}\mu^{*}\left(\frac{1}{\tau}\delta_\varphi v_\varphi + \frac{\overline{v_r}^{r}}{\tau}\right)\right\}\right.$$
$$\left. + \frac{1}{\tau}\delta_r\left\{\tau\,{}^{r}\mu^{*}\left(\tau\overline{\delta}_r\left(\frac{v_\varphi}{\tau}\right) + \frac{1}{\tau}\delta_\varphi v_r\right)\right\} + {}^{v}\mu^{*}\left(\overline{\delta_r\frac{v_\varphi}{\tau} + \frac{1}{\tau}\delta_\varphi\frac{v_r}{\tau}}^{r}\right)\right]^{no}$$

$$\left[\overline{\delta_t v_r}^{t} + \delta_x\left(\overline{\frac{\tau v_x}{\tau}}^{r}\,\overline{v_r}^{x}\right) + \frac{1}{\tau}\delta_\varphi\left(\overline{v_\varphi}^{r}\,\overline{v_r}^{\varphi}\right) + \frac{1}{\tau}\delta_r\left(\frac{\overline{\tau v_r}^{r}\;\overline{\tau v_r}^{r}}{\tau}\right) - \overline{\frac{v_\varphi^2}{\tau}}^{\varphi}\right]^{n1}$$
$$= \left[\delta_r p\right]^{n2} + \left[\delta_x\left\{{}^{x}\mu\left(\delta_x v_r + \overline{\delta}_r v_x\right)\right\} + \frac{1}{\tau}\delta_\varphi\left\{{}^{\varphi}\mu^{*}\left(\tau\overline{\delta}_r\left(\frac{v_\varphi}{\tau}\right) + \frac{1}{\tau}\delta_\varphi v_r\right)\right\}\right.$$
$$\left. + \frac{1}{\tau}\delta_r\left(2\,{}^{r}\mu^{*}\,\tau\,\overline{\delta}_r v_r\right) - 2\,{}^{v}\mu^{*}\left(\overline{\overline{\frac{1}{\tau^2}\delta_\varphi v_\varphi}^{\varphi} + \frac{v_r}{\tau^2}}^{r}\right)\right]^{no} \tag{6-4}$$

$${}^{x}\mu^{*} \equiv {}^{x}\mu + \nu \; ; \quad {}^{\varphi}\mu^{*} \equiv {}^{\varphi}\mu + \nu \; ; \quad {}^{r}\mu^{*} \equiv {}^{r}\mu + \nu \; ; \quad {}^{p}\mu^{*} \equiv {}^{p}\mu + \nu \; ; \quad {}^{v}\mu^{*} \equiv {}^{v}\mu + \nu .$$

The superscripts no, nl, n2 refer to time steps. For the first time step n=1 we have no=1, nl=2, n2=2 and for the following N time steps n = 2,3,.., N we have no=n-1, nl - n,n2 = n+1. After N time steps the solutions at the time N+1 are averaged using a solution which is found from no=nl=N, n2 = N+1. After this, one starts again just like for n= 1. This so-called leapfrog-midpoint or jump method has an accuracy of order Δt^2 for the convective terms except for the first and last step. It has been used many times [29, 33, 42, 79, 141], because it avoids numerical damping in contrast to the Euler one-step method [73, 79], for example. The absence of the numerical damping, however, can lead to $2\Delta t$ oscillations because of the nonlinearities, which are damped by averaging with respect to N steps. The convection terms and the diffusion terms which result for μ = const correspond to the difference formulas of Williams [141] for equidistant meshes. The corresponding formulas for $\mu \neq$ const and non-equidistant meshes have not been formulated up to the present. /75

It is now possible to use different formulas having a higher degree of accuracy in time because of the difficult calculation of the pressure and the associated enlarged storage requirement. It does not seem to be appropriate to use more accurate difference formulas in space, such as for example one suggested by Fromm [41], for the turbulent flow case. Apparently the greatest errors are produced by the fine structure model. In addition, the boundary conditions become much more complicated.

6.2.2. Difference Formulas for the Pressure p and the Auxiliary Potential ψ

The pressure required in (6-4) is in principle to be calculated according to Chapter 1.4.2 from a Poisson equation with inhomogeneous boundary conditions. Since these inhomogeneous boundary conditions have a disturbing effect and also the

calculation of the source term q according to (1-20) is laborious and it must be assumed that the velocity field for the time steps no and nl exactly satisfies the continuity equation [54], or that errors in the adherence to the continuity equation can increase from one time step to another, we will therefore not first calculate the pressure p itself. Instead we will calculate an auxiliary potential φ which will remove all these deficiencies. The method used here was suggested by Chorin [21], and was used by Amsden-Harlow [3]. Compared with the method used by Deardorff, Williams, etc. [29, 141, 54], this represents an improvement so far as accuracy and simplicity are concerned. Compared with the methods suggested in [3, 37], it becomes possible to calculate the pressure directly without solving an additional Poisson equation.

/ 76

First of all a velocity field $\tilde{\underline{u}}^{n2}$ for a new point in time is calculated using formulas (6-4) but without considering the pressure. The velocity component perpendicular to the wall is set equal to zero for the new time step corresponding to the exact wall conditions (1-5):

$$v_r^{n2} = \tilde{v}_r^{n2} = 0 \qquad (6\text{-}5)$$

This velocity field $\tilde{\underline{u}}^{n2}$ is, of course, not the correct one, because the pressure was not considered. However, because of the omitted pressure terms, this solution can only differ by the gradient of a potential from the correct solution $\underline{u}^{n2}$. Therefore, we set

$$\underline{u}^{n2} = \tilde{\underline{u}}^{n2} - \underline{\mathrm{grad}}\,\varphi \qquad (6\text{-}6)$$

Here φ is an auxiliary potential and $\underline{\mathrm{grad}}$ is the difference form of the gradient operator:

$$\underline{\mathrm{grad}} = \left\{ \delta_x, \frac{1}{r}\delta_\varphi, \delta_r \right\} \qquad (6\text{-}7)$$

The direct velocity field $\underline{u}^{n2}$ must satisfy the continuity equation (I-8)

$$div\ \underline{u}^{n2} \equiv \delta_x v_x^{n2} + \frac{1}{r}\delta_\varphi v_\varphi^{n2} + \frac{1}{r}\delta_r(r v_r^{n2}) = 0 \qquad (6\text{-}8)$$

The potential ψ is therefore the solution of the following Poisson equation

$$div\ grad\ \psi = div\ \tilde{\underline{u}}^{n2} \qquad (6\text{-}9)$$

Because of (6-5) we have the homogeneous Neumann boundary conditions

$$\delta_r \psi = 0 \Big|_{wall} \qquad (6\text{-}10)$$

This system of equations can be directly solved using the series expansion described in Section 4 and using the fast Fourier transformation (FFT) in a very effective manner. Then the velocity fields will satisfy the continuity equation after every time step up to a numerical rounding error. This is also true if the initial condition does not satisfy the continuity equation. Corrections suggested by Hirt-Harlow [56] and used in [29, 141], are superfluous here. In the following we will show that the pressure p can be simply calculated as follows without any additional solution of a special Poisson equation: /77

$$p = \frac{\psi}{(n2-n0)\Delta t} \qquad \text{For all meshes inside of the flow space} \qquad (6\text{-}11)$$

$$p_w = \pm \frac{\Delta r}{2} \frac{\partial \tilde{v}_r}{\partial t}\Big|_{wall} + \frac{\psi}{(n2-n0)\Delta t}\Big|_{wall} \qquad \text{At the walls} \qquad (6\text{-}12)$$

(+for r = R1; -for r = R2)

Here $\partial \tilde{v}_r/\partial t|_{wall}$ is the radial acceleration at the wall which is obtained when the pressure is not considered. $\psi/_{wall}$ is the value of the auxiliary potential at the mesh adjacent to the wall. For proof of this, we consider the equation for determining the

pressure, which is given as follows according to (1-19) in difference form:

$$\operatorname{div}\ \underline{\operatorname{grad}}\ \varphi = \operatorname{div}\ \frac{\partial \tilde{\underline{v}}}{\partial t}\Big| \qquad (6\text{-}13)$$

with the boundary condition

$$\delta_r p = \frac{\partial \tilde{v}_r}{\partial t}\Big|_{\text{wall}}. \qquad (6\text{-}14)$$

Because of div $\tilde{\underline{v}}^{n0} = 0$, we have

$$\operatorname{div}\left(\frac{\partial \tilde{\underline{v}}}{\partial t}\right) = \frac{1}{(n2-n0)\Delta t}\ \operatorname{div}\left(\tilde{\underline{v}}^{n2}\right) \qquad (6\text{-}15)$$

for all meshes which are not adjacent to the wall. On the other hand for the wall meshes $\operatorname{div} \tilde{\underline{v}}^{n2}$ does not obtain the contribution to the divergence which is a consequence of $\partial \tilde{v}_r/\partial t|$, because according to (6-5) $\tilde{v}_r^{n2}$ was set equal to the value which was a consequence of the wall condition. Therefore in this case we have

$$\operatorname{div}\left(\frac{\partial \tilde{\underline{v}}}{\partial t}\right) = \frac{1}{(n2-n0)\Delta t}\ \operatorname{div}\ \tilde{\underline{v}}^{n2} + \operatorname{div}\left\{0, 0, \frac{\partial \tilde{v}_r}{\partial t}\Big|_{\text{wall}}\right\}, \qquad (6\text{-}16)$$

and in the second divergence operator the field values located in the interior of the flow are all equal to zero. If we now form the divergence of (6-14) in a corresponding way and if we subtract this from (6-13, 16), we find:

$$\operatorname{div}\ \underline{\operatorname{grad}}\ (p_1) = \frac{1}{(n2-n0)\,\Delta t}\ \operatorname{div}\ \tilde{\underline{v}}^{n2} \qquad (6\text{-}17)$$

$$\delta_r p_1 = 0\Big|_{\text{wall}} \qquad (6\text{-}18)$$

With $p_1 = p$ inside of all the meshes and

$$p_1 = p \mp \frac{\Delta r}{2}\ \frac{\partial \tilde{v}_r}{\partial t}\Big|_{\text{wall}} \quad \text{at the walls.} \qquad (6\text{-}19)$$

Because of the similiarty of the Equations (6-17,18) and (6-9, 10) and the linearity of the operator div grad, we find the result which has to be proved (6-11, 12). See Chapter 7.7 for the calculation of $\partial \tilde{v}_r/\partial t|_{\text{wall}}$.

6.2.3. Difference Form of the Energy Equation

In the numerical integration of the energy Equation (5-44, 100) we must determine that the energy $\sqrt{E'}$ is always larger (or equal for laminar flow) than zero. For this reason we will integrate over time using the single step method. The convective terms are calculated with so-called "upwind", "down stream" or "corner cell" difference Formulas [49, 57, 72, 73, 123]: / 78

$$u\,\delta_x^*\,y \equiv \begin{cases} u(x-\frac{1}{2}\Delta x)\frac{1}{\Delta x}\left(y(x)-y(x-\Delta x)\right); & u(x)>0 \\ u(x+\frac{1}{2}\Delta x)\frac{1}{\Delta x}\left(y(x+\Delta x)-y(x)\right); & u(x)\le 0 \end{cases} \qquad (6\text{-}20)$$

These formulas insure that the new value of y at the next time step will not be negative if only the convection is considered, unless the initial field is non-negative everywhere [123]. As linear stability analysis can show (see Section 6), it is not permissible to use the jump method for the time integration here because it would always be unstable. Therefore we will use the Euler method here.

Negative values of the energy field can occur under some conditions if the energy dissipation was calculated according to

$$\left(\sqrt{E'}\right)^{n+1} = \left(\sqrt{E'}\right)^{n} + \Delta t\cdot\left(\cdots - \frac{c_3}{4}\left(\sqrt{E'}\right)^{3}\right) \qquad (6\text{-}21)$$

and the dots stand for all terms besides the sink term. Since the analytical solution of

$$\frac{\partial y}{\partial t} = -\,a\,y^{3/2} \qquad (6\text{-}22)$$

is given by

$$y(t) = \frac{y(t_0)}{\left(1+\frac{a}{2}(t-t_0)\left[y(t_0)\right]^{1/2}\right)^2}\,, \qquad (6\text{-}23)$$

we integrate as follows here:

$$\left(\sqrt{E'}\right)^{n2} = \frac{\left(\sqrt{E'}\right)^{n1}}{\left(1+\frac{c_3\cdot\Delta t}{2h}(n2-n1)\left[\left(\sqrt{E'}\right)^{n1}\right]^{1/2}\right)^2} + \Delta t\cdot(\cdots\cdots) \quad (6\text{-}24)$$

If we obtain a negative value of $\sqrt{E'}$ in spite of these precautions, then this will be due to instabilities caused by steps which are too large for the integration of the energy diffusion terms. In such cases, the time step Δt is reduced.

6.3. Accuracy and Stability of the Difference Formulas /79

6.3.1. Accuracy

In Section 5 we will discuss several aspects of the accuracy of the difference formulas.

Among these we have:

a) Statistical errors of the linear difference approximations;
b) Truncation errors;
c) Aliasing errors;
d) Agreement of the difference formulas with the physical conservation laws which follow from the integrals of the differential equations
3) Numerical errors

The most important results are the following:

a) The deterministic linear difference approximations are only correct for the statistical average and for sufficiently smooth averaged fields. The instantaneous deviations from the statistical average have a standard

deviation which is proportional to $\langle\varepsilon\rangle^{1/3}\,\Delta x^{4/3}$ and therefore becomes smaller only as the dissipation $\langle\varepsilon\rangle$ and the mesh edge length Δx are decreased. It is likely that the deterministic approximations can be replaced by a statistical method which can be determined quantitatively, but this was not done. The area averaging results in a reduction in the error by only a factor of three compared with the consideration of point velocities.

b) The truncation errors of the difference formulas have the order of Δx^2 for position and are of order Δt^2 in time for the convective terms. Phase errors can be ignored because of the small energy contribution of the short wave Fourier components of the solution. The effect of "false diffusion" will be discussed but does not seem to be important either.

c) The aliasing effect will be discussed. This error can lead to instabilities, but they are controlled in the conservation properties which will be discussed in the following.

d) The difference formulas must satisfy the condition that / 80
if there are no source and sink terms, the time changes of momentum and kinetic energy integrated over the entire flow space must vanish. The same conditions apply for the differential equation. This condition is satisfied by the difference formulas used here.

e) The reasons for the production of numerical errors have been demonstrated. Rules will be given which, if followed, make it possible to avoid these errors, especially when extensive sums are formed.

6.3.2. Stability

As discussed in detail in Appendix 6, stability criteria will be investigated. First of all the permissible time steps are determined for the linearized difference formulas in their three-dimensional form for cylindrical coordinates using the Neumann criterion [111]. Three types of difference formulas are investigated. The first one corresponds to the formulas for the momentum calculation and the second one corresponds to the energy $\sqrt{E^2}$ calculation. As the third type we will investigate often suggested difference formulas which correspond to the first type except for the approximation of the diffusion terms, which are calculated according to DuFort-Frankel. The following results are obtained (see Appendix 6):

a) The permissible time step Δt (except for the second type) can only be given in an explicit algebraic form for the limiting cases of pure convection and pure diffusion. In the first case we have $\Delta t \sim \frac{\Delta x}{|u|}$ and in the second case $\Delta t \sim \frac{\Delta x^2}{\mu}$. For the third type Δt is arbitrarily large for stability and for pure diffusion.

b) For the general case of mixed convection and diffusion, the permissible time step Δt is determined numerically. Comparisons do not yet exist in the literature.

c) The permissible time step Δt can be much smaller than the minimum of the time steps which result for the limiting cases. A formula is given according to which a conservative time step can be easily determined algebraically.

d) When the Du Fort-Frankel form is used for small viscosities, one is led to smaller permissible time steps than those used here for multi-dimensional problems. /81

From the result a) and according to the turbulent viscosity which varies according to (5-69) it follows that at high Reynolds numbers the permissible time step is always proportional to the mesh edge length Δx.

In addition, in Appendix 6 we will discuss the method of Hirt [57] for investigating the influence of nonlinearities on the stability. It will be shown that this method is not practical here.

Finally we would like to state why we do not use an implicit method [44, 111] to avoid instabilities. The reasons are as follows:

a) The numerical cost for solving the large, nonlinear systems of equations which are produced would be very high;
b) The increased numerical effort could not be compensated for by a larger time step Δt, because the inaccuracies, especially regarding the nonlinear convection terms, would become much too large. For example, note the effect of the time step on the fine structure model according to Chapter 5.2.2.5.1.

c) The permissible time step is sufficiently large because $\Delta t \sim \Delta x$.

7. BOUNDARY CONDITIONS

In this chapter we will give the boundary conditions for integrating the difference equations. Periodic boundary conditions are assumed in the azimuthal and axial directions. The period lengths are selected according to experimental results. There are wall conditions in the radial direction. For this the basic equations are integrated over the wall meshes and the strongly varying profiles as well as wall roughnesses are considered by means of logarithmic wall laws.

7.1. Periodicity Condition

The basic equations are elliptical as far as space is concerned and therefore require boundary conditions as all surfaces of the flow field being considered. Such boundary conditions must be introduced artificially in the axial direction and, for plate channels (or annulus channels with radii ratios R2/R1 close to 1) in the azimuth direction. This is because the numerically simulated flow space cannot be selected as large as desired for specified mesh sizes. According to convention [29, 83, 94] periodic boundary conditions are used here:

Cartesian $$y(x_1 + iX_1, x_2 + jX_2, x_3) = y(x_1, x_2, x_3)$$

Cylindrical $$y(x + iX, \varphi + j\Phi, r) = y(x, \varphi, r) \qquad i, j = 0, \pm 1, \pm 2, \ldots \qquad (7\text{-}1)$$

These boundary conditions would be exactly correct if $\Phi = 2\pi$ and the channel were a torus with the circumference length X. In all other cases, this boundary condition does not have a physical reality. In the first approximation, the periodic boundary condition can be justified as follows, for example in the axial direction. If the flow fields y in the axial

direction are only correlated over a length of X/2, i.e., $\langle y(x+z,\varphi,r)\cdot y(x,\varphi,r)\rangle$ equals zero for $z \geq X/2$, then for $z > X/2$ one can prescribe any arbitrary boundary condition without influencing $y(x,\varphi,r)$, and therefore, for example, one can also require periodicity. From the measurements of Comte-Bellot [18] for plate flow, it is evident that the correlation length defined above corresponds to about 1.6 times the plate distance in the axial direction and about 0.8 times the plate distance in the direction perpendicular to the flow direction. Therefore, we selected /83 the following period length:

$$X_1 = 4\,,\quad X_2 = 2$$
$$X = 4,\quad \phi = \begin{cases} 2\pi & R1/R2 \leq 0.2 \\ 2/R1 & R1/R2 > 0.2 \end{cases} \qquad (7\text{-}2)$$

The values used by Deardorff [29], $X_1=3$, $X_2= 0.7$, seemed to be too small based on the measurement results discussed above.

7.2. Exact Wall Condition and Galileo Transformation

The exact wall condition (1-5) is valid at the walls. Since only the reference area of the radial velocity component lies on the wall surface, the exact wall conditions can be simulated here without any problems:

$$\left.{}^{3}\bar{u}_3\right|_{\text{wall}} = \left.{}^{\uparrow}\bar{v}_r\right|_{\text{wall}} = 0 \qquad (7\text{-}3)$$

For the two other components, additional approximations of (1-5) are necessary. For this see the following sections. In order to improve the stability properties and to reduce the numerical inaccuracies, when differences are formed, we carried out a Galileo transformation. It is assumed that the coordinate system is not at rest but itself moves at the velocity VG, which corresponds approximately to the average axial velocity with which the flow is moving in the axial direction. In this way the basic equations are not changed. However, now the

wall condition for the axial velocity component becomes [29]

$$u_1 \Big|_{wall} = v_x \Big|_{wall} = -VG \Big| \qquad (7\text{-}4)$$

7.3. Wall Condition for the Axial Velocity Component v_x

One must start with the momentum conservation equation (3-15) averaged over the mesh volumes in the exact form. If we considered a wall mesh, then the approximation of the convective terms does not cause any problems because of $\bar{v}_r\big|_{wall} = 0$. However, this is not true for the diffusion terms. Here the term

$$\frac{1}{r}\,\delta_r\left\{r\,\overline{\nu\left(\frac{\partial v_x}{\partial r}+\frac{\partial v_r}{\partial x}\right)}\right\}\Big|$$

must be considered separately. For a wall mesh along the inner wall at $r=r_1$ we have: /84

$$\frac{1}{r}\delta_r\left\{r\,\overline{\nu\left(\frac{\partial v_x}{\partial r}+\frac{\partial v_r}{\partial x}\right)}\right\} = \frac{1}{r_1\cdot\Delta r_1}\left\{r_{3/2}\left[\overline{\nu\left(\frac{\partial v_x}{\partial r}+\frac{\partial v_r}{\partial x}\right)}\right]_{3/2} - R1\,\tau_{w_1}\right\}, \qquad (7\text{-}5)$$

with the wall shear stress

$$\tau_{w_1} = \overline{\nu\,\frac{\partial v_x}{\partial r}}\,. \qquad (7\text{-}6)$$

The terms can be approximated at $r=r_{3/2}$ just like in the interior of the flow. However, we cannot set $\tau_{w_1} = \frac{\bar{v}_{x_1}}{\Delta r_{1/2}}$* because the velocity profile varies too much in the vicinity of the wall.

---

* $\bar{v}_{x_1}$ is the value of $\bar{v}_x$ in the wall mesh at n = 1 according to Figure 5.

Instead, we will set:

$$\tau_{w_1} = {}^{x}\bar{v}_{x_1} \frac{\langle \tau_{w_1} \rangle}{\langle {}^{x}\bar{v}_{x_1} \rangle} \qquad (7\text{-}7)$$

If we approximately assume, as is done in general [29, 120], the following logarithmic profile for the average velocity in the vicinity of the wall:

$$\langle v_x \rangle(r) = \frac{\langle \tau_{w_1} \rangle^{1/2}}{k} \ln \left[(r - R_1) E_1 \right],$$

where k is the Karman constant and E_1 is the wall roughness along the inner wall, we have

$$\langle {}^{x}\bar{v}_x \rangle_1 = \frac{\langle \tau_{w_1} \rangle^{1/2}}{k} \left[\ln [\Delta r_1 \cdot E_1] - 1 \right] \qquad (7\text{-}8)$$

and therefore

$$\tau_{w_1} = {}^{x}\bar{v}_{x_1} \frac{k}{\left(\ln [\Delta r_1 E_1] - 1 \right)} \cdot \langle \tau_{w_1} \rangle^{1/2}$$

If we consider the Galileo transformation (7-4), then we have the following complete form

$$\tau_{w_1} = \left({}^{x}\bar{v}_{x_1} + VG \right) \frac{k}{\left(\ln [\Delta r_1 E_1] - 1 \right)} \langle \tau_{w_1} \rangle^{1/2} \qquad (7\text{-}9)$$

For plate flow with the same wall roughness at both walls we can calculate $\langle \tau_{w_1} \rangle$ from a simple force equilibrium as follows:

$$\langle \tau_{w_1} \rangle = \langle \tau_{w_2} \rangle = \frac{P_x (R_2 - R_1)}{2} = 1 \qquad (7\text{-}10)$$

In all other cases it is necessary to determine the average wall shear stress during the integration. See Chapter 7.5 for this.

For the constants k, E_1, E_2, Deardorff [29] used the following values referring to the measurements of Laufer [76]:

$$k = 0.4;\ E_1 = E_2 = 8.8 \cdot 10^4 \qquad (7\text{-}11)$$ /85

If we calculate the average velocity profile using the Prandtl mixing length model (2-5) with the mixing length L according to (2-8), then we obtain the same profile for large distances from the wall if the constant used in (2-8) is set equal to $A_w = 4$. A_w and $E_{1,2}$ are therefore constants which both consider the wall roughness and cannot be selected independently. The value $A_w=4$ will therefore also be used in (5-88).

7.4. Wall Condition for the Azimuth Velocity Component v_φ

For the component $\overline{v_\varphi}/\text{wall}$ we essentially have the same formulas as for the axial component. However, since in this case the average velocity is always zero, we set:

$$\overline{\nu + \frac{\partial}{\partial r}\left(\frac{v_\varphi}{r}\right)} \approx \left(\tau_{\mu_1}+\nu\right) R1 \frac{2}{\Delta r_1}\left(\frac{\overline{v_{\varphi_2}}}{r_1}\right). \qquad (7\text{-}12)$$

Therefore we assume a linear variation of $\left(\frac{v_\varphi}{r}\right)$ and the error thereby produced is somewhat corrected by considering the turbulent viscosity r_μ which is the result of the fine structure model.

7.5. Calculation of the Average Wall Shear Stresses

As already mentioned in Chapter 7.3, the average wall shear stresses $\langle \tau_{w_1} \rangle, \langle \tau_{w_2} \rangle$ can only be calculated for plate flows with the same wall roughnesses of both walls from a force balance and by considering the symmetry. In all other cases it is necessary to calculate $\langle \tau_{w_1} \rangle, \langle \tau_{w_2} \rangle$ from the numerical solution itself. Following we will discuss the computation procedure for the inner wall. For stationary turbulence, we obtain the time

average from a force balance on the ring of wall meshes, according to the following diagram

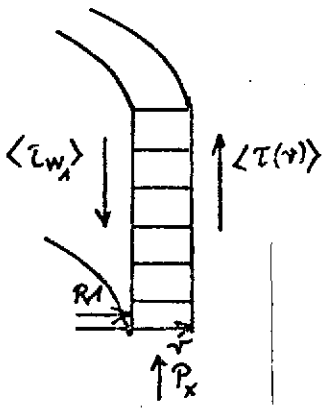

$$\langle \tau_{W_1} \rangle = \langle \tau(r) \rangle \frac{r}{R1} + P_x \frac{r^2 - R1^2}{2\,R1} \qquad (7\text{-}13)$$

The wall shear stress can be calculated from a force balance if the average shear stress variation $\langle \tau(r) \rangle$ is known in the interior. This is calculated from /86

$$\langle \tau(r) \rangle = -\rho \left\langle \tilde{v}_x^r \tilde{v}_r^x \right\rangle + \rho \nu \delta_r \langle v_x \rangle + \rho \left\langle \nu \delta_r \left(\bar{v}_x - \rho \langle \bar{v}_x \rangle \right) \right\rangle \qquad (7\text{-}14)$$

At the beginning of the integration the wall shear stress is specified per input and it is again recalculated when the stationary solution is obtained according to the formulas given above. This process is then repeated after the integration time until the wall shear stresses no longer change. Instead of the time average value we use the periodic average value as an approximation, which does not produce any error for sufficiently large period lengths * .

* However, see Chapter 10.4.7.

7.6. Wall Condition for the Kinetic Energy $\overline{E'}^{\nu}$

All the velocity fluctuations vanish at the wall and therefore the fluctuation motion energy is also zero there. This wall condition can be considered in an exact way for the convective terms. For the diffusion terms it is necessary to know the gradient $\frac{\partial}{\partial r}\overline{E'}^{\nu}\Big|_{Wall}$. It does not make sense to calculate this gradient from $\frac{\partial}{\partial r}\overline{E'}^{\nu}\Big|_{Wall} = \overline{E'}^{\nu}_1/(\Delta r_1/2)$ because $\overline{E'}^{\nu}$ has a maximum very close to the wall, as experiments [18, 76] have shown. Therefore we set

$$\frac{\partial}{\partial r}\overline{E'}^{\nu}\Big|_{Wall} = c_{11}\,\overline{E'}^{\nu}_1/(\Delta r_1/2) \qquad (7\text{-}15)$$

where $0 \leqslant c_{11} \leqslant 1$. For these calculations, we will use $c_{11} = 0.2$ in this paper.

When the source term is calculated for the energy equation, it is necessary to calculate the squares of velocity deformations, and at the wall the radial gradient of the deviation of the velocities from its periodic average value must be known. Here we will use linear gradient approximations.

7.7. Wall Condition for the Pressure

According to (6-12) it is necessary to know $\overline{\partial \tilde{v}_r/\partial t}^{r}\Big|_{Wall}$, and this is the area average value of the radial acceleration of the wall which would be obtained if the pressure were not considered. If we consider the momentum equation of this component for such a mesh area element which occurs at the wall, it can be seen that because of the wall adhesion condition, all terms vanish except for the radial diffusion term: /87

$$\overline{\frac{\partial \tilde{v}_r}{\partial t}}^{r}\Big|_{wall} = \overline{\frac{1}{r}\frac{\partial}{\partial r}\left(r\left(\nu + \nu_\mu\right)\frac{\partial v_r}{\partial r}\right)}^{r}\Big|_{wall} \qquad (7\text{-}16)$$

From the continuity equation (1-8) it follows that

$$\frac{\partial v_r}{\partial r} = -\frac{v_r}{r} - \frac{1}{r}\frac{\partial v_\varphi}{\partial \varphi} - \frac{\partial v_x}{\partial x} \qquad (7\text{-}17)$$

All of these terms vanish at the wall, but not their radial derivative. For calculating it we use the average values over the wall mesh which are available, and we find:

$$\overline{\frac{\partial \tilde{v}_r}{\partial t}}\Big|_{Wall} = -\frac{2(\nu + \overline{\mu}_1)}{\Delta r_1}\left[\frac{\overline{v}_{r_{3/2}}}{R_1} + \frac{\delta_\varphi \overline{v}_{\varphi_1}}{R_1} + \frac{r_1}{R_1}\delta_z \overline{v}_{z_1}\right]. \qquad (7\text{-}18)$$

A similar relationship is obtained for the other wall.

8. INITIAL CONDITIONS

/88

The initial conditions must be prescribed for the velocity fields $\underline{u}$ and the kinetic energy field $\overline{v_{E'}}$ of the fine structure. In order to be effective, these must be prescribed so that they already correspond to the stationary model in the statistical sense as far as possible.

8.1. Initial Values of the Velocity Field

The direct simulation of turbulent flows is based on the hypothesis that the initial values in principle do not have any influence on the statistical properties of the solution when it has reached a statistically stationary state [29]*. In order to make the computation time small up to the point where this stationary state is reached, initial values will be selected which already correspond to the stationary state as much as possible.

---

* This hypothesis can be seen to be valid because according to Chapter 10, the same results are obtained for various grid sizes.

The following requirements are placed on the initial values:

- Fulfillment of the boundary conditions;
- Agreement of the average velocities with corresponding experimental data;
- Agreement of the average kinetic energies with the corresponding measurement data;
- Reasonable energy spectrum which agrees with the Kolmogorov spectrum (4-4) at high wave numbers;
- The incompressibility condition is satisfied.

In order to satisfy the first two requirements, the average velocity profile is specified according to measurements of Laufer [76].

The velocity fluctuations around these average values are calculated from the vector potential $\{Pot_1, Pot_2\}$ [2, 121] in order to observe the incompressibility condition:

$$
\begin{aligned}
{}^{r}\bar{v}_r &= \delta_z \; Pot_1 \\
{}^{\varphi}\bar{v}_\varphi &= \delta_z \; Pot_2 \\
{}^{z}\bar{v}_z &= -\frac{1}{r}\delta_r(r\,Pot_1) - \frac{1}{r}\delta_\varphi(Pot_2) + \langle {}^{z}\bar{v}_z \rangle
\end{aligned}
\qquad (8\text{-}1)
$$

It can easily be seen that the velocity field determined in this way satisfies the continuity equation for all meshes and for arbitrary potentials (Pot_1, Pot_2). /89

In order to produce a velocity field with a reasonable energy distribution, the potentials (Pot_1, Pot_2) are designed by using a random number generator with a given fluctuation width in such a way that the kinetic energy on the average will correspond to the measurements of Comte-Bellot [18] for the three velocity components. In order to produce a Kolmogorov spectrum we use an algorithm which starts with a randomly determined prescribed value at the walls and at the center and which determines

the potential values first at the point which is half-way between the meshes with already specified potential values, so that the resulting velocities are correlated with the neighboring values in proportion to $r^{2/3}$ and where r is the distance between the two reference meshes. According to (4-5), this correlation corresponds to the variation $k^{-5/3}$ of the Kolmogorov spectrum. Figure 16 shows such a randomly produced velocity field in the corresponding energy spectrum for the axial wave numbers. The agreement with the Kolmogorov spectrum is satisfactory even though the produced velocity field may seem somewhat too random. This is based on the calculation of the velocities by differentiation of the potentials according to (8-1).

The method used here only has a heuristic basis. Fox-Deardorff [44] indicate a method briefly for which the energy spectrum is enclosed on the initial values in a mathematically justifiable way by specifying the Fourier transform of the velocity field. However, this method cannot be used for cylindrical coordinates.

8.2. Initial Values of the Kinetic Energy $\sqrt{E'}$

The kinetic energy of the fluctuation velocities inside of the meshes is determined from the velocity field in such a way that if the convection and diffusion terms are ignored, they will correspond to the stationary solution of (5-44):

$$\frac{\partial E'}{\partial t} = c_4 h D^2 \left(\sqrt{E'}\right)^{1/2} - \frac{c_3}{h} \left(\sqrt{E'}\right)^{3/2} \stackrel{!}{=} 0 \qquad (8\text{-}2)$$

$$\sim \quad \sqrt{E'} = \frac{c_4}{c_3} h^2 D^2 \qquad (8\text{-}3)$$

9. THE PROGRAM -TURBIT-1 /90

The numerical simulation of turbulent flows requires an optimal programming technique because of the extensive amounts of data and large calculation times. The programs used here are mostly programmed in FORTRAN. Assembler programs are used for dynamic core storage use and in order to determine the permissible computation time. This is done so that, if the time limit is exceeded, all of the solutions calculated up to that point can be saved on background storage units. A dynamic data management system is used as one of the bases of the program. For this, the required data fields are divided into blocks, except for the auxiliary potential ψ. A block includes all the values of a variable in the same plane parallel to the walls. A subprogram package [126] manages these blocks. Blocks not required at some time are automatically stored on direct access storage units if the core storage space is not sufficient. By corresponding programming, it is possible to have a readout or read-in of one block a maximum of once per time step. Using the assembler subprograms, one is insured that the available core storage is used in the optimal way. A maximum of 34 blocks must fit into the core storage unit at the same time independent of the number of meshes in the radial direction. The subprogram package is so effective that the costs of the calculation take on their minimum when the core storage unit is selected so small that this minimum number of blocks fits into the core storage unit. The program, therefore, requires a 820 K Byte core storage unit for problems with 64*32 meshes for a plane parallel to the walls as well as 32 meshes in the radial direction (without overlay for the program Modulus). Of these, about 260 K are reserved for the auxiliary potential ψ; approximately 200 K are reserved for the program instructions. About 30 K are reserved for an input/output buffer. On the IBM 370/165 in Karlsruhe, the

available core storage space is about 1500 K Byte and therefore problems having 64*64*32 meshes can be calculated. It would be possible to reduce the core storage requirement by dividing the auxiliary potential ψ into data blocks and solving the Poisson equation using the transposition method described in [125,128].

In order to avoid unnecessary calculation operations, all of the expressions which remain unchanged during the calculation are calculated once at the beginning of a calculation. This type of optimization cannot be assigned to an optimizing translator, because it cannot optimize over several subprograms.

In addition, multiple subscripts are avoided and instead the required complicated linear subscripts are calculated without multiplications. In order to minimize the number of square root operations, we do not store the kinetic energy $\overline{E'}$ but $(\overline{E'})^{1/2}$ instead. /91

In order to check the calculations and in order to present the results, we use subprograms [84, 124] for graphical output of the scalar and vector fields in the form of height lines and vector fields. These are especially suited for cylindrical and other curvilinear coordinates. The average quantities as a function of radius or wall distance are produced using the program GRAPHIC [39].

One major problem consists of demonstrating that the programs do not have any errors. There are no test problems having analytical or known numerical solutions for the geometries considered, for which all of the terms in the equations being integrated do not appear in a non-trivial way. The test problems used are laminar flows. See Appendix 8 for this. The solutions for turbulent flows can only be tested using experimental results. For this

see the following chapter.

The program built has been named TURBIT-1. TURBIT is the abbreviation for TURBulenter Impuls Transport, (Turbulent momentum transport)

10. NUMERICAL RESULTS

10.1 Specifications of the Calculated Cases

Two different physical problems are treated: a plate channel and an annulus channel with the radius ratio R2/R1=5. Both problems are characterized by K (Cartesian) or Z (Cylindrical). For each problem case, we consider four different cases K1, K2, K3, K4 and Z1, Z2, Z3, Z4, respectively, which differ regarding the size and shape of the difference grid as well as the period length. K1, Z1 are the cases with the smallest mesh number; K4, Z4 are the cases with the largest mesh number. Tables 12 and 13 contain the exact data for specifying the 8 cases. Non-equidistant meshes are used for cases K4, Z4 in the radial direction:

n	1	2	3	4	5	6	7	8	9	1o	11	12	13	14	15	16
	32	31	3o	29	28	27	26	25	24	23	22	21	2o	19	18	17
$\Delta x_i / \Delta r$	o.o18		o.o2		o.o22		o.o27		o.o33		o.o38		o.o4o		o.o42	

In the other cases we use equidistant meshes. It should be noted that the number of meshes in cases K4, Z4 is 65536 which is substantially larger than the number 6720 used by Deardorff [29] and the 32,000 meshes used in [33]. These numbers do not represent the upper programming limit, which is given only by the available or the sensible computation time. As Figure 12

shows, the computation times (Figure 4) are already so large that a further increase in the number of meshes does not seem to be defensible.

In the cases K1-K3, Z1-Z3 we started with random initial values according to Chapter 8. For the cases K4, Z4, the initial values are obtained by interpolation from the solutions determined in K3, Z3. In this context, the integrated time steps as well as the machine computation times given for K4, Z4, consist of the sum of the values given for K3, Z3 and for K4, Z4 alone.

Table 14 shows the calculation time required per time step. Integration of the $\sqrt{\varepsilon}$ fine structure energy requires on the average of 33% of the computation time. The velocities without pressure correction require 57% and the calculation of the auxiliary potential ψ, or of the pressure p requires only 10% of the computation time per time step.

10.2. Qualitative Description and Evaluation of the Results /93

10.2.1. Three-Dimensional Flow Models

Figure 17 to 20 give an impression of the effort required for the direct numerical simulation of a turbulent flow, as well as the results. These figures show three-dimensional "instantaneous photographs" of the flow fields in the form of vector and contour graphs. Each of them corresponds to an arbitrarily selected plane of the flow space. Only the fluctuation field $\underline{u}'' = \underline{u} - \overset{p}{\langle u \rangle}$ of the velocities is represented. The velocity components in the plane of the drawing are characterized by vectors which start at the point under consideration and which have a length and direction corresponding to the velocity vector. The

fluctuation velocity perpendicular to the plane of the drawing is characterized by contours having a constant contour value difference. In this way we obtain a good plastic representation of the flow processes. In addition, Figures 18, 19 and 20 show the contour representations of the fine structure energy $\overline{v'^2}$ as well as the pressure p defined by (6-3). The contours corresponding to negative function values are given by dashed lines and those corresponding to positive values are given by solid lines. The latter also had markings for identification of the height using the legend given. These figures have markings at the edges which characterize the separations between meshes. For the solid ring figures, these markings are partly inside of the flow space (for example, Figure 17). Here one can clearly see the non-equidistant radial mesh separations as well as how the periodic boundary conditions are satisfied.

The most important results shown by the figures is the fact that the flow fields presented are indeed as irregular as one imagines turbulent flows to be. This fact is an important argument for the fact that the program used does not have any errors. As is well known, many program errors lead to some kind of regular features which cannot be explained physically. The systematic phenomena which are shown are exactly those one would expect from the physics of the problem. Everywhere one can see that in the vicinity of the wall, the greatest fluctuation motions occur. This is exactly where the kinetic energy production is great because of the large velocity gradient. Because of the large velocity fluctuations, / 94
the $\overline{v'^2}$ values are a maximum and the pressures have extreme values. The fine structure tips shown clearly in Figure 19 which are perpendicular to the flow direction and go from the wall to the center are very interesting. This could be one of the often observed intermittence processes [89,115, 120], for

which the flow is relatively quiet over large regions and the stored energy is transported in pulses from the wall to the center now and then. The figures for the problems with many methods are too confused to be able to follow the motions in detail. Figure 20 for case Z1 is probably better suited for this.

10.2.2. Time Functions and Spectra

Figure 21 shows the flow behavior as a function of time at a location r=0.844, where according to Figure 44 the average shear stress $\langle v_r' \cdot v_x' \rangle$ is positive. The velocity components as well as the macroscopic energy calculated from it are shown, as well as the instantaneous product $v_r \cdot v_x$ and the fine structure energy $\overline{e'}$ starting at t=0, where random initial conditions prevail up to $t \approx 5$. In real dimensions, this dimensionless time at $\hat{D}$ = 18 cm, Re_m = 240 000 und $\hat{u}_o$ = 0.80 m/s corresponds to about one second according to [18] in real time. Perhaps one would have expected a motion which fluctuates more here. However, one should consider the fact that because of the space averaging over individual meshes, the time functions are also smoothed. From this figure one can see that the flow apparently does not move towards a true stationary solution (as is the case for laminar flow). In addition it can be seen that after some time, the "Reynolds stress" $v_x \cdot v_r$ does indeed become mainly positive.

From the time functions given, we calculated the energy spectra and show this on the lower right of Figure 21. Because there is no periodicity here at large frequencies (recalculated here for dimensionless wave numbers) an apparently large contribution of the Aliasing error is produced [50, 9]. The spectra of the space functions $v_x(x), v_\varphi(x), v_r(x)$ also shown do not have such errors, because these functions are periodic according to the model. Nevertheless, both types of spectra have similarities

of the type so that in the center there is a region corresponding to $k^{-5/3}$ which drops off in proportion to k^{-7} at the high wave numbers. This is clearly also shown for the spectra corresponding to cases K4, Z3 (Figure 22) where in the axial direction it is possible to represent more meshes and therefore more wave numbers.

10.2.3. Problem of Formation of the Average Values

The statistical properties of a flow should move towards a stationary state independent of the instantaneous space photographs or the unsteady variations at a point. In Chapter 10.4.1 we will discuss whether or not this state is indeed reached. In the stationary state, when there is a large number of meshes in the x-y-m ir x_1-x_2 planes, respectively, the time averaging should be able to be replaced by periodic averaging over these planes. This assumption was always made for the evaluation of the results. However, under the given conditions (not completely stationary, only a small number of points) this did not actually happen and therefore the period average values shown in Figures 26 to 64 show large fluctuations. The replacement of period averaging by time averaging alone is not practical. For example, Figure 65 shows the velocities at a location as a function of time for the case K3. In order to produce this curve, the computation time is 2 hours on an IBM 370/165. Apparently this computation time is not sufficient to obtain average values with sufficiently small fluctuation widths. The combination of both types of averaging seems desirable. For this, all of the evaluations would have to take place simultaneously with the integration, because it is almost impossible to have intermediate storage of the data for later evaluation for the cases with 65,000 meshes. It should be remembered that the values of the three velocity components plus the fine structure energy require

10^6 Byte of storage per time step. A magnetic tape contains about 10^7 Byte.

10.2.3. Contribution of the Macroscopic Structure to the Turbulent Processes

In Figures 43 and 44 we show the shear stresses as a function of radius (or wall distance) for one plate channel and one annulus channel each. Only the shaded region can be attributed to the fine structure model according to Chapter 5.2.3.1. Therefore, we can see the favorable result that most of the momentum transport is brought about by the macroscopic structure. The method used here simulates the turbulent momentum transport primarily by direct integration of the Navier-Stokes equations.

Figures 34 and 35 show the kinetic energy of the solutions coded according to the calculation methods. The contribution between a zero line and the first curve corresponds to the fine structure energy $\overline{v'^2}$ according to Chapter 5.2.2. The next region was calculated according to (5-92) and differs only slightly from zero. The region above it finally is the energy contribution produced by the macroscopic structure. This energy contribution /96 apparently is not much greater than the contribution of the fine structure. The models used for this are therefore not negligible for the local processes.

In the following chapters we will discuss some of the individual results which will support the physical plausibility of the method. In particular we will make clear that even relatively coarse solutions give reasonable results for cases K2, Z2. This means that the greater amount of effort for the finer resolution corresponding to cases K4, Z4 is not absolutely necessary for future problems.

10.3. Quantitative Comparison with Experiments

10.3.1. Maximum Velocity

In the following we will compare the calculated maximum of the average velocity profile $^{P}\langle u \rangle_{max}$ with corresponding data from the literature. See Table 15 for this.

The agreement between the calculated values and the measured values lies within the experimental measurement errors for the corresponding Reynolds numbers.

For the annulus, Barthels [11] and Maubach [88] predict a reduction of the maximum velocity by 1-2% compared with plate flow. The values calculated here lie between 0-10% under those for plate flow. This means that the tendency is represented correctly.

10.3.2. Velocity Profile

Figure 26 shows the velocity profile calculated for plate flow. The measured values reported by Comte-Bellot [18] and Laufer [76] are shown by dashed lines. The differences between the measured values and numerical results can hardly be distinguished. The profiles for the annulus flow according to Figure 27 show the expected displacements of the maxima towards the inner edge. The difference between a maximum and average velocity is a better measure for the agreement between the calculated and measured profiles than is the graphical representation of the profile. Corresponding numbers are given in Table 16.

It can be seen that the calculated values agree well with the measured values. We can clearly see an improvement of the results compared with those of Deardorff. This is probably due to

the division of the fine structure model into a locally isotropic /97
part and an inhomogeneous part (Chapter 5.2.1).

10.3.3. Fluctuation Velocities

In Figures 28-30 we show the average velocity fluctuations $\rho\langle(u'_{ci})^2\rangle^{1/2}$ for the various components for plate flow. Corresponding results are shown in Figures 31-33 for the annulus. For plate flow, we also show the measured values of Comte-Bellot (dashed lines) for comparison purposes. The agreement of the average values can be considered good. The numerical values do not have as large a variation with wall distance as do the experimental values. This is partly due to the fact that the fine structure energy was assigned uniformly to the various components corresponding to the assumption of local isotropy. In any case, these results are much better than those of Deardorff [29]. There the contributions of the fluctuation velocities were all higher than was the case for the measurements. In the vicinity of the wall, maxima of 5 were indicated for the axial velocity fluctuations. This is about twice as high as the corresponding value measured by Comte-Bellot [18]. Here again we had better agreement because of the separation into a local isotropic and an inhomogeneous fine structure model.

Figures 31-33 show that (except for Z4) the fluctuation velocities for annulus flow are smaller at the inner edge than at the outer edge. This corresponds to the physical realities because for R1/R2→0, i.e. for a circular tube, the fluctuation intensity has a minimum at the center, just like a plate. The deviation for Z4 is attributed to insufficient stationary conditions (see Chapter 10.4.1).

10.3.4. Axial Correlations

The two-point correlations of the axial velocity components in the axial direction were calculated and are compared with the measured values of Comte-Bellot [18] in Figure 36 for x_3=0.5 (center) and in Figure 37 for x_3=0.031 (vicinity of the wall). The agreement of the numerical values is satisfactory within the framework of the statistical scatter for cases K2-K4 for which the period length is 4. Corresponding correlations for the other velocity components are shown in Figure 38 for x_3=0.5. Comparison measurements are not known for this case. The correlation curves clearly verify the result found by Deardorff [29] according to which the axial component is correlated over a larger axial interval than the two other components. This result had been found before Deardorff by Comte-Bellot [18] by determining the correlation lengths from spectrum measurements. These correlation lengths are shown in Figures 39 to 41 for the plate channels. The dashed curve corresponds to the measurements of Comte-Bellot. Here again we can consider the agreement to be satisfactory. Figure 42 shows the corresponding results for an annulus, but without any experimental comparison. /98

10.4. Influence of the Model Parameter

10.4.1. Integration Time (Steadiness)

It is not easy to decide whether the solutions discussed here can be considered stationary in the statistical sense. The period average values have large fluctuations after a relatively long integration time. This is especially clearly seen in Figures 45 and 46 in which the period average values of the accelerations are shown. If we remember that the pressure gradient can only produce an acceleration having the magnitude 2, then the fluctuations of the average accelerations are remarkably large.

This is also true for cases Z1 and Z2, where according to (1-41) the required "start-up time" has greatly been exceeded. It is only from the systematic variations of the accelerations for cases K4, Z4 that one can conclude that the stationary state has not been reached at least for this case. A better measure for closeness to the stationary state is the variation in time of the macroscopic energy $^{V}\langle \bar{E} \rangle$ and the fine structure energy $^{V}\langle {}^{V}\bar{E}' \rangle (t)$ averaged over the entire flow volume at a point in time. For cases K1 and Z3, these variables are shown in Figure 47 as a function of time. The oscillations are much smaller for K1 but this is not so for Z3. From these and similar curves we have the following results: the solutions K1, K2, Z1, Z2 can be looked upon as sufficiently stationary. For cases K3, Z3, the deviations are probably only small. The cases /99 K4, Z4, however, are not stationary in this statistical sense. On the other hand, the substantial increase in the problem time for cases K4, Z4 cannot be defended because of the large computation times.

10.4.2. Period Lengths

One measure for sufficient magnitude of the period lengths X_1, X_2 or $X, \emptyset$, respectively, are the deviations of the two-point correlations for the distances $X_1/2$, $X_2/2$ or $X/2$, $\emptyset/2$ from zero, respectively. Axial correlation coefficients were already discussed in Chapter 10.3.4. Figures 24 and 25 give lucid representation of the correlations. In Figure 24 we show the following using contours for K1, K2, K3:

$$R_{ii}(x_3, x_1) = \frac{{}^{P}\langle u_i(x_1', x_2', x_3) \cdot u_i(x_1' + x_1, x_2', x_3) \rangle}{{}^{P}\langle u_i(x_1', x_2', x_3)^2 \rangle}$$

Figure 25 shows the following for cases Z1, Z2, Z3:

$$R_{ii}(r,\varphi) = \frac{\overline{P}\langle u_i(x',\varphi',t)\cdot u_i(x',\varphi'+\varphi,t)\rangle}{\overline{P}\langle u_i(x',\varphi',t)^2\rangle}$$

The apparent symmetries are a consequence of the periodic nature and period averaging. From Figures 24 and 25, one can see that the correlations first decrease rapidly with increasing distance of the correlated points. This effect is reproduced to about the same extent in all cases. However, at a distance of 1/2 of the period length, it is only in the cases with $x_1=4$ or $\phi = 2$, respectively, that we have sufficiently small correlations (about ± 10%. For the cases K1 and Z1 we still have substantial correlations (KL: ± 20%; Z1: -60%). The period lengths $X_1 = 2$ or $\phi = \pi$, respectively, are not sufficient. From similar figures for plate flow, it also follows that $X_2=1$ is too small. This demonstrates a deficiency of the Deardorff calculations with $X_2=0.7$. On the other hand, the period lengths selected for K2-K4, Z2-Z4 seemed to be sufficient.

10.4.3. Mesh Size

The mesh size is very important for determining the numerical effort as well as the period length. The requirement KM>30 as a prerequisite for the existence of local isotropy is only applicable for cases K4, Z4. Nevertheless we were able to show that it is possible to realize these conditions in practice. /100
As can be seen from the results already discussed and from the Figures 26 to 64, the averaged results do not differ significantly from each other for the cases with different mesh sizes. In addition, all the cases having the same geometry were always treated with the same programs and model constants according to Table 13. These results show that for the expenditure used for

cases K2, Z2, it is possible to obtain physically reasonable results.

10.4.4. Time step Δ t

For the case K2 we integrated over an additional time span of 0.096 starting with the solution at t= 3.8. Three cases were considered:

Case a)	Δt = 0.0015	Both with $^{j}c_{9}$
Case b)	Δt = 0.003	According to (5-73)
Case c)	Δt = 0.003	$^{j}c_{9}$ calculated according to (5-73) just as for Δt = 0.0015

Cases b) and c) gave results for the velocities which differed by about 1% from the solutions for case a), (referred to the total change within this time span of 0.096). The results of case b) for the calculated fine structure energy are closer to the reference solution of case a) than for case c). This is also true for the correctness of the correction factor $^{j}c_{9}$. On the other hand, the reverse holds true for the average velocities. Based on this experience, we suggest a correction factor $^{j}c_{9}$ in future calculations which varies somewhat less with Δt than indicated by Equation (5-73).

The variation of the instantaneous results with a decreasing time step cannot be considered negligible. This experience was also reported in [44]. In the statistical sense, the effects seem to be small. However, we have not yet carried out an exact investigation of this.

10.4.5. Effect of Integration of the Fine Structure Energy Equation

For the case K1, we started with the solution at t=5.6 and integrated over additional problem time of 1.8. First of all $\sqrt{E'}$ was determined by integration of the transport equation derived for it, and then we also used Equation (8-3) according to the method of Deardorff without integrating an additional transport equation. In the second case, we first found larger energies /101
than at the wall meshes, which can be explained by the missing convective and diffusion transport. These increased fine structure energies then lead to a correspondingly larger damping of the coarse structure fluctuations. Nevertheless, the statistical average values vary only slightly. This is a remarkable result. One would have expected that the integration of this additional transport equation, which, in particular avoids the weakness of the Deardorff model indicated under a) in Chapter 5.1.2, would be very important for the accuracy of the result. One can show that when the fine structure energies are calculated from one transport equation, these are almost completely correlated with the source term P according to (5-44), especially for small mesh edge lengths h. In order to show this clearly, we integrated the following initial value problem using Dysys [122], which can be considered a model for equation (5-44)

$$\frac{dE}{dt} = c_4 \cdot h \cdot D^2 \, E^{1/2} - \frac{c_3}{h} \, E^{3/2}$$

$$E(t=0) = E_0(0)$$

$$E_0(t) = \frac{c_4}{c_3} \, h^2 \, D^2$$

$$c_3 = 1 \quad , \quad c_4 = 1.6$$

A harmonic function is assumed for the deformation velocity, and its average value approximately agrees with the true values

$$D^2 = 5\, h^{-4/3} \cdot (1 + \sin(t))$$

The factor $h^{-4/3}$ follows from (4-34). Figure 66 shows the calculated results for h = 0.01, 0.1 and (in order to clearly show the effect) h = 1. One can see from this that as the correlation E(t) and the energy $E_0(t)$ corresponding to the simpler model becomes greater, the smaller h becomes. Clear differences are only found for the unnaturally large mesh distance h = 1. This means that we have found an important positive result for future calculations which states that the effort of an additional integration of the energy equation is not necessary. However, the effort saved is not particularly large, because most of the computation time is required for calculating the source term. /102

10.4.6. The Correction Constants σ_1, σ_2, σ_3

An additional measure for the correlation between the fine structure and the macroscopic deformation velocity is the factor σ_3 defined by (5-82). This factor, as well as the factors σ_1, σ_2 according to (5-14, 15), were determined numerically and are shown in Figures 48 and 49 for cases Z2 and K4. It can be seen that the factors σ_1, σ_2 are clearly closer to the assumed value of one than the value σ_3 which was also assumed to be one in earlier theories. However the deviations of 20% are not serious. As the figures show, these factors are mostly independent of position, mesh size, channel geometry and can be considered as "universal" constants in future calculations:

$$\sigma_1 \approx 1.05\,, \quad \sigma_2 \approx 1.1\,, \quad \sigma_3 \approx 1.2$$

The value of σ_1 given here is in contradiction to the data in Table 13, and will now be explained.

10.4.7. Problem of the Model

In the first test calculations using the method described in Chapters 3 to 8, we first had unexplainably large axial correlations. Part of this effect could be explained and correlated according to Appendix 7. In addition it was found that the calculated viscosities of the locally isotropic fine structure model are too large. Using corresponding artificially changed values of the constant σ_1, according to Table 13, we were able to avoid this effect. The reason for this weakness of the fine structure model is attributed to the fact that the correction c_d suggested in Chapter 5.2, 2.5.2 was not considered. The correction is supposed to take into account the deviation of the actual spectrum from the Kolmogorov spectrum for small wave numbers. However, we do not have any quantitative data for the lengths L according to (5-77, 78).

In addition we find that the calculation of the wall shear stresses according to Chapter 7.5 could not be carried out because the period averages used for this had fluctuations which were too large. The ratio of the wall shear stresses used corresponds to the data of Barthels [11].

10.5. Determination of Turbulence Model Constants /103

10.5.1. Energy-Length Model

10.5.1.1. Calculation of Quantities to be Approximated

In order to prove the usefulness of direct numerical simulations for supporting turbulent models, according to Chapter 2, we calculated the length L defined by (2-13) and the length-production term L-PROD defined by (2-14). For the annulus,

integrals $\int_0^{\infty} y(\tau)\,d\tau$ are replaced by

$$\frac{\int_{R_1}^{R_2} y(\tau)\,\tau\,d\tau}{\int_{R_1}^{R_2} \tau\,d\tau}$$

The results are shown in Figures 52 to 55. The length L first increases with wall distance Z more than k·z (k=Kármán constant) and has a maximum of about 0.17 in the center. The main variation corresponds to our physical expectations. The length production term is about zero in the center and increases towards the walls. It is reasonable to have the production term vanish in the center because it is identically zero for homogeneous turbulence.

10.5.1.2. Calculation of the Constant a_1

Since in addition to the length L we know the shear stresses $\rho\langle u'w'\rangle$, the kinetic enbrgy $\rho\langle E'\rangle$ and the average velocity profile, we can calculate the "constant" a_1 according to (2-9) for each location z from

$$a_1(z) = \frac{-\rho\langle u'w'\rangle}{\rho\langle E'\rangle^{1/2}\,\frac{\partial\langle u\rangle}{\partial z}}$$

The results are shown in Figures 56, 57. First of all it becomes clear that this "constant" is not a true "constant". The calculations show that there is a slight increase of the "constants" with wall distance. The large fluctuations in the center are a consequence of the mathematical uncertainty of the definition of (0/0). Negative values indicate that the signs of $\langle u'w'\rangle$ and $\partial\langle u\rangle/\partial z$ can differ, as Maubach-Rehme [90] also discussed. Based on the large fluctuations, the average value a_1 is weighted from $a_1(z)$ and calculated with $\langle u'w'\rangle$. The results calculated are as follows:

Case	K1	K2	K3	K4	Z1	Z2	Z3	Z4
a_1	0.0848	0.0835	0.0685	0.0672	0.0906	0.091	0.0592	0.0463

The average value is about 0.075. The fact that this value is smaller than the usually assumed value is a consequence of the relatively large values of length in the vicinity of the wall. /104

10.5.1.3. Determination of the Constants a_4 and a_5

First a_5 is assumed to be identically zero and only a_4 is considered. Using the definition

$$a_4(z) = \frac{L\text{-}PROD}{a_1 \sqrt{k\varepsilon'} \left(L \frac{\partial \langle u \rangle}{\partial z} \right)^2}$$

we calculate the values for a_4 as a function of position, and this is shown in Figures 58, 59. Just like a_1, the uncertainty in the definition equation leads to large fluctuations in the center. Independent of this, there is a clear increase in the "constant" a_4 with wall distance. The values of a_4 weighted with L-PROD(z) are:

Case	K1	K2	K3	K4	Z1	Z2	Z3	Z4
a_4	1.049	0.775	1.17	0.513	0.655	0.748	1.12	0.50

The general average value is $a_4 = 0.8$.

Because of the apparent variation with wall distance, the separation of additional terms for approximating the length production is desirable. If we use the additional term with the constant a_5 suggested by Rotta, then we obtain the values a_4, a_5 for the individual cases from the minimum of the following expression $f(a_4, a_5)$:

$$f(a_4, a_5) =$$

$$\int_{R1}^{R2} \left\{ L\text{-}PROD(\tau) - \left[a_1 \sqrt{k\varepsilon'} \cdot L \cdot \frac{\partial \langle u \rangle}{\partial \tau} \left(a_4 \cdot L \cdot \frac{\partial \langle u \rangle}{\partial \tau} + a_5 \cdot L^3 \frac{\partial^3 \langle u \rangle}{\partial \tau^3} \right) \right] \right\}^2 \cdot L\text{-}PROD(\tau) \cdot \tau \, d\tau \stackrel{!}{=} Min$$

The results found for this are as follows: /105

Case	K1	K2	K3	K4	Z1	Z2	Z3	Z4
a_4	1.08	0.78	1.6	0.9	0.47	0.44	0.95	0.65
a_5	-0.13	-1.5	-1.1	-1.2	0.39	0.92	0.40	-0.13

From this we can see the following:

a) The magnitudes of the constants can only be calculated with large uncertainties.

b) The magnitudes of the constants a_5 have the same order of magnitude as those of a_4; therefore, it does not seem justified to ignore the additional term weighted with a_5.

c) For the plate and the annulus under consideration, there are different optimum values of a_4, a_5. For the plate in the center we have

$$a_4 = 1. \qquad a_5 = -1.$$

and for the annulus with R2/R1 = 5: we have

$$a_4 = 0.6. \qquad a_5 = 0.4$$

The reason for these differences could be that the minimum of the production term is closest to the inner wall for the annulus than the maximum of the average velocity profile. The approximation theorem assumes that these locations coincide. From these results it becomes clear that new trial solutions must be developed

for approximating the shear stresses as well as the length production term, for which the coincidence of the zero point of these variables and the maximum of the average velocity profile does not have to be assumed in the trial solution. /106

10.5.2. Pressure Deformation Velocity Correlation

10.5.2.1. Calculation of Terms to be Approximated

Turbulence models which contain transport equations for $\langle u_i' u_j' \rangle$ require models for correlations

$$PU_{ij} \equiv \left\langle p' \left(\frac{\partial u_i}{\partial x_j} + \frac{\partial u_j}{\partial x_i} \right) \right\rangle$$

These terms cause the energy exchange of fluctuation components of high intensity to those having a lower intensity [108, 115, p. 123, 53, p. 253]. These correlations are calculated only from the coarse structure of the numerical solutions. Figures 60 and 61 show PU11, PU22, PU33, PU13 for one plate and annulus channel. Figure 62 showed the various results for PU11 alone. Figures 60 and 61 show that the calculated correlations correspond to the expected variation. PU11 is negative and PU22, PU33 are positive. This means that because of the pressure, energy is transferred from the axial component to the other components. PU13 shows the negative proportionality with the shear stress $\langle u_1' u_3' \rangle$ as predicted by Rotta [108]. Figure 62 shows that there are differences in the correlation magnitudes for the various cases. The fact that the magnitudes do not increase with the number of meshes apparently proves the fact that the correlations considered are indeed represented by the coarse structure. On the other hand, PU11 has the smallest magnitude for the case K4. This is probably due to deficient stationary conditions.

10.5.2.2. Determination of the Constant kp

If we use the model trial solution of Rotta (A1-48) and $\langle\varepsilon\rangle$ is calculated from

$$\langle\varepsilon\rangle = a_2 \cdot \frac{\langle e'\rangle^{3/2}}{L}$$

where L is given by Chapter 10.5.1.1 and we use the working variable

$$a_2 = 1,$$

then it is possible to calculate the "constant" kp. As expected (A1-48) only apply for homogeneous turbulence [108] and different values $KP_{ij}(z)$ are obtained for the various indices i, j of PUij and different locations z, as shown in Figures 63, 64. As a rule the values are all positive as predicted. The average value is 0.5. If instead of a_2=1 we use the value suggested by Rotta [116] a_2=0.18, then the magnitudes of the constants will be at 2.8 on the average and then agree well with the 2.5 which follows from experiments [115, p. 126]. After this paper there should be a /107
further evaluation of the numerical results in order to consider the inhomogenuity of the turbulence in the model. In addition, the often-discussed relationship [4] between pressure fluctuations (Figures 50, 51) and the velocity fluctuations could be investigated. Obviously we have proven the usefulness of the numerical method for this purpose by means of the evaluations given above.

11. CONCLUSIONS /108

11.1. Summary of the Most Important Results

A numerical differencing method is presented with which it is possible to simulate three-dimensional, unsteady, incompressible turbulent momentum transport for Reynolds number $Re_m > 10^5$ in plate and, for the first time, in concentric annulus channels by direct integration of the Navier-Stokes equations.

This method is realized in the program TURBIT-1. The maximum useable number of difference meshes is not restricted by the available storage because of a dynamic data management system, but only by the allowable computation times. Eight different cases were simulated, and in two cases, the flow space under consideration was divided into 64*32*32=65536 meshes. This is much higher than mesh numbers used earlier.

Based on this still insufficient number of meshes, a fine structure model is required with which it is possible to calculate Reynold stresses in an approximate way, which appear as unknown variables in the averaging of the Navier-Stokes equations over one difference grid. It is shown that these Reynolds stresses represent area average values of the fluctuation velocity correlations and not volume average values. In this paper we develop a model which differs from earlier suggestions [29, 81] by the following characteristics:

- A distinction is made between the locally isotropic and the inomogeneous contribution. The locally isotropic contribution vanishes according to definition when the time average is taken. The inhomogeneous part makes it possible to apply the method even for relatively large meshes.

- The model considers the different dimensions of the difference meshes in the various directions, as well as the difference quotients used. This is an important assumption for the applicability of the method for curvilinear coordinates, where the mesh shape must vary with location.

- The turbulent viscosity is calculated according to a trial solution of the Boussinesq type from the macroscopic velocity deformation and the kinetic energy of the fluctuation motion within a mesh. A special transport equation is integrated

for this purpose. / 109

- The model for the locally isotropic part of the fine structure is calculated essentially exactly from the assumption of locally isotropic turbulence with the Kolmogorov spectrum. The solutions of the complicated integrals which occur in this case are approximated by convenient approximations.

By evaluating known experimental results, it is shown that the assumption of a locally isotropic fine structure model is valid for Reynolds numbers Re > 10^5 if the mesh edge lengths are less than about 1/30 of the distance between the walls.

The difference method allows radial non-equidistant meshes. Correspondingly, according to the Neumann criterion, stability criteria are established for the linearized difference equations, of the type that have not existed before for such complicated formulas. Among other things, it is shown that the DuFort-Frankel model for approximating the diffusion terms in multi-dimensional flows with small viscosities and simultaneous convection is not suitable. The accuracy of the differencing method is discussed. The pressure is exactly solved in an effective five way by solving the Poisson equation using the fast Fourier transformation, except for rounding errors.

Numerical results have been given for plate flow and one annulus channel (R2/R1=5). Four cases were presented for both problems, and they differ as to the number of difference meshes and period lengths. The numerical results agree well with the experimental values. This is especially true for the velocity profile and the average velocity fluctuations, where we found a substantial improvement over the results of Dearforff [29]. The results are mostly independent of the mesh number used. Physically reasonable results are already obtained for 32·16·16= 8192 meshes. In addition it was shown that the additional effort

for integrating the fine structure energy equation is not necessary. Problems occur in the quantitative determination of the fine structure model and in the calculation of the wall shear stresses.

It is shown that the method is a useful tool for the quantitative determination of turbulence models, using the example of the energy-length model and the pressure-velocity deformation correlation. In particular it is possible to simulate those terms which are primarily determined by the coarse structure of turbulence. From the numerical results, it is possible to also calculate quantities which cannot be measured or are difficult to measure.

11.2. Suggestions for the Application and Further Development of the Methods Presented /110

In the future the methods developed will be used to test turbulence models, to complete such models and to improve such models. In some cases it will be possible to simply refer to the already available space velocity fields without any further integration.

Then one should attempt to remove the deficiencies of the model which were discussed above. Among these we have the following:

- Consideration of the spectrum for small wave numbers (Chapter 5.2.2.5.2).
- Consideration of the random nature (Chapter 5.2.2.5.1
- as well as A5.1) and the removal of the assumption of local isotropy for large mesh sizes.

The program can be extended to annulus flows with simultaneous rotation of the walls or induced angular momentum, as well as flows in four-cornered channels, where it will then be possible

to also consider secondary flows. This can be done without any substantial increased theoretical work. It is more difficult to simulate recirculating flows, but this seems possible, such as for example flows around obstacles [75], around buildings (houses, cooling towers, etc.) [63] and around ribs. One assumption to be made here is that there is a limited flow space with boundary conditions defined on all sides (for example, periodic boundary conditions). The simulation of tube flows or similar problems will be difficult, for which the natural coordinates have singular points.

In addition, the turbulent transport of scalar variables such as for example the enthalpy | can be simulated using the momentum. The additional effort is not excessive, because four of the quantities (3 velocity components, one energy) are already contained in the method. An additional variable will therefore require only about 25% more effort. Fine structure models having a similar accuracy as well as momentum models do not yet exist, especially when one wants to consider small Prandtl numbers, for example. However, it seems possible that a quantitative model can be derived from the theory of isotropic turbulence and by measuring the corresponding spectra [17, 106]. With a major effort, it will probably be possible to investigate problems of environment and local meteorology using the method discussed here. For example, the stability of the atmosphere (already treated by Dearforff [33] for similar problems) could be investigated when there are large heat sources concentrated in space, such as for example power generating stations.

APPENDIX 1

The Theory of Isotropic Turbulence and Its Experimental Verification

In this section we will develop the theoretical bases in detail which are required from the theory of isotropic turbulence so that the fine structure model can be determined quantitatively. The local isotropic condition and the Kolmogorov spectrum are especially important here. We will report on the experimental verification of these factors.

A1.1. Kinematics of Isotropic Turbulence

In this chapter we will describe and define a number of quantities for describing isotropic turbulence. We will derive relationships (according to [53]) which follow only from the invariance condition of isotropy as well as from the continuity equation (1-6). These relationships are therefore of a kinematic nature.

A1.1.1. Correlation $R_{ij}(\underline{r})$

In order to determine the fine structure model we will require correlations of velocities at two locations. We define the two-point correlation as follows [53, 66]

$$R_{ij}(\underline{x},\underline{r}) \equiv \left\langle u_i\left(\underline{x}-\tfrac{1}{2}\underline{r}\right)\cdot u_j\left(\underline{x}+\tfrac{1}{2}\underline{r}\right)\right\rangle. \qquad \text{(A1-1)}$$

For isotropic turbulence because of the invariance with respect to translation we have

$$R_{ij}(\underline{x},\underline{r}) \equiv R_{ij}(\underline{r}) \qquad \text{(A1-2)}$$

From the invariance with respect to rotation we have [66]:

$$R_{ij}(\underline{r}) = \frac{F(r) - G(r)}{r^2} r_i r_j + G(r)\,\delta_{ij} \qquad \text{(A1-3)}$$

Here F and G are scalar functions of the magnitude of $\underline{r}$

$$r \equiv \sqrt{r_i^2}, \qquad \text{(A1-4)}$$

which can be interpreted as longitudinal and transverse correlation:

$$F(r) = \langle u_1(\underline{x} - \tfrac{1}{2} r \underline{e}_1) \cdot u_1(\underline{x} + \tfrac{r}{2} \underline{e}_1) \rangle \qquad \text{(A1-5)}$$

$$G(r) = \langle u_2(\underline{x} - \tfrac{1}{2} r \underline{e}_1) \cdot u_2(\underline{x} + \tfrac{1}{2} r \underline{e}_1) \rangle \qquad \text{(A1-6)}$$

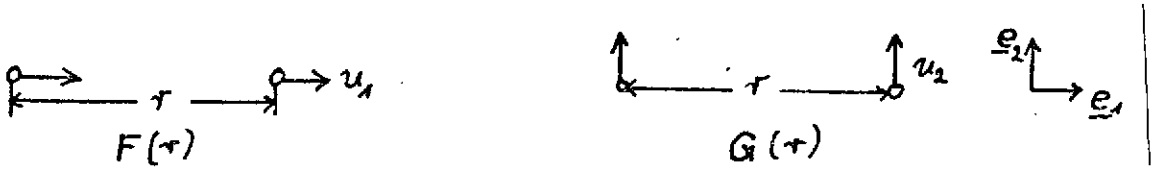

Because of the continuity equation we have: /112

$$\frac{\partial}{\partial r_i} R_{ij}(\underline{r}) = 0 \qquad \text{(A1-7)}$$

from which it follows that [66]:

$$G(r) = \frac{1}{2r} \frac{\partial}{\partial r} \left(r^2 F(r)\right) \qquad \text{(A1-8)}$$

A1.1.2. Energy Spectrum

A turbulent flow can be imagined as a superposition of trigonometric velocity functions where the position $\underline{x}$ is a variable and with different wave numbers $\underline{k}$ [132]:

$$u_i(\underline{x}, t) \sim \int v_i(\underline{k}, t) \exp\left\{\sqrt{-1}\ \underline{k} \cdot \underline{x}\right\} d\underline{k} \qquad \text{(A1-9)}$$

$\underline{k} = \{k_1, k_2, k_3\}$ is the wave number vector with the dimension [1/length]. It is possible to determine the energy contribution of the velocity field within a certain wave number interval.

The distribution of energy into various wave number regions is called the energy spectrum. A distinction is made between a "one-dimensional energy spectrum $E_1(k)$", a "three-dimensional tensor energy spectrum $E_{ij}(\underline{k})$" and a "three-dimensional, average (scalar) energy spectrum $E(k)$".

The tensor energy spectrum $E_{ij}(\underline{k})$ is defined as the Fourier transform of the correlation $R_{ij}(r)$ [53].

$$E_{ij}(\underline{k}) = \frac{1}{8\pi^3} \iiint_{-\infty}^{\infty} R_{ij}(\underline{r}) \exp\{-\sqrt{-1}\, \underline{k}\cdot\underline{r}\}\, d\underline{r} \qquad \text{(A1-10)}$$

The one-dimensional spectrum $E_1(k_1)$ is defined as the (one-dimensional) Fourier transform of the longitudinal correlation $F(r_1)$ according to (A1-5)

$$E_1(k_1) = \frac{1}{\pi} \int_{-\infty}^{\infty} F(r_1) \exp\{-\sqrt{-1}\, k_1 r_1\}\, dr_1 \qquad \text{(A1-11)}$$

The three-dimensional scalar spectrum $E(k)$ is finally defined as the integral of $E_{ii}(\underline{k})$ over all wave numbers $\underline{k}$, which have a magnitude of k:

$$E(k) \equiv \iint_{|\underline{k}|=k} E_{ii}(\underline{k})\, d\underline{k} \qquad \text{(A1-12)}$$

In practice, only $E_{ij}(\underline{k})$ can be described mathematically. $E_1(k_1)$ can be determined by measuring the correlation $F(r)$. We will be most interested in $E(k)$ so that the following calculations will be needed [53] /113

$$E_1(k_1) = \int_{k_1}^{\infty} \frac{E(k)}{k}\left(1 - \frac{k_1^2}{k^2}\right) dk \qquad \text{(A1-13)}$$

$$E(k) = 2\pi k^2 E_{ii}(\underline{k}), \quad |\underline{k}| = k \qquad \text{(A1-14)}$$

Just like (A1-3,8) we can show that:

$$E_{33}(k_1 \underline{e}_1) = E_{22}(k_1 \underline{e}_1) = \frac{1}{2}\left(E_{11}(k_1 \underline{e}_1) - k_1 \frac{dE_{11}(k_1 \underline{e}_1)}{dk_1}\right) \qquad \text{(A1-15)}$$

A.1.1.3. Relationships between the Correlations and the Scalar Energy Spectrum E(k)

According to Hinze [53] as a consequence of (A1-3, 5, 10, 12) we have:

$$F(r) = 2 \int_0^\infty E(k) \left(\frac{\sin(kr)}{k^3 r^3} - \frac{\cos(kr)}{k^2 r^2} \right) dk . \qquad \text{(A1-16)}$$

Because of (A1-3) and (A1-8) we can therefore determine $R_{ij}(\underline{r})$, if E(k) is known using (A1-11) we can also determine $R_{ij}(r)$ from one-dimensional measurements.

In the following we will derive a few formulas which are suitable for the direct calculation of $R_{ij}(\underline{r})$ if E(k) is known and also can be used when E(k) is singular at k=0 in a way which is weaker than k^{-2}.

First we will consider $R_{11}(\underline{r})$ and R_{33} are found in a similar way.

From (A1-3) and (A1-8) it follows that:

$$R_{11}(r) = \frac{1}{2r} \frac{\partial}{\partial r} \left[(r^2 - r_1^2) F(r) \right] \qquad \text{(A1-17)}$$

If Equation (A1-16) is substituted for F(r) and if we subtract $R_{11}(0)$ in order to avoid the singularity at k equal to zero, we find

$$R_{11}(r) - R_{11}(0) = 2 \int_0^\infty E(k) \left\{ A(r \cdot k) - \frac{r_1^2}{r^2} B(r \cdot k) \right\} dk , \qquad \text{(A1-18)}$$

where

$$A(rk) \equiv \frac{\sin(rk)}{rk} - \frac{\sin(rk)}{(rk)^3} + \frac{\cos(rk)}{(rk)^2} - \frac{2}{3} \qquad \text{(A1-19)}$$

and

$$B(rk) \equiv \frac{\sin(rk)}{rk} - 3 \frac{\sin(rk)}{(rk)^3} + 3 \frac{\cos(rk)}{(rk)^2} .$$

A series expansion which is valid in the range from $C \leq rk \leq \frac{\pi}{2}$ /114/ except for an error of 10^{-7} and which is useful for the numerical evaluation* of the integral for a small k·r for arbitrary E(k) results in **:

$$A(rk) = -\frac{2}{15}(rk)^2 + \frac{1}{140}(rk)^4 - \frac{1}{5670}(rk)^6 + \frac{1}{399168}(rk)^8 - \ldots$$
$$B(rk) = -\frac{1}{15}(rk)^2 + \frac{1}{210}(rk)^4 - \frac{1}{7560}(rk)^6 + \frac{1}{498960}(rk)^8 - \ldots \qquad \text{(A1-20)}$$

It can be seen that the integrand is still not non-singular if we have $E(k) \sim k^{-n}$ with $n<2$.

The other correlations $R_{ij}(\underline{r})$ for $i \neq j$ are then found according to (A1-3) and (A1-8) as follows

$$R_{ij}(\underline{r}) = -\frac{r_i r_j}{2r}\frac{\partial F(r)}{\partial r}$$
$$= -\frac{r_i r_j}{2r}\frac{\partial R_{11}(r_1 \cdot e_1)}{\partial r_1}, \quad i \neq j \qquad \text{(A1-21)}$$

from the formulas given above.

A1.1.4 Relationships between the Square of the Deformation Velocity, Dissipation and Energy Spectrum and Correlations, respectively

The dissipation ε according to (1-16) is defined as follows:

$$\varepsilon = \nu\left(\frac{\partial u_i}{\partial x_j} + \frac{\partial u_j}{\partial x_i}\right)\frac{\partial u_i}{\partial x_j}$$

Because of the following relationship which can be derived from the definition (A1-1) for isotropic turbulence

---

* For the Kolmogorov spectrum, an analytical integration is possible, see Chapter 4.3.6.

** When such series expansions are determined, FORMAC [135] is found to be very helpful.

$$\left\langle \frac{\partial u_i}{\partial x_k} \frac{\partial u_j}{\partial x_e} \right\rangle = - \left. \frac{\partial^2 R_{ij}(\vec{r})}{\partial x_k \partial x_e} \right|_{\vec{r}=0} \qquad \text{(A1-22)}$$

we have

$$\left\langle (\partial u_1/\partial x_1)^2 \right\rangle = \left\langle (\partial u_2/\partial x_2)^2 \right\rangle = \left\langle (\partial u_3/\partial x_3)^2 \right\rangle = - \left. \frac{\partial^2 R_{11}(r_1 \cdot e_1)}{\partial r_1^2} \right|_{r_1=0}$$

$$\left\langle (\partial u_1/\partial x_2)^2 \right\rangle = \left\langle (\partial u_2/\partial x_1)^2 \right\rangle = \left\langle (\partial u_3/\partial x_1)^2 \right\rangle = \ldots \qquad \text{(A1-23)}$$

$$\left\langle (\partial u_1/\partial x_2) \cdot (\partial u_2/\partial x_1) \right\rangle = \left\langle (\partial u_1/\partial x_3) \cdot (\partial u_3/\partial x_1) \right\rangle = \ldots$$

$$\left\langle \frac{v_x e}{z_n e} \frac{z_x e}{r_n e} \right\rangle \frac{\tau}{\nu} - = \left\langle \left(\frac{v_x e}{z_n e} \right) \right\rangle \frac{\tau}{\nu} = \left\langle \left(\frac{v_x e}{r_n e} \right) \right\rangle$$

and therefore

$$\langle \varepsilon \rangle = 15 \nu \left\langle (\partial u_1/\partial x_1)^2 \right\rangle = - 15 \nu \left(\frac{\partial^2 F(r)}{\partial r^2} \right)_{r=0} \qquad \text{(A1-24)}$$

/115

From (4-16, 24) it also follows that

$$\langle \varepsilon \rangle = 2 \nu \int_0^\infty E(k) \, k^2 \, dk \qquad \text{(A1-25)}$$

and therefore we find the following for the average square of the deformation velocity

$$\left\langle \tfrac{1}{2} D_{ij}^2 \right\rangle \equiv \langle \varepsilon / \nu \rangle \qquad \text{(A1-26)}$$

$$\langle D_{ij}^2 \rangle = 4 \int_0^\infty E(k) \, k^2 \, dk \qquad \text{(A1-27)}$$

From (A1-24) we find

$$\left. \frac{\partial^2 F(r)}{\partial r^2} \right|_{r=0} = - \frac{2}{15} \int_0^\infty E(k) \, k^2 \, dk \qquad \text{(A1-28)}$$

and in general we have [115, p. 99]:

$$\left. \frac{\partial^{2n} F(r)}{\partial r^{2n}} \right|_{r=0} = \frac{2 (-1)^n}{(2n+1)(2n+3)} \int_0^\infty E(k) \, k^{2n} \, dk \qquad \text{(A1-29)}$$

A1.2 Energy Spectra Based on Models of the Dynamics of Locally Isotropic Turbulence

A1.2.1. Summary

In the previous chapter we saw that many variables used to describe isotropic turbulence are purely kinematic in nature if the scalar energy spectrum E(k) is known. Figure 6 shows the principal variation of the energy spectrum for isotropic turbulence.

E(k) is zero for k = 0, because for isotropic turbulence the average velocity is zero. E(k) then increases and has a maximum at the wave numbers $k_{max} \sim \frac{1}{L_{max}}$, and L_{max} is considered to be the diameter of those turbulence balls which carry the greatest part of the kinetic energy of the fluctuation motion. At large wave numbers (according to equation (A1-25)) the molecular viscosity forces bring about a conversion of the kinetic energy into heat and E(k) then goes to zero for large k. For very large wave numbers, another maximum could be possible which would represent the Brownian molecular motion. In order to be /116 able to consider the flow as a continuum (according to the assumption of Chapter 1.3) this maximum must be located at wave numbers which are much greater than the wave numbers for which the spectrum becomes zero because of the molecular viscosity.

We will now assume that using the differencing method, the wave number range can be explicitly resolved in the grid between k = 0 and $k=k_{grid}$, where we at least have:

$$k_{grid} > k_{max}$$

The region which cannot be resolved in the grid, that is the fine structure, corresponds to wave numbers $k \gtrsim k_{grid}$. Since we require

models for this fine structure, we will present a turbulent model with which it is possible to give a quantitative description of the energy spectrum E(k) for $k \gtrsim k_{grid}$.

In the following section we will discuss the ideas of energy transport set forth by Kolmogorov [67], Weizsäcker [139], and others [92, 93, 52], and this will finally result in a trial solution for E(k) based on dimensional analysis. Part of the model can be explained from consideration of the exact equations [103].

A1.2.2 Model of Energy Transport in the Wave Number Space ("Cascade Process")

For sufficiently large Reynolds numbers it is possible to look upon a turbulent flow as the result of a transition of various sizes of vortices (" turbulence balls" or "spectral elements"). Only the largest of these vortices are a direct consequence of the instability of the average flow. The motion of the largest vortices itself is unstable and produces vortices having a smaller characteristic length or a larger characteristic wave number, respectively.

Taylor-Green [131] gave an explanation for this instability. Accordingly, a turbulence ball having a diameter d_o and a rotation w_o is "swelled" because of turbulent diffusion and (as I would like to add) centrifugal acceleration. However, since we have

$$\omega = \omega_o \cdot \frac{d}{d_o}$$

its rotation will increase in proportion to the diameter d. The /117
ball can only "swell" up to the point where the dissipation $\varepsilon \sim \nu\omega^2$ brings about its decomposition into smaller vortices.

For an incompressible fluid, we can only have an enlargement of the turbulence ball in the radial direction if fluid can flow to the ball parallel to the rotation axis. This is a good example which shows that certain flow processes in turbulent flow can only occur in three dimensions.

After a large number of such "cascade processes" have occurred, the characteristic lengths are so small that the viscosity forces are greater than the inertia forces (the Reynolds number formed with the length becomes small)and the kinetic energy is transformed into heat. It is important to note that the viscosity forces are only effective for small balls or large wave numbers. According to Kolmogorov and others, it is postulated that in wave number space there is a range $k_o < k < k_1$ in which only the inertia forces are effective. This range is called the "inertial subrange" or "range determined by inertia forces". In this range, neither the viscosity ν nor the macroscopic geometry, i.e. the manner of producing the large turbulence balls, are of any consequence.

A1.2.3. Kolmogorov-Pao Spectrum, Kolmogorov Length

According to the model described above, the energy spectrum in the inertial subrange can only be determined by the sizes of the balls or their wave number k as well as by the energy transport from the small wave numbers to the large wave numbers. In the final analysis, this is determined by the total dissipation $\langle\varepsilon\rangle$. From a dimensional analysis we find the following conclusion

$$E(k) = \alpha \langle\varepsilon\rangle^{2/3} k^{-5/3} \qquad \text{(A1-30)}$$

Here α is the Kolmogorov constant (see Chapter A1.2.4 for the value). The upper limit k_o of the inertial subrange is given by

$$k_0 \approx 1/L_0 \qquad \text{(A1-31)}$$

where L_o is an integral length scale such as for example the Prandtl mixing length, which has the order of magnitude between 10^{-2} to 10^{-1}. The upper limit

$$k_1 \approx 1/\eta \qquad \text{(A1-32)}$$

is characterized by the "Kolmogorov length" η (see Chapter 1.6.1) which characterizes the ball diameter for which the viscosity forces and the inertia forces which cause energy transport (proportional to $\langle\varepsilon\rangle$) from the small wave numbers to the large wave numbers have the same order of magnitude. From a dimensional analysis we find in this case

$$\eta \sim \left(\frac{\nu^3}{\langle\varepsilon\rangle}\right)^{1/4} \qquad \text{(A1-33)}$$

Based on the exact model of Pao [103], we find the following for the spectrum.

$$E(k) = \alpha \langle\varepsilon\rangle^{2/3} k^{-5/3} \cdot \exp\left\{-\frac{3}{2}\alpha\left[\left(\frac{\nu^3}{\langle\varepsilon\rangle}\right)^{1/4} \cdot \frac{1}{k}\right]\right\} \qquad \text{(A1-34)}$$

Therefore we assume that the missing proportionality factor in (4-33) is equal to one. The Kolmogorov spectrum (4-30) therefore applies in a range

$$\frac{1}{L_o} < k < \frac{1}{\eta}, \qquad \text{(A1-35)}$$

where it is probably more appropriate to replace the symbol < by the symbol <<. See Chapter 1.6.1 and Figure 2 for an estimation of the order of magnitude of η.

A1.2.4. The Magnitude of the Kolmogorov Constants

Table 3 gives information on measurements, theoretical estimates and recommendations for the magnitude of the Kolmogorov constant α. It can be seen that the measured values scatter between 1.41 and 1.7 for the various types of flows (also in a channel flow). Therefore, the value

$$\alpha = 1.5 \qquad \text{(A1-36)}$$

seems reasonable and will be used in this paper.

A1.2.5. The Spectrum Outside of the Region Determined by Inertia Forces

For very small wave numbers, theoretical predictions [53,115] state that either

$$E(k) \sim k^4 \qquad 0 \leq k \ll \frac{1}{L_0} \tag{A1-37}$$

or

$$E(k) \sim k^2 \qquad 0 \leq k \ll \frac{1}{L_0} \tag{A1-38}$$

/119

For the range $k > k_0 \left(= \frac{1}{L_0}\right)$, Heisenberg gave the following spectrum [52]

$$E(k) = \alpha \langle \varepsilon \rangle^{2/3} k^{-5/3} \left[1 + \frac{27}{8}\alpha^3 \eta^4 k^4\right]^{-4/3} \tag{A1-39}$$

For $k \ll \frac{1}{\eta}$ we also find the Kolmogorov spectrum from this. For $k \gg \frac{1}{\eta}$ we find the proportionality k^{-7}

$$E(k) = \frac{1}{\alpha^3}\left(\frac{2}{3}\right)^4 \frac{\langle \varepsilon \rangle^2}{\nu^4} k^{-7}, \qquad k \gg \frac{1}{\eta} \tag{A1-40}$$

However, this cannot be valid for arbitrarily large wave numbers, because otherwise integrals of the type

$$\int_0^\infty E(k) k^{2n} \, dk$$

would no longer exist for $n \geq 4$, in contrast to the higher derivatives for the longitudinal correlations F(r) according to (A1-24). Therefore it seems that the Pao spectrum (A1-34) is more general.

A1.2.6. Calculation of the Correlation for Turbulence with the Kolmogorov Spectrum

If E(k) is substituted in (A1-18) according to (A1-30), then using the auxiliary formulas [13]

$$\int \frac{\sin(x)}{x^n}\,dx = -\frac{1}{n-1}\,\frac{\sin(x)}{x^{n-1}} + \frac{1}{n-1}\int \frac{\cos(x)}{x^{n-1}}\,dx \qquad \text{(A1-41)}$$

$$\int \frac{\cos(x)}{x^n}\,dx = -\frac{1}{n-1}\,\frac{\cos(x)}{x^{n-1}} - \frac{1}{n-1}\int \frac{\sin(x)}{x^{n-1}}\,dx \qquad \text{(A1-42)}$$

and partial integration, and considering the series expansion for X=0 as well as

$$\int_0^\infty \frac{\sin(x)}{x^{2/3}}\,dx = \frac{1}{2}\,\Gamma\left(\frac{1}{3}\right) \qquad \text{(A1-43)}$$

$$\Gamma\left(\frac{1}{3}\right) \approx 2.678938 \qquad \text{(A1-44)}$$

we finally find

$$R_{11}(\underline{r}) - R_{11}(\underline{0}) = \frac{18}{55}\,\Gamma\left(\frac{1}{3}\right)\alpha\,\langle\varepsilon\rangle^{2/3}\,r^{2/3}\left(1-\frac{r_1^2}{4r^2}\right) \qquad \text{(A1-45)}$$

(similarly R_{22}, R_{33}) as well as using (A1-21)

$$R_{ij}(\underline{r}) = -\frac{18}{55}\,\Gamma\left(\frac{1}{3}\right)\alpha\,\langle\varepsilon\rangle^{2/3}\,\frac{r_i\,r_j}{4\cdot r^{4/3}}\,,\quad i\neq j \qquad \text{(A1-46)}$$

These results can, for example, be found in [80, 53]; the derivations used here make it possible to calculate the correlations for other spectra numerically, for example for the Pao spectrum. /120

Just as the Kolmogorov spectrum is only valid in a limited wave number region (A1-35) these correlations only apply in a limited range

$$\eta < r < L_0 \qquad \text{(A1-47)}$$

This becomes clear if we consider that in contrast to (A1-24) from (A1-45), we would have

$$\left.\frac{\partial^2 F}{\partial r^2}\right|_{r=0} = -\infty \qquad \text{(A1-48)}$$

and in contrast to experience, $R_{11}(r)$ would go to $-\infty$ for $r \to \infty$. A correlation which is valid for $0 < r < L_0$ and which in addition agrees exactly with (A1-24) is obtained when the Pao spectrum (A1-34) is used. However, the lower limit is non-critical for Reynolds numbers $Re \gtrsim 10^6$ according to Figure 2.

A1.3 Experimental Verification of the Validity of Local Isotropic Conditions and the Kolmogorov Spectrum

A1.3.1 Local Isotropy

There are numerous experimental proofs of the existence of local isotropy in turbulent flows which are macroscopically anisotropic. Pao [103] mentions 18 references in this regard. The reason for the existence of local isotropy is the effect of the pressure due to incompressibility. As Rotta [108, 115, p. 123] showed, the pressure-velocity correlations bring about an energy exchange between the velocity fluctuations in the various directions, so that energy is transferred from components with a strong fluctuation intensity to components with a weaker intensity, until there is an isotropic energy distribution. Rotta suggested the following quantitative trial solutions for this

$$\left\langle p \left(\frac{\partial u_i}{\partial x_j} + \frac{\partial u_j}{\partial x_i} \right) \right\rangle \approx -2 k_p \frac{\langle u_i u_j \rangle - \frac{1}{3}\langle u_i u_i \rangle \delta_{ij}}{\langle u_i^2 \rangle} \langle \varepsilon \rangle \qquad \text{(A1-48)}$$

In agreement with measurements of Uberoi [138] we have

$$k_p \approx 2.5 \qquad \text{(A1-49)}$$

as an estimate.

In the following we will mention three papers on the proof of local isotropy. Townsend [133] investigated the wake flow behind a cylinder in a flow by means of experiments. He showed that the velocity-fluctuation field referred to prime averages satisfies the relationships (A1-23) within the framework of measurement accuracy for isotropic conditions.

Laufer [76,77] shows that for a quasi plate flow with $Re_{max} \approx 6 \cdot 10^4$, $x_3 = 0.4$ and for wave numbers*

$$k \geq 12.5$$

we have

$$\frac{E_{13}(k_1)}{E_{11}(k_1)} = 0$$

i.e. the local contribution of the Reynolds stresses $\langle u_1' u_3' \rangle$ vanishes for these wave numbers, just as in the case of isotropic turbulence for all wave numbers.

Since in a grid

$$KM = 2 \times k$$

meshes are required to represent the oscillations with a dimensionless wave number k, approximately 25 meshes were required as shown in Figure 7, in order to be able to assume local isotropy within the mesh.

---

* Laufer measured velocities as a function of time at a position and determined spectra as a function of frequency $\hat{n}$. The recalculation of frequencies into dimensionless wave numbers is usually done based on the Taylor hypothesis of "frozen turbulence" [130] according to the formula

$$k = \frac{\hat{n} \cdot \hat{D}}{\langle \hat{u}_1 \rangle}$$

where

$$\hat{D} = 0.127\,m, \quad \langle \hat{u}_1 \rangle = 15\,m/s$$

Similar data is obtained from the measurements of Comte-Bellot [18] for Reynolds numbers $114000 \leq Re_m \leq 460000$ in a plate flow. Figures 8 to 10 show spectra $E_{22}(k_1)$ and $E_{33}(k_1)$ as well as spectra calculated from $E_{11}(k_1)$ according to the relationship (A1-15) applicable for isotropic turbulence at $X_3 = 0.5, 0.23, 0.02$ for $Re_m = 240000$. In the center $X_3 = 0.5$ and about half-way between the center and the wall, ($X_3 = 0.23$) there is already sufficiently good agreement between the spectra for relatively small wave numbers corresponding to $KM \geq 30$ meshes. Consequently we have determined local isotropic conditions. In the immediate vicinity of the wall ($X_3 = 0.02$), however, this is only valid after $KM \approx 300$. For other Reynolds numbers, the results are only slightly different.

/122

Based on these results, we can assume local isotropic conditions within a mesh for $Re_m \geqq 10^5$ except in the vicinity of the wall, if $KM \geqq 30$.

A1.3.2. Kolmogorov Spectrum

Laufer [76,77] was not able to find a Kolmogorov spectrum in his measurements of a quasi-plate flow at $Re_{max} \approx 60000$. The measured spectrum corresponded more to the k^{-7} variation according to Heisenberg (A1-40). However, Laufer indicates that there are uncertainties in the measurements. Nevertheless, it seems possible that the limits k_o and k_1 (A4-31,32) coincide for such small Reynolds numbers.

On the other hand, Comte-Bellot [18] was able to demonstrate a spectrum similar to the Kolmogorov spectrum for a similar geometry and $114000 \leq Re_m \leq 460000$. This is shown in Figure 11 for $X_3 \approx 0.22$, for example. Accordingly, the limiting wave numbers for $RE_m \approx 240000$ are such that for the mesh numbers

$$15 \leq KM \leq 325$$

we can assume that the Kolmogorov spectrum exists for the fine structure. The limits increase slightly with Reynolds number. The upper limit corresponds to the estimation given in Figure 2. Even in the vicinity of the wall ($X_3 = 0.06$) at wave numbers $KM \gtrsim 20$ there is a $k^{-5/3}$ dependence of the spectrum.

Therefore we can assume that for $Re_m \gtrsim 10^5$ and mesh numbers $KM \gtrsim 20$ (in one direction) that a spectrum according to Kolmogorov (A1-30) exists for the fine structure.

APPENDIX 2

/ 123

Calculation of Correlations Between Space Average Values

In this appendix we will prepare the fundamentals for the quantitative determination of the fine structure model. We will assume isotropic turbulence with the Kolmogorov spectrum and will quantitatively determine the time averages of products of pairs of velocities for velocity derivatives averaged over volumes.

A2.1. Calculation of the Volume Correlations which Occur

In the following we will calculate the volume correlations $\varphi_{12}(\xi)$ defined according to (4-20), which are the averaging volumes used for Cartesian coordinates in this paper. Uberoi-Kavasznay [136] published graphs of the corresponding results for line, circular area and spherical volumes with $V_1=V_2$. Here we will consider rectangular volumes and will algebraically determine the volume correlations.

A2.1.1. n-Dimensional Rectangular Volumes $V_1=V_2=V$

The averaging volume V considered is defined by

$$|\vartheta_i| \leq H_i/2\,;\ i = 1,2,\dots,n \qquad \text{(A2-1)}$$

The weighting functions $K(\underline{s})$ are therefore given by

$$K(\underline{s}) = \prod_{i=1}^{n} K_i(s_i) \qquad \text{(A2-2)}$$

where

$$K_i(s_i) = \begin{cases} 1/H_i & \text{for } |s_i| \leq H_i/2 \\ 0 & \text{otherwise} \end{cases} \qquad \text{(A2-3)}$$

From this it is possible to calculate $\varphi_{12}(\underline{\tau})$

$$\varphi_{12}(\underline{\tau}) = \iiint_{\infty} \prod_{i=1}^{n} K_{[i]}(\tau_i + z_i)\, K_{[i]}(z_i)\, dV(\underline{z}) = \prod_{i=1}^{n} \int_{\infty} K_{[i]}(\tau_i + z_i)\, K_{[i]}(z_i)\, dz_i \qquad \text{(A2-4)}$$

Convolution integrals over rectangular distributions correspond to the individual integrals. This results in triangular distributions [9] according to:

$$\varphi_{12}(\underline{\tau}) = \prod_{i=1}^{n} \frac{1}{H_{[i]}^2} \max\left(0, H_i - |\tau_i|\right) \qquad \text{(A2-5)}$$

A2.1.2. V_1, V_2 Rectangular Area- "Volumes" with Different Orientations

/ 124

In addition to volumes V_1 and V_2 which are equal and can cover each other, in this paper we will also use volume correlations between two rectangular areas having different orthogonal directions of the surface normals. The following sketch shows one basic possibility. All of the other possibilities are the result of rotating the coordinate system.

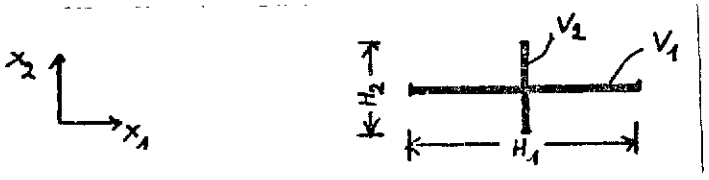

The area centers coincide. The volumes are defined by

$$V_1: \quad |s_1| \le H_1/2 \; ; \; s_2 = 0 \; ; \; |s_3| \le H_3/2 \qquad \text{(A2-6)}$$
$$V_2: \quad s_1 = 0 \; ; \; |s_2| \le H_2/2 \; ; \; |s_3| \le H_3/2$$

The corresponding weighting functions $K_j(\underline{s})$, $j=1,2$ are

$$K_j(\underline{s}) = \prod_{i=1}^{3} K_{ji}(s_i) \quad ; \; j=1,2 \qquad \text{(A2-7)}$$

with

$$K_{13}(s_3) = K_{23}(s_3) = \begin{cases} 1/H_3 & \text{for } |s_3| \le H_3/2 \\ 0 & \text{otherwise} \end{cases}$$

$$K_{11}(s_1) = \begin{cases} 1/H_1 & \text{for } |s_1| \le H_1/2 \\ 0 & \text{otherwise} \end{cases}$$

$$K_{12}(s_2) = \vartheta(0, s_2)$$

$$K_{21}(s_1) = \vartheta(0, s_1)$$

$$K_{22}(s_2) = \begin{cases} 1/H_2 & \text{for } |s_2| \le H_2/2 \\ 0 & \text{otherwise} \end{cases}$$

ϑ is the Dirac function:

$$\int_{-\infty}^{\infty} \vartheta(x,y)\, dy = 1 \; ; \quad \vartheta(x,y) = 0 \quad x \neq y$$

Both weighting functions satisfy the normalization condition (4-14). For this, according to the definition, the volume correlation is:

$$\varphi_{12}(\underline{\tau}) = \iiint_{\infty} \prod_{i=1}^{3} K_{1i}(\tau_i + y_i)\, K_{2i}(y_i)\, dy_i$$
$$= \prod_{i=1}^{3} \int_{\infty} K_{1i}(\tau_i + y_i)\, K_{2i}(y_i)\, dy_i$$

This means that convolution integrals with respect to y_1 and y_2 must be determined among rectangular functions and Dirac functions. Both of these again result in rectangular functions. Just as in 5.2.3.1, for y_3 we again obtain a triangular function

$$\varphi_{12}(\underline{\tau}) = \begin{cases} \frac{1}{H_1 \cdot H_2 \cdot H_3^2} \, Max(0, H_3 - |\tau_3|) & \text{for } (|\tau_1| \le H_1/2) \,\&\, (|\tau_2| \le H_2/2) \\ 0 & \text{otherwise} \end{cases} \quad \text{(A2-8)}$$

A2.2. Calculation of the Average Energies

The correlations to be calculated according to (4-24) are the following:

$$\langle V_n \overline{E'} \rangle = \sum_{i=1}^{3} \frac{1}{2} R(u_i - \langle u_i \rangle, u_i - \langle u_i \rangle, V_n, V_n, \underline{0}) \quad \text{(A2-9)}$$

where V_n is defined by

$$|x_i| \le \frac{\Delta x_i}{2} \quad , i = 1, 2, \ldots, n \quad \text{(A2-10)}$$

From (4-21, A2-5) it follows that:

$$\langle V_n \overline{E'} \rangle = \int_{-\Delta x_1}^{\Delta x_1} \cdots \int_{-\Delta x_n}^{\Delta x_n} \left(\prod_{j=1}^{n} \frac{\Delta x_j - |\tau_j|}{\Delta x_j^2} \right) \cdot \frac{1}{2} \left[R_{ii}(\underline{\tau}) - R_{ii}(\underline{0}) \right] d\tau_1 \cdots d\tau_n \quad \text{(A2-11)}$$

Because of (4-5) and (4-38) we have:

$$\frac{1}{2} \left(R_{ii}(\underline{\tau}) - R_{ii}(0) \right) = f_1 \langle \varepsilon \rangle^{2/3} |\underline{\tau}|^{2/3} \quad \text{(A2-12)}$$

If all lenths are normalized with $h = \sqrt[n]{V_n}$, it follows that

$$\langle V_n \overline{E'} \rangle = f_1 \langle \varepsilon \rangle^{2/3} h^{2/3} \, En(\Delta x_1/h, \Delta x_2/h, \ldots, \Delta x_n/h) \quad \text{(A2-13)}$$

where

$$En(h_1, h_2, \ldots, h_n) = 2^n \int_0^{h_1} \cdots \int_0^{h_n} \left(\prod_{j=1}^{n} (h_j - \tau_j) \right) (\tau^2)^{1/3} d\tau_1 d\tau_2 \cdots d\tau_n \quad \text{(A2-14)}$$

This integral can be determined analytically for n = 1:

$$E1(h_1) = E1(1) = \frac{9}{20} = 0.45 \quad \text{(A2-15)}$$

For volumes of equal length $\Delta x_j = h$ we find the following numerical result:

$$E2(1,1) = 0.6293 \qquad \text{(A2-16)}$$

$$E3(1,1,1) = 0.7461 \qquad \text{(A2-17)}$$

Since we must always have $\prod_{i=1}^{n} \frac{\Delta x_i}{h} = 1$, the volume region V_n approaches a linear region for $\Delta x_1 \to \infty$ and therefore we have

$$\lim_{\Delta x_1 \to \infty} En(\Delta x_1, \Delta x_2, \ldots, \Delta x_n) = 0.45 \cdot \Delta x_1^{2/3} \qquad \text{(A2-18)}$$

The numerical solution of the integrals for various edge lengths Δx_i and for n = 0,1,2,3 can be approximated with the following formula with a maximum error of 1%

$$E_n(h_1, h_2, \ldots, h_n) = 0.45 \left(\sum_{i=1}^{n} h_i^{1/\beta} \right)^{\beta \cdot 2/3} \qquad \text{(A2-19)}$$

and we find the following value by a least squares fit

$$\beta = 0.69687$$

and this approximation function satisfies the limiting value condition (A2-18) exactly.

A2.3. Isotropic Properties of the Squares of the Deformation Velocity

The time averaged squares of various space averages of the deformation velocities to be calculated according to (4-23) to (4-26) consist of the sums of nine sum terms characterized by i, j:

$$_{h}D^2 = \sum_{i=1}^{3} \sum_{j=1}^{3} {}_{h}D^2_{i,j} \qquad \text{(A2-20)}$$

It is sufficient to derive the method of determining ${}_kD^2_{1,1}(\underline{M})$, ${}_kD^2_{1,2}(\underline{M})$ and $\underline{M}$ characterizes the grid.

$$\underline{M} \equiv \{\Delta x_1, \Delta x_2, \Delta x_3\} \qquad \text{(A2-21)}$$

The other sum terms can be calculated with the same methods, if instead of $\underline{M}$ we use a suitably rotated grid, as given by the following formulas

$$\begin{aligned} {}_kD^2_{ii,ii}(\underline{M}) &= {}_kD^2_{11}(\underline{\overset{1}{=}V}\cdot\underline{M}) \\ {}_kD^2_{i,j}(\underline{M}) &= {}_kD^2_{12}(\underline{\overset{2}{=}V}\cdot\underline{M}) \qquad i\neq j \end{aligned} \qquad \text{(A2-22)}$$

$\underline{\overset{1}{=}V}$, $\underline{\overset{2}{=}V}$ described the required rotation:

$$\underline{\overset{1}{=}V} = \begin{pmatrix} \delta_{i1} & \delta_{i2} & \delta_{i3} \\ \delta_{i2} & \delta_{i3} & \delta_{i1} \\ \delta_{i3} & \delta_{i1} & \delta_{i2} \end{pmatrix}; \quad \underline{\overset{2}{=}V} = \begin{pmatrix} \delta_{i1} & \delta_{i2} & \delta_{i3} \\ \delta_{j1} & \delta_{j2} & \delta_{j3} \\ (1-\delta_{i1}-\delta_{j1}) & (1-\delta_{i2}-\delta_{j2}) & (1-\delta_{i3}-\delta_{j3}) \end{pmatrix} \qquad \text{(A2-23)}$$

These relationships follow from geometrical considerations. Therefore in the following we will first only consider ${}_kD^2_{11}$, ${}_kD^2_{12}$.

A2.4. Reduction of the Squares of the Deformation Velocities to Differences of "Space Correlations".

The following derivations will be done in detail for ${}_1D^2_{11}$, ${}_1D^2_{12}$. The results for the other variables are similar. /127

A2.4.1. ${}_1D^2_{11}$

${}_1D^2_{11}$ is as follows according to (4-23):

$${}_1D^2_{11} = 2\left\langle (\delta_{x_1} {}_1\overline{u}_1)^2 \right\rangle$$

If we note the definition of the difference operator δ_{x_1}, we have:

$$
\begin{aligned}
{}_1D_{11}^2 &= \frac{2}{\Delta x_1^2}\left\langle\left[{}^1u_1\left(x_1+\tfrac{\Delta x_1}{2},x_2,x_3\right)-{}^1u_1\left(x_1-\tfrac{\Delta x_1}{2},x_2,x_3\right)\right]^2\right\rangle \\
&= \frac{2}{\Delta x_1^2}\left\{\left\langle\left[{}^1u_1\left(x_1+\tfrac{\Delta x_1}{2},x_2,x_3\right)\right]^2\right\rangle+\left\langle\left[{}^1u_1\left(x_1-\tfrac{\Delta x_1}{2},x_2,x_3\right)\right]^2\right\rangle\right. \\
&\qquad \left.-2\left\langle {}^1u_1\left(x_1+\tfrac{\Delta x_1}{2},x_2,x_3\right)\cdot {}^1u_1\left(x_1-\tfrac{\Delta x_1}{2},x_2,x_3\right)\right\rangle\right\}
\end{aligned}
$$

Since the individual terms do not depend on the actual values x_1, x_2, x_3 but only on the difference vector, we have

$$
{}_1D_{11}^2 = \frac{4}{\Delta x_1^2}\left\{\left\langle {}^1u_1\cdot {}^1u_1(\underline{0})\right\rangle-\left\langle {}^1u_1\,{}^1u_1(\Delta x_1,0,0)\right\rangle\right\} \qquad \text{(A2-24)}
$$

A2.4.2 $\quad {}_1D_{12}^2$

Starting with the definitions, for ${}_1D_{12}^2$ we find:

$$
\begin{aligned}
{}_1D_{12}^2 &= \left\langle \delta_{x2}\,{}^2u_1\left(\delta_{x2}\,{}^2u_1+\delta_{x_1}{}^1u_2\right)\right\rangle \\
&= \left\langle\frac{1}{\Delta x_2^2}\left({}^2u_1\left(x_1,x_2+\tfrac{\Delta x_2}{2},x_3\right)-{}^2u_1\left(x_1,x_2-\tfrac{\Delta x_2}{2},x_3\right)\right)^2\right\rangle \\
&\quad+\left\langle\frac{1}{\Delta x_2\,\Delta x_1}\left[{}^2u_1\left(x_1,x_2+\tfrac{\Delta x_2}{2},x_3\right)-{}^2u_1\left(x_1,x_2-\tfrac{\Delta x_2}{2},x_3\right)\right]\right. \\
&\qquad\left.\cdot\left[{}^1u_2\left(x_1+\tfrac{\Delta x_1}{2},x_2,x_3\right)-{}^1u_2\left(x_1-\tfrac{\Delta x_1}{2},x_2,x_3\right)\right]\right\rangle
\end{aligned}
$$

After evaluating the square and the product, respectively, we can again collect a few terms, because the time averages do not depend on $\underline{x}$. If we consider the following symmetry conditions which are a consequence of (4-6)

$$
\begin{aligned}
\left\langle {}^2u_1\left(0,\tfrac{\Delta x_2}{2},0\right){}^1u_2\left(\tfrac{\Delta x_1}{2},0,0\right)\right\rangle &= \left\langle {}^2u_1\left(0,-\tfrac{\Delta x_1}{2},0\right)\cdot {}^1u_2\left(-\tfrac{\Delta x_2}{2},0,0\right)\right\rangle \\
\left\langle {}^2u_1\left(0,\tfrac{\Delta x_2}{2},0\right){}^1u_2\left(\tfrac{\Delta x_1}{2},0,0\right)\right\rangle &= -\left\langle {}^1u_1\left(0,-\tfrac{\Delta x_1}{2},0\right){}^1u_2\left(\tfrac{\Delta x_2}{2},0,0\right)\right\rangle,
\end{aligned}
$$

then we have

$$ {}_1D_{12}^2 = \frac{2}{\Delta x_2^2}\left\{\langle {}^2\bar{u}_1\, {}^2\bar{u}_1(\underline{0})\rangle - \langle {}^2\bar{u}_1\, {}^2\bar{u}_1(0,+\Delta x_2,0)\rangle\right\} + \frac{4}{\Delta x_2 \Delta x_1}\langle {}^2\bar{u}_1\, {}^1\bar{u}_2\ (\tfrac{\Delta x_1}{2}, \tfrac{\Delta x_2}{2}, 0)\rangle \qquad \text{(A2-25)} $$

A2.4.3. Similar Results

/128

$$ {}_2D_{11}^2 = \frac{4}{\Delta x_1^2}\left(\langle {}^1\bar{u}_1\, {}^1\bar{u}_1\ (\tfrac{\Delta x_1}{2},0,0)\rangle - \langle {}^1\bar{u}_1\, {}^1\bar{u}_1\ (\tfrac{3}{2}\Delta x_1,0,0)\rangle\right) \qquad \text{(A2-26)} $$

$$ {}_2D_{12}^2 = \frac{1}{\Delta x_2^2}\left\{\langle {}^1\bar{u}_1\, {}^2\bar{u}_1\ (0,\tfrac{\Delta x_2}{2},0)\rangle - \langle {}^1\bar{u}_1\, {}^2\bar{u}_1\ (0,\tfrac{3}{2}\Delta x_2,0)\rangle\right\} + \frac{2}{\Delta x_1 \Delta x_2}\langle {}^2\bar{u}_1\, {}^2\bar{u}_2\ (\tfrac{\Delta x_1}{2}, \Delta x_2, 0)\rangle \qquad \text{(A2-27)} $$

$$ {}_3D_{11}^2 = {}_1D_{11}^2 \qquad \text{(A2-28)} $$

$$ {}_3D_{12}^2 = \frac{1}{\Delta x_2^2}\left\{\langle {}^1\bar{u}_1\, {}^1\bar{u}_1\ (\underline{0})\rangle - \langle {}^1\bar{u}_1\, {}^1\bar{u}_1\ (0,\Delta x_2,0)\rangle\right\} + \frac{1}{\Delta x_1^2}\left\{\langle {}^2\bar{u}_2\, {}^2\bar{u}_2\ (\underline{0})\rangle - \langle {}^2\bar{u}_2\, {}^2\bar{u}_2\ (\Delta x_1,0,0)\rangle\right\} + \frac{4}{\Delta x_1 \Delta x_2}\langle {}^2\bar{u}_2\, {}^1\bar{u}_1\ (\tfrac{\Delta x_1}{2}, \tfrac{\Delta x_2}{2}, 0)\rangle \qquad \text{(A2-29)} $$

$$ {}_4D_{11}^2 = \frac{1}{8\Delta x_1^2}\left\{14\langle {}^1\bar{u}_1\, {}^1\bar{u}_1\ (\underline{0})\rangle - 17\langle {}^1\bar{u}_1\, {}^1\bar{u}_1\ (\Delta x_1,0,0)\rangle + 2\langle {}^1\bar{u}_1\, {}^1\bar{u}_1\ (2\Delta x_1,0,0)\rangle + \langle {}^1\bar{u}_1\, {}^1\bar{u}_1\ (3\Delta x_1,0,0)\rangle\right\} \qquad \text{(A2-30)} $$

$$
\begin{aligned}
{}_4D_{12}^2 = {} & \frac{1}{8\Delta x_2^2}\Big\{7\langle {}^1\tilde{u}_1\,{}^1\tilde{u}_1(\underline{0})\rangle - 8\langle {}^1\tilde{u}_1\,{}^1\tilde{u}_1(0,\Delta x_2,0)\rangle \\
& + \langle {}^1\tilde{u}_1\,{}^1\tilde{u}_1(0,2\Delta x_2,0)\rangle + \langle {}^1\tilde{u}_1\,{}^1\tilde{u}_1(\Delta x_1,2\Delta x_2,0)\rangle - \langle {}^1\tilde{u}_1\,{}^1\tilde{u}_1(\Delta x_1,0,0)\rangle\Big\} \\
& + \frac{1}{8\Delta x_1^2}\Big\{7\langle {}^2\tilde{u}_2\,{}^2\tilde{u}_2(\underline{0})\rangle - 8\langle {}^2\tilde{u}_2\,{}^2\tilde{u}_2(\Delta x_1,0,0)\rangle \\
& + \langle {}^2\tilde{u}_2\,{}^2\tilde{u}_2(2\Delta x_1,0,0)\rangle + \langle {}^2\tilde{u}_2\,{}^2\tilde{u}_2(2\Delta x_1,\Delta x_2,0)\rangle - \langle {}^2\tilde{u}_2\,{}^2\tilde{u}_2(0,\Delta x_2,0)\rangle\Big\} \\
& + \frac{1}{4\Delta x_1\Delta x_2}\Big\{15\langle {}^2\tilde{u}_2\,{}^1\tilde{u}_1\left(\tfrac{\Delta x_1}{2},\tfrac{\Delta x_2}{2},0\right)\rangle - \langle {}^2\tilde{u}_2\,{}^1\tilde{u}_1\left(\tfrac{3}{2}\Delta x_1,\tfrac{\Delta x_2}{2},0\right)\rangle \\
& - \langle {}^2\tilde{u}_2\,{}^1\tilde{u}_1\left(\tfrac{\Delta x_1}{2},\tfrac{3}{2}\Delta x_2,0\right) - \langle {}^2\tilde{u}_2\,{}^1\tilde{u}_1\left(\tfrac{3}{2}\Delta x_1,\tfrac{3}{2}\Delta x_2,0\right)\rangle\Big\}
\end{aligned}
\qquad \text{(A2-31)}
$$

A2.4.4. Definition

/129

We should note: the squares of the deformation velocity averaged over time according to (4-23) to (4-26) can be calculated if the "space correlations"

$$\langle {}^{\ell}\tilde{u}_i\,{}^{m}\tilde{u}_j(\xi_1,\xi_2,0)\rangle$$

are known. In particular we require

$$
\begin{aligned}
d_1(\Delta x_1,\Delta x_2,\Delta x_3,\xi_1,\xi_2) &\equiv \langle {}^1\tilde{u}_1\,{}^1\tilde{u}_1(\xi_1,\xi_2,0)\rangle \\
d_2(\Delta x_1,\Delta x_2,\Delta x_3,\xi_1,\xi_2) &\equiv \langle {}^2\tilde{u}_1\,{}^2\tilde{u}_1(\xi_1,\xi_2,0)\rangle \\
d_3(\Delta x_1,\Delta x_2,\Delta x_3,\xi_1,\xi_2) &\equiv \langle {}^1\tilde{u}_1\,{}^2\tilde{u}_1(\xi_1,\xi_2,0)\rangle \\
d_4(\Delta x_1,\Delta x_2,\Delta x_3,\xi_1,\xi_2) &\equiv \langle {}^1\tilde{u}_1\,{}^2\tilde{u}_2(\xi_1,\xi_2,0)\rangle \\
d_5(\Delta x_1,\Delta x_2,\Delta x_3,\xi_1,\xi_2) &\equiv \langle {}^2\tilde{u}_1\,{}^2\tilde{u}_2(\xi_1,\xi_2,0)\rangle
\end{aligned}
\qquad \text{(A2-32)}
$$

The other correlations $\langle {}^2\bar{u}_2\, {}^2\bar{u}_2\,(\underline{\xi})\rangle$ can be calculated from d_1 corresponding to the development in Chapter A2.3:

$$\langle {}^2\bar{u}_2\, {}^2\bar{u}_2\,(\xi_1,\xi_2,0)\rangle = d_1(\Delta x_2,\Delta x_1,\Delta x_3,\xi_2,\xi_1) \tag{A2-33}$$

Also we can calculate $\langle {}^2\bar{u}_1\, {}^1\bar{u}_2\,(\xi_1,\xi_2,0)\rangle$ according to

$$\langle {}^2\bar{u}_1\, {}^1\bar{u}_2(\xi_1,\xi_2,0)\rangle = \langle {}^1\bar{u}_1\, {}^2\bar{u}_2\,(\xi_1,\xi_2,0)\rangle = d_4(\Delta x_1,\Delta x_2,\Delta x_3,\xi_1,\xi_2) \tag{A2-34}$$

because the exchange averaging operations lead to the same volume correlations as according to (4-20).

The correlations d_k, k=1,2,...,5 defined above will be calculated in the following section .

A2.5 Calculation of the Correlations Defined in A2.4.4

The calculation of the correlations $d_k(\xi_1,\xi_2)$, k=1,2,...,5 according to Chapter A2.4.4, is carried out using the methods prepared in Chapters 4.2 and A2.1.2, where $R_{11}(\underline{r})$ and $R_{12}(\underline{r})$ are given by (4-5) and (4-6) and f_2 is given by (4-39).

A2.5.1. Solution in Integral Form

/130

We define the following abbreviations

$$\begin{aligned} h &\equiv \sqrt[3]{\Delta x_1 \cdot \Delta x_2 \cdot \Delta x_3} \\ h_i &\equiv \Delta x_i / h \quad ; \; i=1,2,3 \\ z_i &\equiv \xi_i / h \quad ; \; i=1,2,3 \end{aligned} \tag{A2-35}$$

Therefore the results can be given in integral form:

$$d_k(\Delta x_1,\Delta x_2,\Delta x_3,\xi_1,\xi_2) = R_{11}(\underline{0}) - f_2 \langle\varepsilon\rangle^{2/3} h^{2/3} \cdot d_k^*(h_1,h_2,h_3,z_1,z_2), \quad k=1,2,3. \tag{A2-36}$$

$$\alpha_1^* = 2\int_{-h_2}^{h_2}\int_{0}^{h_3} \frac{(h_2-|\tau_2|)(h_3-\tau_3)}{h_2^2 h_3^2}\,(r^2)^{1/3}\left(1-\frac{z_1^2}{4r^2}\right)d\tau_3\,d\tau_2 \qquad \text{(A2-37)}$$

$$r^2 = z_1^2 + (\tau_2+z_2)^2 + \tau_3^2 \quad ;$$

$$\alpha_2^* = 2\int_{-h_1}^{h_1}\int_{0}^{h_3} \frac{(h_1-|\tau_1|)(h_3-\tau_3)}{h_1^2 h_3^2}\,(r^2)^{1/3}\left(1-\frac{(z_1+\tau_1)^2}{4r^2}\right)d\tau_3\,d\tau_1 \qquad \text{(A2-38)}$$

$$r^2 = (\tau_1+z_1)^2 + (\tau_2+z_2)^2 + \tau_3^2 \quad ;$$

$$\alpha_3^* = 2\int_{-\frac{h_1}{2}}^{\frac{h_1}{2}}\int_{-\frac{h_2}{2}}^{\frac{h_2}{2}}\int_{0}^{h_3} \frac{(h_3-\tau_3)}{h_3}\,(r^2)^{1/3}\left(1-\frac{(z_1+\tau_1)^2}{4r^2}\right)d\tau_3\,d\tau_2\,d\tau_1 \qquad \text{(A2-39)}$$

$$r^2 = (\tau_1+z_1)^2 + (\tau_2+z_2)^2 + \tau_3^2 \quad ;$$

$$\alpha_k(\Delta x_1, \Delta x_2, \Delta x_3, \varphi_1, \varphi_2) = f_2\langle\varepsilon\rangle^{2/3} h^{2/3}\,\alpha_k^*(h_1, h_2, h_3, z_1, z_2); \qquad \text{(A2-40)}$$

$$k = 4, 5.$$

$$\alpha_5^* = -\frac{1}{2}\int_{-h_1}^{h_1}\int_{0}^{h_3} \frac{(h_1-|\tau_1|)(h_2-|\tau_2|)}{h_1^2 h_3^2}\cdot\frac{(\tau_1+z_1)\,z_2}{\left[(\tau_1+z_1)^2+z_2^2+\tau_3^2\right]^{2/3}}\,d\tau_3\,d\tau_1 \qquad \text{(A2-41)}$$

$$\alpha_4^* = -\frac{1}{2}\int_{-\frac{h_1}{2}}^{\frac{h_1}{2}}\int_{-\frac{h_2}{2}}^{\frac{h_2}{2}}\int_{0}^{h_3} \frac{h_3-\tau_3}{h_3}\,\frac{(\tau_1+z_1)(\tau_2+z_2)}{\left[(\tau_1+z_1)^2+(\tau_2+z_2)^2+\tau_3^2\right]^{2/3}}\,d\tau_3\,d\tau_2\,d\tau_1 \qquad \text{(A2-42)}$$

Table 4 shows FORTRAN subprograms with which these integrals /131 can be calculated numerically. For the integration, the subprogram QSF [65] is used which integrates equidistant tabulated functions using the Simpson rule. The number NN of the support values of an integration variable to be specified in the COMMON region NNNNNN must be about 50 in order to have an accuracy of 10^{-3}. The COMMON region CWORK contains the working region required for integration. It is designed for NN<100.

A2.5.2. Limiting Values of the Integrals and Approximations

The numerical evaluation of the integrals given above requires a large computation time. Therefore it is desirable to prepare approximations which approximate these exact solutions as well as possible. The approximations must provide the same results for special values of the parameters. Among these we have the following limiting values:

$$\lim_{h_2\to\infty} \alpha_1^*(h_1,h_2,h_3,0,0) = \frac{9}{20}\, h_2^{2/3}$$

$$\lim_{h_3\to\infty} \alpha_1^*(h_1,h_2,h_3,0,0) = \frac{9}{20}\, h_3^{2/3}$$

$$\lim_{\substack{z_1\to\infty\\ z_2\to\infty}} \alpha_1^*(h_1,h_2,h_3,z_1,z_2) = (z_1^2+z_2^2)^{1/3}\left(1-\frac{z_1^2}{4(z_1^2+z_2^2)}\right)$$

$$\lim_{h_1\to\infty} \alpha_2^*(h_1,h_2,h_3,0,0) = \frac{27}{80}\, h_1^{2/3}$$

$$\lim_{h_3\to\infty} \alpha_2^*(h_1,h_2,h_3,0,0) = \frac{9}{20}\, h_3^{2/3}$$

$$\lim_{\substack{z_1\to\infty\\ z_2\to\infty}} \alpha_2^*(h_1,h_2,h_3,z_1,z_2) = (z_1^2+z_2^2)\left(1-\frac{z_1^2}{4(z_1^2+z_2^2)}\right)$$

$$\lim_{h_1\to\infty} \alpha_3^*(h_1,h_2,h_3,0,0) = \frac{9}{10}\left(\frac{1}{2}\right)^{5/3} h_1^{2/3}$$

$$\lim_{h_2\to\infty} \alpha_3^*(h_1,h_2,h_3,0,0) = \frac{6}{5}\left(\frac{1}{2}\right)^{5/3} h_2^{2/3}$$

$$\lim_{h_3\to\infty} \alpha_3^*(h_1,h_2,h_3,0,0) = \frac{9}{20}\, h_3^{2/3}$$

$$\lim_{z_1, z_2 \to \infty} d3^*(h_1, h_2, h_3, z_1, z_2) = (z_1^2+z_2^2)^{1/3}\left(1-\frac{z_1^2}{4(z_1^2+z_2^2)}\right)$$

$$d4^*(h_1, h_2, h_3, 0, z_2) = d4^*(h_1, h_2, h_3, z_1, 0) = 0$$

$$\lim_{h_3 \to \infty} d4^*(h_1, h_2, h_3, z_1, z_2) = 0$$

$$d5^*(h_1, h_2, h_3, 0, z_2) = d5^*(h_1, h_2, h_3, z_1, 0) = 0$$

$$\lim_{h_3 \to \infty} d5^*(h_1, h_2, h_3, z_1, z_2) = 0$$

In addition we require that the approximations for d_k, k=1,2,3 must agree exactly with the numerically obtained integral solutions at $(h_1, h_2, h_3, z_1, z_2) = (1,1,1,0,0)$. These reference values are:

k	d_k^* (1,1,1,0,0)
1	0.6293
2	0.5506
3	0.6104

Since d4* is required the most for $z_1 = \frac{\Delta x_1}{2}, z_2 = \frac{\Delta x_2}{2}$ and d5* is only required for $z_1 = \frac{\Delta x_1}{2}, z_2 = \Delta x_2$, the approximation must satisfy the following requirement in agreement with the numerical results:

$$d4^*(1,1,1,1/2,1/2) = -0.1376 \qquad d5^*(1,1,1,1/2,1) = -0.0846$$

Approximations corresponding to these requirements are shown in Table 5 in the form of FORTRAN subprograms. Table 6 contains a comparison of the results obtained by direct integration or from the approximation functions. The errors of the approximations are not especially small, but they can be tolerated because the constants of the fine structure model calculated according to the approximations deviate at the most by about 20% from those for the exact solutions. /133

A2.6. Results for $_2D^2$ and FED

Using the relationships derived in Chapter A2.3 to A2.5, it is possible to calculate the quantities $_kD^2$ and FED. These results are best presented in the form of a program. Considering the subprograms D11, D12, D13, D14 and FED1 given in Table 7, the results are as follows after extracting the variables having dimensions

$$_RD^2 = f_2 \langle \varepsilon \rangle^{2/3} h^{-4/3} \, D1R\left(\frac{\Delta x_1}{h}, \frac{\Delta x_2}{h}, \frac{\Delta x_3}{h}\right), \quad R=1,2,3,4 \qquad \text{(A2-43)}$$

$$FED = f_3 \langle \varepsilon \rangle \, FED1\left(\frac{\Delta x_1}{h}, \frac{\Delta x_2}{h}, \frac{\Delta x_3}{h}\right). \qquad \text{(A2-44)}$$

f_2, f_3 are given by (4-39, 40). See Chapter 4.3 for numerical results.

/134

APPENDIX 3

Determination of a Constant c_1

Here we will report on the calculations of Smagorinsky and Lilly of the value of the constant c_1 contained in the trial solution

$$\overline{u_i' u_j'} = (c_1 h)^2 \left[\frac{1}{2}\left(\overline{D}_{ij}\right)^2\right]^{1/2} \overline{D}_{ij} + \frac{1}{3}\delta_{ij}\overline{u_\ell' u_\ell'} \qquad \text{(A3-1)}$$

We will discuss the assumptions and approximations. In addition we will summarize the experience of Deardorff and discuss his method for calculating the kinetic energy. At the end of this appendix we will calculate the constant c_1 according to methods of this paper.

A3.1 Calculation of c_1 according to Smagorinsky

Smagorinsky [118] uses a trial solution corresponding to (A3-1) for the two-dimensional, global, meteorological simulation where

$$c_1 = k, \qquad \text{(A3-2)}$$

and k is the Karman constant [120]:

$$k \approx 0.4 \qquad \text{(A3-3)}$$

One obtains this result [32] if μ and $\overline{D}_{ij}$ are set equal to their time-average values in a boundary layer with constant shear stresses. For this we have the logarithmic wall law [120]:

$$\langle u_1 \rangle = \frac{1}{k} \ln (z' \cdot E_W) \qquad \text{(A3-4)}$$

(z' = wall distance, E_W a constant which considers wall roughness)
Here we therefore have

$$\langle \tau_W \rangle = \mu \frac{\partial}{\partial z'} \langle u_1 \rangle = 1 = (c_1 h)^2 (k z')^{-2} \qquad \text{(A3-5)}$$

If the height at which μ is being determined is equal to h, then (A3-2) follows. This result can at best only apply for the immediate vicinity of the wall, according to our assumption.

A3.2. Calculation of c_1 according to Lilly [80, 81]

A3.2.1. Averaging Operation and Determination Equation for c_1

For the derivation of the mesh averages of the basic equations Lilly [80, 81] and Deardorff [29,33,44] made use of the following averaging operations.

$$\text{a)}\quad \overline{y}^{v}(x_1,x_2,x_3,t) \equiv \frac{1}{h^3}\int_{-\frac{h}{2}}^{\frac{h}{2}}\int_{-\frac{h}{2}}^{\frac{h}{2}}\int_{-\frac{h}{2}}^{\frac{h}{2}} y(x_1+z_1, x_2+z_2, x_3+z_3, t)\, dz_3\, dz_2\, dz_1 \qquad \text{(A3-6)}$$

/135

$$\text{b)}\quad \overline{y}^{v}(x_1,x_2,x_3,t) \equiv \frac{1}{h^3}\int_{x_1-\frac{h}{2}}^{x_1+\frac{h}{2}}\int_{x_2-\frac{h}{2}}^{x_2+\frac{h}{2}}\int_{x_3-\frac{h}{2}}^{x_3+\frac{h}{2}} y(z_1,z_2,z_3,t)\, dz_3\, dz_2\, dz_1 \qquad \text{(A3-7)}$$

For the first one we have:

$$\overline{\frac{\partial y}{\partial x_i}}^{v} = \frac{\partial}{\partial x_i}\overline{y}^{v} \qquad \text{(A3-8)}$$

and for the second one we have:

$$\overline{\frac{\partial y}{\partial x_i}}^{v} \neq \frac{\partial}{\partial x_i}\overline{y}^{v} \qquad \text{(A3-9)}$$

Neither of the two averaging operations was selected consistently. The basic equations for determining the constant c_1 were derived by Lilly [81] using the first operation. Deardorff [29] used the second operation, and in addition he used (A3-8) as an approximation. The conservation equation for $\overline{E'}^{v}$ derived by Lilly using (A3-6) has the following main terms:

$$\frac{\partial \overline{E'}^{v}}{\partial t} = -\,Konv + Diff - \overline{u_i' u_j'}^{v}\frac{\overline{D_{ij}}^{v}}{2} - \overline{\varepsilon'}^{v} \qquad \text{(A3-10)}$$

The convection and diffusion terms Konv and Diff are of no consequence. $\overline{\varepsilon'}^{v}$ is defined as

$$\overline{\varepsilon'}^{v} = \nu\left[\overline{\left(\frac{\partial u_i}{\partial x_j}\right)^2}^{v} - \left(\frac{\partial \overline{u_i}^{v}}{\partial x_j}\right)^2\right] \qquad \text{(A3-11)}$$

and there is also a term corresponding to the dissipation. It is assumed that the velocity field is locally isotropic and that it has an energy spectrum E(k) which corresponds to the Kolmogorov spectrum. The trial solution (A3-1) is substituted into (A3-10). The additional term $\frac{1}{3}\delta_{ij}\sqrt{u_\ell' u_\ell'}$ vanishes because of the continuity equation

$$\frac{1}{3}\sqrt{u_\ell' u_\ell'}\,\delta_{ij}\sqrt{D_{ij}} = \sqrt{u_\ell' u_\ell'}\,\frac{2}{3}\sqrt{\frac{\partial u_i}{\partial x_i}} = 0 \qquad \text{(A3-12)}$$

For stationary and locally isotropic turbulence, averaged over time we have

$$\left\langle \sqrt{\frac{\partial E'}{\partial t}} \right\rangle = \langle Konv \rangle - \langle Diff \rangle = 0 \qquad \text{(A3-13)}$$

/136

and therefore we obtain an equation for the determination of c_1:

$$c_1 = \left[\frac{\langle \sqrt{\varepsilon'} \rangle}{h^2 \left\langle \left[\frac{1}{2}\left(\sqrt{D_{ij}}\right)^2\right]^{1/2} \cdot \frac{1}{2}\left(\sqrt{D_{ij}}\right)^2 \right\rangle} \right]^{1/2}. \qquad \text{(A3-14)}$$

Here we will use the approximation

$$\left\langle \left(\frac{1}{2}\left(\sqrt{D_{ij}}\right)^2\right)^{3/2} \right\rangle = \left\langle \frac{1}{2}\left(\sqrt{D_{ij}}\right)^2 \right\rangle^{3/2}, \qquad \text{(A3-15)}$$

as well as

$$\langle \varepsilon' \rangle = \langle \varepsilon \rangle, \qquad \text{(A3-16)}$$

where ε is defined (1-16). Therefore we have

$$c_1 \approx \left(\frac{\langle \varepsilon \rangle}{h^2 \left\langle \frac{1}{2}\left(\sqrt{D_{ij}}\right)^2 \right\rangle^{3/2}} \right)^{1/2} \qquad \text{(A3-17)}$$

A3.2.2 Estimation of $\left\langle \left(\sqrt{D_{ij}}\right)^2 \right\rangle$ [81]

According to (A1-27) we have

$$\left\langle D_{ij}^2 \right\rangle = 4 \int_0^\infty E(k)\, k^2\, dk. \qquad \text{(A3-18)}$$

If the cube-shaped mesh with edge lengths h is approximated by a sphere with a diameter h and if we consider that only those parts of the energy spectrum contribute to $\langle(\overline{{}^{v}D_{ij}})^2\rangle$ whose wave numbers $k \leq k_o$ can be represented by the macroscopic structure of the average velocity field, and if we assume the following according to Lilly [81]

$$k_o = \frac{\pi}{h}, \tag{A3-19}$$

it follows that

$$\langle(\overline{{}^{v}D_{ij}})^2\rangle = 4 \int_0^{\pi/h} k^2 E(k)\, dk\,. \tag{A3-20}$$

If we substitute (4-4) for E(k) according to definition, then we have

$$\langle(\overline{{}^{v}D_{ij}})^2\rangle = 3 \left(\frac{\pi}{h}\right)^{4/3} \alpha \langle\varepsilon\rangle^{2/3} \tag{A3-21}$$

and therefore we obtain the following for c_1 together with (A3-14):

$$c_1 = \frac{1}{\pi}\left(\frac{2}{3\alpha}\right)^{3/4}. \tag{A3-22}$$

For $\alpha = 1.5$ we have

$$c_1 = 0.173 \tag{A3-23}$$

/137

A3.2.3 Numerical Calculation of $\langle(\overline{{}^{v}D_{ij}})^2\rangle$ for a Cube Volume

If we assume the following approximation [80]:

$$\left\langle \overline{{}^{v}\frac{\partial u_2}{\partial x_1}} \cdot \overline{{}^{v}\frac{\partial u_1}{\partial x_2}} \right\rangle = -\frac{1}{2}\left\langle \left(\overline{{}^{v}\frac{\partial u_1}{\partial x_1}}\right)^2 \right\rangle, \tag{A3-24}$$

then because of (A1-23) we have:

$$\left\langle \frac{1}{2}(\overline{{}^{v}D_{ij}})^2 \right\rangle = 3\left\langle \left(\overline{{}^{v}\partial u_1/\partial x_1}\right)^2 \right\rangle + 6\left\langle \left(\overline{{}^{v}\partial u_2/\partial x_1}\right)^2 \right\rangle. \tag{A3-25}$$

(A3-24) only applies exactly, as Lilly [80] himself determined, if the averaging volume V includes the entire flow space. Lilly [80] numerically calculated the correlations which occur in (A3-25) according to Appendix 2 for a cube volume V having equal side lengths and by using the averaging operation (A3-7). For $\alpha = 1.5$ he obtains the following result:

$$\left\langle \tfrac{1}{2} \left(\sqrt{\bar{D}_{ij}} \right)^2 \right\rangle = 10.05 \, \langle \varepsilon \rangle^{2/3} \, h^{-4/3} \qquad \text{(A3-26)}$$

$$c_1 = 0.177 \qquad \text{(A3-27)}$$

Lilly [80] also investigated the influence of difference formulas on the constant c_1. For this he assumed that instead of

$$\tfrac{1}{2} \sqrt{\bar{D}_{ij}}^2 = \sqrt{\frac{\partial u_i}{\partial x_j}} \left(\sqrt{\frac{\partial u_i}{\partial x_j}} + \sqrt{\frac{\partial u_j}{\partial x_i}} \right) \qquad \text{(A3-28)}$$

we must substitute the following in (A3-17)

$$\tfrac{1}{2} \sqrt{\bar{D}_{h\,ij}}^2 = \sqrt{\Delta_j u_i} \left(\sqrt{\Delta_j u_i} + \sqrt{\Delta_i u_j} \right) \qquad \text{(A3-29)}$$

The following difference operator Δ_i is defined:

$$\Delta_i \, y(x) \equiv \left[y\left(x + \tfrac{h}{2} e_i\right) - y\left(x - \tfrac{h}{2} e_i\right) \right] / h \qquad \text{(A3-30)}$$

For the numerical evaluation of the expression (A3-28) defined in this way, Lilly numerically evaluates six-fold integrals according to the method given in Chapter 4.2.2 and obtains the following results for $\alpha = 1.5$:

$$\left\langle \tfrac{1}{2} \left(\sqrt{\bar{D}_{h\,ij}} \right)^2 \right\rangle = 7.5 \, \langle \varepsilon \rangle^{2/3} \, h^{-4/3} \qquad \text{(A3-31)}$$

and

$$c_1 = 0.22. \qquad \text{(A3-32)}$$

A3.3. Values of c_1 according to Deardorff

Deardorff [29, 30, 31, 32, 33] performed numerical calculations for plate flows according to Chapter 1.5.3. The square of the deformation velocity in (5-3) is calculated according to the following difference formulas (using the notation in Chapter 3):

$$\frac{1}{2}\left(\overline{D_{ij}}\right)^2 = \frac{1}{2}\overline{\left(\delta_{x_i}\overline{u_j} + \delta_{x_j}\overline{u_i}\right)^2}^{i}\,(1-\delta_{[i][j]}) + 2\left(\delta_{x_j}\overline{u_i}\right)^2\delta_{[i][j]} \qquad \text{(A3-33)}$$

/ 138

The calculations for the plate flow with a constant axial pressure gradient [28, 29, 30] showed that the values of c_1 calculated by Lilly using (A3-33) are too large. In order to obtain turbulence statistics which would agree with experience, c_1 would have to be in the range

$$0.08 \leq c_1 \leq 0.12 \qquad \text{(A3-34)}$$

For the investigation of the stability of the atmosphere the influence of buoyancy forces caused by a temperature gradient and the Coriolis acceleration [33], which is considered as a plate flow, it was found that we also have $c_1 \approx 0.13$ in the isothermal case (except in the wall mesh, where the calculations are performed with $c_1 = 0.10$). However

$$c_1 \approx 0.21 \qquad \text{(A3-35)}$$

is used when there is a temperature gradient. This change is justified by the fact that a large contribution of the average deformation velocity is made to (A3-33) because of the Coriolis force in the isothermal case, which would lead to large turbulent viscosities according to (5-3) if c_1 were not reduced. It was found [33] that the value $c_1 \approx 0.21$ can always be used if the average velocity is first subtracted when $\left(\overline{D_{ij}}\right)^2$ is calculated according to (A3-33), therefore

$$\frac{1}{2}\left(\sqrt{\bar{D}_{ij}}\right)^2 = \frac{1}{2}\overline{\left(\delta_{x_i}\left(\bar{u}_j - \langle u_j\rangle\right) + \delta_{x_j}\left(\bar{u}_i - \langle u_i\rangle\right)\right)^2}^{ij}\left(1 - \delta_{[i][j]}\right) + 2\left(\delta_{x_j}\left(\bar{u}_i - \langle u_i\rangle\right)\right)^2 \cdot \delta_{[i][j]} \qquad \text{(A3-36)}$$

A3.4. Calculation of the Kinetic Energy $\sqrt{\bar{E}'}$

The kinetic energy is an additional term in (A3-1), but it can be treated together with the pressure per unit of mass. Therefore it must not be explicitly known for the integration of the momentum equations, but it is required for the evaluation.

A rough approximation corresponding to the approximation for $\langle\sqrt{\bar{D}_{ij}}^2\rangle$ in Chapter A3.2.2, results in the following:

$$\langle\sqrt{\bar{E}'}\rangle = \int_{\pi/h}^{\infty} E(k)\,dk \qquad \text{(A3-37)}$$

and with (4-4):

$$\langle\sqrt{\bar{E}'}\rangle = \frac{3}{2}\,\alpha\,\langle\varepsilon\rangle^{2/3}\left(\frac{h}{\pi}\right)^{2/3} \qquad \text{(A3-38)}$$

/139

With $\langle\varepsilon\rangle^{2/3}$ according to (A3-21) it follows that

$$\langle\sqrt{\bar{E}'}\rangle = \langle\left(\sqrt{\bar{D}_{ij}}\right)^2\rangle \cdot h^2/(2\pi^2) \approx 0.050 \cdot h^2 \cdot \langle\left(\sqrt{\bar{D}_{ij}}\right)^2\rangle \qquad \text{(A3-39)}$$

Deardorff [29, 33] calculates $\sqrt{\bar{E}'}$ while referring to Lilly [81] from the following equation

$$\sqrt{\bar{E}'} = 2\mu^2/(c_e \cdot h)^2 \quad \text{with} \quad c_e = 0.094 \qquad \text{(A3-40)}$$

If μ is given by (5-3) and c_1 is given by (A3-32), it follows that:

$$\langle\sqrt{\bar{E}'}\rangle = \frac{c_1^2}{c_e^2}\,h^2\langle\left(\bar{D}_{ij}\right)^2\rangle = 0.27 \cdot h^2\langle\left(\bar{D}_{ij}\right)^2\rangle \qquad \text{(A3-41,42)}$$

The kinetic energies of the fluctuation velocities calculated by Deardorff are therefore too large.

A3.5. Calculation of the Constant c_1 using the Method of Chapter 5.2.2.3.2. and of Appendix 2

If the trial solution (A3-1) is substituted in the conservation equation (3-31) for $\overline{E'}$ and if the time average is taken according to Chapter 5.2.2.3.2, and then if the average is taken over the entire flow space and if one ignores the molecular dissipation due to the macroscopic velocities, then with

$$\sigma_3 \equiv \left\langle \left(\tfrac{1}{2} \overline{D_{ij}}^2 \right)^{3/2} \right\rangle \Big/ \left\langle \tfrac{1}{2} \overline{D_{ij}}^2 \right\rangle^{3/2} \qquad \text{(A3-43)}$$

we obtain the following for constant c_1:

$$c_1 = \left(\frac{\langle \varepsilon \rangle}{h^2 \left({}_3D^2 \right)^{1/2} {}_2D^2 \cdot \sigma_3} \right)^{1/2}, \qquad \text{(A3-44)}$$

where ${}_3D^2$ and ${}_2D^2$ are defined by (4-25, 26).

If we use the results of Appendix 2 we find

$$c_1 = \left[f_2^3 \; D12^2(\Delta x_1/h, \Delta x_2/h, \Delta x_3/h) \cdot D13(\Delta x_1/h, \Delta x_2/h, \Delta x_3/h) \right]^{1/4} \qquad \text{(A3-45)}$$

D12, D13 are the FORTRAN subprograms given in Table 7. For $\alpha = 1.5$, $\sigma_3 = 1.$ we find the following numerical results:

	$\Delta x_1 : \Delta x_2 : \Delta x_3 = 1:1:1$	$\Delta x_1 : \Delta x_2 : \Delta x_3 = 0.125 : 0.05 : 0.05$
$c_1 =$	0.215	0.225

(A3-46)

These values agree very well with the value $c_1 = 0.21$, which had proved itself in [33]. Equation (A3-46) also showed that the error in assuming (5-6) for the mesh sizes used by Deardorff [29] is small as far as the magnitude of the constant c_1 is concerned. However, this does not mean that the viscosities calculated with this are correct for meshes not having equal lengths. This was

discussed in Chapter 5. / 140

APPENDIX 4

Solution of the Poisson Equation using the Fast Fourier Transformation

A4.1. Problem

In Chapter 6.2.2 we established a Poisson equation with Neumann boundary conditions for calculating the auxiliary potential ψ or the true pressure p. Written out, it has the following difference form for cylindrical coordinates (see Section 5):

$$\frac{1}{\tau_k}\frac{1}{\Delta\tau_k}\left(\frac{\tau_{k+1/2}}{\Delta\tau_{k+1/2}}\psi_{i,j,k+1}-\left(\frac{\tau_{k+1/2}}{\Delta\tau_{k+1/2}}+\frac{\tau_{k-1/2}}{\Delta\tau_{k-1/2}}\right)\psi_{i,j,k}+\frac{\tau_{k-1/2}}{\Delta\tau_{k-1/2}}\psi_{i,j,k-1}\right)$$
$$+\frac{1}{(\tau_k\Delta\varphi)^2}\left(\psi_{i,j+1,k}-2\psi_{i,j,k}+\psi_{i,j-1,k}\right)+\frac{1}{\Delta x^2}\left(\psi_{i+1,j,k}-2\psi_{i,j,k}+\psi_{i-1,j,k}\right)$$
$$=q_{i,j,k};\quad i=1,2,\dots,IM;\quad j=1,2,\dots,JM;\quad k=1,2,\dots,KM \qquad (A4\text{-}1)$$

Boundary conditions:

a) Periodicity in the φ,z direction:

$$\psi_{i,j,k}=\psi_{i+I\cdot IM,\,j+J\cdot JM,\,k};\quad I=0,\pm1,\pm2,\dots;\quad J=0,\pm1,\pm2,\dots \qquad (A4\text{-}2)$$

b) $\delta_\tau\psi=0$ at the wall:

$$\psi_{i,j,0}=\psi_{i,j,1};\quad \psi_{i,j,KM}=\psi_{i,j,KM+1};\quad i=1,2,\dots,IM;\ j=1,2,\dots,JM. \qquad (A4\text{-}3)$$

With these boundary conditions, ψ is determined to within an additional constant. We must satisfy the following consistency condition [87] to guarantee the existence of the solution:

$$\sum_{k=1}^{KM}\sum_{j=1}^{JM}\sum_{i=1}^{IM} q_{i,j,k}\;\Delta z\cdot\Delta\varphi\cdot\Delta\tau_k\cdot\tau_k=0 \qquad (A4\text{-}4)$$

A4.2. Solution Method

In the following we will describe the solution method, the principle of which was first given by Hockney [55]. A direct method is used which is much faster than the iteration method [16] and does not have any stability problems [61]. The method is very similar to the one used by Williams [141]. The periodic boundary conditions make it possible to use the fast Fourier transformation routines.

In addition, the method used here makes it possible to use variable mesh separations in the radial direction. In conjunction with the transposition algorithm described in [38, 125], the method used here can also be used effectively if the fields ψ and q, respectively, cannot be completely stored in storage [128]. /141

The solution method is based on a series expansion of the source term q and the solution ψ in the azimuth and axial direction into trigonometric functions, which identically satisfy the periodic boundary conditions (A4-2):

$$\psi_{i,j,k} = \sum_{\nu=0}^{JM-1} \sum_{\mu=0}^{IM-1} CP(\mu+1, \nu+1, k)\, e^{\sqrt{-1}\frac{\nu 2\pi (j-1)}{JM}} \cdot e^{\sqrt{-1}\frac{\mu 2\pi (i-1)}{IM}} \qquad \text{(A4-5)}$$

$$q_{i,j,k} = \sum_{\nu=0}^{JM-1} \sum_{\mu=0}^{IM-1} CQ(\mu+1, \nu+1, k)\, e^{\sqrt{-1}\frac{\nu 2\pi (j-1)}{JM}} \cdot e^{\sqrt{-1}\frac{\mu 2\pi (i-1)}{IM}} \qquad \text{(A4-6)}$$

No series expansion in terms of eigen functions is used in the radial direction, because in this case it is necessary to use Bessel functions, which are much more complicated numerically. It is more advantageous to use complex eigen functions instead of real eigen functions (sin and cos) (as in [141]). This is because instead of one product of two eigen functions, it will be necessary to deal with four products. Also, special situations occur for D=M=0 which are avoided when the complex notation is used [50].

The complex coefficients CQ in (A4-6) can be calculated as follows based on the orthogonality properties of the eigen functions

$$CQ(\mu+1,\nu+1,k)=\frac{1}{IM\cdot JM}\sum_{j=1}^{JM}\sum_{i=1}^{IM} q_{i,j,k}\, e^{-\sqrt{-1}\,\frac{\nu 2\pi(j-1)}{JM}}\, e^{-\sqrt{-1}\,\frac{\mu 2\pi(i-1)}{IM}} \qquad \text{(A4-7)}$$

$$\mu = 0,1,2,\ldots,IM-1;\quad \nu = 0,1,2,\ldots,JM-1;\quad k = 1,2,\ldots,KM.$$

The initial data $q_{i,j,k}$ consists of IM·JM real numbers for K = const and the Fourier coefficients are made up of CQ IM·JM complex numbers, which is twice as many individual values. However, it is only necessary to store one-half of this data because we have:

$$CQ(\mu+1,\nu+1,k) = CQ^{*}(IM-\mu+1,\,JM-\nu+1,\,k) \qquad \text{(A4-8)}$$

$$\nu = 0,1,2,\ldots,(JM-1)/2$$

$$\mu = 0,1,2,\ldots,(IM-1)/2$$

$$\nu,\mu \neq 0,0$$

$$CQ(1,1,k) = CQ^{*}(1,1,k) \quad \text{(real)}$$

(The star characterizes the conjugate complex value) /142

A4.3. Evaluation of the Fast Fourier Transformation (FFT)

Equation (A4-7) and Equation (A4-5), if CP values are known, are calculated according to the fast Fourier (FFT) method developed by Cooley and Tukey [19]. Reference [20] contains a detailed description of this transformation. For the FFT, the periodic properties of harmonic functions are exploited in order to reduce a large number of multiplications to a single multiplication. When the sums in (A4-5,7) are evaluated directly, the number of multiplications increases in proportion to $(IM.JM)^2$. For the FFT, the number of operations is only proportional to (IM·JM)ln(IM.JM). The FFT therefore is especially effective (also for transposition [125], if the factors IM and JM can be decomposed into as many small prime numbers as possible. The algorithms also become especially simple if these prime factors

are all equal to two. Brenner [14] developed a program "FOUR2" which corresponds to the FFT. It is used here.

A4.4 Establishment of the Difference Equation for CP

(Abbreviation $CP_{\mu,\nu,k} \equiv CP(\mu+1, \nu+1, k)$
$CQ_{\mu,\nu,k} \equiv CQ(\mu+1, \nu+1, k)$)

The coefficients $CP_{\mu,\nu,k}$ are determined from the difference equation (A4-1), which is substituted into the trial solution (A4-5,6). We find

$$\frac{1}{\tau_k \Delta\tau_k}\frac{\tau_{k+1/2}}{\Delta\tau_{k+1/2}} CP_{\mu,\nu,k+1} - \left\{\frac{1}{\tau_k \Delta\tau_k}\left(\frac{\tau_{k+1/2}}{\Delta\tau_{k+1/2}} + \frac{\tau_{k-1/2}}{\Delta\tau_{k-1/2}}\right) + \frac{\lambda_\nu}{(\Delta\varphi\tau_k)^2} + \lambda_\mu\right\} CP_{\mu,\nu,k} \tag{A4-9}$$

$$+ \frac{1}{\tau_k \Delta\tau_k}\frac{\tau_{k-1/2}}{\Delta\tau_{k-1/2}} CP_{\mu,\nu,k-1} = CQ_{\mu,\nu,k}$$

$$k = 1, 2, \ldots, KM$$

$$\lambda_\mu = \frac{2}{\Delta x^2}\left(1 - \cos\left(\mu\frac{2\pi}{IM}\right)\right); \quad \lambda_\nu = 2\left(1 - \cos\left(\nu\frac{2\pi}{JM}\right)\right) \tag{A4-10}$$

$$\nu = 0, 1, 2, \ldots, (JM-1); \quad \mu = 0, 1, 2, \ldots, (IM-1).$$

From the boundary conditions (A4-3) it also follows that /143

$$CP_{\mu,\nu,1} = CP_{\mu,\nu,0}$$
$$CP_{\mu,\nu,KM} = CP_{\mu,\nu,KM+1} \tag{A4-11}$$

The equations (A4-9, 10, 11) represent IM·JM linear equations for the complex coefficients $CP_{\mu,\nu,k}$; k=0,1,2..., KM,KM+1/. These equations have unique solutions only if $\left(\frac{\lambda_\nu}{(\Delta\varphi\tau_k)^2} + \lambda_\mu\right) \neq 0$ because otherwise the solution is only determined up to an additional constant, that is, only for $\nu, \mu \neq 0,0$. The case $\nu,\mu = 0,0$ must be treated separately. After dividing by $\left\{-\frac{\tau_{k+1/2}}{\tau_k \Delta\tau_k \Delta\tau_{k+1/2}}\right\}$ we obtain the following result in an abbreviated form from (A4-9)

$$-CP_{\mu,\nu,k+1} + B(k)\, CP_{\mu,\nu,k} - C(k)\, CP_{\mu,\nu,k-1} = D_k \tag{A4-12}$$

$$C(k) = \frac{\Delta\tau_{k+1/2} \cdot \tau_{k-1/2}}{\Delta\tau_{k-1/2} \cdot \tau_{k+1/2}}$$

where $B(k) = 1 + C(k) + \frac{\Delta\tau_k \cdot \Delta\tau_{k+1/2} \cdot \tau_k}{\tau_{k+1/2}} \left(\frac{\lambda_\nu}{(\Delta p \tau_k)^2} + \lambda_\mu \right)$

$$D(k) = -\frac{\tau_k}{\tau_{k+1/2}} \Delta\tau_k \Delta\tau_{k+1/2} \cdot CQ_{\mu,\nu,k} \qquad \text{(A4-13)}$$

A4.5. Solution of the Differential Equation for CP

A4.5.1. Case $\nu, \mu \neq 0,0$

The system of equations (A4-12) can be solved for $\nu, \mu \neq 0,0$ using the Gaussian elimination algorithm, which is simple and fast for such triple diagonal systems. However, there is a simple recursion solution [111, 141], for these equations, which corresponds to the Gaussian algorithm. In addition it is very stable [111, p. 198].

The following trial solution is used:

$$CP_{\mu,\nu,k} = CP_{\mu,\nu,k+1} \cdot E(k) + F(k); \quad k = KM, KM-1, \ldots, 1; \qquad \text{(A4-14)}$$

From this it follows that:

$$CP_{\mu,\nu,k-1} = CP_{\mu,\nu,k+1} \cdot E(k)E(k-1) + F(k) \cdot E(k-1) + F(k-1).$$

We will substitute both relationships (A4-12) and therefore we obtain the following conditions for arbitrary CP

$$\begin{aligned} E(k) &= 1/(B(k)-C(k).E(K-1)) \\ F(k) &= (C(k)F(k-1)+D(k)) \cdot E(k) \end{aligned} \qquad \text{(A4-15)}$$

/144

The boundary condition (A4-11) is satisfied for k=1 if we have

$$\begin{aligned} E(0) &= 1 \\ F(0) &= 0 \end{aligned}$$

Starting with these values it is possible to calculate all the E(k), F(k) for k = 1,2....,KM from (A4-15). E(k) just like

B(k) is independent of μ,ν and therefore cannot be calculated once and for all as stated in [141]. From the boundary condition (A4-11) for k=KM and (A4-14) it follows that

$$CP_{\mu,\nu,KM} = F(KM)/(1.-E(KM)) \qquad \text{(A4-16)}$$

With this initial value then it is possible to calculate all the $CP_{\mu,\nu,k}$ for k=KM-1,KM-2,...,1, according to (A4-14).

A4.5.2 Case ν,μ = 0.0 Consistency Condition

For ν = μ = o we may arbitrarily set, for example

$$CP_{0,0,1} = 0$$

From the boundary condition (A4-11) and for (A4-12) it then follows that

$$CP_{0,0,2} = -D(1)$$

The remaining $CP_{0,0,k}$ can be calculated for k=3,4,...,KM according to (A4-12) from

$$CP_{0,0,k} = B(k-1)\cdot CP_{0,0,k-1} - C(k-1)CP_{0,0,k-2} - D(k-1) \qquad \text{(A4-17)}$$

In order to also satisfy the boundary condition k=KM (A4-11), D(k) must satisfy a condition which corresponds to the consistency condition (A4-4) and which will now be derived:

Using the following abbreviation for the gradient of CP

$$g_{k+1/2} \equiv \tau_{k+1/2}\,(CP_{0,0,k+1} - CP_{0,0,k})/\Delta\tau_{k+1/2}$$

it follows from (A4-9) that

$$\frac{1}{\tau_k\,\Delta\tau_k}\,(g_{k+1/2} - g_{k-1/2}) = CQ_{0,0,k}$$

and from (A4-11) it follows that $g_{1/2}=0$

By complete induction it is easily shown that we have

$$g_{k+1/2} = \sum_{k'=1}^{k} \tau_{k'} \cdot \Delta\tau_{k'} \cdot CQ_{0,0,k'}$$

In order for the boundary conditions (A4-11) /145

$$g_{KM+1/2} = 0$$

to be satisfied, we must therefore have

$$\sum_{k=1}^{KM} CQ_{0,0,k} \cdot \tau_k \cdot \Delta\tau_k = 0$$

This condition is directly equivalent to the requirement (A4-4) because for $\nu=\mu=0$ and from (A4-7) it follows that

$$CQ_{0,0,k} = \frac{1}{IM \cdot JM} \sum_{j=1}^{JM} \sum_{i=1}^{IM} q_{i,j,k} .$$

Since $q_{i,j,k}$ is equal to the divergence of the velocity field $\{\tilde{v}_x, \tilde{v}_\varphi, \tilde{v}_r\}$, and its component $\tilde{v}_r$ must always be equal to zero at the wall according to (6-5), the consistency condition given above is always theoretically satisfied according to (A5-11). Because of rounding errors, the sum (A4-4) can be slightly different from zero. This can cause non-convergence of the iteration solution procedure, as our own numerical experiments have shown. The method described here is not sensitive to such rounding errors.

The method described, therefore, has the following advantages:

- exact solution (if rounding errors are ignored) after a finite computation time
- very small computation time (see Chapter 10)

The disadvantages are the requirement that the values IM, JM be powers of 2. Also it is not possible to transfer the results to complicated geometric boundaries.

APPENDIX 5:

Accuracy and Consistency of the Difference Formulas

A5.1 Statistical Errors of the Linear Difference Approximations

/146

A typical linear difference approximation is the approximation

$$\overline{{}^{2}u_1}(x_1,x_2,x_3,t) = \overline{{}^{1}\overline{u}_1}^{1} = \frac{1}{2}\left({}^{1}u_1(x_1+\frac{\Delta x_1}{2},x_2,x_3,t)+{}^{1}u_1(x_1-\frac{\Delta x_1}{2},x_2,x_3,t)\right) \quad \text{(A5-1)}$$

This approximation assumes that ${}^{1}u_1(x_1,x_2,x_3,t)$ is a sufficiently smooth field, so that linear interpolations are possible. For locally homogeneous turbulence, this approximation is certainly correct in the statistical sense. Nevertheless, the approximation given above can have an error at a certain point in time, which is characterized by the following standard deviation f:

$$f^2 = \left\langle \left[{}^{2}u_1(x_1,x_2,x_3) - \frac{1}{2}\left({}^{1}u_1(x_1+\frac{\Delta x_1}{2},x_2,x_3)+{}^{1}u_1(x_1-\frac{\Delta x_1}{2},x_2,x_3)\right)\right]^2\right\rangle \quad \text{(A5-2)}$$

Assuming locally isotropic turbulence, we find the following according to Appendix 2:

$$f^2 = \langle {}^{2}u_1\,{}^{2}u_1(0)\rangle + \frac{1}{2}\langle {}^{1}u_1\,{}^{1}u_1(0)\rangle + \frac{1}{2}\langle {}^{1}u_1\,{}^{1}u_1(\Delta x_1,0,0)\rangle - 2\langle {}^{2}u_1\,{}^{1}u_1(\tfrac{\Delta x_1}{2},0,0)\rangle \quad \text{(A5-3)}$$

For meshes of equal side lengths, using (A2-40, 41, 42) we have

$$f^2 = f_2\cdot\langle\varepsilon\rangle^{2/3}\Delta x_1^{2/3}\left[2\alpha_3^*(1,1,1,\tfrac{1}{2},0)-\alpha_2^*(1,1,1,0,0)-\frac{1}{2}\alpha_1^*(1,1,1,0,0)-\alpha_1^*(1,1,1,1,0)\right] \quad \text{(A5-4)}$$

$$= 0.0641\, f_2\langle\varepsilon\rangle^{2/3}\Delta x_1^{2/3}$$

$$f = 0.253\, f_2^{1/2}\langle\varepsilon\rangle^{1/3}\Delta x_1^{1/3} \quad \text{(A5-5)}$$

This statistical error therefore decreases as the mesh edge length Δx_1 is decreased, but only slowly according to the power 1/3. This result is, of course, only to be applied in the

region in which the Kolmogorov spectrum is valid according to (4-6). For very large mesh sizes, where $\overline{u}_1^2, \overline{u}_1^4$ strive to constant values for homogeneous turbulence, as well as for very small mesh separations, where the smoothing becomes noticeable because of the molecular viscosity, the error is probably smaller. The result given above is therefore a pessimistic one.

If point velocities and not area averages were approximated by arithmetic averaging according to

$$u_1 = \overline{u}_1^1$$

then from (4-6) we obtain:

$$f = \left[\frac{3}{2}\left(\frac{1}{2}\right)^{2/3} - \frac{3}{8}\right]^{1/2} f_2^{1/2} \langle\varepsilon\rangle^{1/3} \Delta x_1^{1/3} = 0.755 \cdot f_2^{1/2} \langle\varepsilon\rangle^{1/3} \Delta x_1^{1/3} \quad \text{(A5-6)}$$ /147

i.e. the averaging operation reduces the error by about a factor of 3 but does not change it in principle.

Just like in the fine structure model (Chapter 5.2.2.5.3), instead of the deterministic approximation (A5-1) given above, one could think of a statistical approximation which has an average value corresponding to (A5-1). In contrast to the fine structure model, we even have a trial solution for specifying the standard deviation, given by (A5-5).

A5.2 Truncation Error

A5.2.1. Limited Phase and Wave Number Resolution

As Orszag [96] discussed in great detail, difference approximations lead to errors which can cause erroneous amplitudes and phases of the solutions. These errors are especially large for Fourier components corresponding to large wave numbers. The phase errors would disappear if the Galerkin method (see Chapter 1.5.2) were used. Deardorff [33] points out

that the energy spectra of the kinetic energy dissolved in the grid drop off very rapidly at the maximum wave numbers which can be resolved (approximately according to k^{-4}), so that these errors have only a relatively small weight (see Figure 23).

With difference approximations for grids with an edge length of Δx, it is in principle impossible to represent Fourier components with wavelengths smaller than $2 \cdot \Delta x$ [94].

A5.2.2. Truncation Error of the Convective Terms

If we assume that the average velocity fields $\bar{u}_i$ can be represented by Taylor series expansions, then it is possible to determine the truncation error of the difference formulas. The truncation errors of the convective terms are especially important here. If we consider Cartesian coordinates, we obtain for example

$$\delta_{x_1}(\bar{u}_1^1 \bar{u}_1^1) = \frac{\partial}{\partial x_1}(u_1 \cdot u_1) + f$$
$$f = \frac{\partial^2 u_1}{\partial x_1^2}\frac{\partial u_1}{\partial x_1}\frac{\Delta x_1^2}{2} + \frac{\partial^3 u_1}{\partial x_1^3} u_1 \frac{\Delta x_1^2}{3} + O(\Delta x_1^4) \qquad \text{(A5-7)}$$

/148

It seems more favorable to use the approximation of Amsden-Harlow [3]

$$2 u_1 \delta_{x_1} \bar{u}_1^1 = \frac{\partial}{\partial x_1}(u_1 \cdot u_1) + f$$
$$f = \frac{\partial^2 u_1}{\partial x_1^2} u_1 \frac{\Delta x_1^2}{3} + O(\Delta x_1^4), \qquad \text{(A5-8)}$$

because here the truncation error does not have any second derivative. This has a favorable effect on the stability behavior. However, one disadvantage of this approximation is the fact that the difference formulas do not correspond to the conservation equations for kinetic energy, which can lead to instabilities because of aliasing (see Chapter A5.3 and A5.4). This type of approximation is therefore not used here, as was done in [54, 79, 94].

A5.2.3. False Diffusion

False diffusion is discussed in [49], for example. It is produced by the limited resolution capacity in the difference grid for large gradients. For example, the function y(x) has a ramp at x_o

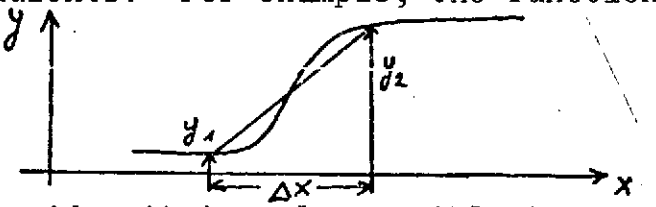

In the difference grids, it is only possible to represent the gradient $(y_2-y_1)/\Delta x$ as a maximum. The field y is therefore artificially smoothed which appears as a false diffusion. This error becomes large if the maximum gradient is not in the direction of the coordinate line but along the diagonal of the mesh. The mesh and length should therefore be parallel or perpendicular to the streamlines as much as possible. This assumption is satisfied for the average flow.

A5.3. Aliasing Errors

The aliasing error is produced by nonlinear terms. It was first demonstrated by Phillips [100] for the convective terms. Miyakoda [87] showed that it can be produced by nonlinear viscosity. This error is also discussed in [1,10,79,96, 100]. The error is based on the finite wave number resolution. If two position dependent functions are multiplied which contain both Fourier components with the wave numbers k = 0,1,2...,N, /149 then a product is produced which contains Fourier components with k = 0,1,2,..,2N. However, only the components with $k \leq N$ can be represented by the difference grid. The components with a higher wave number are added to the components with the smaller wave numbers. In this way part of the physical energy transport from small wave numbers to large wave numbers is reversed. This effect can lead to instabilities. One solution for this is to

structure the difference formulas in such a way that they contain energy according to Chapter A5.4.

A5.4. Consistency with the Physical Conservation Laws

Based on the wall adhesion condition and the periodic boundary conditions, if there are no field forces and if the viscosities are zero, we have

Momentum conservation:

$$\iiint_V \frac{\partial u_i}{\partial t}\, dV = 0\,; \quad i = 1,2,3 \tag{A5-9}$$

Energy conservation:

$$\iiint_V \frac{\partial (u_i^2/2)}{\partial t}\, dV = 0\,, \tag{A5-10}$$

where V is the total flow volume and the velocity field satisfies the continuity equation exactly. The different formulas must be consistent with these physical laws and therefore we must require that the sums over the corresponding difference approximations over all of the difference meshes also vanish.

These conservation laws apparently are satisfied for the difference formulas of the momentum, because the convective terms were used in their conservative form and therefore, for example,

$$\sum_{k=1}^{KM} \delta_{x_3}\left(\bar{u}_3^1 \bar{u}_1^3\right) = \left[\bar{u}_3^1 \bar{u}_1^3\Big|_{k=KM+\frac{1}{2}} - \bar{u}_3^1 \bar{u}_1^3\Big|_{k=\frac{1}{2}}\right] \Big/ \left[x_{KM+\frac{1}{2}} - x_{\frac{1}{2}}\right] \tag{A5-11}$$

and the right side vanished because of $u_3=0$. A similar statement can be proven for the energy according to [78]. However, it must be assumed that the continuity equation is also satisfied exactly in the difference form.

Piacsek-Williams [105] derived difference formulas for which the requirement for energy conservation is not necessary. However, in this case, the momentum is only conserved if the continuity equation is satisfied. Nevertheless, the suggestions of Piacsek-Williams are attractive if the continuity equation is exactly satisfied, for example because of the iterative solution of the Poisson Equation (6-9), because it is probably more important to conserve the energy than the momentum because of the quadratic type of stability. In this paper, the continuity equation is always satisfied to within a very small error because of the very accurate pressure calculation. It seems that the formulas of Piacsek-Williams are not required.

A5.5. Numerical Errors

As is well known, numerical errors are produced because of the limited number of decimal or dual locations which are available in the computer for representing floating decimal numbers. This limited number of places is especially apparent in the calculation of the difference of two approximately equal numbers. For example, for three decimal places we have

$$0.164E2 - 0.163E2 = 0.1??E0$$

The difference is only accurate to one place in the example. This effect is known for the calculation of differences, but is usually ignored for the summation of a very large number of numbers having the same order of magnitude in a sum accumulator.

For example, if a 3. floating point installation is used to represent the addition of 10,000 numbers A(I) having the order of magnitude of 1. according to the prescription FORTRAN:

```
      S   =   0.
      DO 1 I = 1,10000
    1 S   =   S+A(I) ,
```

then after 1,000 summations, the intermediate result in S differs by 3 powers of ten from the A(I), and the sum S no longer changes because of

```
0.100E4 + 0.1E1  =  0.100E4
```

Such numerical errors can be kept small if the following rules are observed.

Difference formation: /151

Rule 1:

Transform the numbers such that their average value is equal to zero.

Sum formation:

Rule 2:

When sum terms having different orders of magnitude are summed in an accumulator, the sum must first be taken over the smallest order of magnitude.

Rule 3:

When the sum of many numbers having the same order of magnitude is taken, as many partial sums as possible should be formed, and the sum of them is then formed. The summation given above is better programmed as follows:

```
      S0   =  0.
      DO 1  I = 1,100
      S1   =  0.
      DO 2  J = 1, 100
    2 S1   =  S1+A(J+(I-1)*100)
    1 S0   =  S0+S1
```

Rule 1 is considered by means of a Galileo transformation (see Chapter 7.2). The other rules have been taken into account in the programming.

/152

APPENDIX 6:

Stability of the Difference Formulas

A6.1. Linear Stability Analysis

A6.1.1. Summary and Linearization

In this chapter we will establish stability criteria for the linearized difference formulas.

In addition to the formulas used

Type a) According to (6-4), jump method in time, central difference quotients for convective terms, time delayed diffusion terms

Type b) According to (5-100, 6-20, 24), Euler method in the time "upwind" differences for the convection terms

another possible difference formula which has often been recommended [42, 44, 112] is investigated.

Type c) Jump method in time, central difference formulas for the convective terms and DuFort-Frankel method [111] for the diffusion terms

It is found that this method is worse than the other methods for small viscosities for more than one dimension.

In addition we investigated the possibility of using "upwind" differences for the convective terms for Type a) as well. We found that the method would then become unstable. Therefore we did not investigate the details.

The linearization refers to the following:

- Assumption of constant convection velocities $\{V_x, V_\varphi, V_r\}$
- Assumption of constant viscosities μ
- Pressure gradients and field forces are ignored
- Decrease of boundary conditions in all directions

In addition, the momentum equations are simplified so they become uncoupled. This uncoupling is exactly valid for Cartesian coordinates. In addition, equidistant meshes and isotropic viscosities are assumed. In this way we obtain the following linearized equations (y stands for one of the velocity components v_x, v_φ, v_r or the kinetic energy $\sqrt{E}$', respectively): / 153

Type a)
$$\frac{y_{i,j,k}^{n+1} - y_{i,j,k}^{n-1}}{2\Delta t} + K_a^n = D_a^{n-1} \qquad \text{(A6-1)}$$

Type b)
$$\frac{y_{i,j,k}^{n+1} - y_{i,j,k}^{n}}{\Delta t} + K_b^n = D_a^n \qquad \text{(A6-2)}$$

Type c) $$\frac{y^{n+1}_{i,j,k} - y^{n-1}_{i,j,k}}{2\Delta t} + K_a^n = D_c^n \qquad \text{(A6-3)}$$

where

$$K_a^n = V_x \frac{y^n_{i+1,j,k} - y^n_{i-1,j,k}}{2\Delta x} + V_\varphi \frac{y^n_{i,j+1,k} - y^n_{i,j-1,k}}{2r\Delta\varphi} + V_r \frac{y^n_{i,j,k+1} - y^n_{i,j,k-1}}{2\Delta r} + V_r \frac{y^n}{r} \delta_{y v_\varphi} \qquad \text{(A6-4)}$$

$$K_b^n = \frac{V_x + |V_x|}{2} \cdot \frac{y^n_{i,j,k} - y^n_{i-1,j,k}}{\Delta x} + \frac{V_x - |V_x|}{2} \cdot \frac{y^n_{i+1,j,k} - y^n_{i,j,k}}{\Delta x}$$
$$+ \frac{V_\varphi + |V_\varphi|}{2} \frac{y^n_{i,j,k} - y^n_{i,j-1,k}}{r\Delta\varphi} + \frac{V_\varphi - |V_\varphi|}{2} \frac{y^n_{i,j+1,k} - y^n_{i,j,k}}{r\Delta\varphi} \qquad \text{(A6-5)}$$
$$+ \frac{V_r + |V_r|}{2} \frac{y^n_{i,j,k} - y^n_{i,j,k-1}}{\Delta r} + \frac{V_r - |V_r|}{2} \frac{y^n_{i,j,k+1} - y^n_{i,j,k}}{\Delta r} + V_r \frac{y^n}{r} \delta_{y v_\varphi}$$

$$D_a^n = \mu \Big\{ \frac{y^n_{i+1,j,k} - 2y^n_{i,j,k} + y^n_{i-1,j,k}}{\Delta x^2}$$
$$+ \frac{y^n_{i,j+1,k} - 2y^n_{i,j,k} + y^n_{i,j-1,k}}{r^2\Delta\varphi^2} - \frac{y^n_{i,j,k}}{r^2}\left(\delta_{y v_\varphi} + \delta_{y v_r}\right) \qquad \text{(A6-6)}$$
$$+ \frac{y^n_{i,j,k+1} - 2y^n_{i,j,k} + y^n_{i,j,k-1}}{\Delta r^2} + \frac{y^n_{i,j,k+1} - y^n_{i,j,k-1}}{r\cdot\Delta r} \Big\}$$

$$D_c^n = \mu \Big\{ \frac{y^n_{i+1,j,k} - \left(y^{n+1}_{i,j,k} + y^{n-1}_{i,j,k}\right) + y^n_{i-1,j,k}}{\Delta x^2}$$
$$+ \frac{y^n_{i,j+1,k} - \left(y^{n+1}_{i,j,k} + y^{n-1}_{i,j,k}\right) + y^n_{i,j-1,k}}{r^2\Delta\varphi^2} - \frac{y^n_{i,j,k}}{r^2}\left(\delta_{y v_\varphi} + \delta_{y v_r}\right) \qquad \text{(A6-7)}$$
$$+ \frac{y^n_{i,j,k+1} - \left(y^{n+1}_{i,j,k} + y^{n-1}_{i,j,k}\right) + y_{i,j,k-1}}{\Delta r^2} + \frac{y^n_{i,j,k+1} - y^n_{i,j,k-1}}{r\Delta r} \Big\}$$

$$\delta_{y v_\varphi} = \begin{cases} 0, & y \neq v_\varphi \\ 1, & y = v_\varphi \end{cases} \qquad \delta_{y v_r} = \begin{cases} 0, & y \neq v_r \\ 1, & y = v_r \end{cases} \qquad \text{(A6-8)}$$

The notation for the "upwind" differences according to (A6-5)/154 corresponds to the suggestion of Kirsch [72].

A6.1.2. General Stability Criterion [111, 140]

The linear homogeneous difference equations can be represented as follows in matrix form

$$y^{n+1}_{i,j,k} = \underline{A1} \cdot \underline{Y^{n}_{i,j,k}} + \underline{A2} \cdot \underline{Y^{n-1}_{i,j,k}} \qquad \text{(A6-9)}$$

where

$$Y_{i,j,k} = \left\{ y_{i,j,k};\ y_{i-1,j,k};\ y_{i+1,j,k};\ y_{i,j-1,k};\ y_{i,j+1,k};\ y_{i,j,k-1};\ y_{i,j,k+1} \right\}^{T}$$

The vectors A1, A2 which are made up of seven elements each are given in Table 8 for the various formula types. These difference equations have the general solution

$$y^{n}_{i',j',k'} = U^{n}_{i,j,k} \exp\left\{ \underset{\sim}{i} \left[k_1 (i'-i)\Delta x + k_2 (j'-j)\Delta\varphi + k_3 (k'-k)\Delta\tau \right] \right\} \qquad \text{(A6-10)}$$

$$\underset{\sim}{i} \equiv \sqrt{-1}$$

and k_1, k_2, k_3 are arbitrary weight numbers. For the vector $\underline{Y_{i,j,k}}$, because of $\{\underset{\sim}{i}\, x\} = \cos(x) + \underset{\sim}{i} \sin(x)$ we have:

$$\underline{Y^{n}_{i,j,k}} = U^{n}_{i,j,k} \cdot \underline{E} \qquad \text{(A6-11)}$$

$$\underline{E} \equiv \left\{ 1;\ -\underset{\sim}{i} S_1 + C_1;\ \underset{\sim}{i} S_1 + C_1;\ -\underset{\sim}{i} S_2 + C_2;\ \underset{\sim}{i} S_2 + C_2;\ -\underset{\sim}{i} S_3 + C_3;\ \underset{\sim}{i} S_3 + C_3 \right\}^{T}$$

$$S_1 \equiv \sin(k_1 \Delta x);\ S_2 \equiv \sin(k_2 \Delta\varphi);\ S_3 \equiv \sin(k_3 \Delta\tau) \qquad \text{(A6-12)}$$

$$C_1 \equiv \cos(k_1 \Delta x);\ C_2 \equiv \cos(k_2 \Delta\varphi);\ C_3 \equiv \cos(k_3 \Delta\tau)$$

$$Si^2 + Ci^2 = 1 \quad ; \quad i = 1,2,3 \qquad \text{(A6-13)}$$

From (A6-9) we therefore find an equation for the variation of the amplitude U with the time step n:

$$U_{i,j,k}^{n+1} = \underline{A1} \cdot \underline{E} \; U_{i,j,k}^{n} + \underline{A2} \cdot \underline{E} \; U_{i,j,k}^{n-1} \qquad \text{(A6-14)}$$

According to Richtmyer [111] the variation of the amplitudes for one step to the next time step n can be described by / 155

$$\begin{pmatrix} U_{i,j,k}^{n+1} \\ U_{i,j,k}^{n} \end{pmatrix} = \underline{\underline{G}} \begin{pmatrix} U_{i,j,k}^{n} \\ U_{i,j,k}^{n-1} \end{pmatrix} \qquad \text{(A6-15)}$$

with the amplification matrix

$$\underline{\underline{G}} \equiv \begin{pmatrix} \underline{A1} \cdot \underline{E} & \underline{A2} \cdot \underline{E} \\ 1 & 0 \end{pmatrix} \equiv \begin{pmatrix} 2(A_{11} + \underset{\sim}{i} B_{11}) & A_{12} + \underset{\sim}{i} B_{12} \\ 1 & 0 \end{pmatrix} \qquad \text{(A6-16)}$$

The real constants A_{11}, B_{11}, A_{12}, B_{12} are given in Table 9 for the various formula types.

The eigenvalues of this amplification matrix $\underline{\underline{G}}$ are

$$\lambda_{1,2} = A_{11} + \underset{\sim}{i} B_{11} \pm \sqrt{(A_{11} + \underset{\sim}{i} B_{11})^2 + A_{12} + \underset{\sim}{i} B_{12}} \qquad \text{(A6-17)}$$

The stability criterion according to Neumann [110, 111] then results from the requirement that the amplitudes of the perturbations U^{n} of the solution cannot increase when the time step n is enlarged. From this we obtain the following necessary condition

$$|\lambda_i| \leq 1 \qquad i = 1,2 \qquad \text{(A6-18)}$$

This condition is also sufficient if $\underline{\underline{G}}$ is equal to its hermitic conjugate term [110], which is assumed as a rule [110, 111, 73, 140].

Just like the requirement (A6-18), of course we have

$$|\lambda_{1/2}^2| \leq 1 \qquad \text{(A6-19)}$$

where

$$|a + \underline{i}\, b| = \sqrt{a^2 + b^2} \quad ; \quad a, b \text{ real} \qquad \text{(A6-20)}$$

From this we can determine the maximum permissible time step Δt, as will be done in the following sections for the individual difference formula types.

A6.1.3. Results for the Permissible Time Step Δt

A6.1.3.1. Type a Difference Formulas (Jump, Delayed Diffusion)

The permissible time step can only be specified in explicit algebraic form for the extreme cases of negligible diffusion or negligible convection:

Case a) Pure convection ($\mu = 0$, $v \neq 0$)

The eigenvalues $\lambda_{1,2}$ here have the following values

$$\lambda_{1,2} = -\underline{i}\,\Delta t \left(\frac{v_x}{\Delta x} S_1 + \frac{v_\varphi}{r\Delta\varphi} S_2 + \frac{v_r}{\Delta r} S_3\right) \pm \sqrt{1 - \Delta t^2 \left(\frac{v_x}{\Delta x} S_1 + \frac{v_\varphi}{r\Delta\varphi} S_2 + \frac{v_r}{\Delta r} S_3\right)^2}$$

From $|\lambda_{1,2}| \leq 1$ it follows that

$$\Delta t^2 \left(\frac{v_x}{\Delta x} S_1 + \frac{v_\varphi}{r\Delta\varphi} S_2 + \frac{v_r}{\Delta r} S_3\right)^2 \leq 1$$

The minimum Δt_K for

$$S_1 = sign(V_x), \quad S_2 = sign(V_\varphi), \quad S_3 = sign(V_r)$$

which results from this is

$$\Delta t_K \leq \left(\frac{|V_x|}{\Delta x} + \frac{|V_\varphi|}{r \Delta \varphi} + \frac{|V_r|}{\Delta r} \right)^{-1} \qquad \text{(A6-21)}$$

Case b) Pure diffusion ($V_x = V_\varphi = V_r = 0$, $r \gg \Delta r$)

$$\lambda_{1,2} = \pm \sqrt{1 + 2\mu\Delta t \left[\frac{2}{\Delta x^2}(C_1 - 1) + \frac{2}{r^2 \Delta \varphi^2}(C_2 - 1) + \frac{2}{\Delta r^2}(C_3 - 1) - \frac{1}{r^2}(\delta_{y u_\varphi} + \delta_{y u_1}) + \frac{2 S_3 k}{r \Delta r} \right]}$$

The magnitudes of these eigenvalues have their maximum at $C_1 = C_2 = C_3 = -1, S_3 = 0$ and we obtain the following permissible time step

$$\Delta t_D \leq \frac{1}{4\mu} \left[\frac{1}{\Delta x^2} + \frac{1}{r^2 \Delta \varphi^2} + \frac{1}{\Delta r^2} - \frac{\delta_{y u_\varphi} + \delta_{y u_r}}{2 r^2} \right]^{-1} \qquad \text{(A6-22)}$$

Case c) Arbitrary parameter values

For the general case, it is necessary to determine the permissible time step Δt numerically. For this, an optimization program is used which operates according to the evolution strategy [60]. The independent variables C_1, C_2, C_3, I_1, I_2, I_3, I_4 where

$$-1 \leq C_i \leq 1, \quad S_i = I_i \sqrt{1 - C_i^2}, \quad i = 1,2,3$$

$$I_i \in \{-1, +1\}, \quad i = 1,2,3,4$$

are varied (I_4 is the sign in front of the square root in (A6-17)) so that a target function ZF is minimized. /157

By means of interval containment, and with a relative accuracy of 10^{-4}, ZF produces the $\Delta t \geq 0$ so that the following relationship holds for the variables specified above

$$|\lambda(\Delta t)| \leq 1, \quad |\lambda(\Delta t + \varepsilon)| > 1.$$

The numerically determined permissible Δt is a function of 10 parameters:

$$\Delta t = \Delta t\left(\mu, V_x, V_\varphi, V_r, \Delta x, r\Delta\varphi, \Delta r, r, \delta_{yu_r}, \delta_{yu_\varphi}\right) \quad \text{(A6-23)}$$

Figure 12 shows a numerical value for

$$\Delta t = \Delta t\left(\mu, V_x, V_x/10, V_x/10, 0.125, 0.05, 0.05, 10^{10}, 0, 0\right) \quad \text{(A6-24)}$$

as a function of viscosity μ for three values of the convection velocity $V_x = 10, 30, 50$. For comparison purposes we also show

$$\Delta t_1 = \min\left\{\Delta t\left(0, V_x, V_x/10, V_x/10, 0.125, 0.05, 0.05, 10^{10}, 0, 0\right), \Delta t\left(\mu, 0, 0, 0, 0.125, 0.05, 0.05, 10^{10}, 0, 0\right)\right\} \quad \text{(A6-25)}$$

as well as

$$\Delta t_2 = \Delta t\left(\mu + \frac{\frac{|V_x|}{\Delta x} + \frac{|V_\varphi|}{r\Delta\varphi} + \frac{|V_r|}{\Delta r}}{4\left(\frac{1}{\Delta x^2} + \frac{1}{(r\Delta\varphi)^2} + \frac{1}{\Delta r^2} - \frac{\delta_{yu_\varphi} + \delta_{yu_r}}{2r^2}\right)}, 0, 0, 0, 0.125, 0.05, 0.05, 10^{10}, 0, 0\right) \quad \text{(A6-26)}$$

Δt_1 is the minimum of the permissible resulting time steps which result for pure convection (Δt_K and pure diffusion (Δt_D), respectively. Δt_2 is the asymptote which results for pure diffusion corresponding to a viscosity which has been enlarged so much that Δt_2 takes on the same value for $\mu = 0$ as Δt_K. These comparison values can be calculated algebraically according to (A6-21,22).

From Figure 12 we can see the following:

a) The permissible time step decreases with increasing viscosity μ and increasing convection velocity V_x.

b) The permissible time step Δt is smaller than the value Δt_K, Δt_D for the limiting cases a and b considered above.

c) The function Δt_2 is a conservative assumption for the permissible time step Δt.

The practical calculations are therefore carried out by a time step determined by Δt_2. As an additional safety factor, it is reduced by a factor which is input, which typically has the value of 0.5. /158

A6.1.3.2. Type b Difference Formula (Euler Method "Upwind" Differences)

For this one step method, the amplification matrix $\underline{\underline{G}}$ is reduced to a scalar value. The eigenvalue is

$$\lambda = \Delta t \left[(C_1-1)\left(\frac{|V_x|}{\Delta x}+\frac{2\mu}{\Delta x^2}\right)+(C_2-1)\left(\frac{|V_\varphi|}{r\Delta\varphi}+\frac{2\mu}{r^2\Delta\varphi^2}\right)\right.$$
$$+(C_3-1)\left(\frac{|V_r|}{\Delta r}+\frac{2\mu}{\Delta r^2}\right)-\frac{V_r}{r}\delta_{yu_\varphi}-\frac{\mu}{r^2}\left(\delta_{yu_\varphi}+\delta_{yv_r}\right)$$
$$\left.-S_1 i\frac{V_x}{\Delta x}-S_2 i\frac{V_\varphi}{r\Delta\varphi}-S_3 i\left(\frac{V_r}{\Delta r}-\frac{2\mu}{r\Delta r}\right)\right]$$

The magnitude of the eigenvalue has a maximum for $r \gg \Delta r$ and for $C_1=C_2=C_3=-1$; $S_1=S_2=S_3=0$. The permissible time step is therefore

$$\Delta t \leq \left[\frac{|V_x|}{\Delta}+\frac{|V_\varphi|}{r\Delta\varphi}+\frac{|V_r|}{\Delta r}+\frac{V_r}{2r}\delta_{yv_\varphi}+2\mu\left(\frac{1}{\Delta x^2}+\frac{1}{r^2\Delta\varphi^2}+\frac{1}{\Delta r^2}+\frac{\delta_{yo_\varphi}+\delta_{yv_r}}{4r^2}\right)\right]^{-1} \quad \text{(A6-27)}$$

This result was derived in a different way by Krause [73, 74]. Figure 13 shows Δt as a function of μ for the same parameter values as in (A6-24). The functions Δt_1, Δt_2 also shown for comparison purposes according to (A6-25, 26) clearly show that for these difference formulas, the permissible time step Δt can take on the same value as for Type a, corresponding to pure convection. For pure diffusion, its value can be twice as large. This means that the time step according to (A6-26) is also conservative in this case, i.e. for the integration of the energy equation (5-100).

A6.1.3.3. Type c Difference Method (Jump Method with Du-Fort-Frankel for the Diffusion Terms)

In this case as well as for Type a, the permissible time step Δt cannot be calculated algebraically for the general case. For pure convection, we find the same permissible time step Δt_k as for Type a, according to (A6-21). For pure diffusion ($V_x = V_\varphi = V_r = 0, \tau = \infty$) the magnitudes of the eigenvalues have a maximum for $C_1 = C_2 = C_3 \in \{-1, +1\}$; $S_1 = S_2 = S_3 = 0$:

$$|\lambda_1| = 1$$
$$|\lambda_2| = \frac{1 - 2\mu\Delta t\left(\frac{1}{\Delta x^2} + \frac{1}{r^2\Delta\varphi^2} + \frac{1}{\Delta r^2}\right)}{1 + 2\mu\Delta t\left(\frac{1}{\Delta x^2} + \frac{1}{r^2\Delta\varphi^2} + \frac{1}{\Delta r^2}\right)} < 1 \quad \text{for } \Delta t > 0. \tag{A6-28}$$

that is, for pure diffusion the difference formulas according to Du Fort Frankel are always stable (this result corresponds to the three-dimensional generalization of the data in [111]).

/159

For the general case of simultaneous convection and diffusion, the permissible time step must be calculated numerically as discussed in Chapter 6.1.3.1. Figure 14 shows the calculated results for the parameter values corresponding to (A6-24). For comparison purposes, we also show the functions Δt_1, Δt_2 (A6-25,26). From this we can see the remarkable result that for positive viscosities μ (not too large), the permissible time step Δt is considerably smaller (by a factor of 1/2 to 1/3 here) than for the Type a difference formulas. For small viscosities μ , it even goes below the otherwise conservative function Δt_2. One would expect that Δt would take on a minimum for pure convection, as was assumed in [112], for example. Figure 15 showed that this limiting value is only exceeded for viscosities μ which are large compared with μ_0.

$$\mu_0 = \left(\frac{|V_x|}{\Delta x} + \frac{|V_\varphi|}{r\Delta\varphi} + \frac{|V_r|}{\Delta r} \right) \left(\frac{1}{\Delta x^2} + \frac{1}{r^2\Delta\varphi^2} + \frac{1}{\Delta r^2} \right)^{-1} \quad \text{(A6-29)}$$

In this paper, however, the viscosity μ is small and the Du Fort-Frankel method is not suitable.

In the following we will show that this statement is directly related to the three dimensionality, because it can be proven that, for the one-dimensional case $\left(\frac{1}{\Delta r} = \frac{1}{r\Delta\varphi} = \infty \;,\; r = \infty \right)$ Δt does indeed take on a minimum for $\mu = 0$.

In the one-dimensional case, the eigenvalues of the matrix $\underline{\underline{G}}$ are:

$$\lambda_{1/2} = \frac{AC_1 - i\,BS_1 \pm \sqrt{(AC_1 - i\,BS_1)^2 + 1 - A^2}}{1+A}$$

where

$$A \equiv \frac{2\Delta t\,\mu}{\Delta x^2} \geq 0 \;, \quad B \equiv \frac{\Delta t \cdot |V_x|}{\Delta x} \geq 0$$

Since we wish to show that $\Delta t = \frac{\Delta x}{|V_x|}$ is permissible, we set B=1. The expression under the square root operator can be transformed as follows:

$$(AC_1 - i\,S_1)^2 + 1 - A^2 = A^2(C_1^2 - 1) + 1 - S_1^2 - i\,2S_1C_1$$

Because of (A6-13) we have:

$$(AC_1 - i\,S_1)^2 + 1 - A^2 = (C_1 - i\,AS_1)^2$$

The root can be taken and the eigenvalues have the following values for B = 1

$$\lambda_1 = C_1 - i\,S_1$$
$$\lambda_2 = \frac{1-A}{1+A}(C_1 + i\,S_1)$$

$$|\lambda_1| = \sqrt{C_1^2 + S_1^2} = 1$$
$$|\lambda_2| = \frac{1-A}{1+A}\sqrt{C_1^2+S_1^2} = \frac{1-A}{1+A} \leq 1 \qquad \text{(A6-30)}$$

Here B = 1 is permissible, i.e. $\Delta t = \Delta x/|V_x|$ is a permissible time step for arbitrary viscosity $\mu \geq 0$. /160

In the two-dimensional case, the eigenvalues are

$$\lambda_{1,2} = \frac{A_1C_1 + A_2C_2 - i(B_1S_1 + B_2S_2) \pm \sqrt{[A_1C_1 + A_2C_2 - i(B_1S_1 + B_2S_2)]^2 + 1 - A^2}}{1+A}$$

where
$$A_1 \equiv \frac{2\Delta t\,\mu}{\Delta x^2} \qquad A_2 \equiv \frac{2\Delta t\,\mu}{\Delta r^2} \qquad A \equiv A_1 + A_2$$
$$B_1 \equiv \frac{\Delta t \cdot |V_x|}{\Delta x} \qquad B_2 \equiv \frac{\Delta t\,|V_r|}{\Delta r} \qquad B \equiv B_1 + B_2$$

If the time step $\Delta t = \left[\frac{|V_x|}{\Delta x} + \frac{|V_r|}{\Delta r}\right]^{-1}$ is to be permissible for pure convection in this case as well, then we must have B = 1. In contrast to the one-dimensional case, the expression under the square root operator cannot be converted into a quadratic form, and we cannot show that $|\lambda_{1,2}| \leq 1$. This is not a proof for the fact that $|\lambda_{1,2}| > 1$ and that the time step given above is too large. This is proven by the numerical result. For example if we assume A1=1/2, A2=2, B1=0.7, B2=0.3, we find that the maximum magnitude of the eigenvalue for $C_1 \approx 0.4$, $C_2 \approx 0.9$ is $|\lambda| = 1.0875$. This example shows that the condition $|\lambda| \leq 1$ is not always satisfied in the two-dimensional case for $\Delta t = [|V_x|/\Delta x + |V_r|/\Delta r]^{-1}$. Consequently this time step is not the minimum of the permissible time steps for arbitrary viscosities μ.

Because of the small viscosities which occur for the simulation of three-dimensional turbulent flows, it is not recommended that the Du Fort-Frankel method be used.

A6.2. The Heuristic Nonlinear Stability Analysis according to Hirt

Hirt [57] gave a heuristic derivation of the fact that nonlinear instabilities are based on truncation errors of the nonlinear terms, which are made up of products having the form

$$a(x)\,\frac{\partial^2 u}{\partial x^2}$$

The factor a(x) is a function of the velocities and of the grid. For example, see the example in (A5-7). In other words the truncation errors appear as additional diffusion terms with variable viscosities a(x). If a(x) is a sufficiently smooth function, it can be linearized and stability criteria for this case can be derived as was done in A6.1. In this way one obtains the results of the type

/ 161

$$\mu > \alpha\, u^2/\Delta t\,;\quad \mu > \beta\, \Delta x^2\, \partial u/\partial x \qquad \text{(A6-31)}$$

where α, β are numerical values. Hirt [57] derives such criteria only for the two-dimensional one-step method. In this paper we attempted to also derive stability criteria of this type for nonlinear terms for the three-dimensional two-step distant formulas used. We encountered the following problems:

a) The truncation errors differ depending on whether the reference point of the Taylor series expansion is the central location point for the time step no or for the time step nl (according to Chapter 6.2.1). We could not decide which was the "correct" reference point, because no exact theory is available.

b) The resulting factors a(x) which result are so complex, that no practical stability criteria can be derived.

For these reasons we did not pursue the stability analysis further, but only used the criteria which were derived from the linearized theory as well as additional safety factors discussed in Chapter A6.1.3.1. /162

APPENDIX

Consideration of Non-Equal Meshes in the Source Term of the Fine Structure Energy Equation

After conclusion of the theory discussed in Chapters 1-8, the first test calculations which had highly unequal meshes

$$\Delta x_1 \gg \Delta x_2 \gg \Delta x_3 \qquad \text{(A7-1)}$$

resulted in velocity fields which did not have the expected random structure. Instead they were definitely regular. This was expressed by the fact that the velocity fields only varied as a function of x_1 with long wave, large amplitude oscillations. They were almost constant as a function of x_2 and x_3, that is:

$$\left\langle \left(\partial \underline{u}/\partial x_1\right)^2 \right\rangle \gg \left\langle \left(\partial \underline{u}/\partial x_2\right)^2 \right\rangle \gtrapprox \left\langle \left(\partial \underline{u}/\partial x_3\right)^2 \right\rangle . \qquad \text{(A7-2)}$$

We found that this effect could be explained because of the unequalness of the mesh edge lengths and its effect on the energy equation. Therefore, we were able to remove it in a corresponding way:

The source term P in (5-44) is proportional to a difference form of the square of the deformation velocity D_{ij}^2, which consists of 9 sum terms $(D_{[i][j]})^2$ (however, here we have $(D_{[i][j]})^2 = (D_{[j][i]})^2$. Because of the unequal mesh edge lengths, the time

averages of the sum terms are unequal. For locally isotropic turbulence with the Kolmogorov spectrum, $\langle (D_{[ij][ij]})^2 \rangle$ approximately varies according to (A3-21) and approximately proportional to $\Delta x_i^{-4/3}$ or $\Delta x_j^{-4/3}$. Therefore, in the expression for the ratio (A7-1) of the mesh edge lengths, for example $\langle D_{11}^2 \rangle$ is much smaller than $\langle D_{33}^2 \rangle$, i.e. a variation of the velocity field in the x_1 direction results in a lower contribution to the source term P than a variation in the x_3 direction. Therefore, at all locations where by chance there is a large gradient $|\partial u / \partial x_3|$, the energy $\sqrt{E}$ and therefore the viscosity μ are large. At these points, the velocity field is rapidly smooth again. However, this is not the case for locations at which $|\partial u / \partial x_3|$ is large, and this is why the result (A7-2) is produced. In order to remove this effect, the individual sum terms $(D_{[ij][ij]})^2$ were multiplied by the weights

$$\frac{\langle D_{ij}^2 \rangle}{\langle D_{[ij][ij]}^2 \rangle} \qquad \text{(A7-3)}$$

which can be calculated for locally isotropic turbulence with the Kolmogorov spectrum using the programs given in Appendix 2. /163
After multiplying with these weights, the time average of all the sum terms will be of the same size if this restriction is observed. With the incorporation of this correction (A7-3), the calculated velocity fields take on the expected random structure which will be discussed in Chapter 10.

APPENDIX 8

Program tests for Laminar Flows

A8.1. Starting Flow

A starting flow is calculated which is obtained for constant viscosity ν (laminar) if a pressure gradient $P_x=2$ accelerates this fluid in the axial direction starting at the

time t = 0, where $\underline{u}(t=0)=\underline{0}$. The solutions of the differencing method are compared with the "exact" solutions calculated according to the program ANLAUF [36] from series "expansion". The calculations are carried out for an annulus with

$$R1=0.25, \quad R2=1.25, \quad \nu = 1$$

Three cases are considered:

Case a) $\Delta t = 0.001, \quad \Delta r = 1/8 \quad (=\text{const})$

Case b) $\Delta t = 0.001,$
$\Delta r = \{0.1, 0.1, 0.13, 0.17, 0.17, 0.13, 0.1, 0.1\}$

Case c) $\Delta t = 0.00025, \quad \Delta r = 1/16 \quad (=\text{const})$

Table 10 shows the deviations ε between the exact solution and the difference method solution at various times. ε_1 are the deviations in the mesh at the inner wall (the largest deviations occur there) and ε_2 are the deviations at r = (R1+R2)/2. The data are presented for $0 < t \leq 0.40$. At the time t = 0.40 the maximum acceleration only amounts to 0.062 instead of 2 at the beginning, and therefore at this time the solution has come quite close to the stationary state.

From Table 10 it can be seen that by using non-equidistant meshes, there is only a slight reduction of the error for very small times at the wall mesh. However, this still leaves open the possibility that a finer resolution for representing the turbulent fields, which fluctuate greatly in the vicinity of the wall, could be advantageous.

A8.2. Flow Between Rotating Cylinders

As a second laminar test problem we consider the stationary flow between two concentric rotating cylinders, which rotate at different rotation rates ω_1 (inside cylinder) and ω_2 (outside). For this case we have the exact solution [120]:

$$v_\varphi(r) = \frac{1}{R2^2 - R1^2}\left[r\left(\omega_2 R2^2 - \omega_1 R1^2\right) - \frac{R1^2 \cdot R2^2}{r}(\omega_2 - \omega_1)\right]$$

Since the solution is in the center of the axial flow, it was investigated at the same time as problem A8.1 was investigated. For $\omega_1 = \omega_2$, $v_\varphi(r)$ is a linear function of the radius r which is obtained exactly by numerical methods. In addition to the azimuth diffusion terms, this example also tests the calculation of the pressure. Because of the centrifugal acceleration, we have the pressure distribution

$$p(r) = \int_{R1}^{r} v_\varphi^2 / r \; dr + p_{w_1}$$

For $\omega_1 = \omega_2 = \omega$ we have

$$p(r) = \frac{\omega^2}{2}\left[r^2 - R1^2\right] + p_{w_1}$$

This solution was reproduced with a relative error of < 1‰ for KM=8 meshes in the radial direction using the difference method.

A8.3 Two-Dimensional Taylor-Green Vortex

For the initial conditions

$$u_1^0 = -\cos(x_1)\cdot\sin(x_1) \quad ; \quad u_2^0 = \sin(x_1)\cos(x_2) \; ; \quad u_3^0 = 0$$

and if no external forces are present, we have the following exact solution [94, 131, 102] for the case of periodic boundary conditions:

$$u_1 = u_1^0 \cdot \exp(-2\nu t)$$
$$u_2 = u_2^0 \cdot \exp(-2\nu t$$
$$u_3 = 0$$
$$p = -\frac{1}{4}\left[\cos(2x_1) + \cos(2x_2)\right] \cdot \exp(-2\nu t)$$

This test problem was also used by Orszag [94] and Chorin [21]. Table 11 shows the errors of the velocity components for

$$\Delta x_1 = \Delta x_2 = \pi/16 \quad ; \quad \nu = 0.05 \quad ; \quad \Delta t = 0.0648$$

Column I contains the errors of the numerical solution, which was calculated using the described difference method. Column II has the errors calculated by Orszag for the same problem. The errors for the method used by Chorin were higher than those of Orszag by several powers of ten. Column III shows the factor by which the errors increase when the mesh size is multiplied by four. Table 11 shows that the method used here is much more accurate for small times than the method used by Orszag. The /166
reason for this is the implicit calculation of the pressure p at the time n2 according to (6-4). Theoretically, for an accuracy of order Δx^2, when Δx is multiplied by four, the error should increase by a factor of 16. This is approximately verified by Column III of Table 11 for the present difference method.

REFERENCES

1. Arakawa, A. Computational Design for Long-Term Numerical Integration of the Equations of Fluid Motion. J. Comp. Phys. Vol. 1, (1966), pp. 116-143.

2. Aziz, K. and J. D. Hellums. Numerical Solution of the Three-Dimensional Equations of Motion for Laminar Natural Convection. Phys. Fluids, Vol. 10, 1967, pp. 314-324.

3. Amsden, A. A. and F. H. Harlow. The SMAC Method: a Numerical Technique for Calculating Incompressible Fluid Flows. LA-4370, 1970.

4. Arndt, R. E. A. and A. W. Nilsen. On the Measurement of Fluctuating Pressure in the Mixing Zone of a Round Jet. ASME: Fluid Dynamic Measurement, Paper 71-FE-31, 1971.

5. Boussinesq, J. Theory of Turbulent Flow. Mém. prés. Acad. Sci. XXIII, 46, Paris, 1877.

6. Batchelor, G. K. The Theory of Homogeneous Turbulence. Cambridge University Press, 1953.

7. Brown, C. E. Basic Concepts. Chapter 68 in Flügge, W.: Handbook of Engineering Mechanics. McGraw Hill, New York 1962.

8. Buleev, N. I. Theoretical Model for Turbulent Transfer in Three-Dimensional Fluid Flow. 3. U. N. Int. Conf. on the Peaceful Use of Atomic Energy, A/Conf. 28/P/329, May, 1964.

9. Bracewell, R. The Fourier Transform and its Applications. McGraw Hill, New York, 1965, pp. 381.

10. Bryan, K. A Scheme for Numerical Integration of the Equations of Motion on an Irregular Grid Free of Nonlinear Instability. Monthly Weather Rev. Vol. 94, 1966, pp. 39-40.

11. Barthels, H. Representation of Heat Transfer in Concentric Annuli Using the Momentum-Heat Exchange Analogy. Jül-506-RB, 1967.

12. Beran, M. J. Statistical Continuum Theories. Interscience Publ., 1968.

13. Bronstein, I. N. and K. A. Semendjajew. Taschenbuch der Mathematik (Handbook of Mathematics). Verlag Harri Deutsch, Zürich, 1968.

14. Brenner, N. Cooley-Tukey Fast Fourier Transform — FOUR 2. IBM Contributed Program Library. Progr. Ord. No. 360 D - 13.4.003, 1969.

15. Bourke, P. J. et al. A Study of the Spatial Structure of Turbulent Flow by Intensity-Fluctuation Spectroscopy. J. Phys. A: Gen. Phys. Vol. 3, 1970, pp. 216-228.

16. Birkhoff, G. The Numerical Solution of Elliptic Equations. Regional Conf. Ser. in Appl. Mathm. Vol. 1, 1971.

17. Boston, N. E. J. and R. W. Burling. An Investigation of High-Wavenumber Temperature and Velocity Spectra in Air. J. Fluid Mech. Vol. 55, 1972, pp. 473-492.

18. Comte-Bellot, G. Turbulent Flow Between Two Parallel Walls. Publications Scientifiques et Techniques du Ministère de l'Air, No. 419, 1965, p. 159.

19. Cooley, J. W. and J. W. Tukey. An Algorithm for the Machine Calculation of Complex Fourier Series. Math Comput. Vol. 19, 1965, pp. 297-301.

20. Cochran, W. T. et al. What is the Fast Fourier Transform? Proc. IEEE, Vol. 55, 1967, pp. 1664-1674.

21. Chorin, A. J. Numerical Solution of the Navier-Stokes Equations. Math. Comp. Vol. 22, 1968, pp. 745-762.

22. Clark, J. A. A Study of Incompressible Turbulent Boundary Layers in Channel Flow. J. Basic Engng. (Transact. ASME) Vol. 90, 1968, pp. 455-467.

23. Chorin, A. J. On the Convergence of Discrete Approximations to the Navier-Stokes-Equations. Math. Comp. Vol. 23, 1969, pp. 341-353.

24. Crastan, V. and J. E. Devos. Finite Element Solution of the Three-Dimensional Flow Problem and of Reynold's Equation for Incompressible and Compressible Fluids. Nucl. Eng. Design, Vol. 22, 1972, pp. 225-232.

25. Van Driest, E. R. On Turbulent Flow Near a Wall. J. Aeronaut. Sci. Vol. 23, 1956, p. 1007.

26. Deissler, R. G. Weak Locally Homogeneous Turbulence in Idealized Flow Through a Cone. ZAMP, Vol. 19, 1967, pp. 165-183.

27. Deardorff, J. W. Numerical Study of Heat Transfer by Internal Gravity Waves above a Growing Unstable Layer. Phys. Fluids Suppl. II, High-Speed Comp. in Fluid Dynamics 1969, pp. II 184-194.

28. Deardorff, J. W. A Three-Dimensional Numerical Study of Turbulent Channel Flow at Large Reynolds Numbers. NCAR Manuscript No. 69 - 19, Jan. 1969.

29. Deardorff, J. W. A Numerical Study of Three-Dimensional Turbulent Channel Flow at Large Reynolds Numbers. J. Fluid Mech. Vol. 41, 1970, pp. 453-480.

30. Deardorff, J. W. A Three-Dimensional Numerical Investigation of the Idealized Planetary Boundary Layer. Geophys. Fluid Dynamics, Vol. 1, 1970, pp. 377-410.

31. Deardorff, J. W. Lagrangian Statistics from Numerically Integrated Turbulent Shear Flow. Phys. Fluids, Vol. 13, 1970, pp. 584-595.

32. Deardorff, J. W. On the Magnitude of the Subgrid Scale Eddy Coefficient. J. Comp. Phys. Vol. 7, 1971, pp. 120 - 133.

33. Deardorff, J. W. Numerical Investigation of Neutral and Unstable Planetary Boundary Layers. J. Atmosp. Sci. Vol. 29, 1972, pp. 91-115.

34. Donaldson, C. du P. Calculation of Turbulent Shear Flows for Atmospheric and Vortex Motion. AIAA J. Vol. 10, 1972, pp. 4-12.

35. Emmons, H. W. Critique of Numerical Modeling of Fluid-Mechanics Phenomena. Ann. Rev. Fluid Mechanics, Vol. 2, 1970, pp. 15-36.

36. Enderle, G. and U. Schumann. FORTRAN Programs for Analytical Description of Starting Flow in One-Dimensional Geometries. KFK-Ext. 8/71-6, 1971. / 177

37. Easton, C. R. Homogeneous Boundary Conditions for Pressure in the MAC Method. J. Comp. Phys. Vol. 9, 1972, pp. 375 - 379.

38. Eklundh, J. O. A Fast Computer Method for Matrix Transposing. IEEE Transact. Computers, 1972, pp. 801-803.

39. Enderle, G., E. G. Schlechtendahl, U. Schumann and R. Schuster. Design Principles of the GRAPHIC System. KFK 1722, 1973.

40. Fromm, J. The Time Dependent Flow of an Incompressible Fluid. (B. Alder, et al. ed.) Methods in Computational Physics, Vol. 3, 1964, pp. 346 - 382.

41. Fromm, J. E. Numerical Method for Computing Nonlinear, Time Dependent Circulation of Air in Rooms. IBM J. Res. Develop. Vol. 15, 1971, pp. 186-196.

42. Fox, D. G. Numerical Simulation of Three-Dimensional, Shape-Preserving Convective Elements. J. Atmosp. Sci. Vol. 29, 1972, pp. 322-341.

43. Fox, D. G. and D. K. Lilly. Numerical Simulation of Turbulent Flows. Rev. Geophys. Space Phys. Vol. 10, 1972, pp. 51-72.

44. Fox, D. G. and J. W. Deardorff. Computer Methods for Simulation of Multidimensional, Nonlinear, Subsonic, Incompressible Flow. Transact. ASME, Journal of Heat Transfer, Vol. 94, Ser. C., 1972, pp. 337-346.

45. Göring, H. Sammelband zur Statistischen Theorie der Turbulenz (Article Collection on Statistical Theory of Turbulence). Akademie-Verlag, Berlin, (1958)

46. Grant, H. L., R. W. Stewart and A. Moilliet. Turbulence Spectra from a Tidal | Channel. J. Fluid Mech., Vol. 12, 1962, pp. 241-268.

47. Gibson, M. M. Spectra of Turbulence in a Round Jet. J. Fluid Mech., Vol. 15, 1963, p. 161.

48. Gröber; Erk; and U. Grigull. Die Grundgesetze der Wärme-übertragung (Basics of Heat Transfer). Springer-Verlag, Berlin, 1963.

49. Gosman, A. D., W. M. Pun, A. K. Runchal, D. B. Spalding and M. Wolfshtein. Heat and Mass Transfer in Recirculating Flows. Academic Press, London, 1969.

50. Günther, G. Advances in Fourier Transformation. Elektronische Datenverarbeitung, 1969, pp. 275-280.

51. Gregorig, R. Developed Turbulent Tube Flow for Very Large Reynolds Numbers. The Principle of Hamilton. Wärme and Stoffübertragung, Vol. 5, 1972, pp. 73-80.

52. Heisenberg, W. Statistical Theory of Turbulence. Z. Physik, Vol. 124, 1948, pp. 628-657.

53. Hinze, J. O. Turbulence. McGraw-Hill, New York, 1959, p. 586.

54. Harlow, F. H. and J. E. Welch. Numerical Calculation of Time-Dependent Viscous Incompressible Flow of Fluid with Free Surface. Phys. Fluids, Vol. 8, 1965, pp. 2182-2189.

55. Hockney, R. W. A Fast Direct Solution of Poisson's Equation Using Fourier Analysis. JACM, Vol. 12, 1965, pp. 95-113.

56. Hirt, C. W. and F. H. Harlow. A General Corrective Procedure for the Numerical Solution of Initial-Value Problems. J. Comp. Physics, Vol. 2, 1967, pp. 114-119.

57. Hirt, C. W. Heuristic Stability Theory for Finite-Difference Equations. J. Comp. Physics, Vol. 2, 1968, pp. 339-355.

58. Harlow, F. H. Numerical Methods for Fluid Dynamics; an Annoted Bibliography. LA-4281, 1969.

59. Harlow, F. H. and C. W. Hirt. Generalized Transport Theory of Anisotropic Turbulence. LA-4086, 1969.

60. Heusener, G. Optimization of Sodium-Cooled Fast Breeding Reactors using Monolinear Programming Methods. KFK 1238, 1970. /179

61. Hockney, R. W. The Potential Calculation and Some Applications. (Alder, et al., ed.): Methods in Comp. Physics 9, Acad. Press, 1970, pp. 135-211.

62. Harlow, F. H. and A. A. Amsden. A Numerical Fluid Dynamics Calculation Method for All Flow Speeds. J. Comp. Phys. Vol. 8, 1971, pp. 197-213.

63. Hirt, C. W. and J. L. Cook. Calculating Three-Dimensional Flows around Structures and over Rough Terrain. J. Comp. Phys., Vol. 10, 1972, pp. 324-340.

64. Hinkelmann, K. Status and Possibilities of Numerical Weather Prediction. Annal. der Meteorol., Neue Folge No. 6, 1973, pp. 11-23.

65. IBM: System/360 Scientific Subroutine Package, Programmer's Manual, IBM-Form H20-0205.

66. Kármán, T. von. The Fundamentals of the Statistical Theory of Turbulence. J. Aeron, Sci., 1937, pp. 131-138.

67. Kolmogorov, A. N. Local Structure of Turbulence in a Viscous Compressible Liquid. C. R. Acad. Sci. U.S.S.R., Vol. 30, 1941, p. 301 (Russian) German Translation in /44/, pp. 71-76.

68. Kolmogorov, A. N. Equations of Turbulent Motion of an Incompressible Fluid. Izv. Akad. Nauk, SSSR, Ser. Phys., Vol. 6, 1942, pp. 56-58. Translated into English by: Imperial College, Mech. Eng. Dept. Report No. ON/6, 1968.

69. Kraichnan, R. H. Lagrangeian History Closure Approximation for Turbulence. Phys. Fluids, Vol. 8, 1965, pp. 575-598.

70. Kraichnan, R. H. Isotropic Turbulence and Inertial-Range Structure in the Abridged LHDI Approximation. Unpublished Research Report No. 8, 1966, Office of Naval Research, Contract No. 4307 (oo), reported by Lilly [81].

71. Kolsky, H. G. Some Computer Aspects of Meteorology. IBM-Journal, 1967, pp. 584-600.

72. Kirsch, D. The Solution of Heat Convection Problems by the Monte Carlo Method. KFK 1315, 1970.

73. Krause, E. Numerical Solution of the Navier-Stokes Equations for Calculating Incompressible Centrifugal Flows. In: Krause, E. and E. H. Hirschel (Publ.): Strömungsmechanische Vorgänge in Gaszentrifugen (Fluid Mechanical Processes in Gas Centrifuges). DFVLR, Institut für Gasdynamik, Porz-Wahn, 1970, pp. 93-119.

74. Krause, E. Numerical Solutions of the Navier-Stokes Equations for Incompressible, Axisymmetric Flows. ZAMM, Vol. 51, 1971, p. 156.

75. Kirsch, D. Investigations of the Flow and Temperature Distribution in the Region of Local Cooling Channel Blockages in Rod Bundle Fuel Elements. Dissertation TU Karlsruhe, 1973, KFK, 1794.

76. Laufer, J. Investigation of Turbulent Flow in a Two-Dimensional Channel. NACA Report 1053, 1950.

77. Laufer, J. Some Recent Measurements in a Two-Dimensional Turbulent Channel. J. Aeronautical Sci., 1950, pp. 277-287.

78. Lilly, D. K. Numerical Solutions for the Shape-Preserving Two-Dimensional Thermal Convection Element. J. Atmosph. Sci., Vol. 21, 1964, pp. 83-98.

79. Lilly, D. K. On the Computational Stability of Numerical Solutions of Time-Dependent Non-Linear Geophysical Fluid Dynamics Problems. Monthly Weath. Rev. 93, 1965, pp. 11-26.

80. Lilly, D. K. On the Application of the Eddy Viscosity Concept in the Inertial Sub-range of Turbulence. NCAR Manuscript No. 123, Jan. 1966.

81. Lilly, D. K. The Representation of Small-Scale Turbulence in Numerical Simulation Experiments. (Goldstine, H. H. ed.:) Proc. of the IBM Scientific Computing Symposium on Environmental Sciences. (14.- 16. Nov. 1966, New York), IBM Form No. 320 - 1951, 1967, pp. 195-210.

82. Leith, C. E. Two-Dimensional Eddy Viscosity Coefficients. Proc. WMO-IUGG Symposium on Numerical Weather Prediction, Tokyo, Japan, 1968, pp. I-41 to I-44.

83. Lilly, D. K. Numerical Simulation of Developing and Decaying Two-Dimensional Turbulence. J. Fluid Mech. Vol. 45, 1971, pp. 395-415.

84. Leinemann, K. Programs for Representing Plane and Three-Dimensional Vector Fields. KFK 1637, 1972.

85. Lorenz, E. N. Investigating the Predictability of Turbulent Motion. Lecture Notes in Physics, Statistical Models and Turbulence, Proc. Symp. San Diego, Springer-Verlag, 1972, pp. 195-204.

86. Navier, C. L. M. H. Memoir of the Laws of Motion of Fluids. Mém. Acad. Sci, Vol. 6, 1822, p. 389.

87. Miyakoda, K. Contribution to the Numerical Weather Prediction — Computation with Finite Difference. Japanese J. Geophysics, Tokyo, Japan, Vol. 3, 1962, pp. 75-190.

88. Maubach, K. Friction Loss of Turbulent Flows. Chemie-Ing. Techn. Vol. 42, 1970, pp. 995-1003.

89. Mollo-Christensen, E. Physics of Turbulent Flow. AIAA J. Vol. 9, 1971, pp. 1217-1228.

90. Maubach, K. and K. Rehme. Negative Eddy Diffusivities for Asymmetric Turbulent Velocities Profiles? Int. J. Heat Mass Transf. Vol. 15, 1972, pp. 425-432.

91. Ng, K. H. and D. B. Spalding. Turbulence Model for Boundary Layers near Walls. Phys. Fluids, Vol. 15, 1972, pp. 20-30.

92. Obuchow, A. M. The Energy Distribution in the Spectrum of the Turbulent Flow. German Translation in [44], 1941, pp. 83-96.

93. Obuchow, A. M. and A. M. Jaglom. Microstructure of a Turbulent Flow. German Translation in [44], 1941, p. 97.

94. Orszag, S. A. Numerical Methods for the Simulation of Turbulence. High-Speed Comput. Fluid Mech., Phys. Fluids Suppl II, 1969, pp. II-250 - II-257.

95. Orszag, S. A. Numerical Simulation of Incompressible Flows Within Simple Boundaries. I. Galerkin (Spectral) Representations. Stud. Appl. Mathm. L, 1971, pp. 293-327.

96. Orszag, S. A. Numerical Simulation of Incompressible Flows Within Simple Boundaries: Accuracy. J. Fluid Mech., Vol. 49, 1971, pp. 75-112.

97. Orszag, S. A. Galerkin Approximations to Flows Within Slabs, Spheres and Cylinders. Phys. Rev. Lett. Vol. 26, 1971, pp. 1100 - 1103.

98. Prandtl, L. Report on Investigations of Fully Developed Turbulence. ZAMM, Vol. 5, 1925, pp. 136-139. /182

99. Prandtl, L. and K. Wieghardt. A New Formula System for Developed Turbulence. Nachr. der Akad. Wiss. Göttingen, Mathphys. Van den Loeck & Ruprecht, 1945.

100. Phillips, N. A. An Example of Non-Linear Computational Instability in: The Atmosphere and Sea in Motion, Rockefeller Inst. Press & Oxford Univ. Press, New York, 1959.

101. Pond, S., R. W. Stewart and R. W. Burling. Turbulence Spectra in the Wind over Waves. J. Atmos. Sci., Vol. 20, 1963, pp. 319-324.

102. Pearson, C. E. A Computational Method for Time-Dependent Two-Dimensional Incompressible Viscous Flow Problems. SRRC-RR-64-17, 1964.

103. Pao, Y. H. Structure of Turbulent Velocity and Scalar Fields at Large Wavenumbers. Phys. Fluids, Vol. 8, 1965, pp. 1063-1075.

104. Patankar, S. V. and D. B. Spalding. Heat and Mass Transfer in Boundary Layers. Intertext Books, London, 1970, p. 225.

105. Piacsek, S. A. and G. P. Williams. Conservation Properties of Convective Difference Schemes. J. Comp. Phys. Vol. 6, 1970, pp. 392-405.

106. Paquin, J. E. and S. Pond. The Determination of the Kolmogoroff Constants for Velocity, Temperature and Humidity Fluctuations from Second- and Third-Order Structure Functions. J. Fluid Mech. Vol. 50, 1971, pp. 257-269.

107. Reynolds, O. On the Dynamical Theory of Incompressible Viscous Fluids and the Determination of the Criterion. Phil. Trans. Roy. Soc. London A, Vol. 186, 1894, p. 123.

108. Rotta, J. Statistical Theory of Nonhomogeneous Turbulence. First Report. Z. Physik, Vol. 129, 1951, pp. 547-572.

109. Rotta, J. C. Statistical Theory of Nonhomogeneous Turbulence. Second Report. Z. F. Physik, Vol. 131, 1951, pp. 51-77.

110. Richtmyer, R. D. A Survey of Difference Methods for Non-Steady Fluid Dynamics. NCAR T. N. 63-2, 1962.

111. Richtmyer, R. D. and K. W. Morton. Difference Methods for Initial Value Problems. Second Ed., Interscience Publ. 1967, p. 403.

112. Rimon, Y. Numerical Solution of the Time-Dependent Incompressible Viscous Flow Over a Disk or a Sphere. Ph. D. thesis, Princeton University, 1968.

113. Rodi, W. and D. B. Spalding. A Two-Parameter Model of Turbulence, and its Application to Free Jets. Wärme- and Stoffübertragung, Vol. 3, 1970, pp. 85-95.

114. Rotta, J. C. A Method for Calculating Turbulent Shear Flow Fields. ZAMM, Vol. 50, 1970, pp. 204-205

115. Rotta, J. C. Turbulente Strömungen (Turbulent Flows). B. G. Teubner-Verlag Stuttgart, 1972.

116. Runchal, A. K. and D. B. Spalding; Steady Turbulent Flow and Heat Transfer Downstream of a Sudden Enlargement in a Pipe of Circular Cross Section. Wärme- und Stoffübertragung, Vol. 5, 1972, pp. 31-38.

117. Stokes, G. G. On the Theories of the Internal Friction of Fluids in Motion. Trans. Cambridge Phil. Soc. Vol. 8, 1845, pp. 287-305.

118. Smagorinsky, J. S. General Circulation Experiments with the Primitive Equations: I. The Basic Experiment. Mon. Weather Rev., Vol. 91, 1963, pp. 99-164; esp. pp. 103-106.

119. Szabó, I. Einfuhrung in die Technische Mechanik (Introduction to Technical Mechanics). Springer-Verlag, 1963, p. 240.

120. Schlichting, H. Grenzschicht Theorie (Boundary Layer Theory). Verlag G. Braun, Karlsruhe, 5th Edition, 1965.

121. Schönauer, W. Solution of the Three-Dimensional, Unsteady Navier-Stokes Equation using the Difference Method. Habilitation Lecture at the University of Karlsruhe, 1969. DFVLR Report, 1970, DLR FB 70-15.

122. Schlechtendahl, E. G. DYSYS - A Dynamic System Simulator for Continuous and Discrete Changes in state. KFK 1209, 1970.

123. Spalding, D. B. A Noval Finite-Difference Formulation for Differential Expressions Involving Both First and Second Derivatives. Imperial College, London BL/TN/A/39, November, 1970.

124. Schumann, U. PLOTHL - a FORTRAN IV Subprogram for Presenting Functions having Two Independent Variables by Contours on a Plotter. KFK 1486, 1971. /184

125. Schumann, U. A Method for Transposing Large, Sequentially Stored Matrices. Angewandte Informatik, 1972, pp. 213-216.

126. Schumann, U. A Subprogram Package for Dynamic Management of Very Large Data Blocks Arranged in Constant Length Units into the Main and External Storage Units. (Unpublished IRE, 6th Notice, 1972).

127. Spalding, D. B. A Two-Equation Model of Turbulence. VDI-Forsch.-Heft, Vol. 549, 1972, pp. 5-16.

128. Schumann, U. Comments on "A Fast Computer Method for Matrix Transposing" and Application to the Solution of Poisson's Equation. IEEE Transact. Comp. 1973.

129. Smidt, D. Is there an Appropriation Method Bottleneck? Atomwirtschaft, 1973, pp. 116-121.

130. Taylor, G. I. Statistical Theory of Trubulence. Proc. Royal Soc. A 151, 1935, pp. 421-464.

131. Taylor, G. I. and A. E. Green. Mechanism of the Production of Small Eddies from Large Ones. Proc. Royal Soc. A 158, 1937, pp. 499-521.

132. Taylor, G. I. The Spectrum of Turbulence. Proc. Roy. Soc. London A 164, 1938, pp. 476-490.

133. Townsend, A. A. Local Isotropy in the Turbulent Wake of of a Cylinder. Australian J. of Sci. Res. 1, No. 2, 1948, pp. 161-174.

134. Townsend, A. A. The Structure of Turbulent Shear Flow. Cambridge, Univ. Press, 1956.

135. Tobey, R., et al. PL/1-FORMAC Interpreter, User's Reference Mannual, IBM, 1967, Progr. No. 306 D, 03.3.004.

136. Uberoi, M. S. and L. S. G. Kovasznay. On Mapping and Measurement of Random Fields. Quart. Appl. Math. Vol. 10, 1952, pp. 375-393.

137. Uberoi, M. S. Correlations Involving Pressure Fluctuations in Homogeneous Turbulence. NACA TN 3116, 1954.

138. Uberoi, M. S. Equipartition of Energy and Local Isotropy in Turbulent Flows. J. Appl. Phys., Vol. 28, 1957, pp. 1165-1170.

139. Weizsäcker, G. F. von: The Spectrum of Turbulence for Large Reynolds numbers. Z. Physik, Vol. 124, 1948, pp. 614-627. Proc. Roy. Soc. London 195 A, 1948, p. 402. /185

140. Williamson, D. Stability of Difference Approximations to Certain Partial Difference Equations of Fluid Dynamics. J. Comp. Phys., Vol. 1, 1966, pp. 51-67.

141. Williams, G. P. Numerical Integration of the Three-Dimensional Navier-Stokes Equations for Incompressible Flow. J. Fluid Mech., Vol. 37, 1969, pp. 727-750.

142. Wyngaard, J. C. and Y. H. Pao. Some Measurements of the Fine Structure of Large Reynolds Number Turbulence. (Ehlers, J. et al. (ed.):) Lecture Notes in Physics 12, Statistical Models and Turbulence, Proc. of a Symposium at San Diego, July 15-21, 1971, Springer-Verlag, 1972.

TABLE 1. PREVIOUS DATA FOR a_1 - a_8 [115,113,91,116] /186

(For comparison purposes, the table also contains the notation used in the various papers)

Term, a_i		Rotta (1972)		Rodi-Spalding (1970)		Ng-Spalding (1972)		Runchal-Spalding(1972)	
			*)		***)				
$\langle u'w' \rangle$	a_1	k	0.56	C_μ	1.	-	1.	C_μ	0.20
$\langle \varepsilon' \rangle$, Dissipation	a_2	c	0,18	C_D	0.055, 0.09	C_D	0.1	C_ε	0.31
$\langle \varepsilon' \rangle$, Diffusion	a_3	k_q	0,38	C_μ/σ_{kL}	1.	$\frac{1}{\sigma_e}$	0.5	$\frac{C_\mu}{\sigma_{e,k}}$	0.133
L-Production	a_4	ξ	1.2	C_B	1.	C_p	0.84	-	
	a_5	ξ_3	?**)	-	0.	-	0.	-	
L-Sink	a_6	C_L	0.667 0.8	C_S/K_D	0.634 0.723	C_M/C_D	X****)	-	
L-Diffusion	a_7	k_{qL}	?**)	$\frac{C_\mu(1-C_{kL})}{\sigma_{kL}}$	1.	$1/\sigma_2$	0.5	-	
	a_8	L	?**)	$\frac{1}{(1+C_{kL})}$	3.33	σ_2/σ_1	1.67	-	

*) The values were derived from the data of Wieghardt [99].

**) One of the constants a_5, a_7, a_8 follows from $-a_4-2k^2a_5+a_6-k^2a_7a_8/a_2 = 0$; $k \approx 0.4$.

***) First number for free jet from a rectangular nozzle; second for circular nozzle.

****) $X = \frac{1}{C_D}\left[C_M + C_W (L/z)^q\right]$, $C_M = 0.055$, $C_W = 22.$, $q = 4.$

TABLE 2. ACCORDING TO Ng-SPALDING (1972): /187
(Variation of the calculated target values
for variation of one constant each by 5% [91].)

Varied constant		Average variation of the target values in percent
L-Production	a_4	4.9
$\langle E' \rangle$ - Dissipation	a_2	3.9
L-Sink	$a_2 \cdot a_6$	3.1
Var. of the L-Sink with location z.	q C_w	1.2 0.7
L-Diffusion	$a_7 \cdot a_8$	0.5
"	a_7	0.4
$\langle E' \rangle$ - Diffusion	a_3	0.4

TABLE 3 *

/188

Kolmogorov - constant α

a) Experimental findings

Authors	Ref.	Year	Flow type	Standard deviation	Average value
Grant et al	46	1962	Tidal flow	1,22 - 1,81	1,44
Gibson	47	1963	Free jet	1,57 - 1,62	1,6o
Pond et al.	1o1	1963	Wind over waves	10%	1,41
Comte-Bellot	18	1965	Flat plate flow		1,55
Paquin, Pond	1o6	1971	Wind	+ 0,28	1,58
Wyngaard, Pao	142	1971	Wind over the ground: height 5,66 - 22,6	± 0,06	1,7
Boston, Burling	17	1972	" 4 m	± 0.06	1,56
b) Theoretical predictions					
Kraichnan	69	1965	-	-	1,77
Kraichnan	7o	1966	-	-	1,5
c) Recommendation					
Pao	1o3	1965	-	-	1,5
Lilly	8o	1966	-	-	1,41
Rotta	115	1972	-	-	1,44
This paper	-	-	-	-	1,5

* Translator's note: Commas in numbers represent decimal points.

TABLE 4. FORTRAN SUBPROGRAMS FOR DIRECT NUMERICAL INTEGRATION OF THE INTEGRALS d_k^*, k=1,2,...,5

```
      FUNCTION  D1(A1,A2,A3,XS1,XS2)
      COMMON/CWORK/ Y1(100),Y2(100),Y3(100),Z1(100),Z2(100),Z3(100)
      COMMON/NNNNNN/NN
      LOGICAL FIRST
      DR=1./3.
      N=AMAX1(1.,A2)*NN
        N2=MAX0(10,MIN0(99,2*N))
      N=AMAX1(1.,A3)*NN
      N3=MAX0(10,MIN0(99,N))
      H2=2.*A2/N2
      H3=A3/N3
      N2=N2+1
      N3=N3+1
      FIRST=      (ABS(XS1).GT.1.E-10)
      T2=-A2
      DO 2 I2=1,N2
      IF(FIRST)GOTO5
      IF(ABS(XS2-T2).GT.1.E-10)GOTO5
      Y2(I2)=(A2-ABS(T2))**0.225*A3**2.666666666E0
      GOTO 4
    5 CONTINUE
      XS12=XS1*XS1
      X2T2=(XS2-T2)**2
      AT2=A2-ABS(T2)
      T3=0.
      DO 3 I3=1,N3
      T3T3=T3*T3
      R=XS12+X2T2+T3T3
      Y3(I3)=(A3-T3)*AT2*(R**DR)*(1.-XS12/(4.*R))
    3 T3=T3+H3
      CALL QSF(H3,Y3,Z3,N3)
      Y2(I2)=Z3(N3)
      CONTINUE
    2 T2=T2+H2
      CALL QSF(H2,Y2,Z2,N2)
      D1=2.*Z2(N2)/(A2*A2*A3*A3)
      RETURN
      END
      FUNCTION  D2(A1,A2,A3,XS1,XS2)
      COMMON/CWORK/ Y1(100),Y2(100),Y3(100),Z1(100),Z2(100),Z3(100)
      COMMON/NNNNNN/NN
      DR3=1./3.
      DR83=8./3.
      DR940=27./160.
      N1=MAX0(10,MIN0(99,IFIX(NN*AMAX1(1.,A1)*2)))
      N3=MAX0(10,MIN0(99,IFIX(NN*AMAX1(1.,A3))))
      H1=2.*A1/N1
      N1=N1+1
      H3=A3/N3
      N3=N3+1
      T1= A1
      DO 1 I1=1,N1
      R1=(T1+XS1)**2+XS2*XS2
      T3=0.
      IF(R1.LT.1.E-10)GOTO 21
      DO 3 I3=1,N3
      R=R1+T3*T3
      F=1.
      IF(R.GT.1.E-10)F=1.- (XS1+T1)**2/(4.*R)
      Y3(I3)= (A3-T3)*R**DR3*F
    3 T3=T3+H3
      CALL QSF(H3,Y3,Z3,N3)
      GOTO 22
   21 Z3(N3)= DR940*A3**DR83
   22 Y1(I1)= Z3(N3)*(A1-ABS(T1))
    1 T1=T1+H1
      CALL QSF(H1,Y1,Z1,N1)
      D2=2.*Z1(N1)/(A1*A1*A3*A3)
      RETURN
      END
      FUNCTION  D3(A1,A2,A3,XS1,XS2)
      COMMON/CWORK/ Y1(100),Y2(100),Y3(100),Z1(100),Z2(100),Z3(100)
      COMMON/NNNNNN/NN
      DR3=1./3.
      DR83=8./3.
      DR940=9./40.
      N1=MAX0(10,MIN0(99,IFIX(NN*AMAX1(1.,A1))))
      N2=MAX0(10,MIN0(99,IFIX(NN*AMAX1(1.,A2))))
      N3=MAX0(10,MIN0(99,IFIX(NN*AMAX1(1.,A3))))
      H1=A1/N1
      N1=N1+1
      H2=A2/N2
      N2=N2+1
      H3=A3/N3
      N3=N3+1
      T1=-A1/2.
      DO 1 I1=1,N1
      T2=-A2/2.
      R1=(T1+XS1)**2
      FXS1=R1
      DO 2 I2=1,N2
      T3=0.
      R2=R1+(T2+XS2)**2
      IF(R2.LT.1.E-10) GOTO  21
      DO 3 I3=1,N3
      R=R2+T3*T3
      F=1.
      IF(R.GT.1.E-10) F=1.-FXS1/(4.*R)
      Y3(I3)=(A3-T3)*R**DR3*F
    3 T3=T3+H3
      CALL QSF(H3,Y3,Z3,N3)
      Y2(I2)=Z3(N3)
      GOTO  2
   21 Y2(I2)=DR940*A3**DR83
    2 T2=T2+H2
      CALL QSF(H2,Y2,Z2,N2)
      Y1(I1)=Z2(N2)
    1 T1=T1+H1
      CALL QSF(H1,Y1,Z1,N1)
      D3=2.*Z1(N1)/A3
      RETURN
      END
      FUNCTION  D4(A1,A2,A3,XS1,XS2)
      COMMON/CWORK/ Y1(100),Y2(100),Y3(100),Z1(100),Z2(100),Z3(100)
      COMMON/NNNNNN/NN
      R=XS1*XS2
      R=R*R
      N1=1
      Z1(N1)=0.
```

Continued on next page

TABLE 4 (CONTINUED)

```
      IF(R.LT.1.E-10)GOTO999
      DR3=2./3.
      N1=MAXO(10,MINO(99,IFIX(NN*AMAX1(1.,A1))))
      N2=MAXO(10,MINO(99,IFIX(NN*AMAX1(1.,A2))))
      N3=MAXO(10,MINO(99,IFIX(NN*AMAX1(1.,A3))))
      H1=A1/N1
      N1=N1+1
      H2=A2/N2
      N2=N2+1
      H3=A3/N3
      N3=N3+1
      T1=-0.5*H1
      DO 1 I1=1,N1
      T2=-0.5*H2
      R1=(T1+XS1)
      R12=R1*R1
      DO 2 I2=1,N2
      T3=0.
      R2=T2+XS2
      R13=R12+R2*R2
      R2=R1*R2
      DO 3 I3=1,N3
      R=R13+T3*T3
      Y3(I3)=(R2 /R**DR3)*(A3-T3)
    3 T3=T3+H3
      CALL QSF(H3,Y3,Z3,N3)
      Y2(I2)=Z3(N3)
    2 T2=T2+H2
      CALL QSF(H2,Y2,Z2,N2)
      Y1(I1)=Z2(N2)
    1 T1=T1+H1
      CALL QSF(H1,Y1,Z1,N1)
  999 CONTINUE
      D4=-0.5*Z1(N1)/A3
      RETURN
      END
      FUNCTION  D5(A1,A2,A3,XS1,XS2)
      COMMON/CWORK/ Y1(100),Y2(100),Y3(100),Z1(100),Z2(100),Z3(100)
      COMMON/NNNNNN/NN
      DATA DR3/0.6666667/
      N1=MAXO(10,MINO(99,IFIX(NN*AMAX1(1.,A1))))
C     XS1=.5*A1
C     XS2=A2
      Z1(N1)=0.
      R=XS1*XS2
      R=R*R
      IF(R.LT.1.E-10) GOTO 999
      N3=MAXO(10,MINO(99,IFIX(NN*AMAX1(1.,A3))))
      H1= 2.*A1/N1
      N1=N1+1
      H3=    A3/N3
      N3=N3+1
      T1=-A1
      XS2Q=XS2*XS2
      DO 1 I1=1,N1
      T3=0.
      A= A1-ABS(T1)
      B= T1+XS1
      B2=B*B+XS2Q
      DO 3 I3=1,N3
      Y3(I3)=  A*(A3-T3)*B*XS2/(B2+T3*T3)**DR3
    3 T3=T3+H3
      CALL QSF(H3,Y3,Z3,N3)
      Y1(I1)=Z3(N3)
    1 T1=T1+H1
      CALL QSF(H1,Y1,Z1,N1)
  999 D5=-.5*Z1(N1)/(A1*A1*A3*A3)
      RETURN
      END
```

TABLE 5. FORTRAN SUBPROGRAM FOR APPROXIMATE CALCULATION OF THE INTEGRALS d_k^*, k = 1, 2, ..., 5

```
      FUNCTION  D1N(H1,H2,H3,X1,X2)
      REAL X(10)/-.375,-.4375,-.1611328,.15625E-1,.9765625E-3,4.078125
     1,3.220215,2.390625,1.807861,1.000488/
      DU=1./0.7257
      DO= 0.45*(H2**DU+H3**DU)**(0.7257*0.66666667E0)
      DU=  X1*X1+X2*X2
      IF(DU.GT.0.) DU= (1.-X1*X1/(4.*DU))*DU**0.3333333E0
      Q= DO/(DO+DU)
      P1= X1*X1*Q
      P2= X2*X2*Q
      P3= (1.-H3)
      P3= P3*P3*Q
      P4= (1.-H1)
      P4= P4*P4*Q
      P5= (1. H2)
      P5= P5*P5*Q
      P1= P1/(1.+ (X(6)*P1)**2)
      P2= P2/(1.+ (X(7)*P2)**2)
      P3= P3/(1.+ (X(8)*P3)**2)
      P4= P4/(1.+ (X(9)*P4)**2)
      P5= P5/(1.+(X(10)*P5)**2)
      B=AMIN1(DU/DO,160.)
      B= DU+DO*EXP(-B)+X(1)*P1+X(2)*P2+X(3)*P3+X(4)*P4+X(5)*P5
      D1N=B
      D1=D1N
      RETURN
      END
      FUNCTION  D2N(H1,H2,H3,X1,X2)
      REAL X(10)/-.2480469,-.28125,.4196777,-.2958984,.1464844E-1,
     1,.812988,3.25,1.812256,.921875,.0/
      DO=((.3375*H1**.6666667E0)**2.140541E0
     1   +(.45  *H3**.6666667E0)**2.140541E0)**.4672
      DU=  X1*X1+X2*X2
      IF(DU.GT.0.) DU= (1.-X1*X1/(4.*DU))*DU**.3333333E0
      Q= DO/(DO+DU)
      P1= X1*X1*Q
      P2= X2*X2*Q
      P3= (1. H3)
      P3= P3*P3*Q
      P4= (1.-H1)
      P4= P4*P4*Q
      P5= (1. H2)
      P5= P5*P5*Q
      P1= P1/(1.+ (X(6)*P1)**2)
      P2= P2/(1.+ (X(7)*P2)**2)
      P3= P3/(1.+ (X(8)*P3)**2)
      P4= P4/(1.+ (X(9)*P4)**2)
      P5= P5/(1.+(X(10)*P5)**2)
      B=AMIN1(DU/DO,160.)
      B= DU+DO*EXP(-B)+X(1)*P1+X(2)*P2+X(3)*P3+X(4)*P4+X(5)*P5
      D2N=B
      D2=D2N
      RETURN
      END
      FUNCTION  D3N(H1,H2,H3,X1,X2)
      REAL X(10)/-.234375,-.640625,.3540039E-1,-.2851562,-.2441406E-1
     1,2.156494,4.377868,.1171875,1.3125,.7668457/
      DO=(1.9 *(.03125*H1*H1)**.3333333E01**2.29894
     1   +(1.2*(.03125*H2*H2)**.3333333E01**2.29894
     1   +(.45      * (H3*H3)**.3333333E01**2.29894)**.4350
      DU= X1*X1+X2*X2
      IF(DU.GT.0.) DU= (1.-X1*X1/(4.*DU))*DU**.3333333E0
      Q= DO/(DO+DU)
      P1= X1*X1*Q
      P2= X2*X2*Q
      P3= (1.-H3)
      P3= P3*P3*Q
      P4= (1.-H1)
      P4= P4*P4*Q
      P5= (1.-H2)
      P5= P5*P5*Q
      P1= P1/(1.+ (X(6)*P1)**2)
      P2= P2/(1.+ (X(7)*P2)**2)
      P3= P3/(1.+ (X(8)*P3)**2)
      P4= P4/(1.+ (X(9)*P4)**2)
      P5= P5/(1.+(X(10)*P5)**2)
      B=AMIN1(DU/DO,160.)
      B= DU+DO*EXP(-B)+X(1)*P1+X(2)*P2+X(3)*P3+X(4)*P4+X(5)*P5
      D3N=B
      D3=D3N
      RETURN
      END
      FUNCTION  D4N(H1,H2,H3,X1,X2)
      REAL X(9)/9.369141,19.125,11.17114,2.078125,1.30957,.0,.6953125
     1,.9990234,.0/
      B=X1*X2
      IF(ABS(B).LT.1.E-10) GOTO 999
      B=    .6* (((1.+X(1)*.5)**2+(1.+X(2)*.5)**2+ X(3)*X(3))
     1 /((H1+X(1)*X1)**2+(H2+X(2)*X2)**2+ (X(3)*H3)**2))*.6666666E0
      P1= (1. H1)
      P1=  P1*P1
      P1=  P1/(1.+(X(4)*P1)**2)
      P2= (1.-H2)
      P2=  P2*P2
      P2=  P2/(1.+(X(5)*P2)**2)
      P3= (1.-H3)
      P3=  P3*P3
      P3=  P3/(1.+(X(6)*P3)**2)
      P1=  X(7)*P1+X(8)*P2+X(9)*P3
      B=  X1*X2*(B+P1)
99$   D4N= -0.13761*B
      D4=D4N
      RETURN
      END
      FUNCTION  D5N (H1,H2,H3,X1,X2)
      REAL X(9)/5.642822,6.376953,1.511719,12.57422,.3793945,1.,
     1 6.076904,-.191123,.0/
      B=X1*X2
      IF(ABS(B).LT.1.E-10) GOTO 999
      B=  2.*(((1.+X(1)*.5)**2+(1.+X(2))**2 +X(3)*X(3))
     1    /((H1+X(1)*X1)**2+(H2+X(2)*X2)**2+(X(3)*H3)**2))**.6666667E0
      P1= 1.- H1
      P1= P1*P1
      P1= P1/(1.+(X(4)*P1)**2)
      P2= 1.-H2
      P2= P2*P2
      P2= P2/(1.+(X(5)*P2)**2)
      P3= 1.-H3
      P3= P3*P3
      P3= P3/(1.+(X(6)*P3)**2)
      B=  X1*X2*(B+X(7)*P1+X(8)*P2+X(9)*P2)
99$   D5N= -.845673E-1*B
      D5=D5N
      RETURN
      END
```

TABLE 6. COMPARISON BETWEEN EXACT AND APPROXIMATE SOLUTION OF THE INTEGRALS d_k^*, k=1, 2, ..., 5

/192

EXAKTE WERTE FUER NN= * 50

DX1	DX2	DX3	XS1	XS2	D1	D2	D3	D4	D5
1.000 **	1.000	1.000	.0	.0	.629273	.550611	.610374	.0	.0
NAEHERUNGSWERTE=					.629293	.550591	.610363	.0	.0
1.250	.8000	1.000	.0	.0	.587434	.583699	.601811	.0	.0
NAEHERUNGSWERTE=					.588521	.565463	.584646	.0	.0
.8000	1.250	1.000	.0	.0	.681658	.524992	.635318	.0	.0
NAEHERUNGSWERTE=					.682437	.514422	.619722	.0	.0
2.000	.8000	.6250	.0	.0	.502878	.617508	.599134	.0	.0
NAEHERUNGSWERTE=					.486339	.512840	.502591	.0	.0
.8000	2.000	.6250	.0	.0	.779179	.429627	.690003	.0	.0
NAEHERUNGSWERTE=					.761372	.487552	.667991	.0	.0
1.000	1.000	1.000	1.000	.0	.884836	.819854	.857132	.0	.0
NAEHERUNGSWERTE=					.902753	.824927	.874311	.0	.0
1.000	1.000	1.000	.0	1.000	1.04151	1.05414	1.05290	.0	.0
NAEHERUNGSWERTE=					1.06213	1.04672	1.05389	.0	.0
1.000	1.000	1.000	2.000	.0	1.25253	1.21832	1.23629	.0	.0
NAEHERUNGSWERTE=					1.26763	1.20377	1.24406	.0	.0
1.000	1.000	1.000	.0	2.000	1.60253	1.61436	1.60853	.0	.0
NAEHERUNGSWERTE=					1.63334	1.59448	1.60383	.0	.0
1.000	1.000	1.000	3.000	.0	1.59738	1.57613	1.58706	.0	.0
NAEHERUNGSWERTE=					1.60417	1.56198	1.58817	.0	.0
1.000	1.000	1.000	.0	3.000	2.08859	2.09591	2.09238	.0	.0
NAEHERUNGSWERTE=					2.08342	2.07891	2.08412	.0	.0
1.000	1.000	1.000	.5000	1.000	1.07322	1.08759	1.07857	-.156930	-.845573E-01
NAEHERUNGSWERTE=					1.04955	1.04511	1.05133	-.876968E-01	-.845573E-01
1.000	1.000	1.000	2.000	1.000	1.41316	1.39668	1.40314	-.217366	-.165805
NAEHERUNGSWERTE=					1.35439	1.31730	1.32711	-.214470	-.165887
4.000	.5000	.5000	4.000	.0	1.89534	1.85482	1.87729	.0	.0
NAEHERUNGSWERTE=					1.88134	1.90877	1.88864	.0	.0
.5000	4.000	.5000	4.000	.0	2.07186	1.89255	1.99081	.0	.0
NAEHERUNGSWERTE=					2.10323	1.88756	1.99329	.0	.0
4.000	.5000	.5000	2.000	4.000	2.58322	2.62638	2.60454	-.387563	-.226155
NAEHERUNGSWERTE=					2.52298	2.46739	2.48395	-.389743	-.226165
.5000	4.000	.5000	1.000	4.000	2.49312	2.53617	2.51448	-.167111	-.150400
NAEHERUNGSWERTE=					2.50211	2.51128	2.52312	-.170391	-.150400
1.000	1.000	1.000	.5000	.5000	.822632	.810274	.811418	-.137926	-.642200E-01
NAEHERUNGSWERTE=					.921765	.796553	.804990	-.917400E-01	-.687301E-01
.1526E-04	.5004	.1309E+06	.7539	.5671	1160.07	1160.08	1160.12	-.887003E-03	-.778719E-03
NAEHERUNGSWERTE=					1160.12	1160.45	1160.30	-.209434E-01	-.483762E-03
1.179	1.495	.5672	.4402E-01	.5547E-01	.660351	.484572	.620180	-.909008E-01	-.105170E-02
NAEHERUNGSWERTE=					.552873	.548969	.631080	-.497372E-02	-.214463E-02
.5051	.8858	2.235	.8165E-01	.5208	.976992	.962490	.966936	-.556944E-01	-.122855E-01
NAEHERUNGSWERTE=					.978648	1.03023	.953560	-.651390E-02	-.134583E-01
1.985	.8386E-01	6.006	.5722	.3971E-01	1.53683	1.58315	1.55947	-.101013E-01	-.225960E-02
NAEHERUNGSWERTE=					1.52613	1.45553	1.55411	-.209490E-02	-.276192E-02
1.174	1.603	.5316	.8629	.7943	1.04097	1.00474	1.01253	-.194115	-.117807
NAEHERUNGSWERTE=					1.03459	.961849	.977707	-.200665	-.116538
1.361	1.526	.4815	.9325E-01	.7213	.849997	.869887	.845786	-.127162	-.140615E-01
NAEHERUNGSWERTE=					.911773	.887366	.891261	-.277261E-01	-.176788E-01
.4891	1.425	1.435	.4391	.2948	.873158	.750833	.819140	-.106793	-.483967E-01
NAEHERUNGSWERTE=					.874864	.751760	.791416	-.444264E-01	-.463789E-01
1.422	1.838	.3825	.9645	.9943	1.14938	1.12704	1.12505	-.215942	-.129191
NAEHERUNGSWERTE=					1.11657	1.07605	1.08718	-.232628	-.129708
.1895	1.458	3.617	.1929	.2957E-01	1.25135	1.07653	1.15612	-.348292E-01	-.265150E-02
NAEHERUNGSWERTE=					1.21371	.983607	1.18651	-.621171E-03	-.159498E-02
.8316	.1272	9.450	.6303	.8847	2.16542	2.16995	2.16782	-.674606E-01	-.436002E-01
NAEHERUNGSWERTE=					2.13827	2.13849	2.15344	-.355640E-01	-.447302E-01
1.474	1.784	.3804	.9127	.2352	.925362	.761321	.860252	-.163858	-.465344E-01
NAEHERUNGSWERTE=					.934152	.814433	.857378	-.148743	-.452523E-01
.2496	1.481	2.706	.4112	.8112	1.21811	1.18160	1.19412	-.862264E-01	-.628895E-01
NAEHERUNGSWERTE=					1.22267	1.14885	1.16759	-.442654E-01	-.599843E-01

* Exact values for NN = 50.
** Approximate values

TABLE 7. FORTRAN SUBPROGRAMS D11, D12, D13, D14 and FEDI ACCORDING TO CHAPTER A 2.6.

```
      FUNCTION  D11(X1,X2,X3)
      EXTERNAL  D1111,D1112
      D11=SDIJ(X1,X2,X3,D1111,D1112)
      RETURN
      END
      FUNCTION  D12(X1,X2,X3)
      EXTERNAL  D1211,D1212
      D12=SDIJ(X1,X2,X3,D1211,D1212)
      RETURN
      END
      FUNCTION  D13(X1,X2,X3)
      EXTERNAL  D1311,D1312
      D13=SDIJ(X1,X2,X3,D1311,D1312)
      RETURN
      END
      FUNCTION  D14(X1,X2,X3)
      EXTERNAL  D1411,D1412
      D14=SDIJ(X1,X2,X3,D1411,D1412)
      RETURN
      END
      FUNCTION  SDIJ(X1,X2,X3,/F11/,/F12/)
      IF(ABS(1.-H1)+ABS(1.-H2)+ABS(1.-H3) .LT.1.E-4) GOTO 2
      S=0.
      DO  1  I= 1,3
      F=1.
      DO 1 J=I,3
      S=S+F*DIJ(X1,X2,X3,I,J,F11,F12)
    1 F=2.
      SDIJ=S
      RETURN
    2 SDIJ= 3.*DIJ(X1,X2,X3,1,1,F11,F12)+6.*DIJ(X1,X2,X3,1,2,F11,F12)
      RETURN
      END
      FUNCTION  DIJ(H1,H2,H3,I,J,D11,D12)
      DIMENSION HH(3),H(3)
      HH(1)=H1
      HH(2)=H2
      HH(3)=H3
      IF(I.EQ.J) GOTO 200
      H(1)=HH(I)
      H(2)=HH(J)
      H(3)=HH(6-I-J)
      DIJ= D12(H(1),H(2),H(3))
      RETURN
  200 JJ=MOD(I,3)+1
      H(1)=HH(I)
      H(2)=HH(JJ)
      H(3)=HH(6-I-JJ)
      DIJ= D11(H(1),H(2),H(3))
      RETURN
      END
      FUNCTION D1111(H1,H2,H3)
      D1111=-4.*(D1(H1,H2,H3,0.,0.)-D1(H1,H2,H3,H1,0.))/(H1*H1)
      RETURN
      END
      FUNCTION D1112(H1,H2,H3)
      D1112=-2.*(D2(H1,H2,H3,0.,0.)-D2(H1,H2,H3,0.,H2))/(H2*H2)
     1       +4.*D4(H1,H2,H3,.5*H1,.5*H2)/(H1*H2)
      RETURN
      END
      FUNCTION D1211(H1,H2,H3)
      D1211=-4.*(D1(H1,H2,H3,.5*H1,0.)-D1(H1,H2,H3,1.5*H1,0.))/(H1*H1)
      RETURN
      END
      FUNCTION D1212(H1,H2,H3)
      D1212=-   (D3(H1,H2,H3,0.,0.5*H2)-D3(H1,H2,H3,0.,1.5*H2))/(H2*H2)
     1       +2.*D5(H1,H2,H3,.5*H1,H2)/(H1*H2)
      RETURN
      END
      FUNCTION D1311(H1,H2,H3)
      D1311=D1111(H1,H2,H3)
      RETURN
      END
      FUNCTION D1312(H1,H2,H3)
      D1312=-(D1(H1,H2,H3,0.,0.)-D1(H1,H2,H3,0.,H2))/(H2*H2)
     1       -(D1(H2,H1,H3,0.,0.)-D1(H2,H1,H3,H2,0.))/(H1*H1)
     2       +4.*D4(H1,H2,H3,.5*H1,.5*H2)/(H1*H2)
      RETURN
      END
      FUNCTION D1411(H1,H2,H3)
      D1411=-(14.*D1(H1,H2,H3,0.,0.)-17.*D1(H1,H2,H3,H1,0.)
     1        +2.*D1(H1,H2,H3,2.*H1,0.)+D1(H1,H2,H3,3.*H1,0.))/(8.*H1*H1
     2)
      RETURN
      END
      FUNCTION D1412(H1,H2,H3)
      D1412=-(7.*D1(H1,H2,H3,0.,0.)-8.*D1(H1,H2,H3,0.,H2)
     1       +D1(H1,H2,H3,0.,2.*H2 )+D1(H1,H2,H3,H1,2.*H2)
     2       -D1(H1,H2,H3,H1,0.))/(8.*H2*H2)
     3       -(7.*D1(H2,H1,H3,0.,0.)-8.*D1(H2,H1,H3,0.,H1)
     4         +D1(H2,H1,H3,0.,2.*H1)+D1(H2,H1,H3,H2,2.*H1)
     5         -D1(H2,H1,H3,H2,0.))/(8.*H1*H1)
     6      +(15.*D4(H1,H2,H3,.5*H1,.5*H2)-D4(H1,H2,H3,1.5*H1,.5*H2)
     7        -D4(H1,H2,H3,.5*H1,1.5*H2)-D4(H1,H2,H3,1.5*H1,1.5*H2))
     8 /(4.*H1*H2)
      RETURN
      END
      FUNCTION  FEDI(X1,X2,X3)
      EXTERNAL FED11,FED12
      FEDI = SDIJ(X1,X2,X3,FED11,FED12)
      RETURN
      END
      FUNCTION  FED11(H1,H2,H3)
      FED11=SQRT(H2*H3*ENERG2(H3,H3))*D1211(H1,H2,H3)
      RETURN
      END
      FUNCTION  FED12(H1,H2,H3)
      FED12=.5*(SQRT(H2*H3*ENERG2(H2,H3))*D1212(H1,H2,H3)
     1         +SQRT(H1*H3*ENERG2(H1,H3))*D1212(H2,H1,H3))
      RETURN
      END
```

TABLE 8. COEFFICIENTS OF THE VECTORS A1, A2
ACCORDING TO (A6-9)

/194

A1	Type a) (Jump)	Type b) (Euler)	Type c) (DuFort-Frankel)
A1(1)	$-2\Delta t\,\frac{V_r}{r}\,\delta_{y v_\varphi}$	$-\Delta t\left(\frac{\lvert V_r\rvert}{\Delta r}+\frac{\lvert V_\varphi\rvert}{r\Delta\varphi}+\frac{\lvert V_x\rvert}{\Delta x}+\frac{V_r}{r}\delta_{y v_\varphi}\right)$ $-2\Delta t\mu\left(\frac{1}{\Delta x^2}+\frac{1}{r^2\Delta\varphi^2}+\frac{1}{\Delta r^2}+\frac{1}{2r^2}\left(\delta_{y v_\varphi}+\delta_{y v_r}\right)\right)$	$\frac{2\Delta t}{1+\gamma}\,\frac{V_r}{r}\,\delta_{\alpha y j}$; $\gamma=2\mu\Delta t\left[\frac{1}{\Delta x^2}+\frac{1}{r^2\Delta\varphi^2}+\frac{1}{\Delta r^2}-\frac{\delta_{y v_r}+\delta_{y v_\varphi}}{2r^2}\right]$
A1(2)	$\frac{\Delta t\cdot V_x}{\Delta x}$	$\frac{\Delta t}{2\Delta x}\left(V_x+\lvert V_x\rvert\right)+\frac{\Delta t\mu}{\Delta x^2}$	$\frac{2\Delta t}{1+\gamma}\left(\frac{V_x}{2\Delta x}+\frac{\mu}{\Delta x^2}\right)$
A1(3)	$-\frac{\Delta t\cdot V_x}{\Delta x}$	$\frac{\Delta t}{2\Delta x}\left(-V_x+\lvert V_x\rvert\right)+\frac{\Delta t\mu}{\Delta x^2}$	$\frac{2\Delta t}{1+\gamma}\left(-\frac{V_x}{2\Delta x}+\frac{\mu}{\Delta x^2}\right)$
A1(4)	$\frac{\Delta t\,V_\varphi}{r\Delta\varphi}$	$\frac{\Delta t}{2r\Delta\varphi}\left(V_\varphi+\lvert V_\varphi\rvert\right)+\frac{\Delta t\mu}{r^2\Delta\varphi^2}$	$\frac{2\Delta t}{1+\gamma}\left(\frac{V_\varphi}{2r\Delta\varphi}+\frac{\mu}{r^2\Delta\varphi^2}\right)$
A1(5)	$-\frac{\Delta t\,V_\varphi}{r\Delta\varphi}$	$\frac{\Delta t}{2r\Delta\varphi}\left(-V_\varphi+\lvert V_\varphi\rvert\right)+\frac{\Delta t\mu}{r^2\Delta\varphi^2}$	$\frac{2\Delta t}{1+\gamma}\left(-\frac{V_\varphi}{2r\Delta\varphi}+\frac{\mu}{r^2\Delta\varphi^2}\right)$
A1(6)	$\frac{\Delta t\,V_r}{\Delta r}$	$\frac{\Delta t}{2\Delta r}\left(V_r+\lvert V_r\rvert\right)+\frac{\Delta t\mu}{\Delta r}\left(\frac{1}{\Delta r}-\frac{1}{r}\right)$	$\frac{2\Delta t}{1+\gamma}\left(\frac{V_r}{2\Delta r}+\frac{\mu}{\Delta r^2}-\frac{\mu}{r\Delta r}\right)$
A1(7)	$-\frac{\Delta t\,V_r}{\Delta r}$	$\frac{\Delta t}{2\Delta r}\left(-V_r+\lvert V_r\rvert\right)+\frac{\Delta t\mu}{\Delta r}\left(\frac{1}{\Delta r}+\frac{1}{r}\right)$	$\frac{2\Delta t}{1+\gamma}\left(-\frac{V_r}{2\Delta r}+\frac{\mu}{\Delta r^2}+\frac{\mu}{r\Delta r}\right)$

Continued on next page

TABLE 8 (CONTINUED)

A2	Type a) (Jump)	Type b) (Euler)	Type c) (DuFort-Frankel)
A2(1)	$1 - 4\Delta t\mu\left[\frac{1}{\Delta x^2} + \frac{1}{\tau^2\Delta\varphi^2} + \frac{1}{\Delta\tau^2} + \frac{1}{2\tau^2}(\delta_{yu_r} + \delta_{yu_\varphi})\right]$	0	$\frac{1-\gamma}{1+\gamma}$ $\gamma \equiv 2\mu\Delta t\left[\frac{1}{\Delta x^2} + \frac{1}{\tau^2\Delta\varphi^2} + \frac{1}{\Delta\tau^2} - \frac{\delta_{yu_r} + \delta_{yu_\varphi}}{2\tau^2}\right]$
A2(2)	$\frac{2\Delta t\mu}{\Delta x^2}$	0	0
A2(3)	$\frac{2\Delta t\mu}{\Delta x^2}$	0	0
A2(4)	$\frac{2\Delta t\mu}{\tau^2\Delta\varphi^2}$	0	0
A2(5)	$\frac{2\Delta t\mu}{\tau^2\Delta\varphi^2}$	0	0
A2(6)	$2\Delta t\mu\left(\frac{1}{\Delta\tau^2} - \frac{1}{\tau\Delta\tau}\right)$	0	0
A2(7)	$2\Delta t\mu\left(\frac{1}{\Delta\tau^2} + \frac{1}{\tau\Delta\tau}\right)$	0	0

TABLE 9. COEFFICIENTS OF THE AMPLIFICATION MATRIX $\underline{\underline{G}}$ ACCORDING TO (A6-16) /195

Type a) (Jump)

$$A_{11} = -\Delta t \frac{V_r}{r} \delta_{y v_\varphi}$$

$$B_{11} = -\Delta t \left(\frac{V_x}{\Delta x} S_1 + \frac{V_\varphi}{r \Delta \varphi} S_2 + \frac{V_r}{\Delta r} S_3 \right)$$

$$A_{12} = 1 + 2\mu \Delta t \left[\frac{2}{\Delta x^2} (C_1 - 1) + \frac{2}{r^2 \Delta \varphi^2} (C_1 - 1) + \frac{2}{\Delta r^2} (C_3 - 1) - \frac{1}{r^2} \left(\delta_{y v_\varphi} + \delta_{y v_r} \right) \right]$$

$$B_{12} = 2\mu \Delta t \left[\frac{2}{r \Delta r} S_3 \right]$$

Type b) (Euler)

$$A_{11} = \Delta t \left[(C_1 - 1) \left(\frac{|V_x|}{\Delta x} + \frac{2\mu}{\Delta x^2} \right) + (C_2 - 1) \left(\frac{|V_\varphi|}{r \Delta \varphi} + \frac{2\mu}{r^2 \Delta \varphi^2} \right) + (C_3 - 1) \left(\frac{|V_r|}{\Delta r} + \frac{2\mu}{\Delta r^2} \right) - \delta_{y v_\varphi} \frac{V_r}{r} - \mu \left(\delta_{y v_\varphi} + \delta_{y v_r} \right) \frac{1}{r^2} \right]$$

$$B_{11} = -S_1 \frac{V_x}{\Delta x} - S_2 \frac{V_\varphi}{r \Delta \varphi} - S_3 \frac{V_r}{\Delta r} + S_3 \frac{2\mu}{r \Delta r}$$

$$A_{12} = B_{12} = 0$$

Type c) (DuFort-Frankel)

$$A_{11} = \frac{\Delta t}{(1+\gamma)} \left[\frac{2\mu}{\Delta x^2} C_1 + \frac{2\mu}{r^2 \Delta \varphi^2} C_2 + \frac{2\mu}{\Delta r^2} C_3 - \frac{V_r}{r} \delta_{v_\varphi y} \right]$$

$$B_{11} = \frac{\Delta t}{(1+\gamma)} \left[-\frac{V_x}{\Delta x} S_1 - \frac{V_\varphi}{r \Delta \varphi} S_2 + \left(\frac{2\mu}{r \Delta r} - \frac{V_r}{\Delta r} \right) S_3 \right]$$

$$A_{12} = \frac{1-\gamma}{1+\gamma} \quad ; \gamma = 2\mu \Delta t \left[\frac{1}{\Delta x^2} + \frac{1}{r^2 \Delta \varphi^2} + \frac{1}{\Delta r^2} - \frac{\delta_{y v_r} + \delta_{y v_\varphi}}{2 r^2} \right]$$

$$B_{12} = 0$$

TABLE 10. ERRORS IN THE DIFFERENCING METHOD FOR LAMINAR INCIDENT FLOW

	$\varepsilon_1 \cdot 1000$ (Wall mesh)			$\varepsilon_2 \cdot 1000$ (Center)		
Fall:	a) $\Delta r = 1/8$ = const	b) $\Delta r \approx 1/8$ ≠ const	c) $\Delta r = 1/16$ = const	a) $\Delta r = 1/8$ = const	b) $\Delta r \approx 1/8$ ≠ const	c) $\Delta r = 1/16$ = const
t						
0.04	- 2.36	- 2.01	- 0.72	- 0.24	- 0.39	- 0.06
0.08	- 2.24	- 2.22	- 0.68	- 0.47	- 0.69	- 0.13
0.12	- 2.06	- 2.31	- 0.63	- 0.48	- 0.93	- 0.12
0.16	- 1.89	- 2.34	- 0.60	- 0.25	- 0.86	- 0.08
0.20	- 1.74	- 2.34	- 0.57	- 0.11	- 0.92	- 0.01
0.24	- 1.61	- 2.32	- 0.55	+ 0.21	- 0.63	+ 0.02
0.40	- 1.30	- 2.21	- 0.49	+ 0.97	+ 0.25	+ 0.23

TABLE 11. TEST PROBLEM TAYLOR-GREEN VORTICES

Time step	I Error of the method used here $\cdot 10^5$	II Error of the method used by Orszag $\cdot 10^5$	III Factor of error enlargement when increasing mesh size by four.
1	0.107	2.1	26
3	4.26	6.1	19
5	8.29	10	16
7	12.3	14	14
9	16.1	17	13
20	37	37	12

FOLDOUT FRAME 1

FOLDOUT FRAME 2

/198/

TABLE 12. SPECIFICATION OF CASES K1 - K4, Z1 - Z4.

	K1	K2	K3	K4	Z1	Z2	Z3	Z4
R2/R1	1	1	1	1	5	5	5	5
$\Delta x_1, \Delta x$	0.125	0.125	0.0625	0.0625	0.25	0.25	0.125	0.125
$\Delta x_2, \Delta \varphi$	0.125	0.125	0.0625	0.0625	$\pi/16$	$\pi/16$	$\pi/32$	$\pi/32$
$\Delta x_3, \Delta \tau$	0.0625	0.0625	0.0625	0.018+ 0.042	0.0625	0.0625	0.0625	0.018+ 0.042
X_1, X	2	4	4	4	2	4	4	4
X_2, ϕ	1	2	2	2	π	2π	2π	2π
IM	16	32	64	64	8	16	32	32
JM	8	16	32	32	16	32	64	64
KM	16	16	16	32	16	16	16	32
IM·JM·KM	2048	8192	32768	65536	2048	8192	32768	65536
N	64	64	32	32	64	64	32	32
$\Delta t \cdot 10^3$	3.13	2.81	1.46	1.13	4.60	3.88	1,43	1.04
Problem time	5.6	3.8	0.9	1.1	7.4	12.3	1.4	1.8
Time steps	1440	1408	736	916	1664	3200	1088	1488
Mesh computation time	35'	2h30'	6h	9h	40'	5h30'	7h40'	14h

TABLE 13. CONSTANT CASE PARAMETERS

/199

Symbol	Def. Eq.	Value
Re	(1 - 13)	10000
Re_m	(1 - 14)	300000
$Re_{m_{krit}}$	(5 - 90)	2100
α	(4 - 4)	1.5
c_7	(5 - 65)	0.3
c_{10}	(5 - 87)	0.01
c_{11}	(7 - 15)	0.2
$E_{1,2}$	(7 - 8)	88000
$A_{w\ 1,2}$	(5-88)	4
$\langle \tau_{w_2} / \tau_{w_1} \rangle$	(7 - 9)	Plate 1 Annulus 0.87
φ_1	(5 - 38)	Plate 3 Annulus 6.r
φ_2	(5 - 55)	1.1
D^2	(5 - 46)	3^{D^2}

TABLE 14. CALCULATION TIMES PER TIME STEP ON THE IBM 370/165

/200

Contri-butions	K1 Z1		K2 Z2		K3 Z3		K4 Z4	
	sec	%	sec	%	sec	%	sec	%
Energy			1.9	31	8.5	34	17.6	33.6
$\underline{\tilde{u}}$			3.7	60	14.1	56.5	29.8	57
ψ			0.54	9	2.33	9.5	4.9	9.4
Total	1.4	100	6.1	100	24.9	100	52.3	100

TABLE 15. COMPARISON OF MAXIMUM VELOCITIES /201

$\langle u_1 \rangle_{max}$	R2/R1	$10^{-5} \cdot Re_m$	Reference
31.8	1	1	Clark [22]
31.5	1	4.6	Comte-Bellot [18]
27.7	1	2.4	"
27	1	1	Laufer [76]
30.1	1	∞	Deardorff [29]
28.89	1	3	K1
31.3	1	3	K2
27.4	1	3	K3
27.6	1	3	K4
28.0	5	3	Z1
28.3	5	3	Z2
27.6	5	3	Z3
27.9	5	3	Z4

TABLE 16. COMPARISON OF THE DIFFERENCES BETWEEN THE MAXIMUM AND MINIMUM VELOCITY

/202

$\langle u_1 \rangle_{max} - \langle u_1 \rangle$	R2/R1	$Re_m \cdot 10^{-5}$	Reference
2.32	1	1	Clark [22]
2.70	1	3	Barthels [11]
2.68	5	3	"
5	1	∞	Deardorff [29]
3.19	1	3	K1
3.17	1	3	K2
2.60	1	3	K3
2.87	1	3	K4
2.75	5	3	Z1
2.52	5	3	Z2
2.74	5	3	Z3
3.15	5	3	Z4

Plate flow

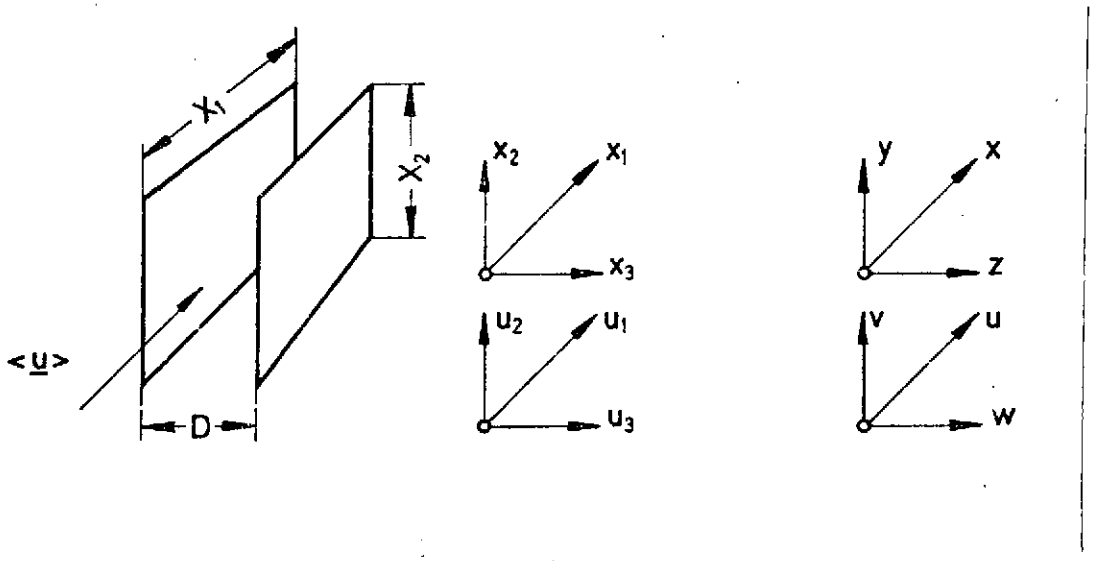

Annulus flow

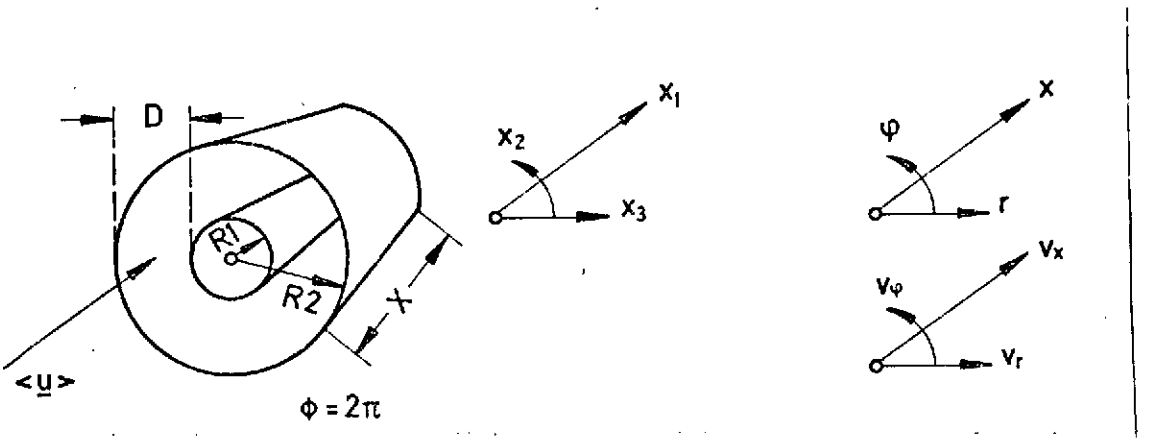

Figure 1. Channel geometries considered

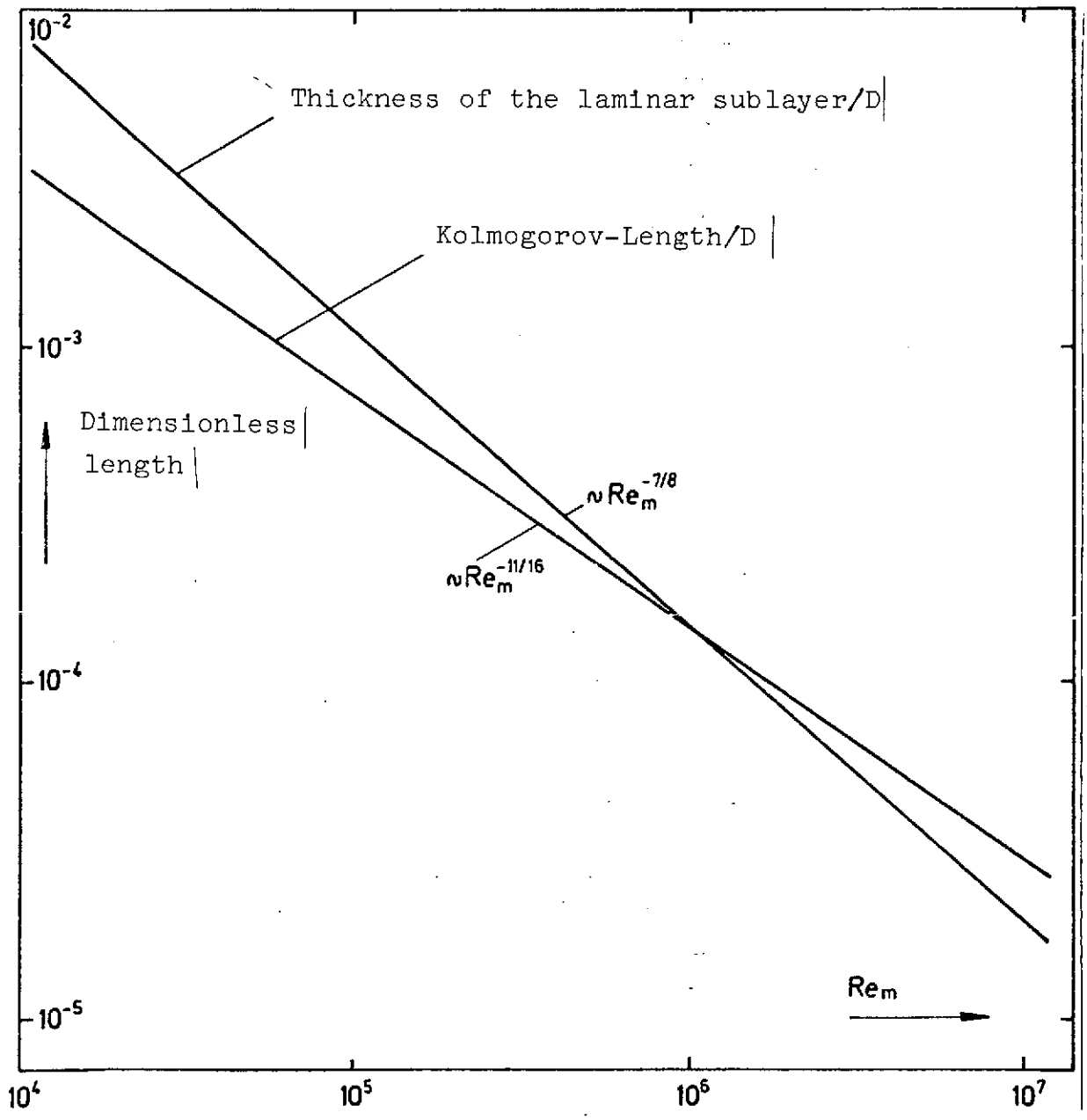

Figure 2. Estimation of required resolution

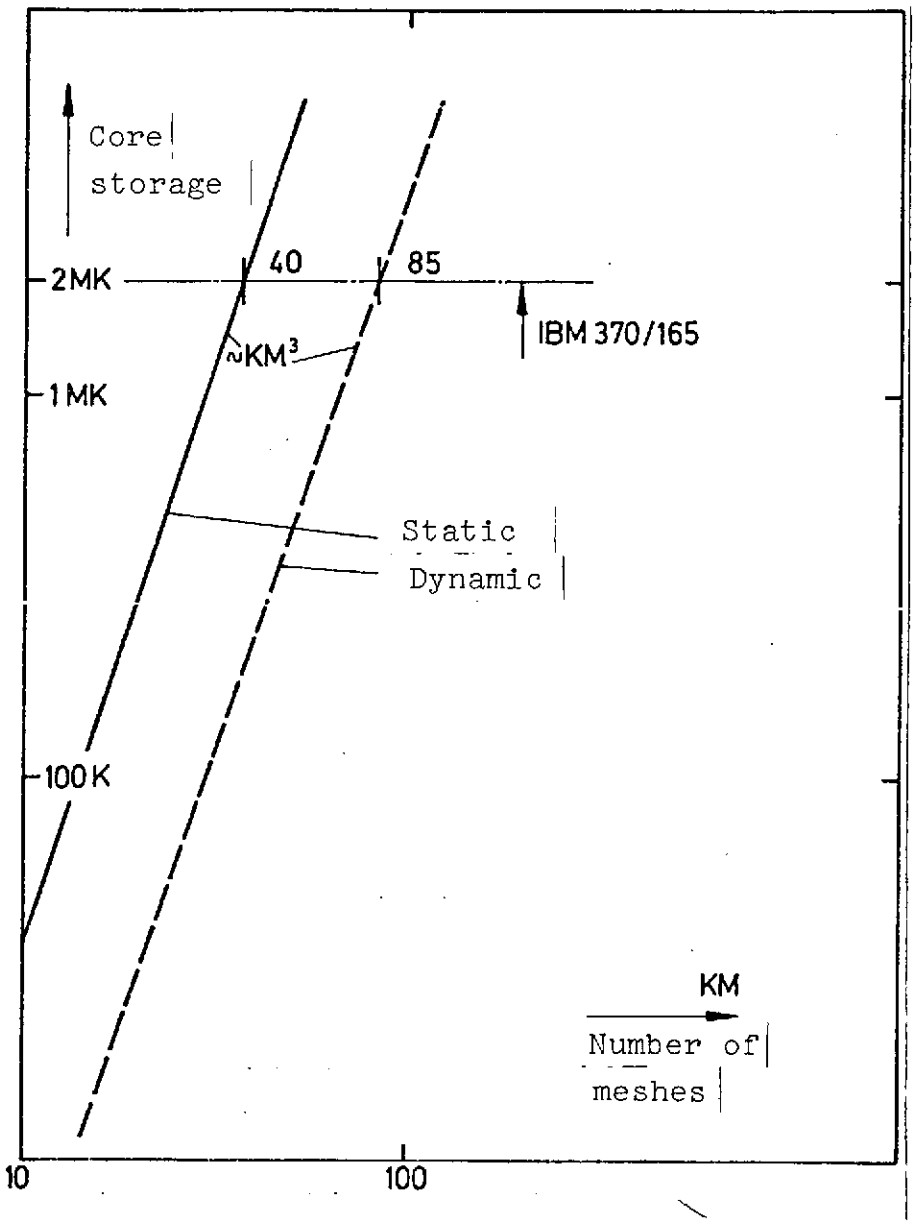

Figure 3. Required storage capacity as a function of meshes in one direction

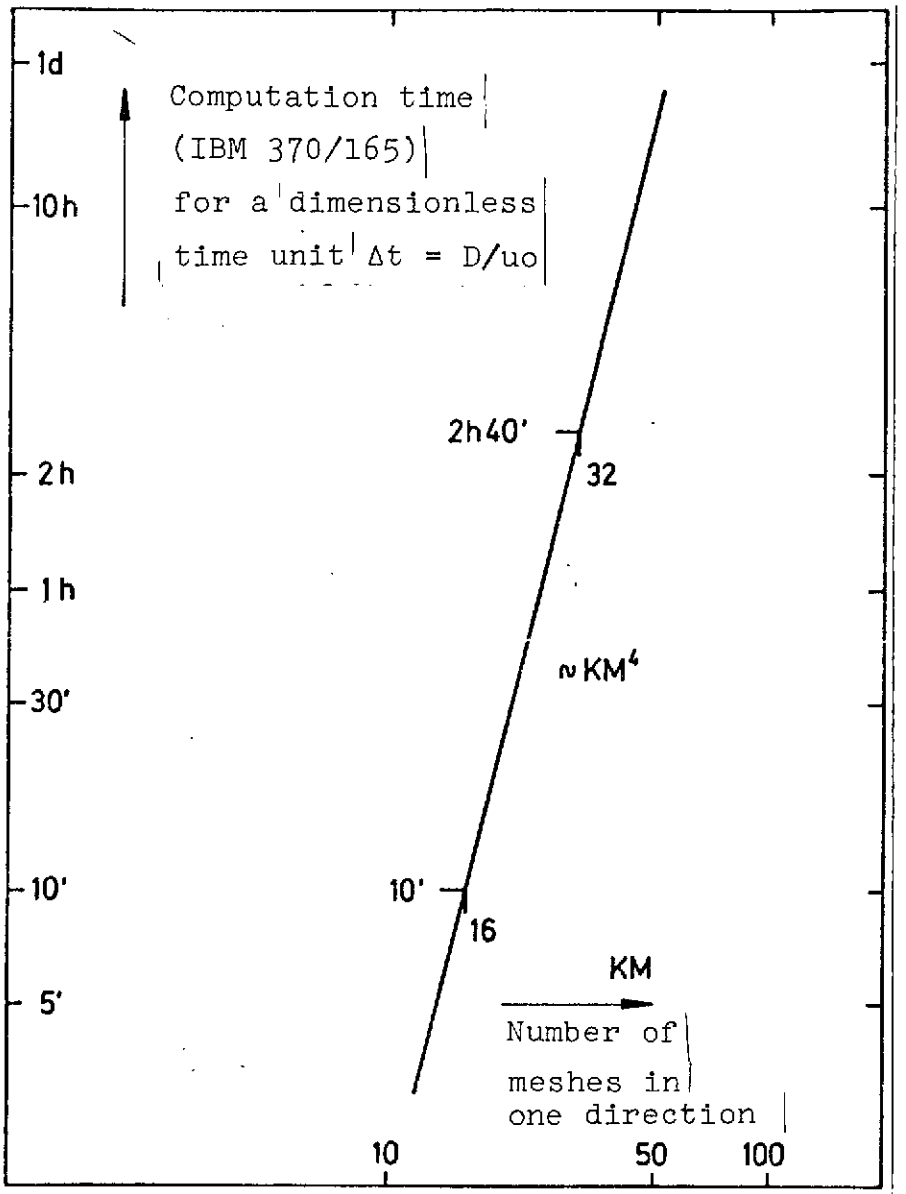

Figure 4. Required computation time as a function of number of meshes in one direction

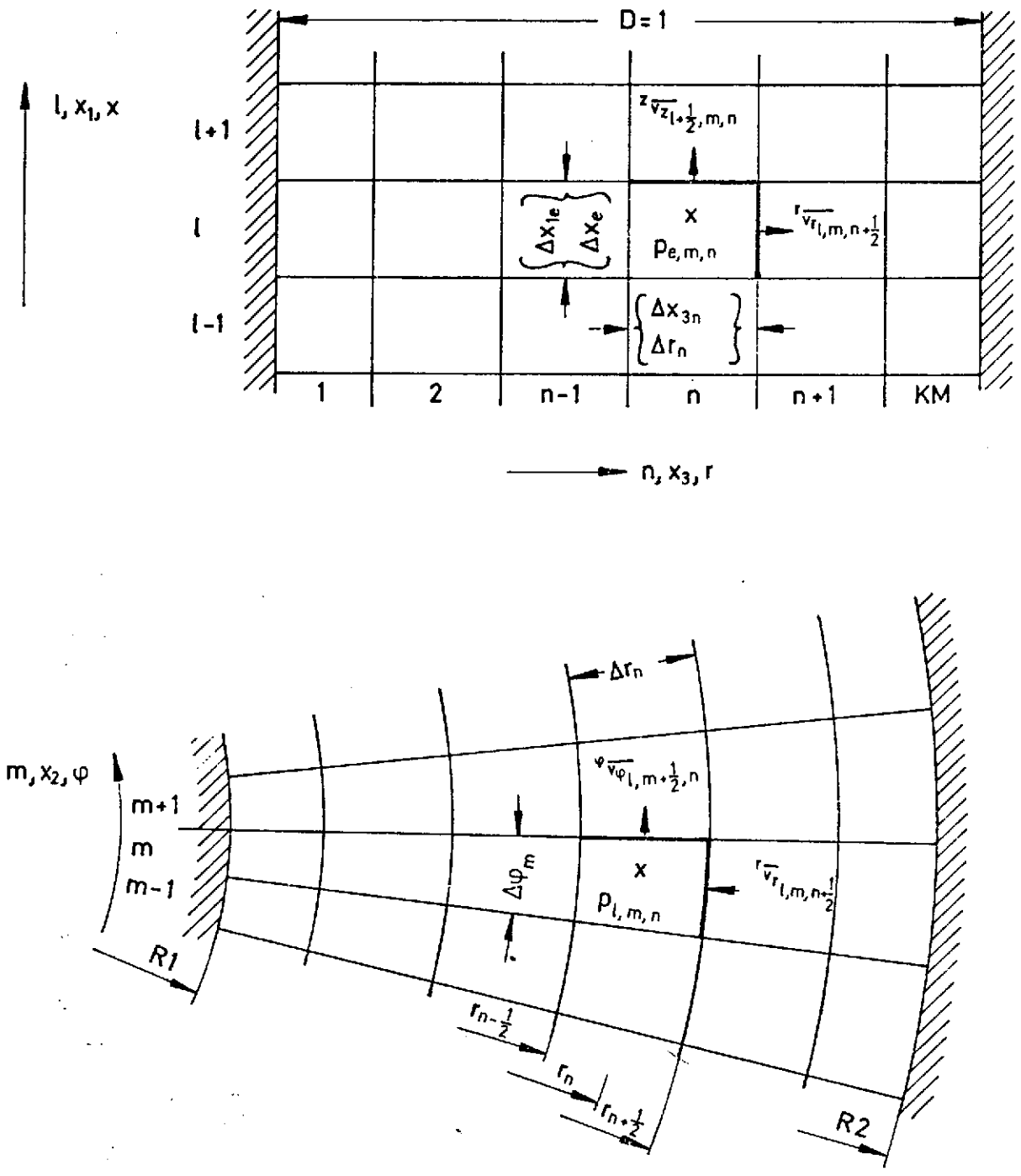

Figure 5. Overlapping mesh grid (staggered grid)

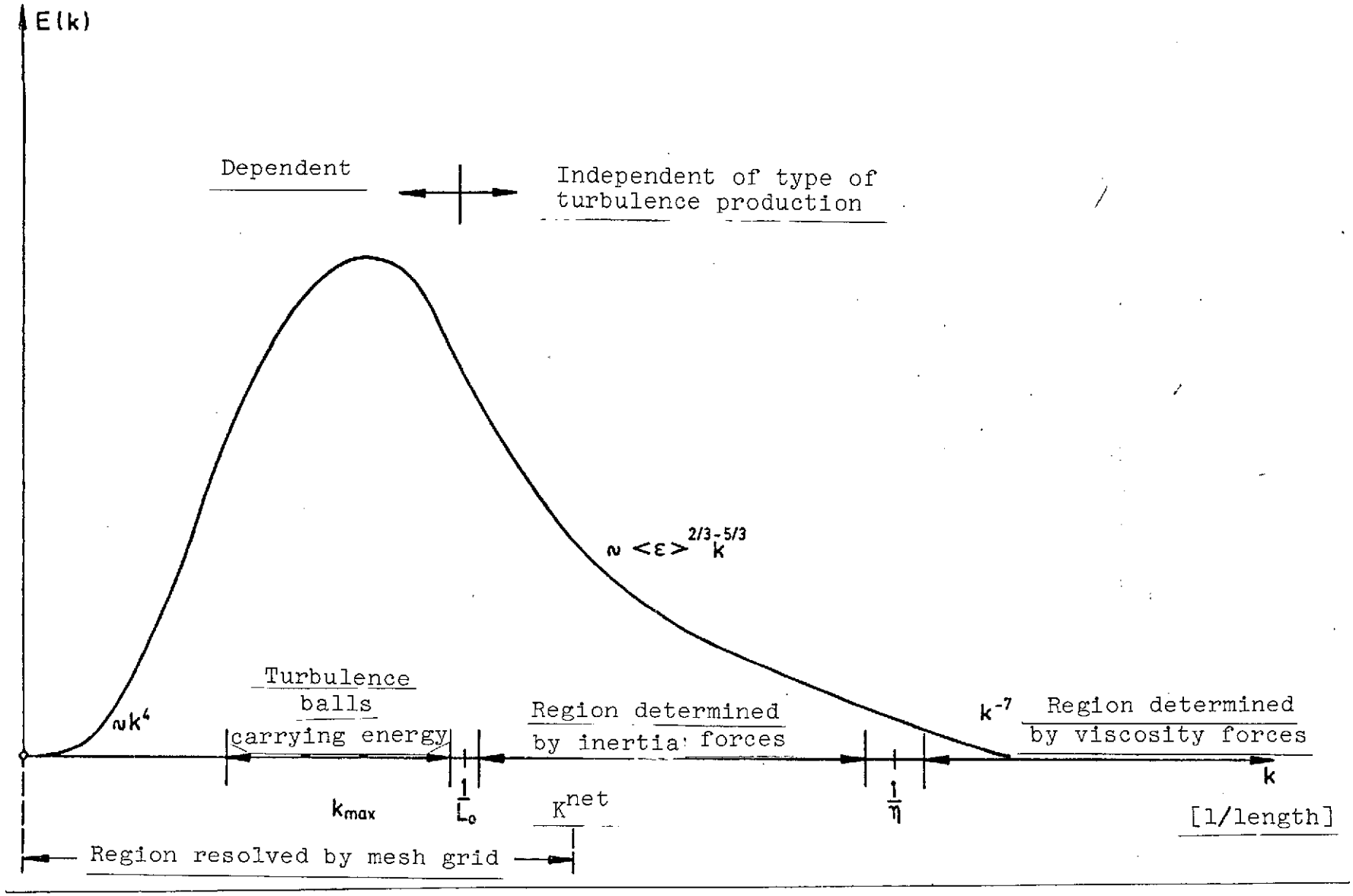

Figure 6. Principle variation of the energy spectrum of isotropic turbulence at large Reynolds numbers

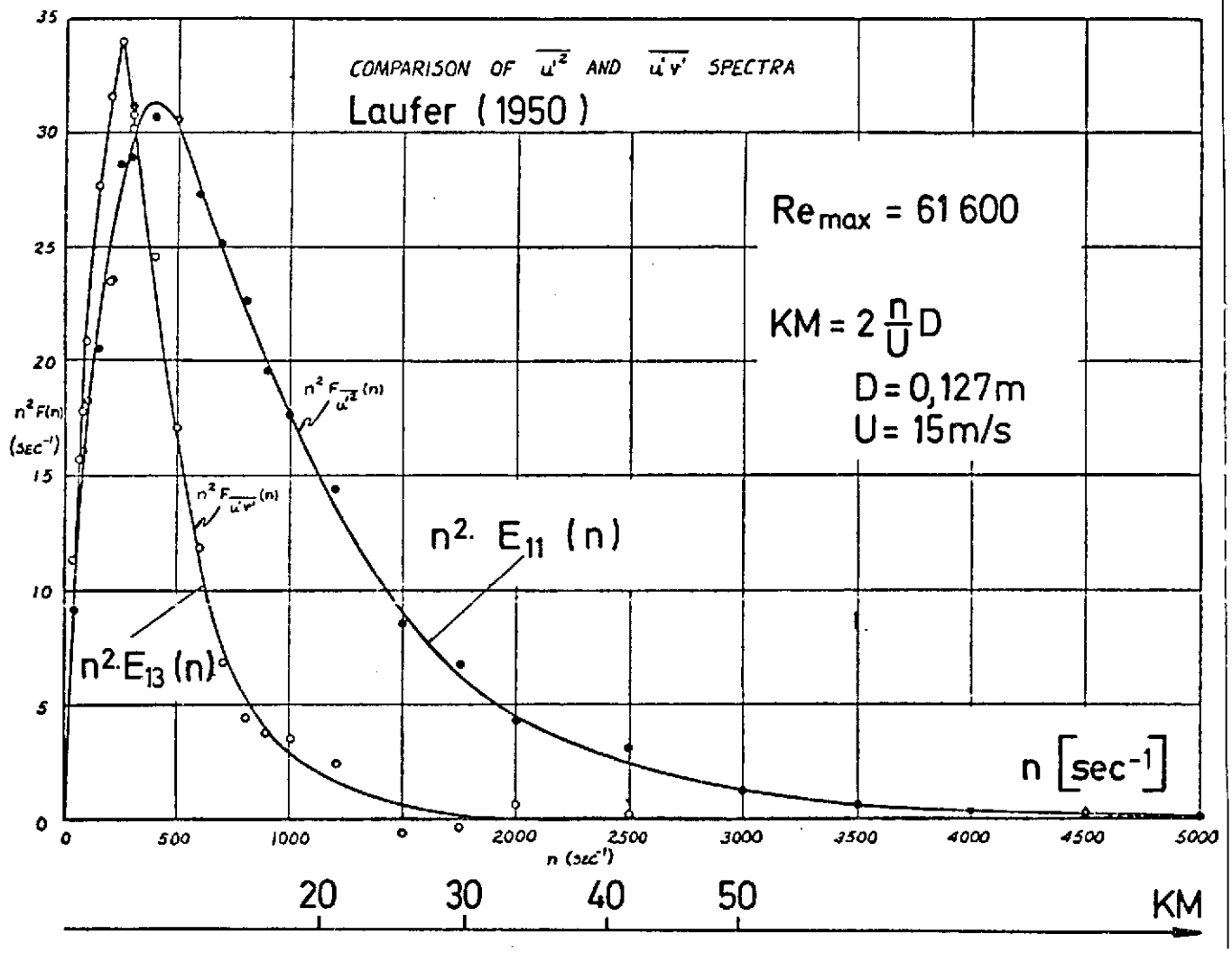

Figure 7. Estimation of required mesh number KM for allowing the local isotropic assumption, according to measurements of Laufer [77]

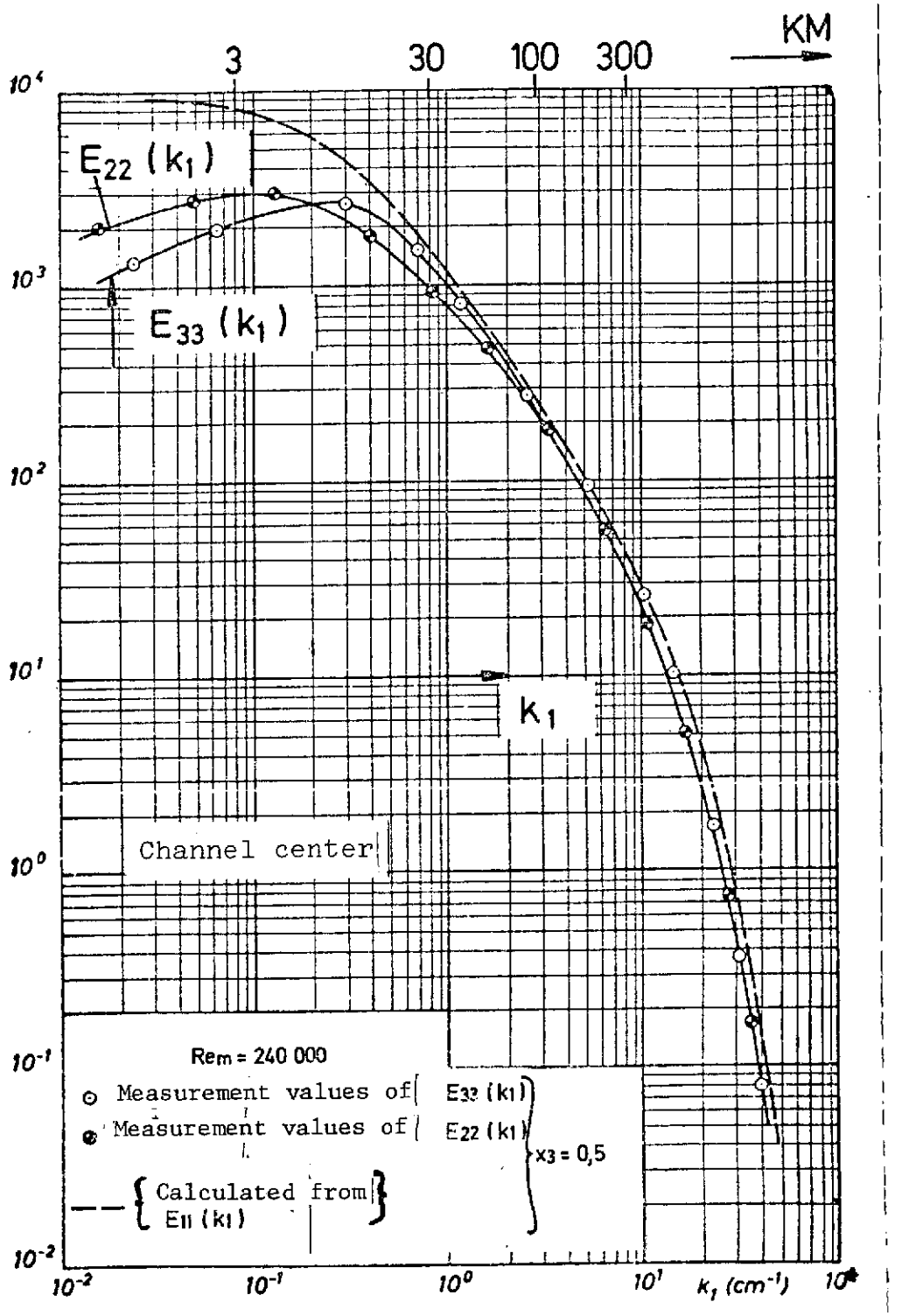

Figure 8. Estimation of required mesh number KM for reliability of local isotropic assumption according to measured value of Comte-Bellot [18] for the channel center (X_3=0.5)

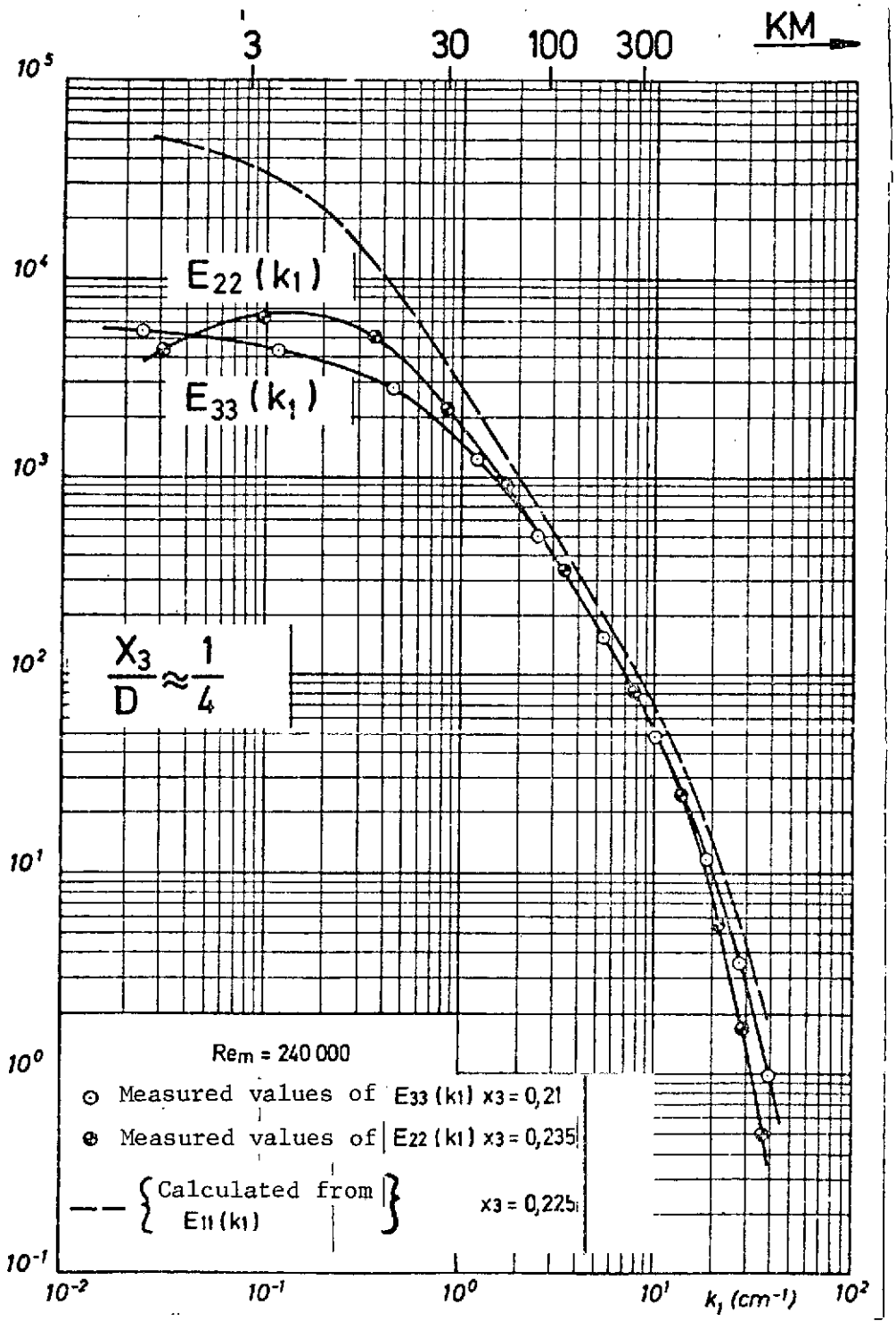

Figure 9. Estimation of required mesh number KM for reliability of local isotropic assumption, according to measured values of Comte-Bellot [18] for x_3=1/4

/212

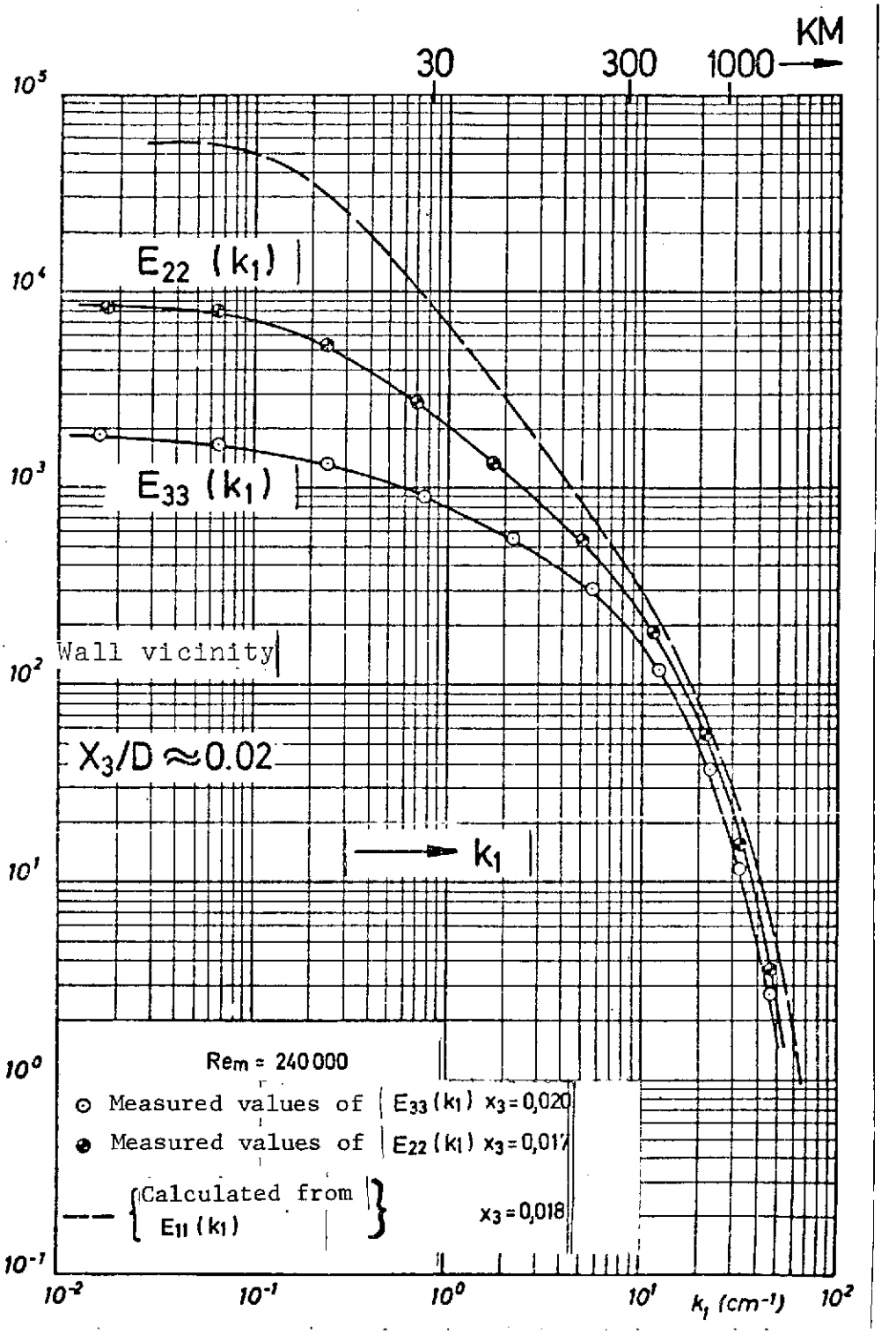

Figure 10. Estimation of required mesh number KM for reliability of local isotropic assumption, according to measured values of Comte-Bellot [18] near the wall (x_3=0.02)

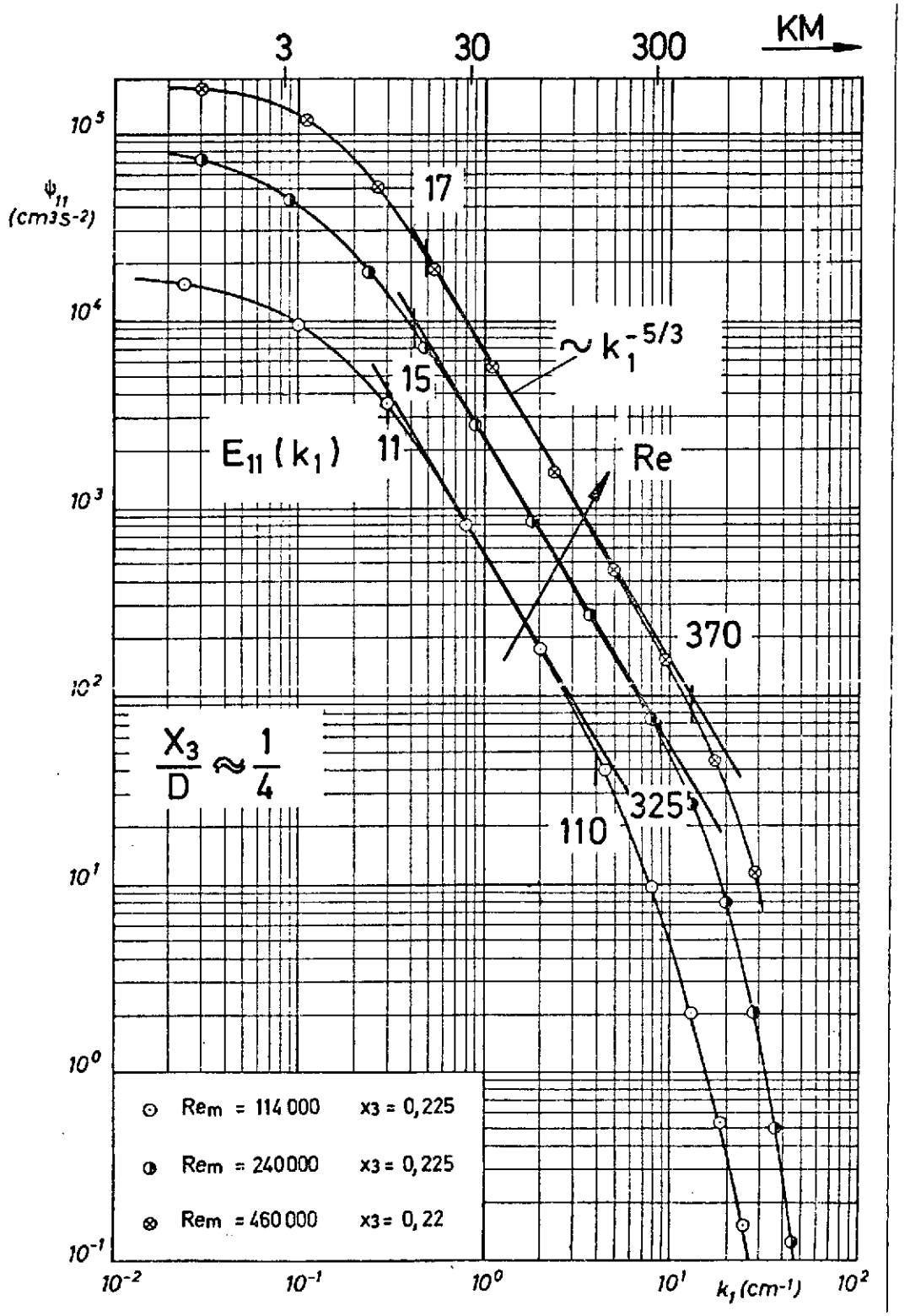

Figure 11. The range of validity of the Kolmogorov spectrum based on measurements of Comte-Bellot [18] for $x_3=1/4$

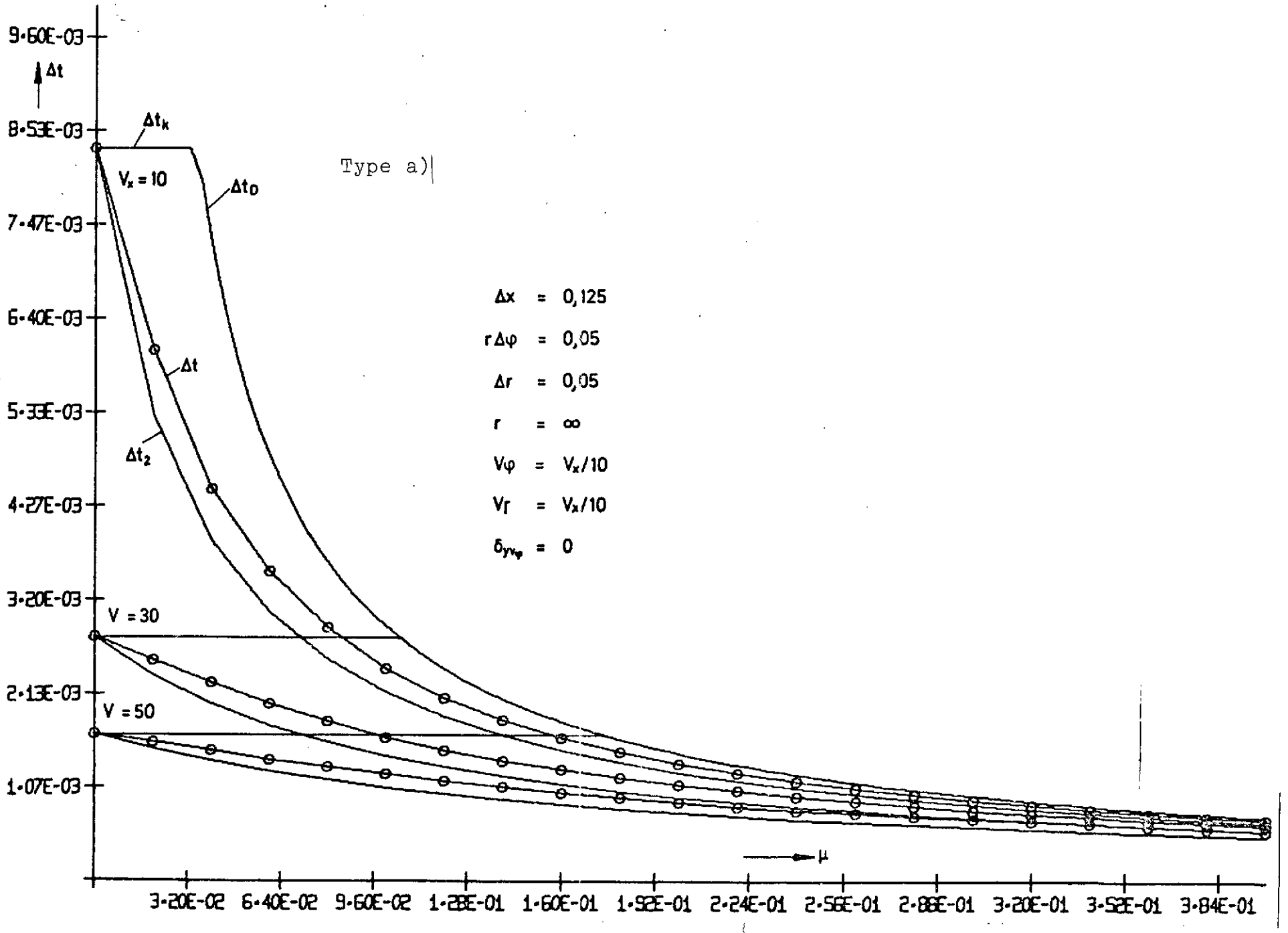

Type a)

$\Delta x = 0{,}125$

$r\Delta\varphi = 0{,}05$

$\Delta r = 0{,}05$

$r = \infty$

$V\varphi = V_x/10$

$V_r = V_x/10$

$\delta_{yv_\varphi} = 0$

Figure 12. Allowable time interval Δt as a function of viscosity μ where convection velocity V_x is the parameter, for Type a) difference formulas

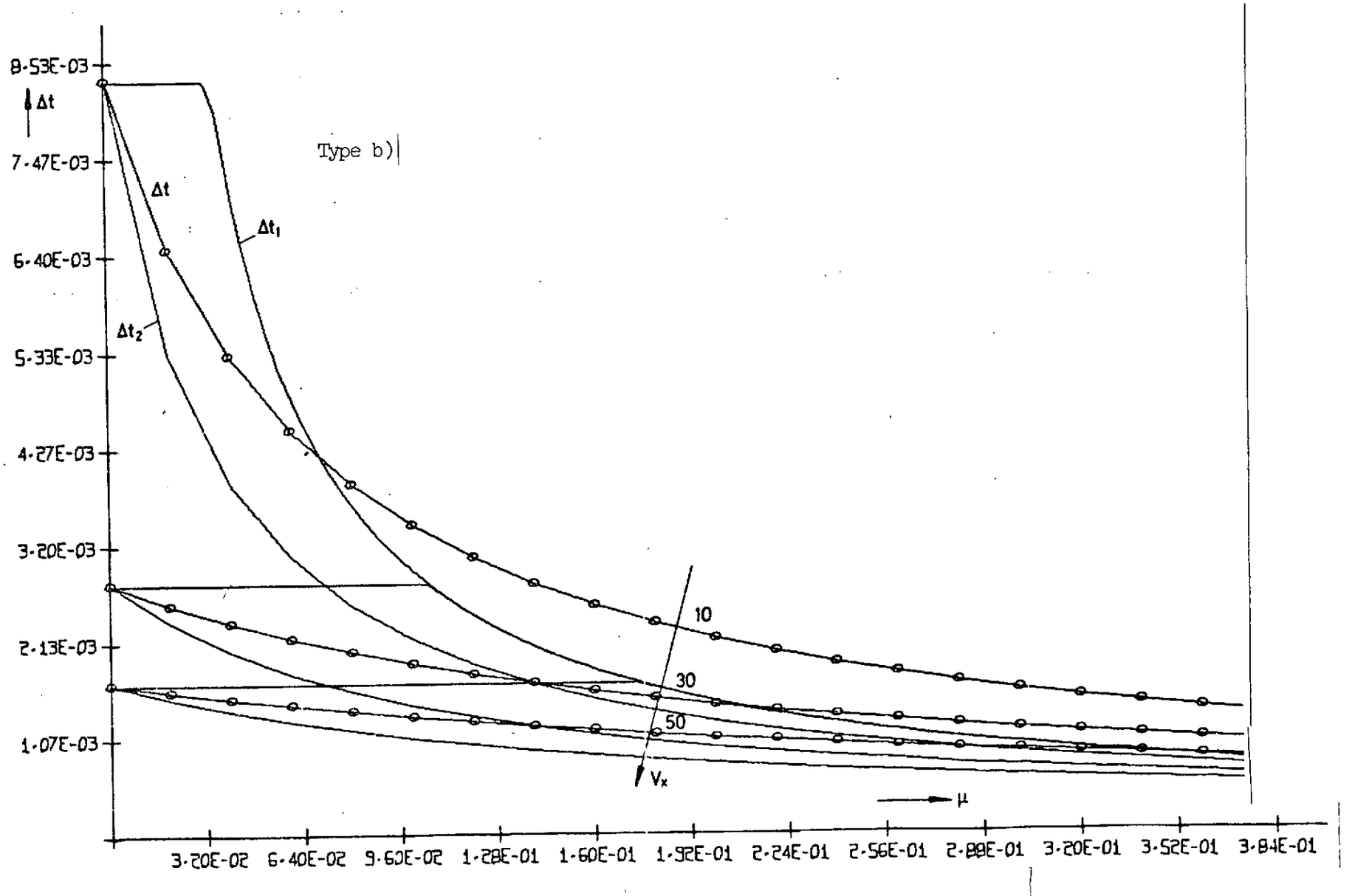

Figure 13. Allowable time interval Δt as a function of viscosity μ where convection velocity V_x is the parameter, for Type b) (other parameters as in Figure 12)

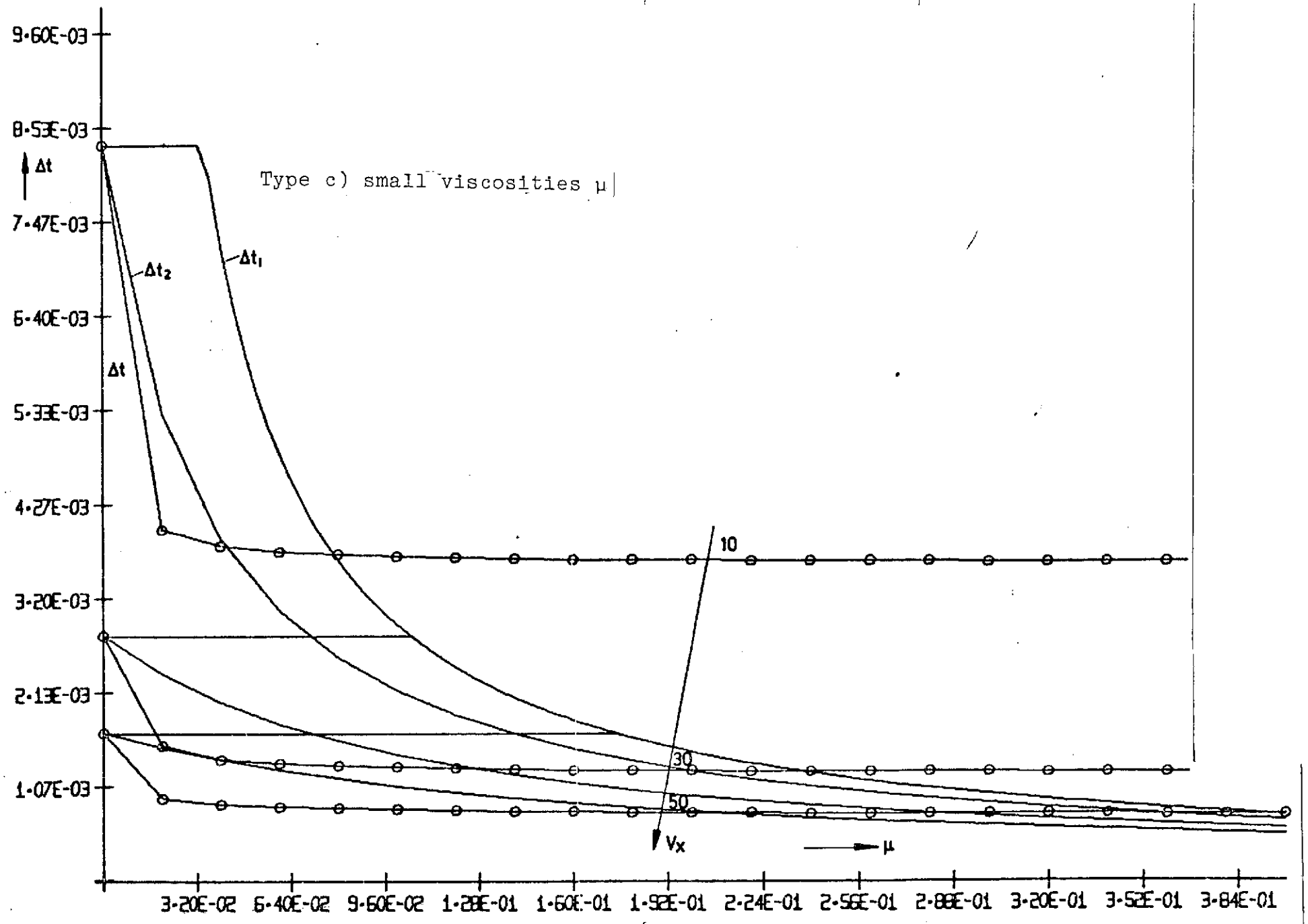

Figure 14. Allowable time interval Δt as a function of viscosity μ where convection velocity V_x is the parameter, for Type c) (DuFort-Frankel) and small viscosities (other parameters as in Figure 12)

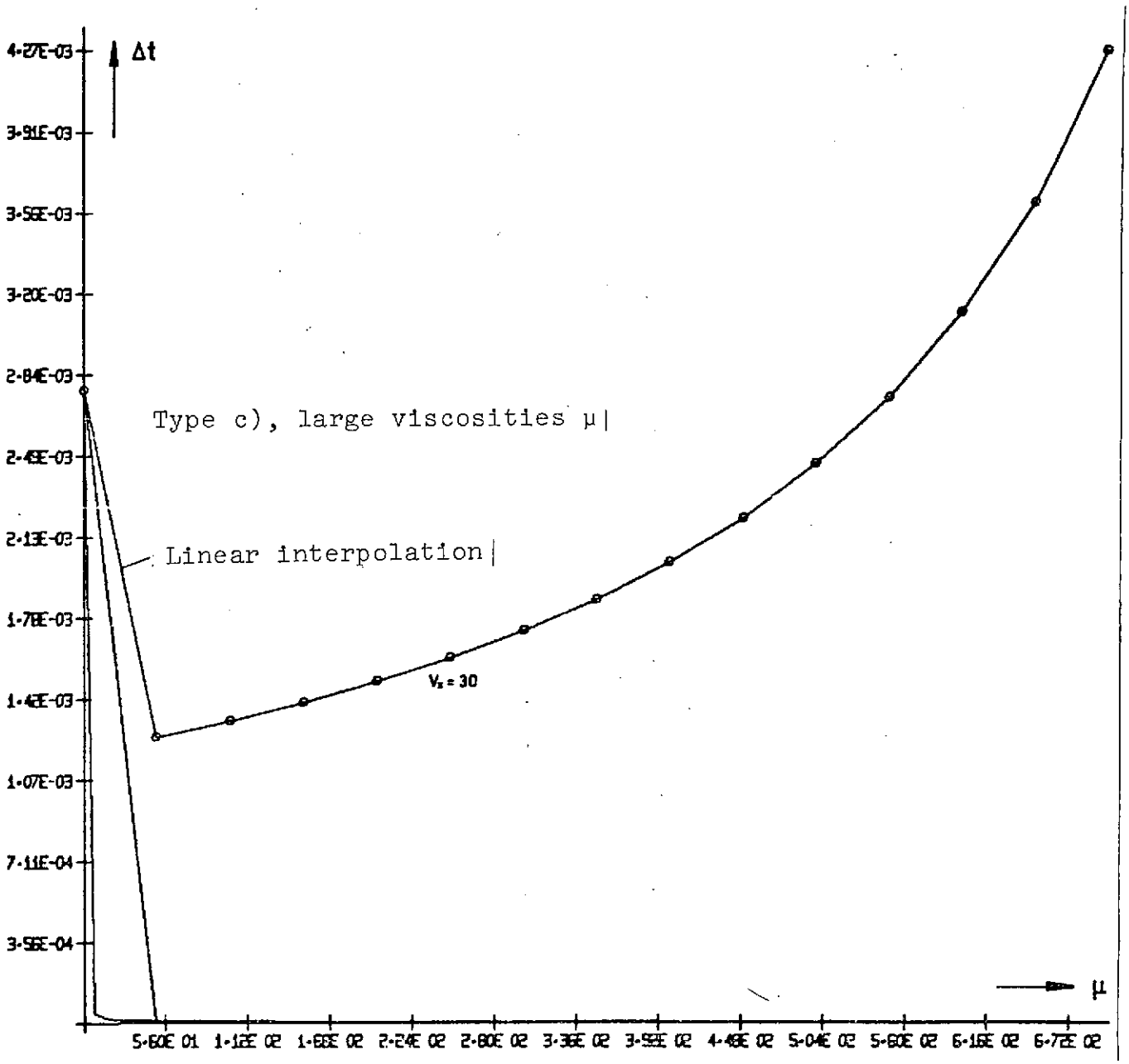

Figure 15. Allowable time interval Δt as a function of viscosity μ for Type c) difference formulas (DuFort-Frankel) and large viscosities (other parameters as in Figure 12)

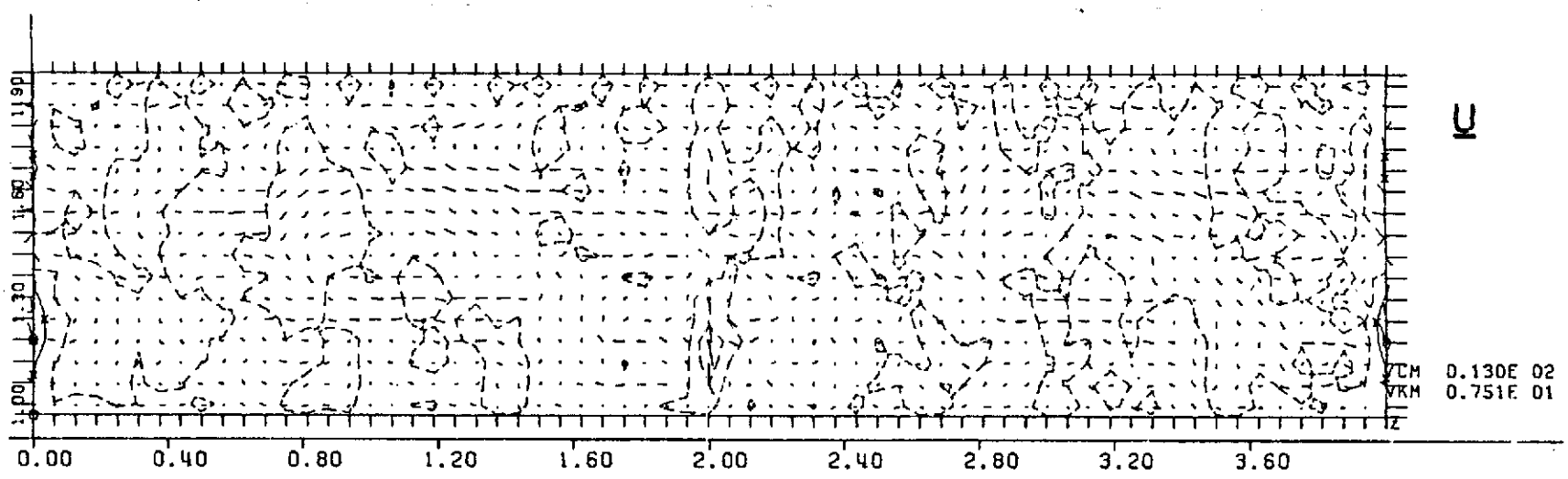

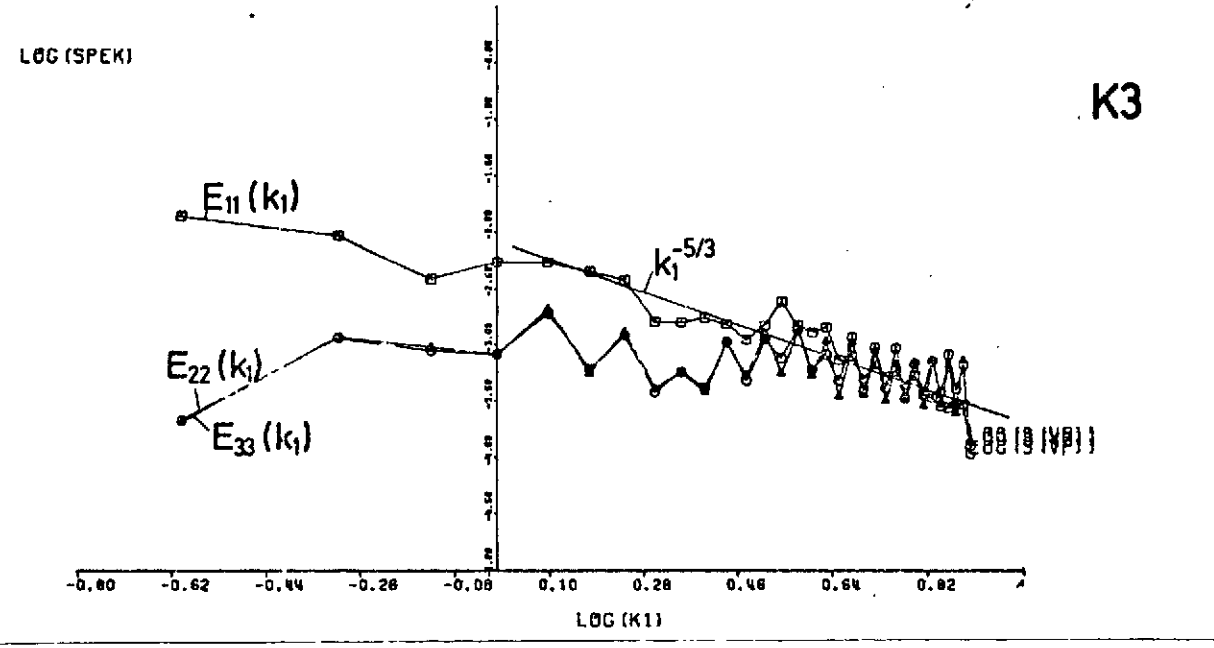

Figure 16. Initial values of the velocity field $(\underline{u} - {}^{P}\langle \underline{u} \rangle)$ in the x_3-x_1 plane and corresponding energy spectra

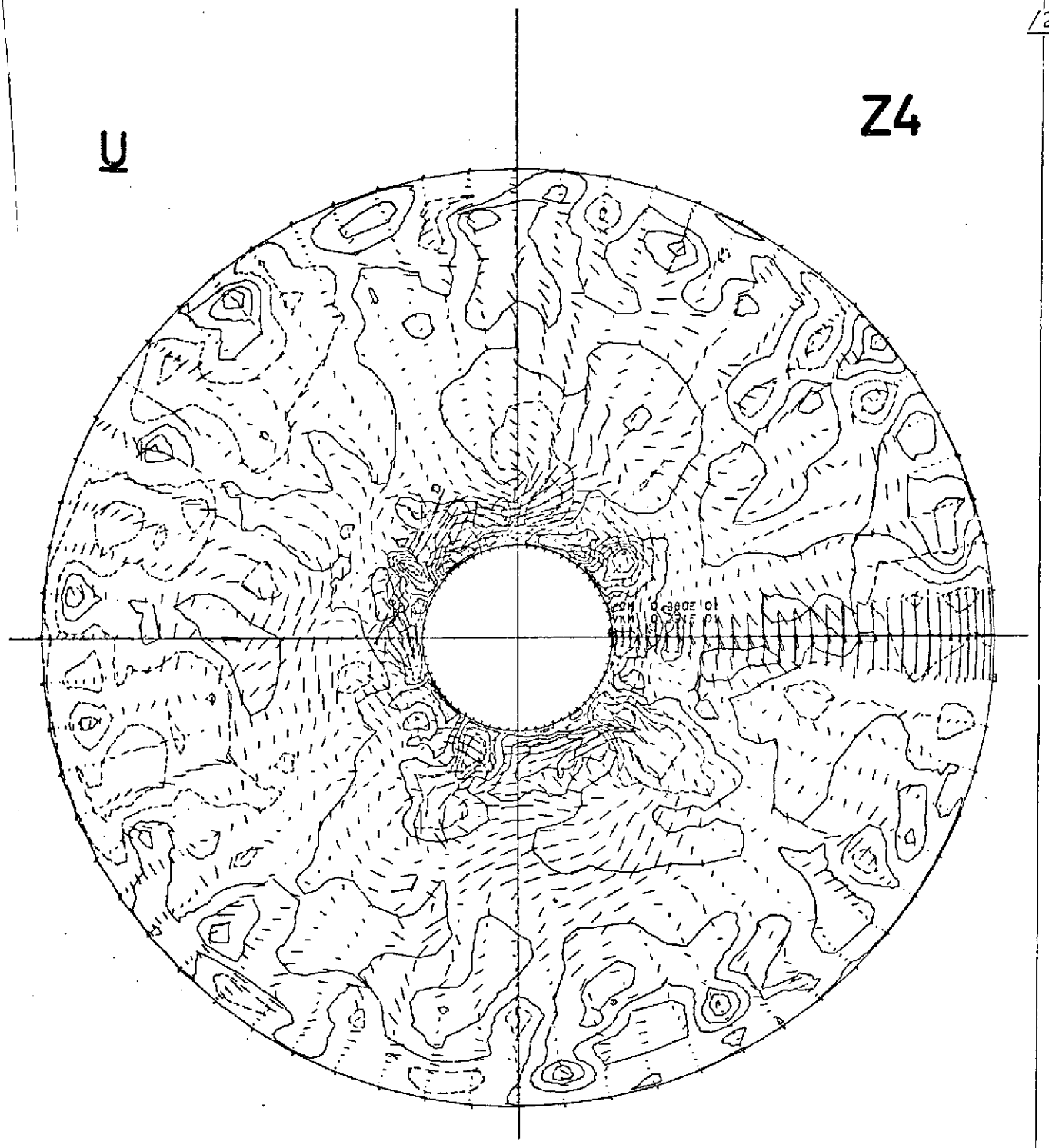

Figure 17. Turbulence velocity field in an annulus: $(u - \langle u \rangle)$

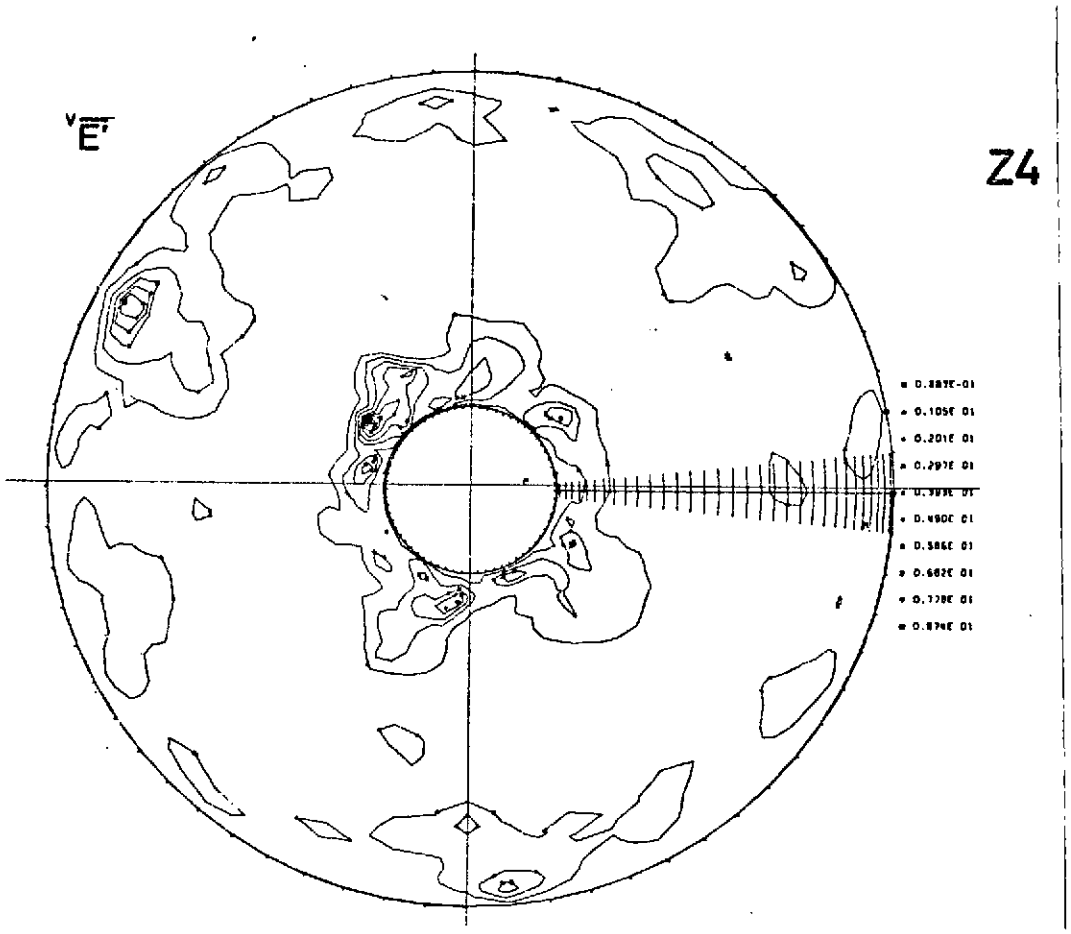

Figure 18. Kinetic energy of the fine structure $\sqrt{E'}$ and pressure p in annulus

(Continued on next page)

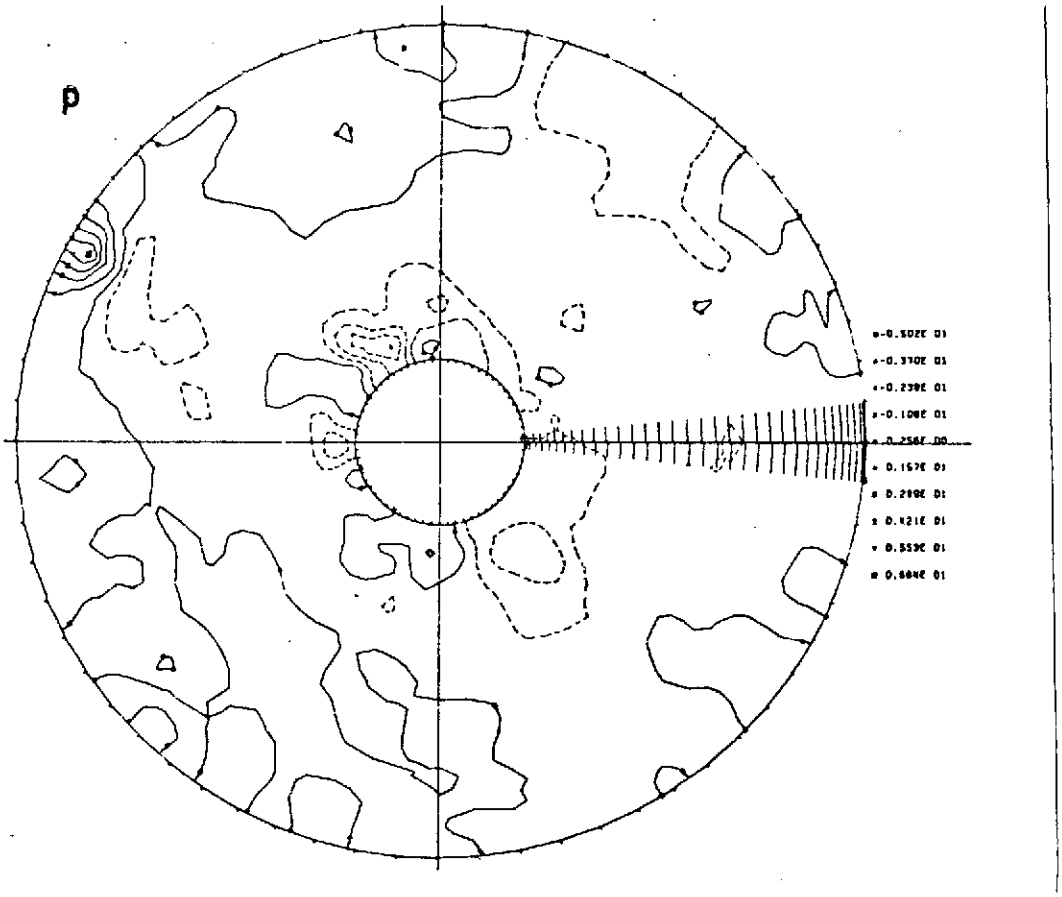

Figure 18 (Continued from preceding page)

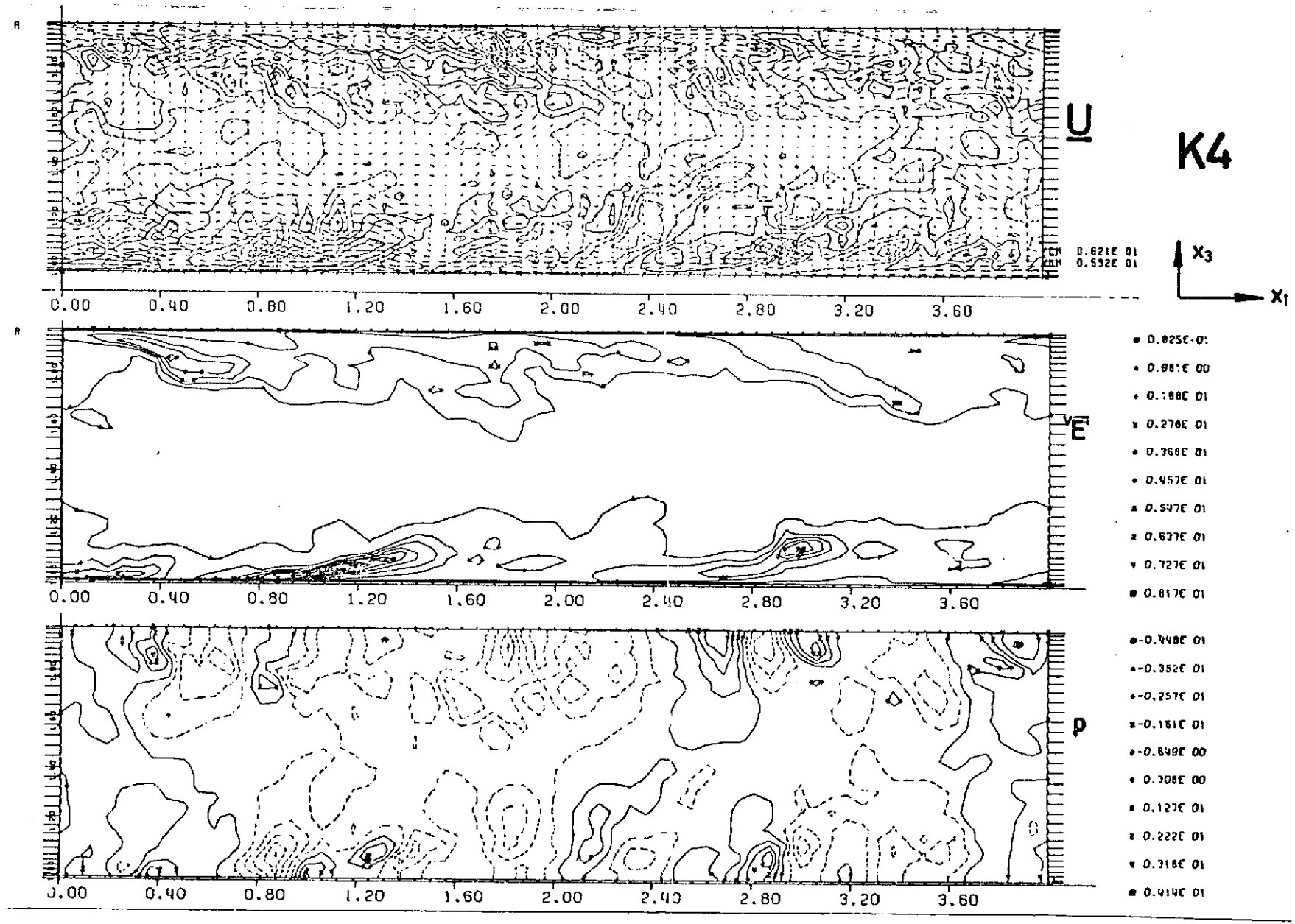

Figure 19. Turbulent velocity field $(u - \langle u \rangle)$, kinetic energy of fine structure $\sqrt{E}$ and pressure p in the x_3-x_1 plane of a plate channel

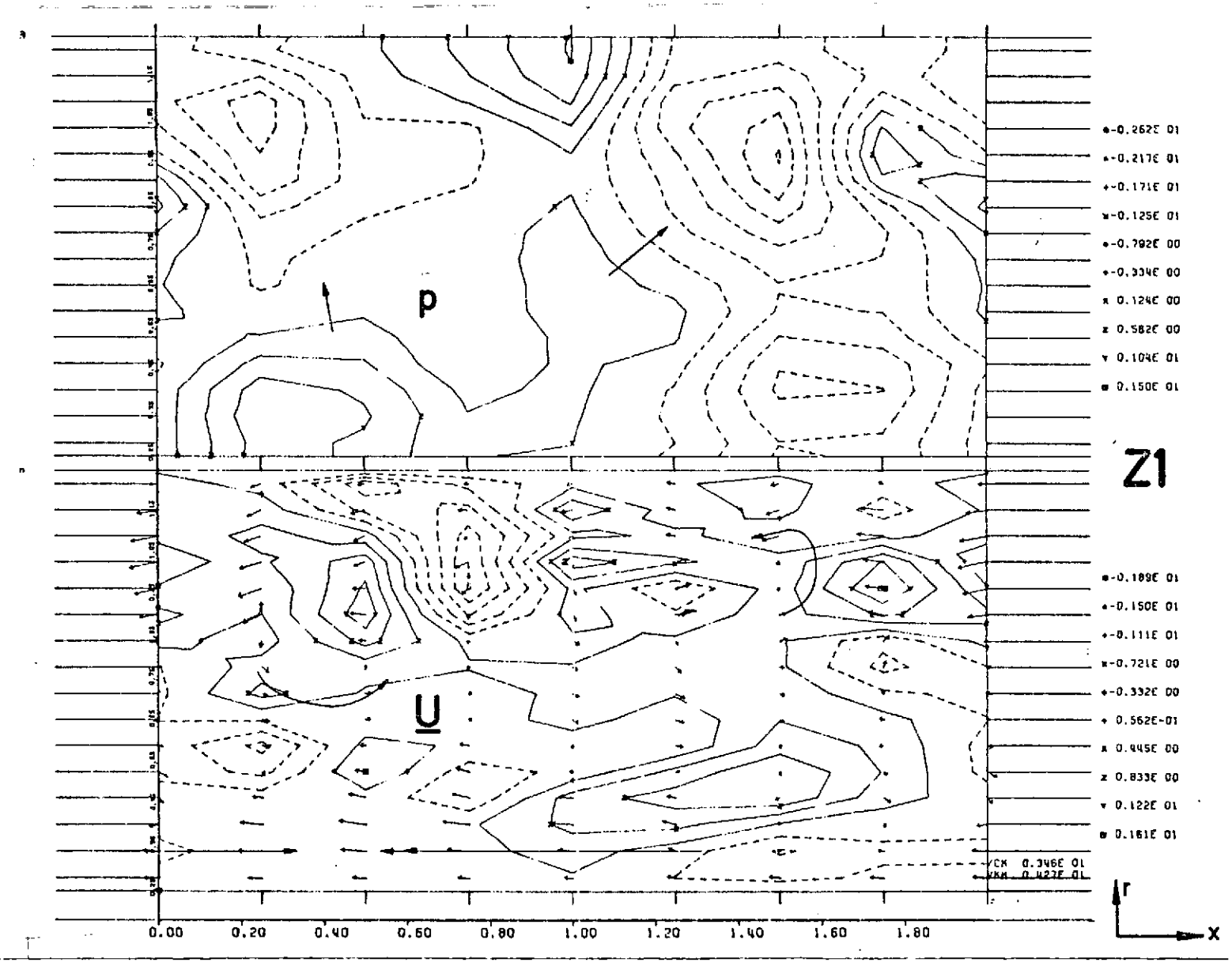

Figure 20. Turbulent pressure field p and velocity field $(u - \langle u \rangle)$ in the r-x plane of an annulus

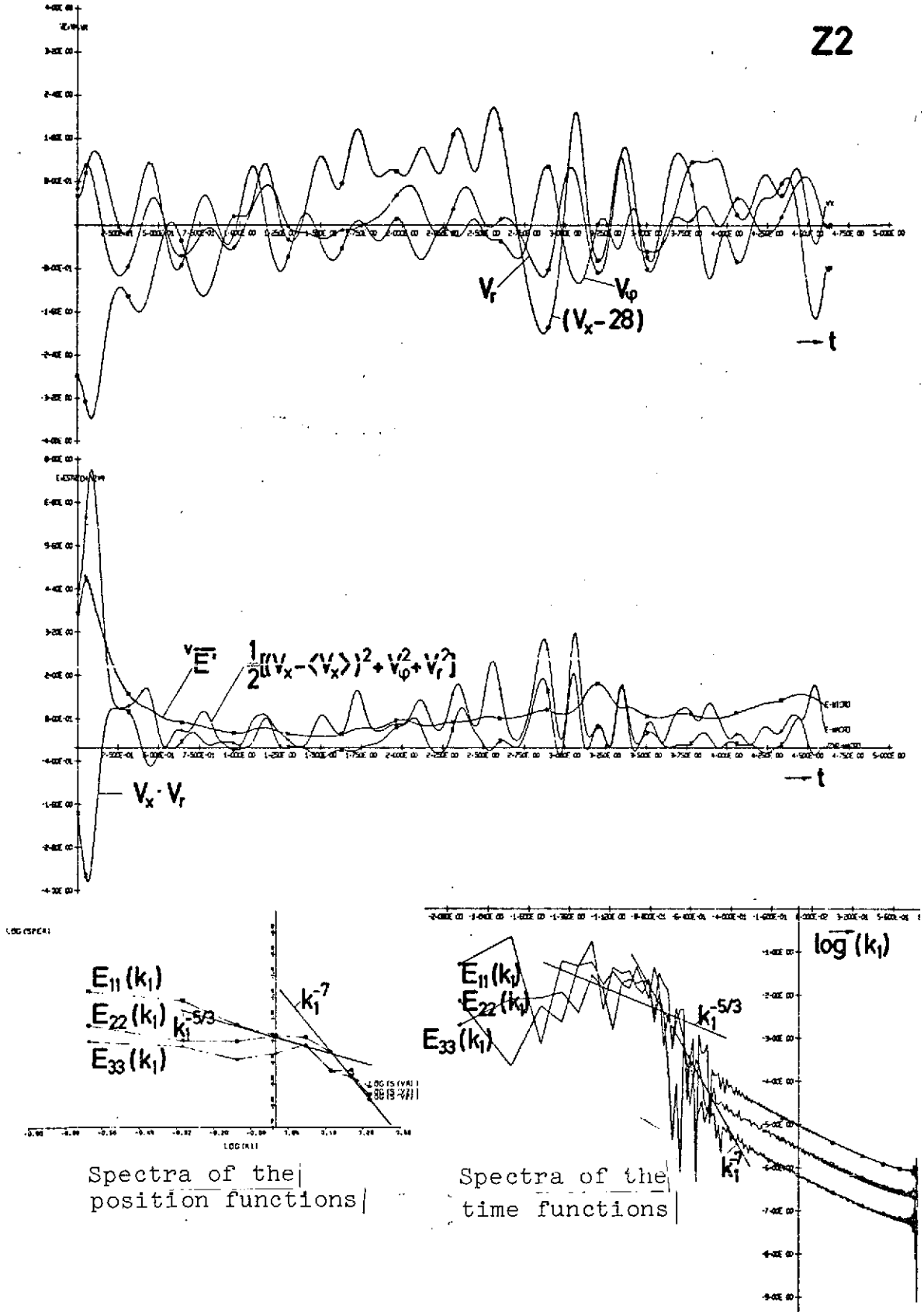

Spectra of the position functions

Spectra of the time functions

Figure 21. Turbulent fluctuations of the coarse structure as a function of time t at a location of r=0.844, and comparison of corresponding spatial and temporal energy spectra

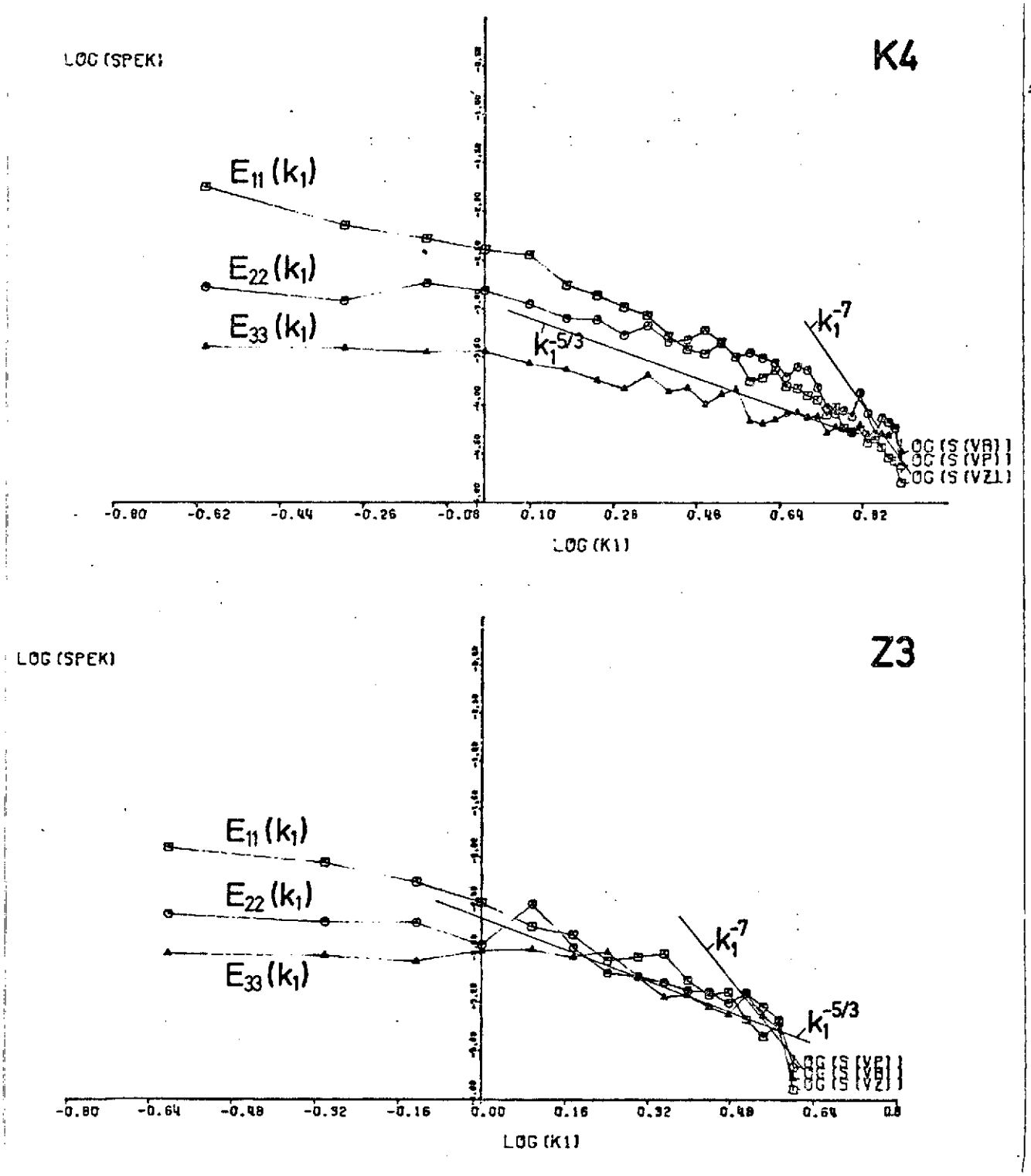

Figure 22. Energy spectra of the velocity fluctuations as a function of the axial coordinate, averaged over the plane parallel to the wall at x_3=0.07 and r=0.47 for the plate and annulus, respectively.

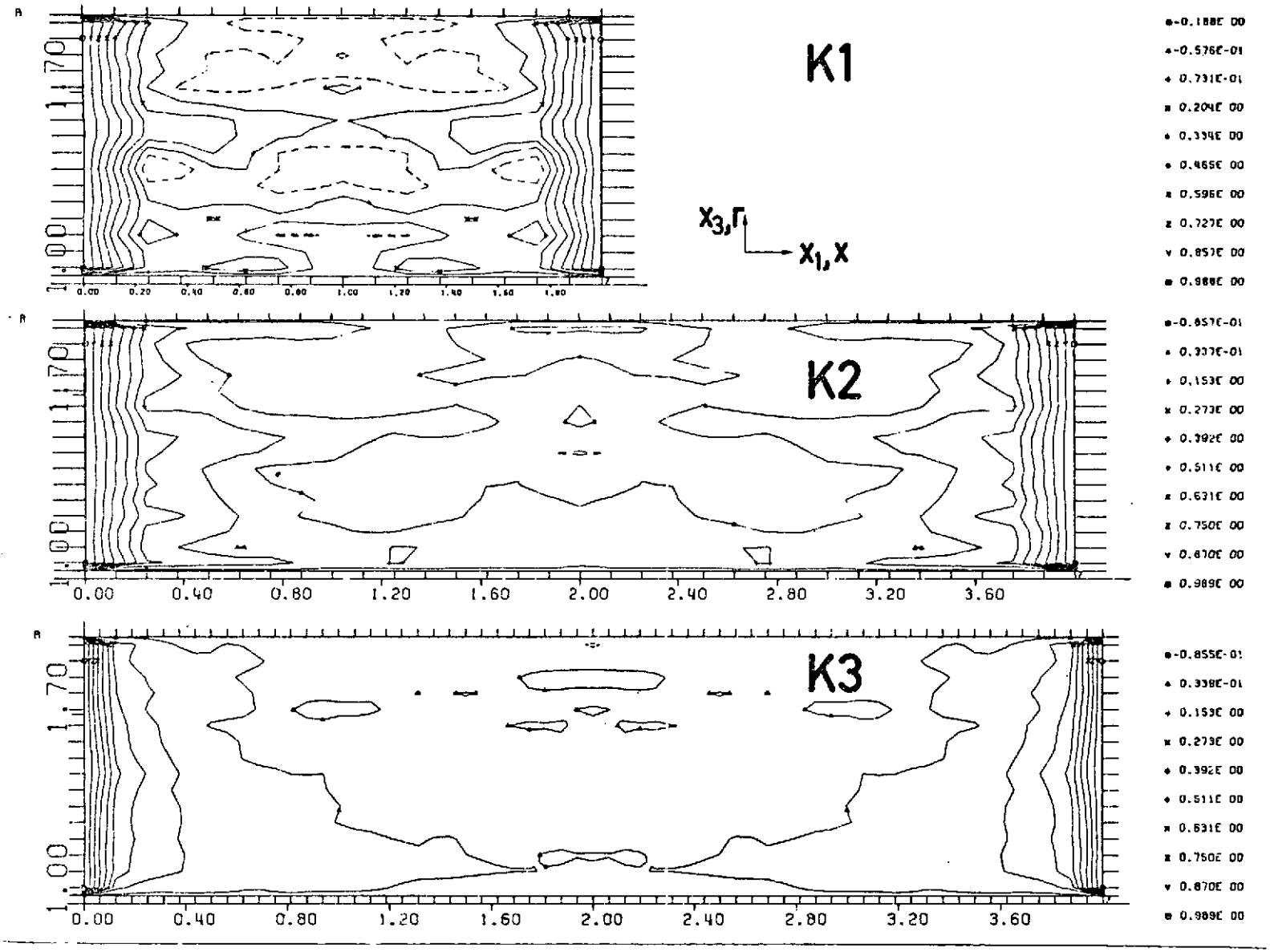

Figure 23. Correlation $R_{ii}(x_3, x_1)$ for plate flows with various period lengths and mesh sizes

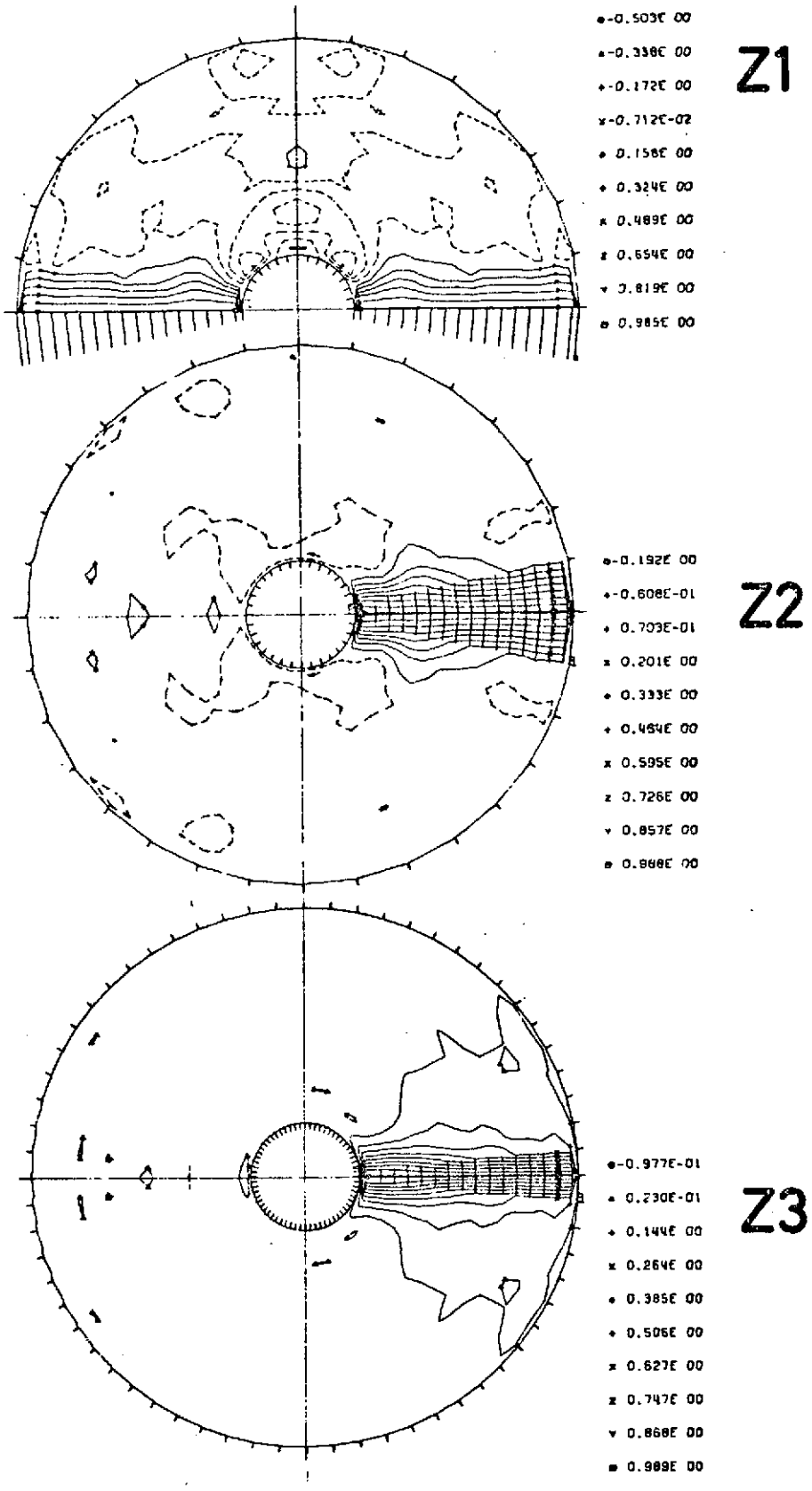

Figure 24. Correlations $R_{ii}(r,\varphi)$ for annulus flows with various period lengths and mesh sizes

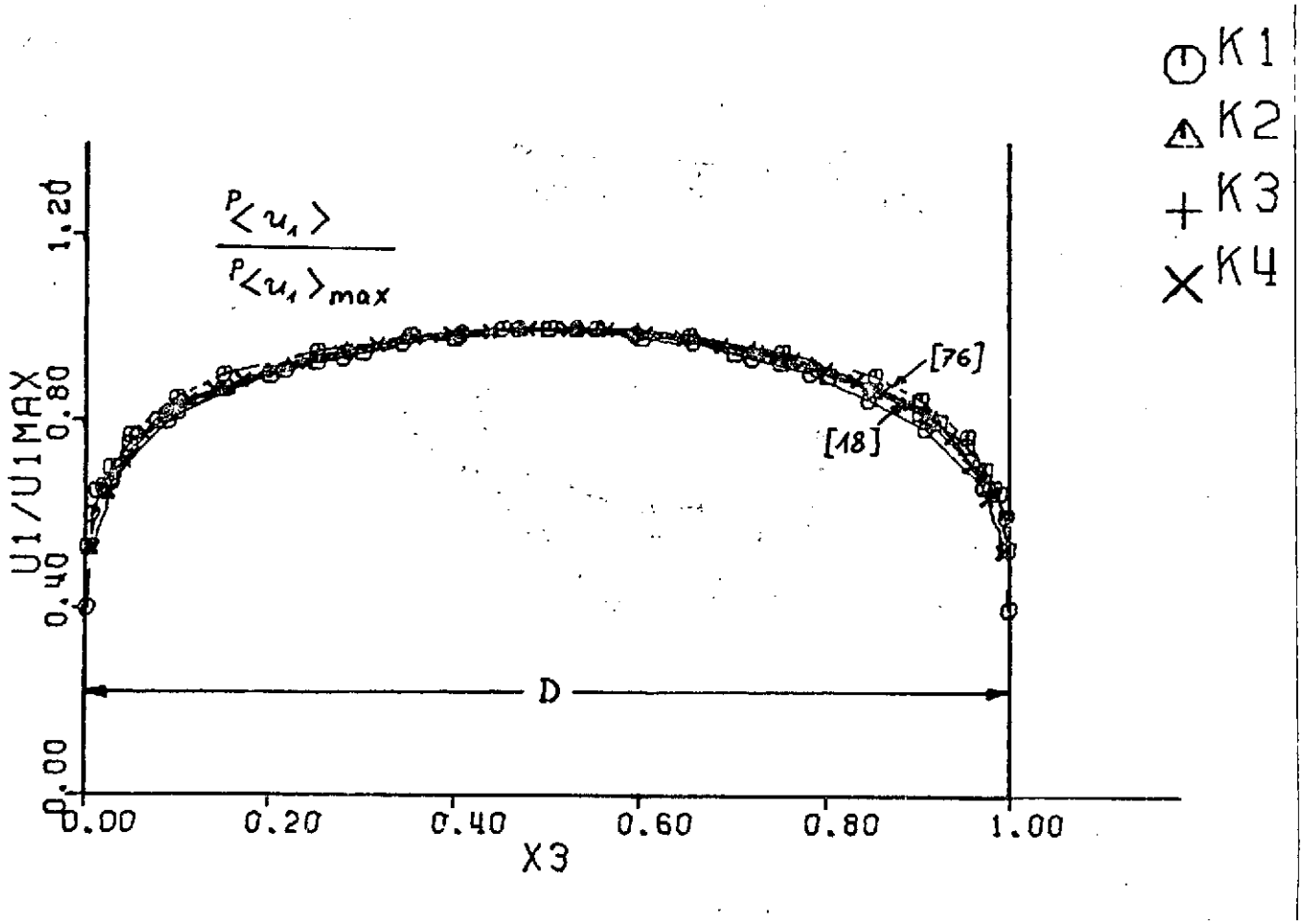

Figure 26. *

* Translator's note: Figure 25 missing from German text.

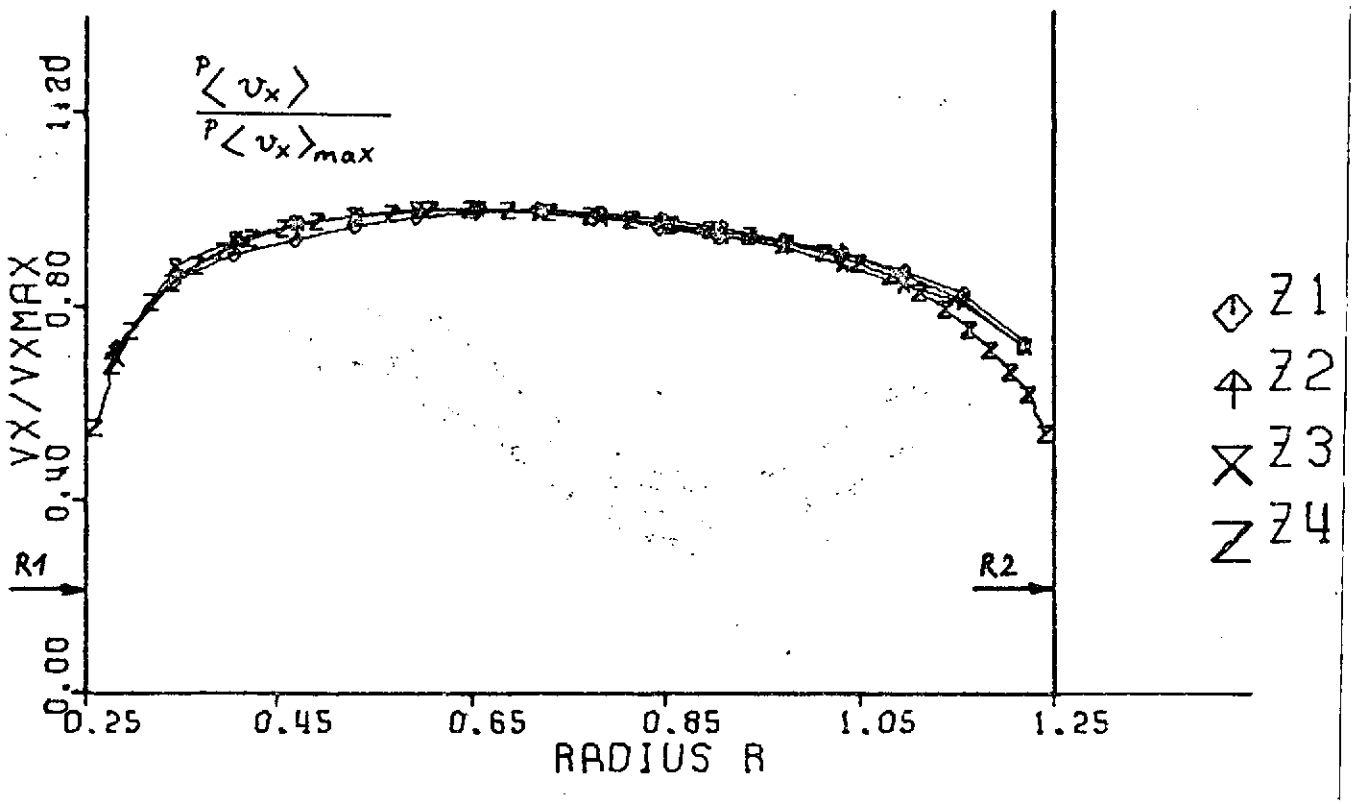
$\frac{P\langle v_x \rangle}{P\langle v_x \rangle_{max}}$
VX/VXMAX
1.20
0.80
0.40
0.00
R1
R2
0.25
0.45
0.65
0.85
1.05
1.25
RADIUS R
Z1
Z2
Z3
Z4

Figure 27.

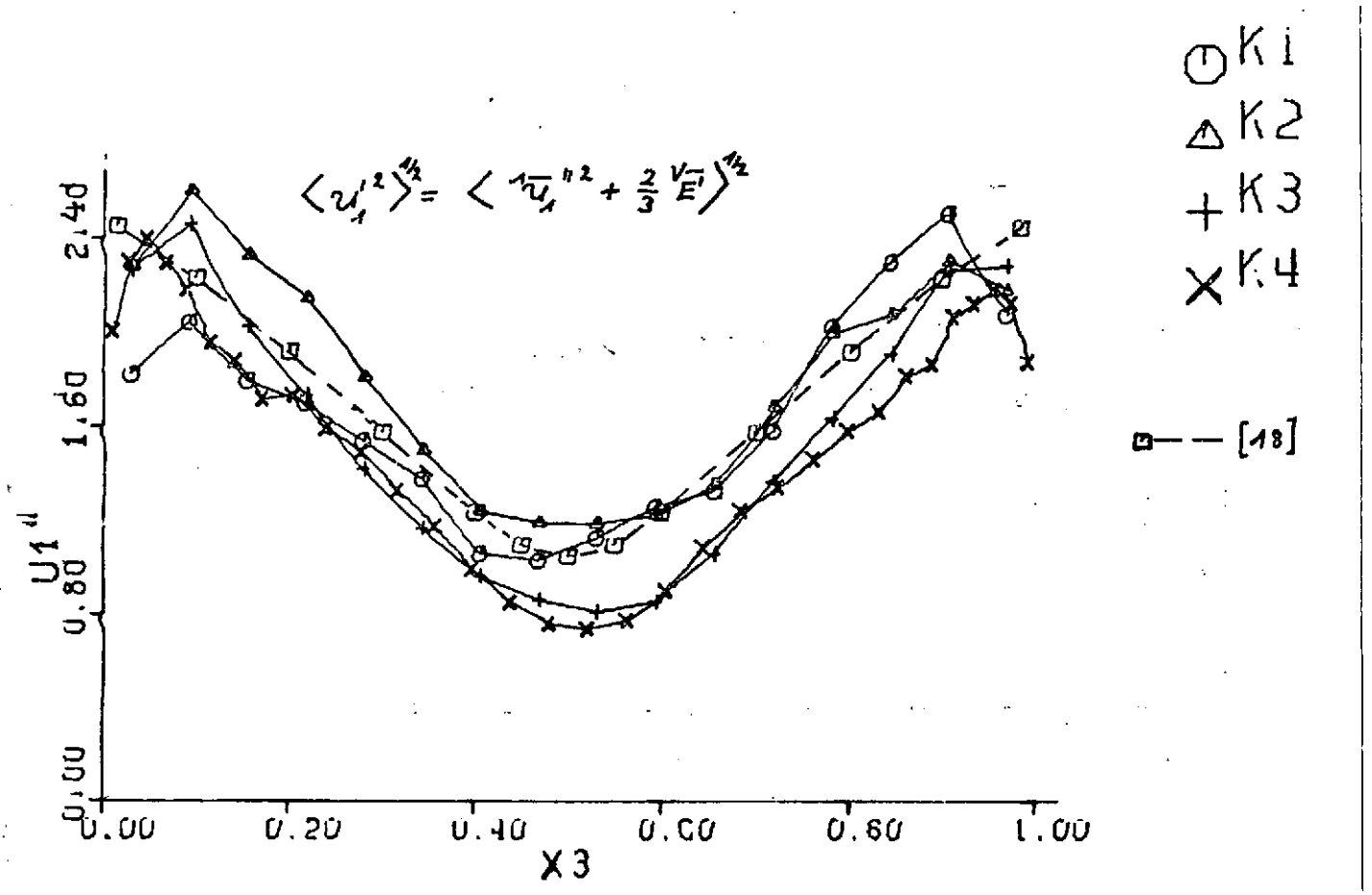
$\langle u_1'^2 \rangle^{1/2} = \langle {}^{1}\overline{u}_1''^2 + \frac{2}{3} \overline{E}^1 \rangle^{1/2}$
U1''
2,40
1,60
0,80
0,00
0.00
0.20
0.40
0.60
0.80
1.00
X3
K i
K2
K3
K4
[18]

Figure 28.

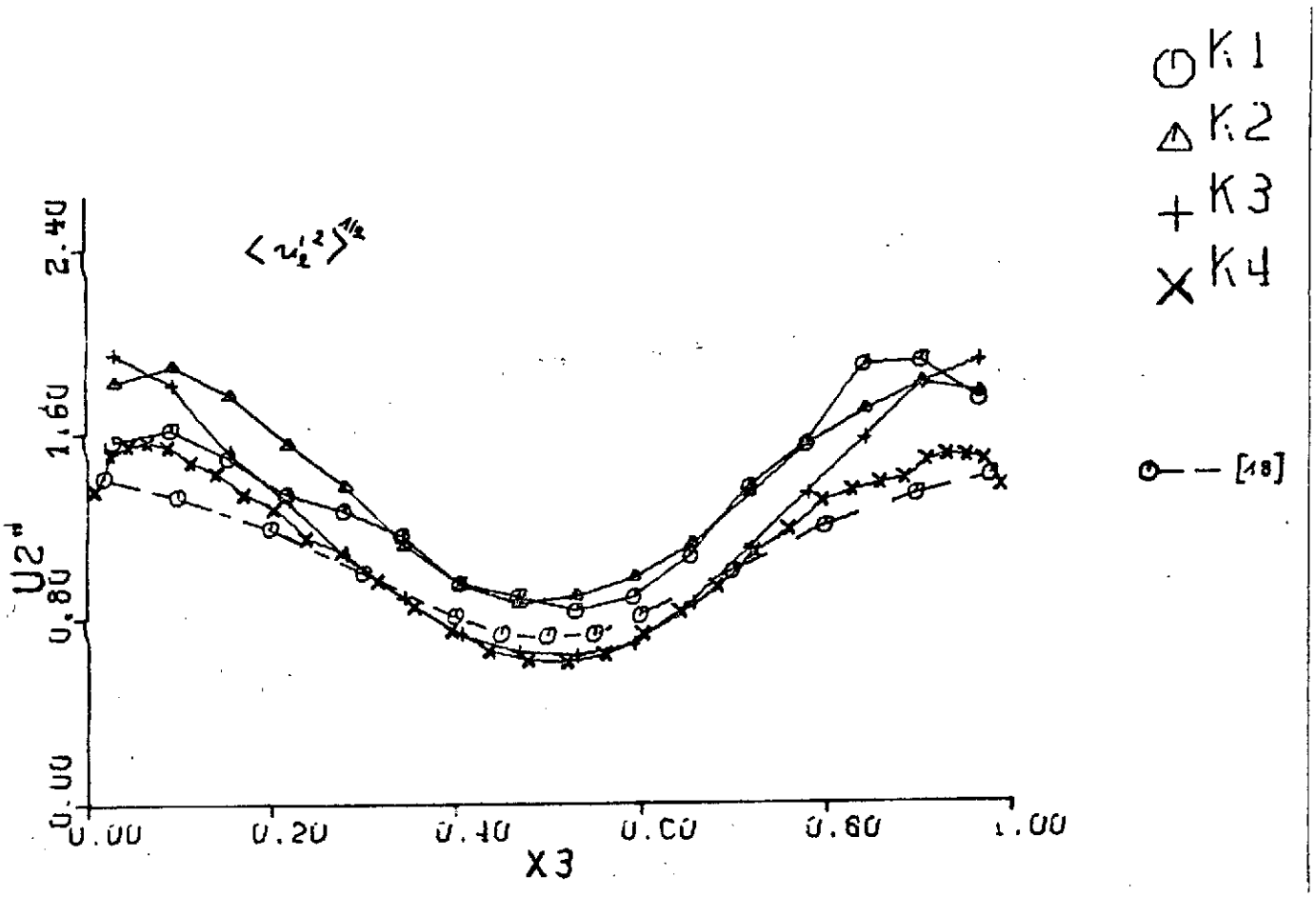

Figure 29.

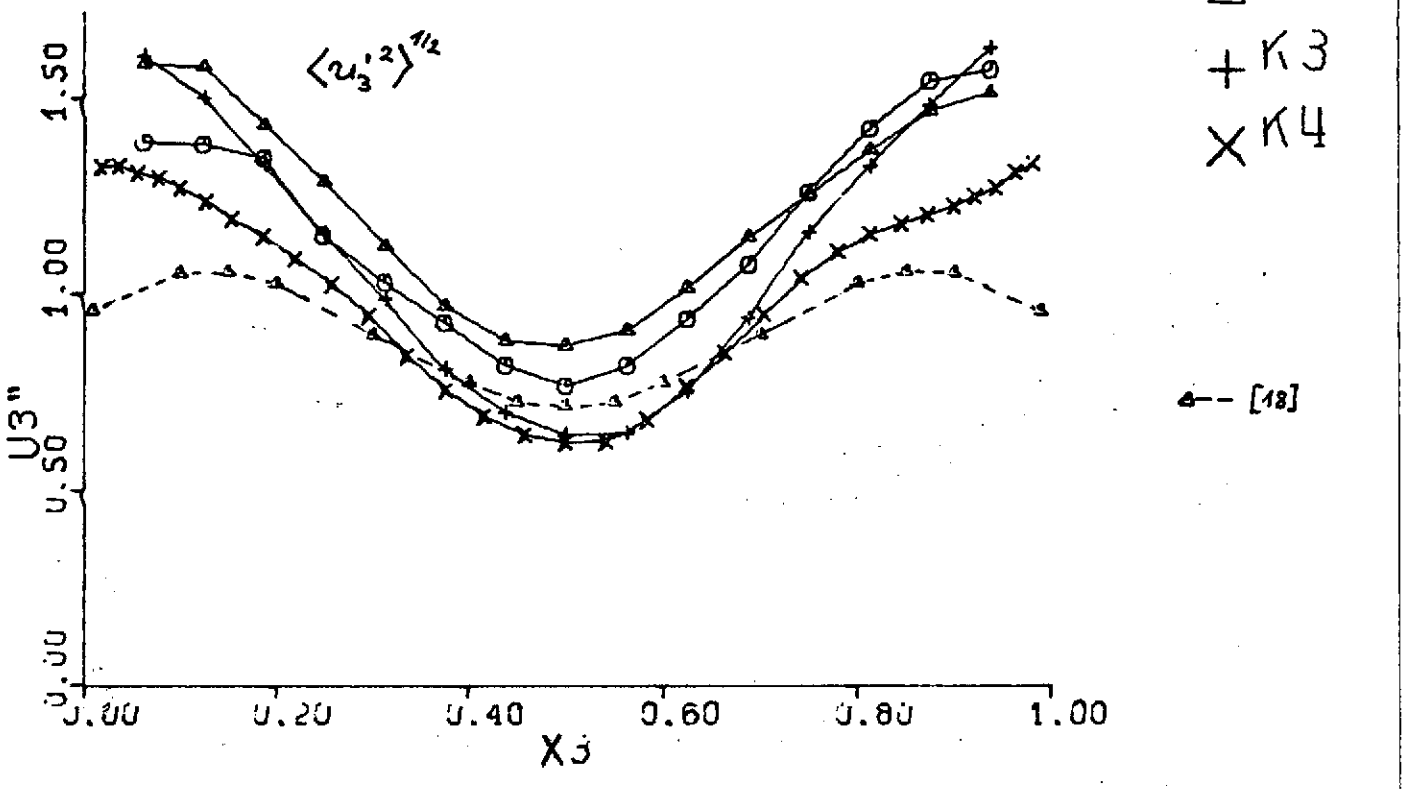
$\langle u_3'^2 \rangle^{1/2}$
U3"
1.50
1.00
0.50
0.00
0.00
0.20
0.40
0.60
0.80
1.00
X3
K1
K2
K3
K4
[18]

Figure 30.

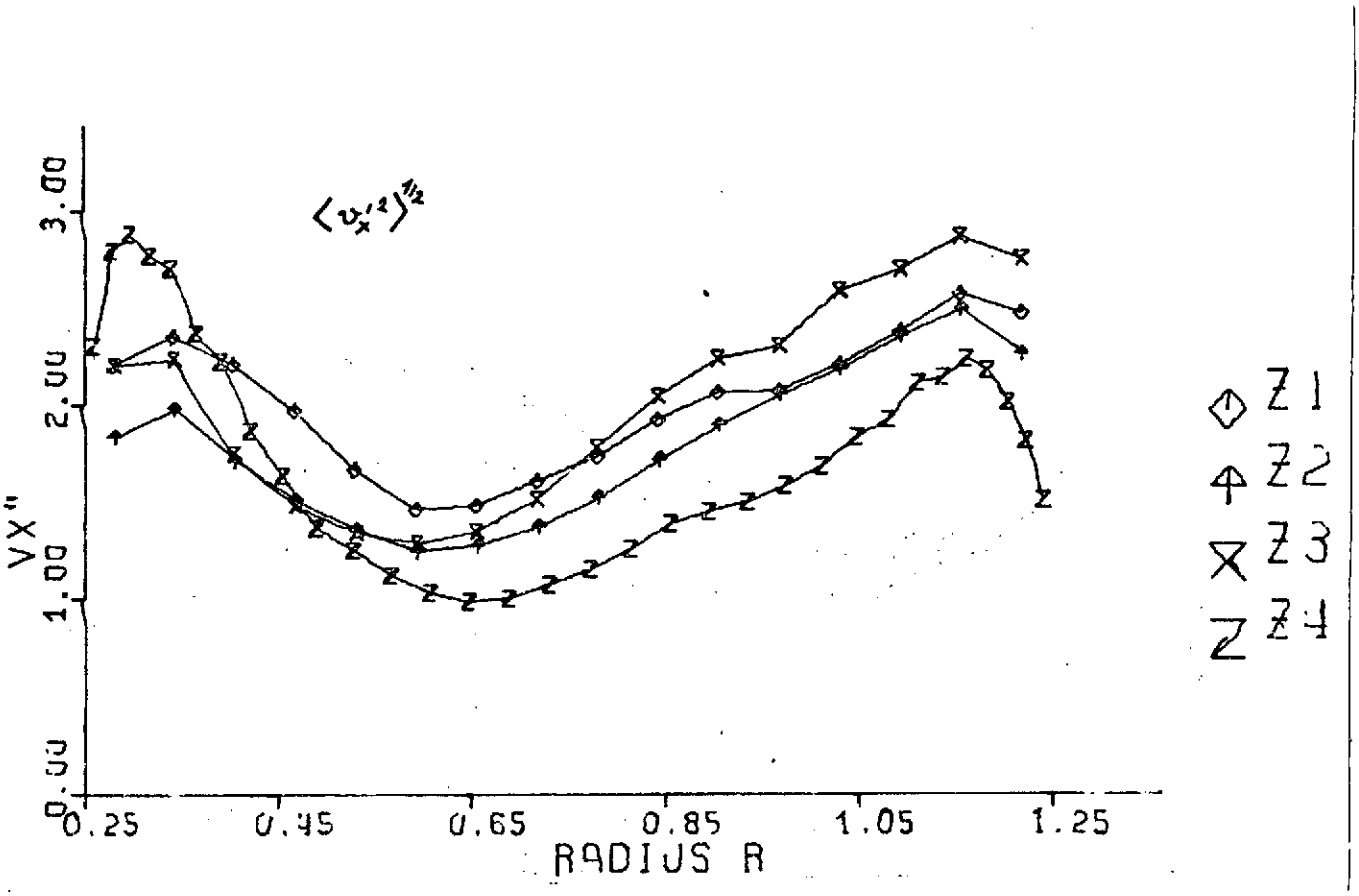
$\langle v_x'^2 \rangle^{1/2}$
VX"
3.00
2.00
1.00
0.00
0.25
0.45
0.65
0.85
1.05
1.25
RADIUS R
Z 1
Z 2
Z 3
Z 4

Figure 31.

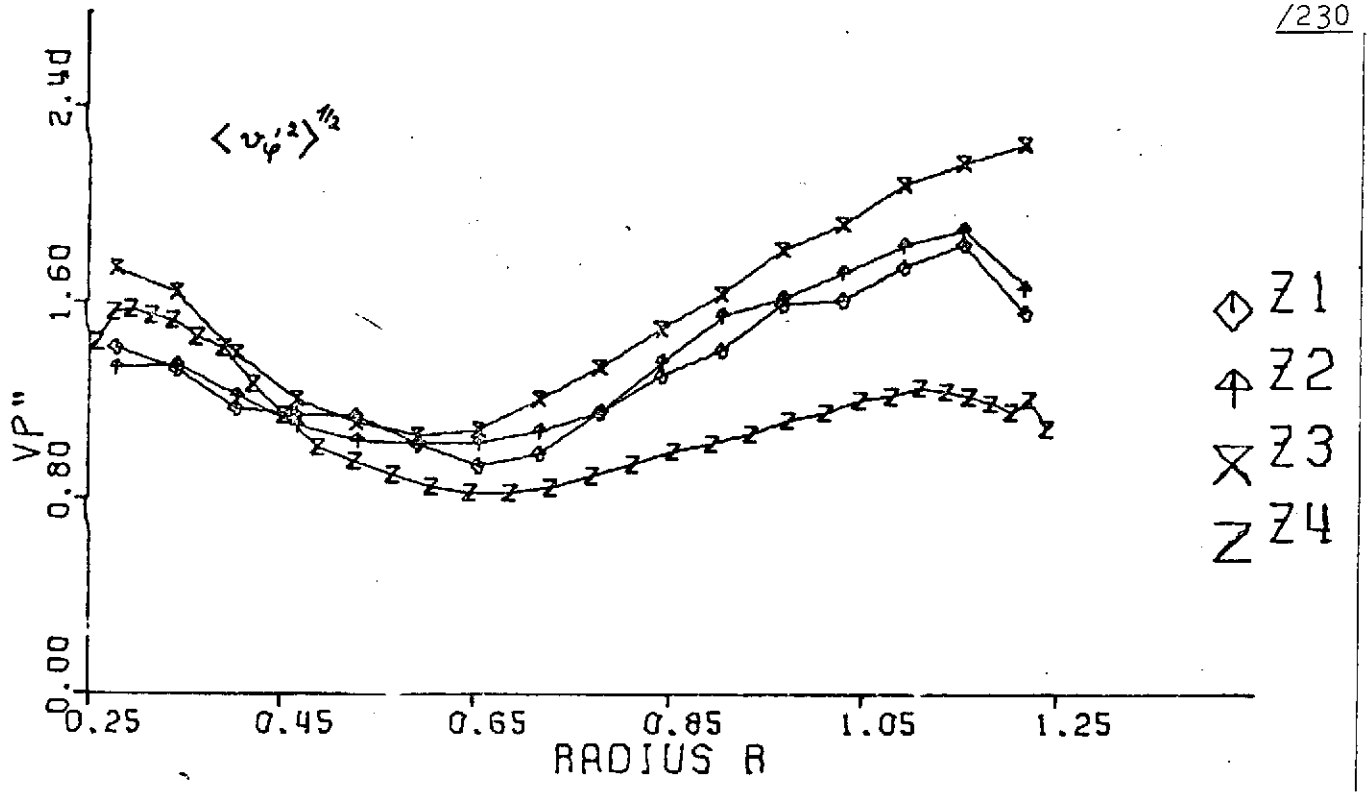
$\langle v_\varphi'^2 \rangle^{1/2}$
2.40
1.60
0.80
0.00
VP"
0.25
0.45
0.65
0.85
1.05
1.25
RADIUS R
Z1
Z2
Z3
Z4

Figure 32.

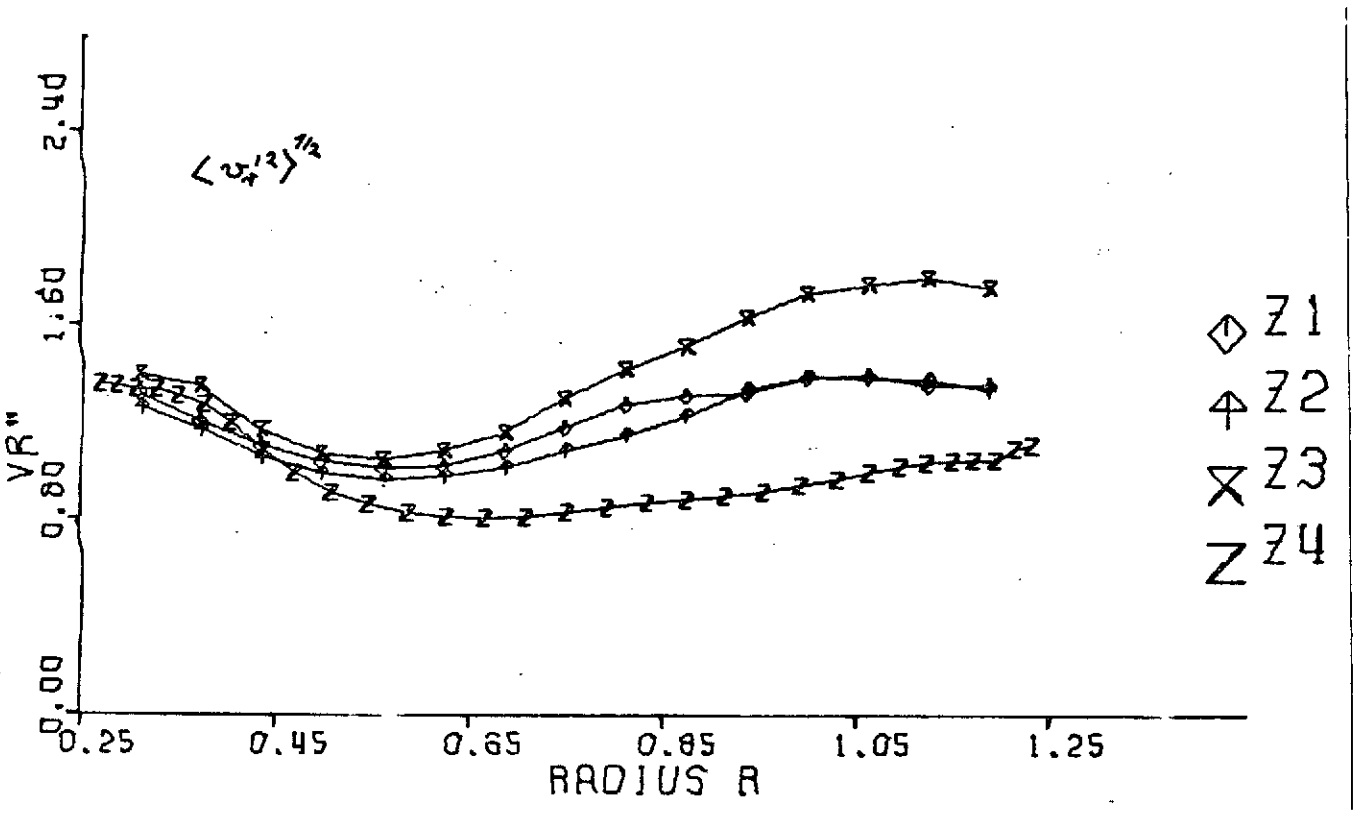

Figure 33.

/231

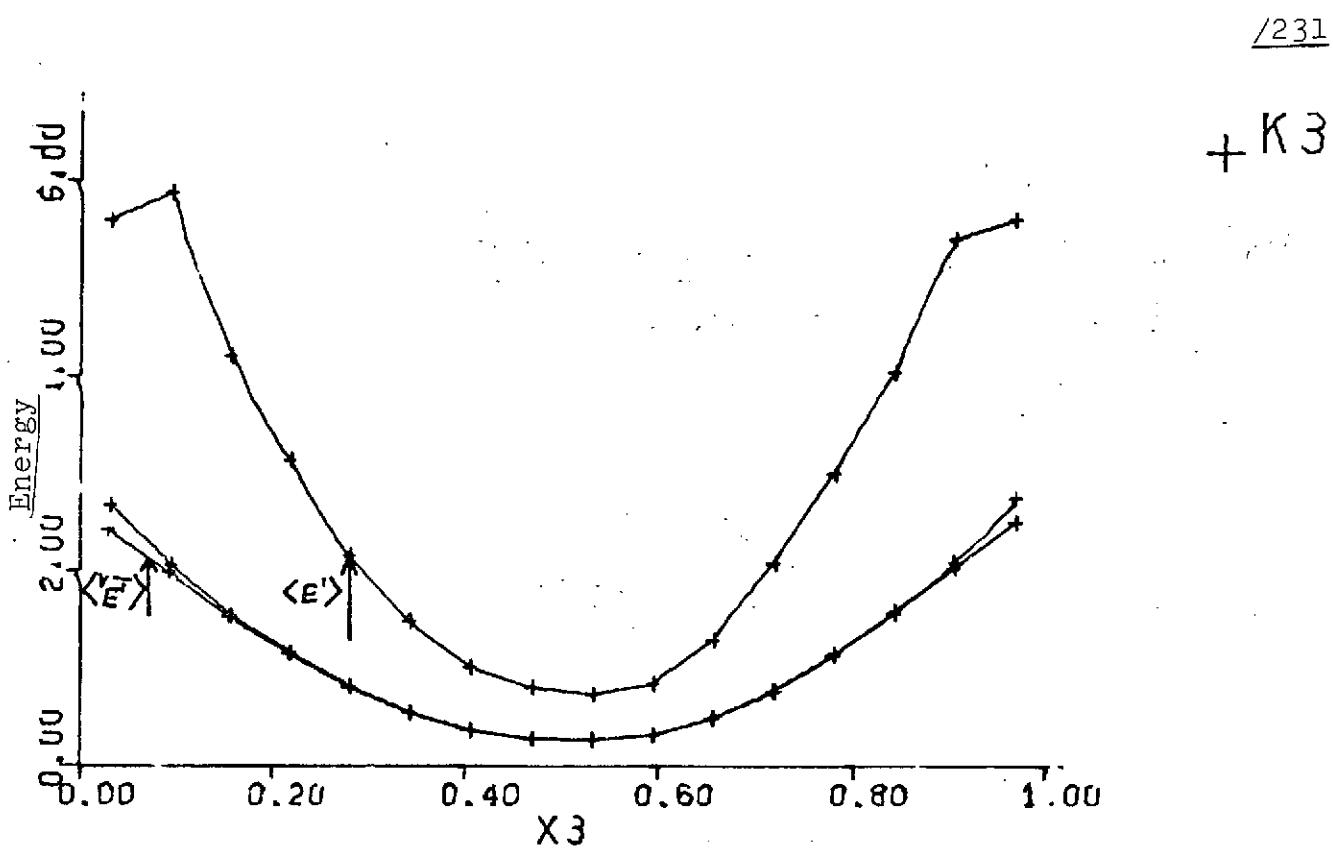

Figure 34.

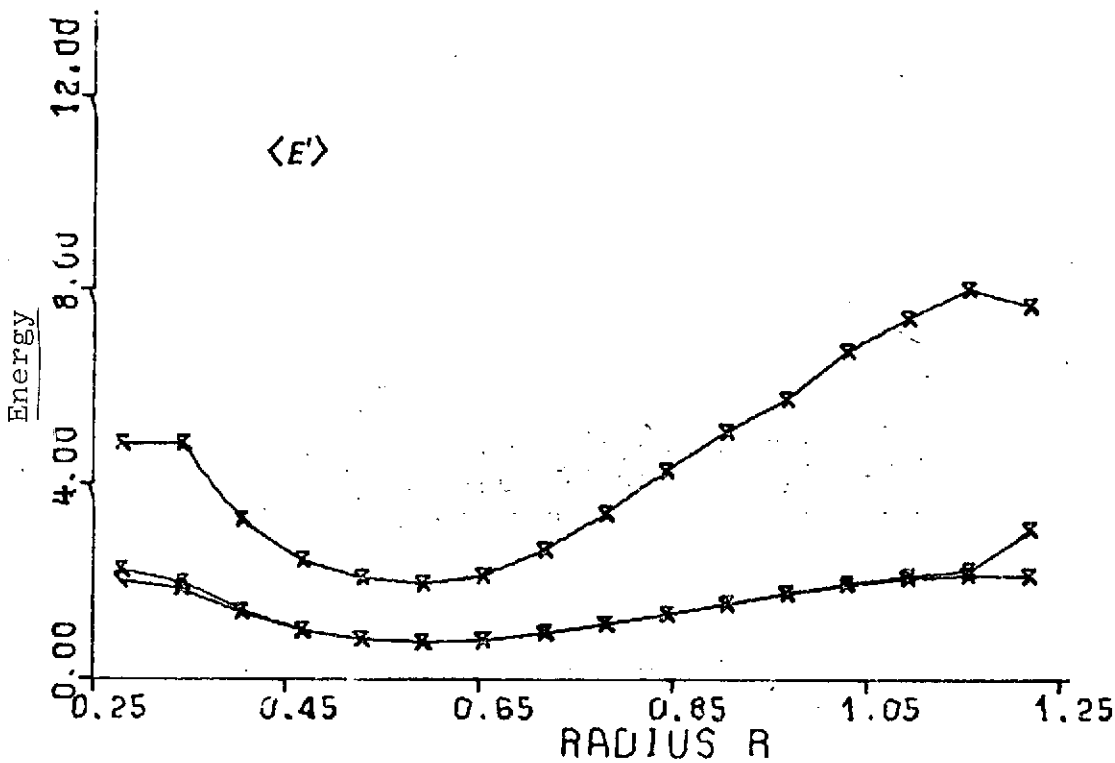

Figure 35.

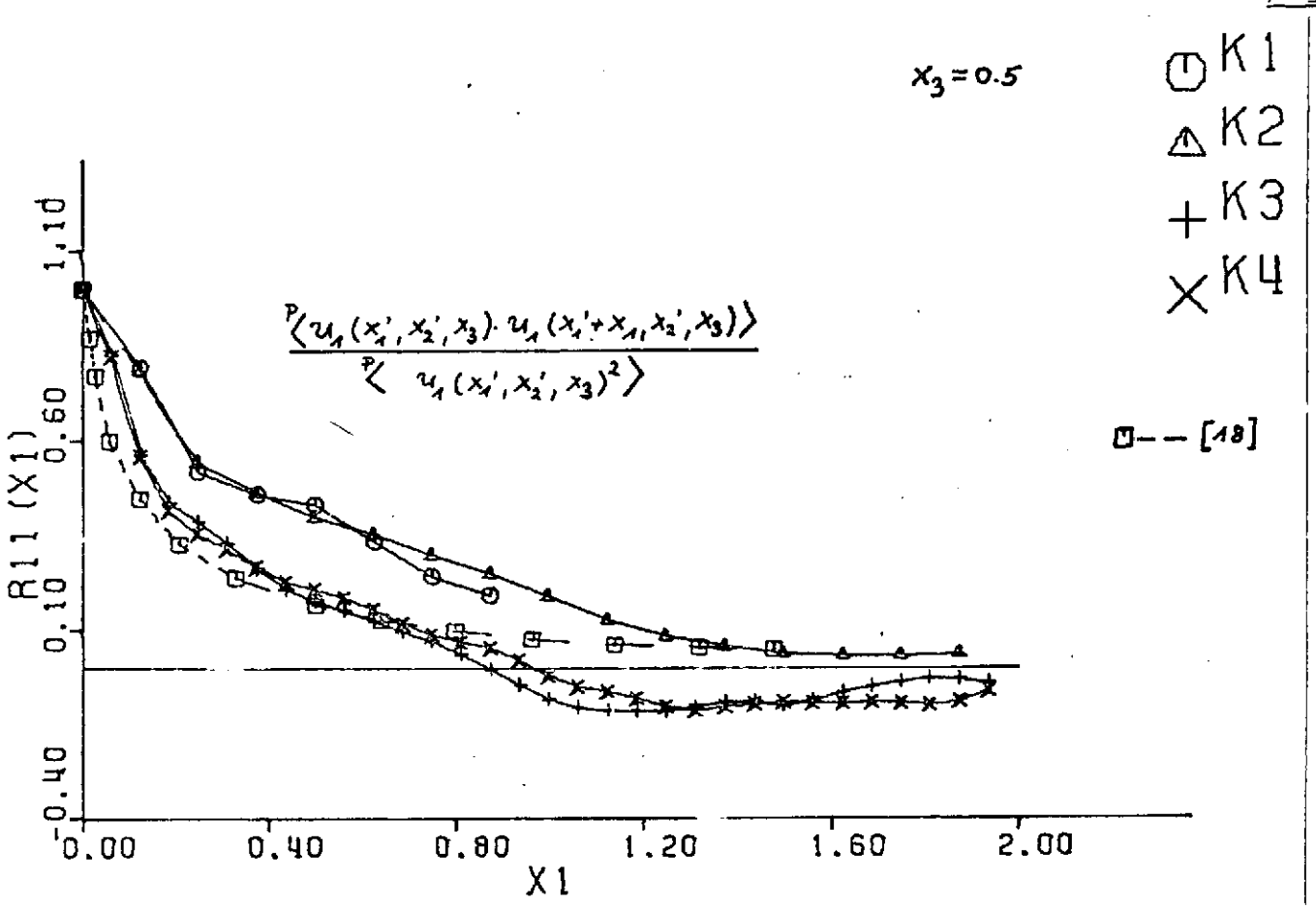
$x_3 = 0.5$
K1
K2
K3
K4
$\frac{P\langle u_1(x_1', x_2', x_3) \cdot u_1(x_1' + x_{11}, x_2', x_3)\rangle}{P\langle u_1(x_1', x_2', x_3)^2\rangle}$
[18]
R11 (X1)
1.10
0.60
0.10
-0.40
0.00
0.40
0.80
1.20
1.60
2.00
X1

Figure 36. |

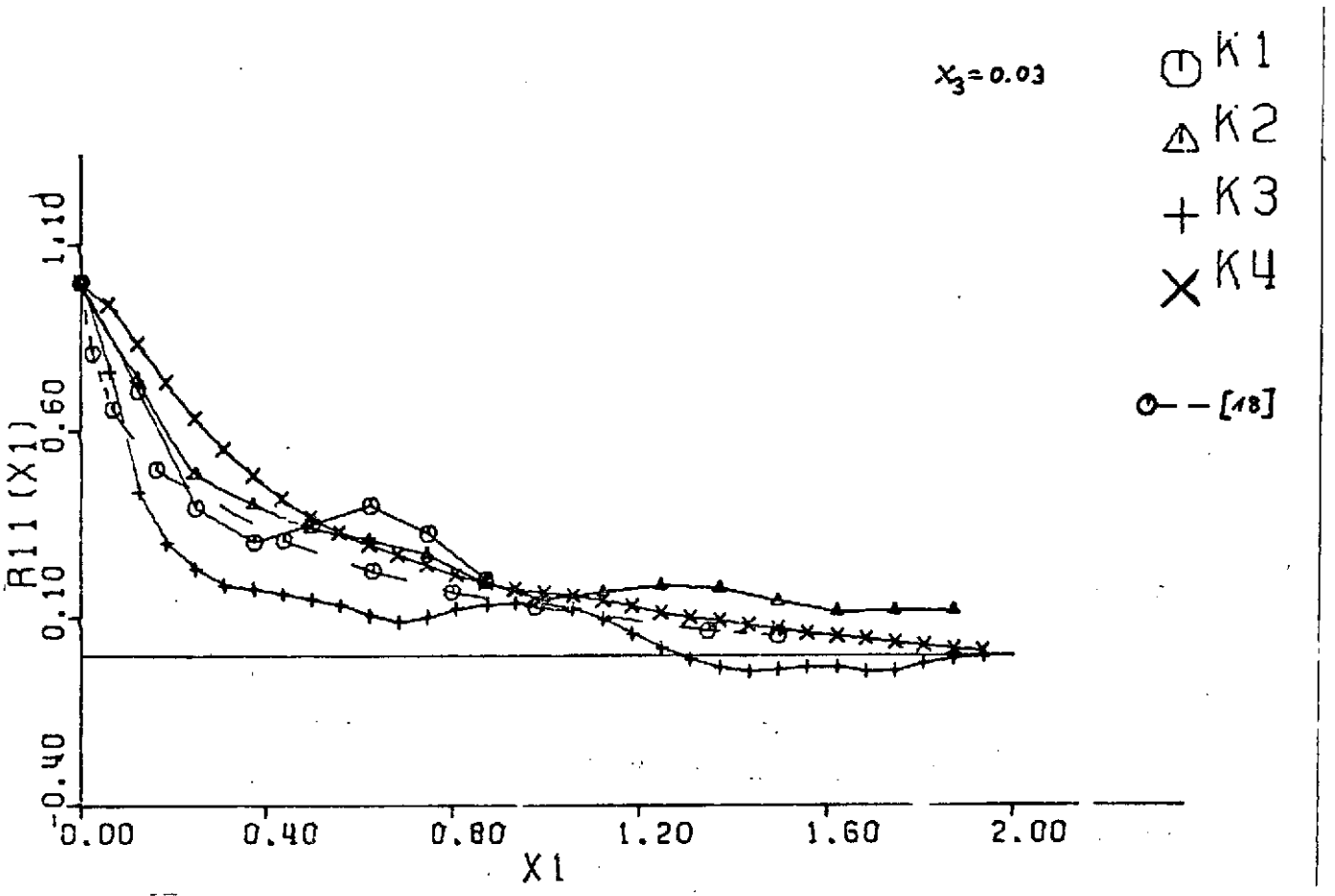
$x_3 = 0.03$
K1
K2
K3
K4
[18]
R11 (X1)
1.10
0.60
0.10
-0.40
0.00
0.40
0.80
1.20
1.60
2.00
X1

Figure 37.

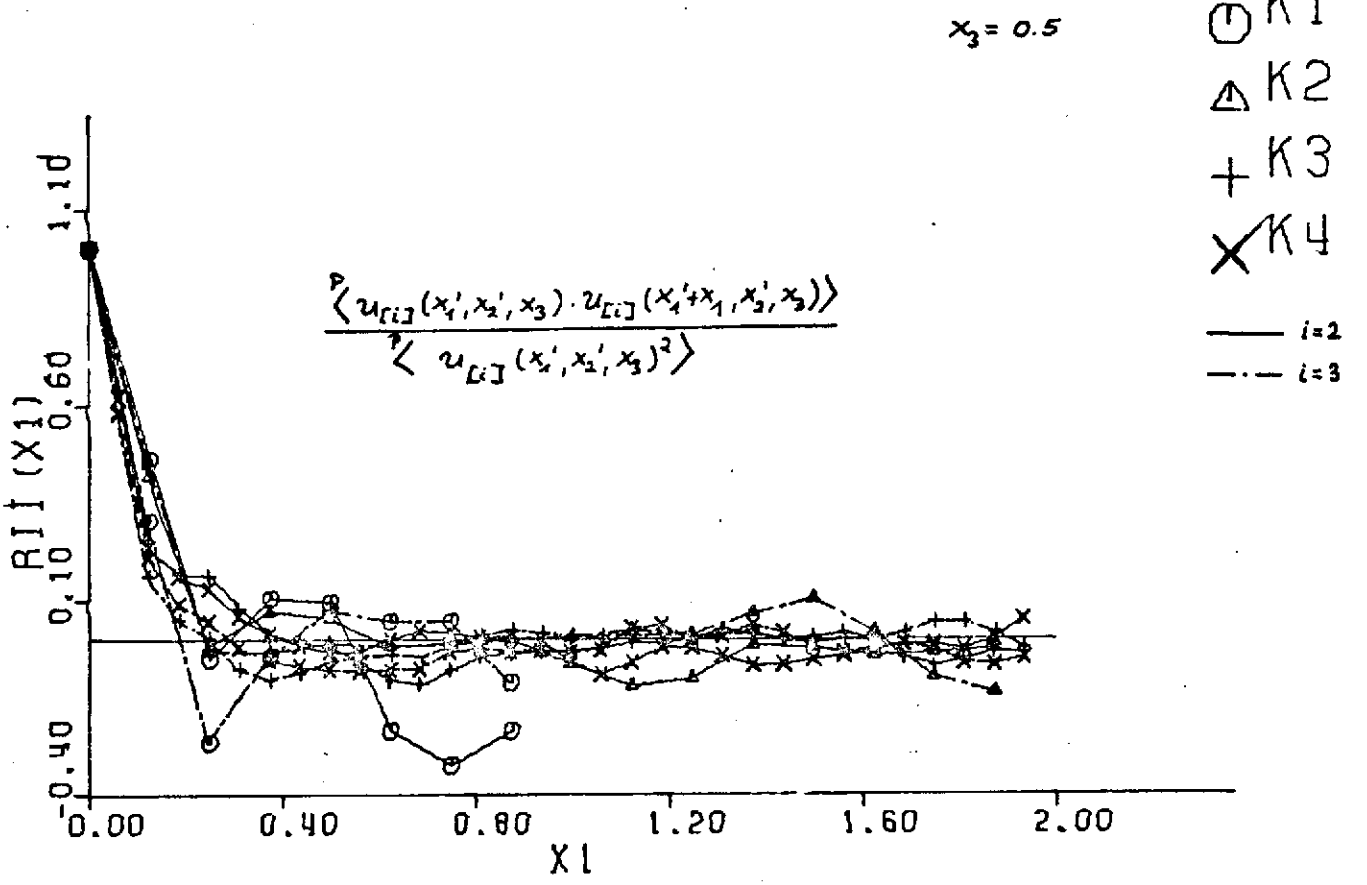
$x_3 = 0.5$
K1
K2
K3
K4
i=2
i=3
$\frac{P\langle u_{[i]}(x_1', x_2', x_3) \cdot u_{[i]}(x_1'+x_1, x_2', x_3)\rangle}{\langle u_{[i]}(x_1', x_2', x_3)^2\rangle}$
RII (X1)
1.10
0.60
0.10
-0.40
0.00
0.40
0.80
1.20
1.60
2.00
X1

Figure 38.

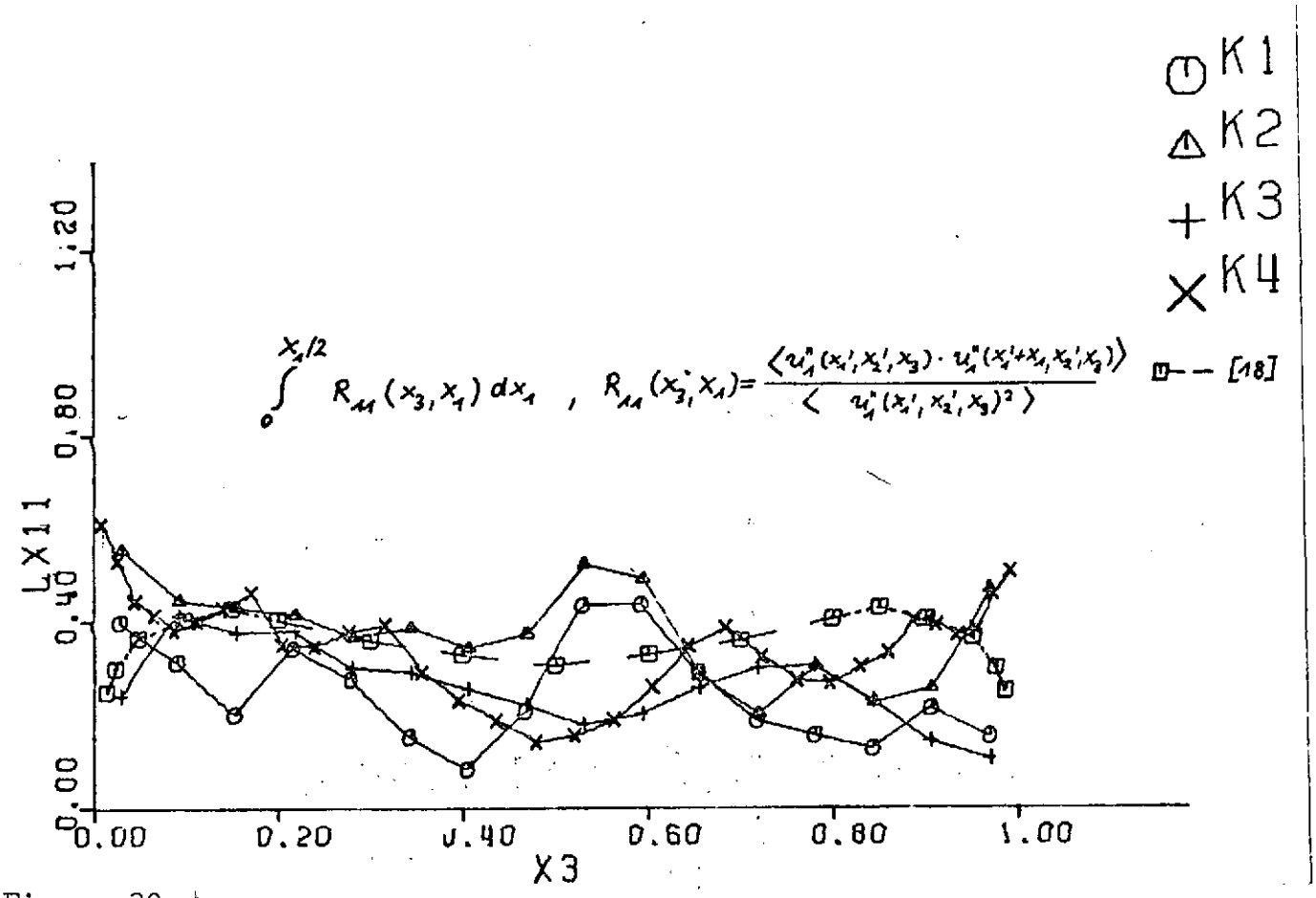
K1
K2
K3
K4
[18]
$\int_0^{x_1/2} R_{11}(x_3, x_1)\, dx_1$, $R_{11}(x_3, x_1) = \frac{\langle u_1''(x_1', x_2', x_3) \cdot u_1''(x_1'+x_1, x_2', x_3) \rangle}{\langle u_1''(x_1', x_2', x_3)^2 \rangle}$
LX11
0.00
0.40
0.80
1:20
0.00
0.20
0.40
0.60
0.80
1.00
X3

Figure 39.

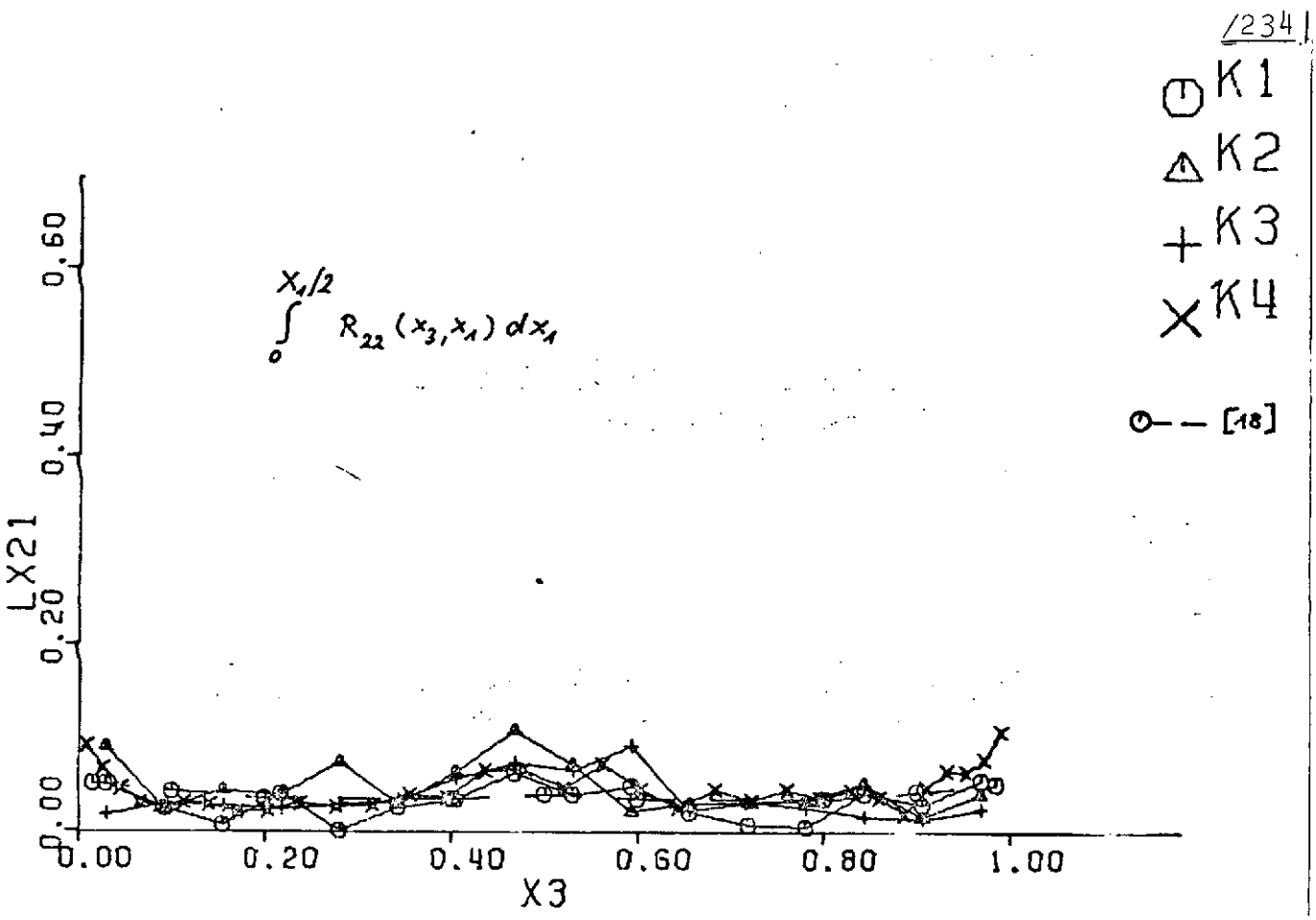
/234/
K1
K2
K3
K4
[18]
$\int_0^{X_1/2} R_{22}(x_3, x_1)\, dx_1$
LX21
0.00
0.20
0.40
0.60
0.00
0.20
0.40
0.60
0.80
1.00
X3

Figure 40.

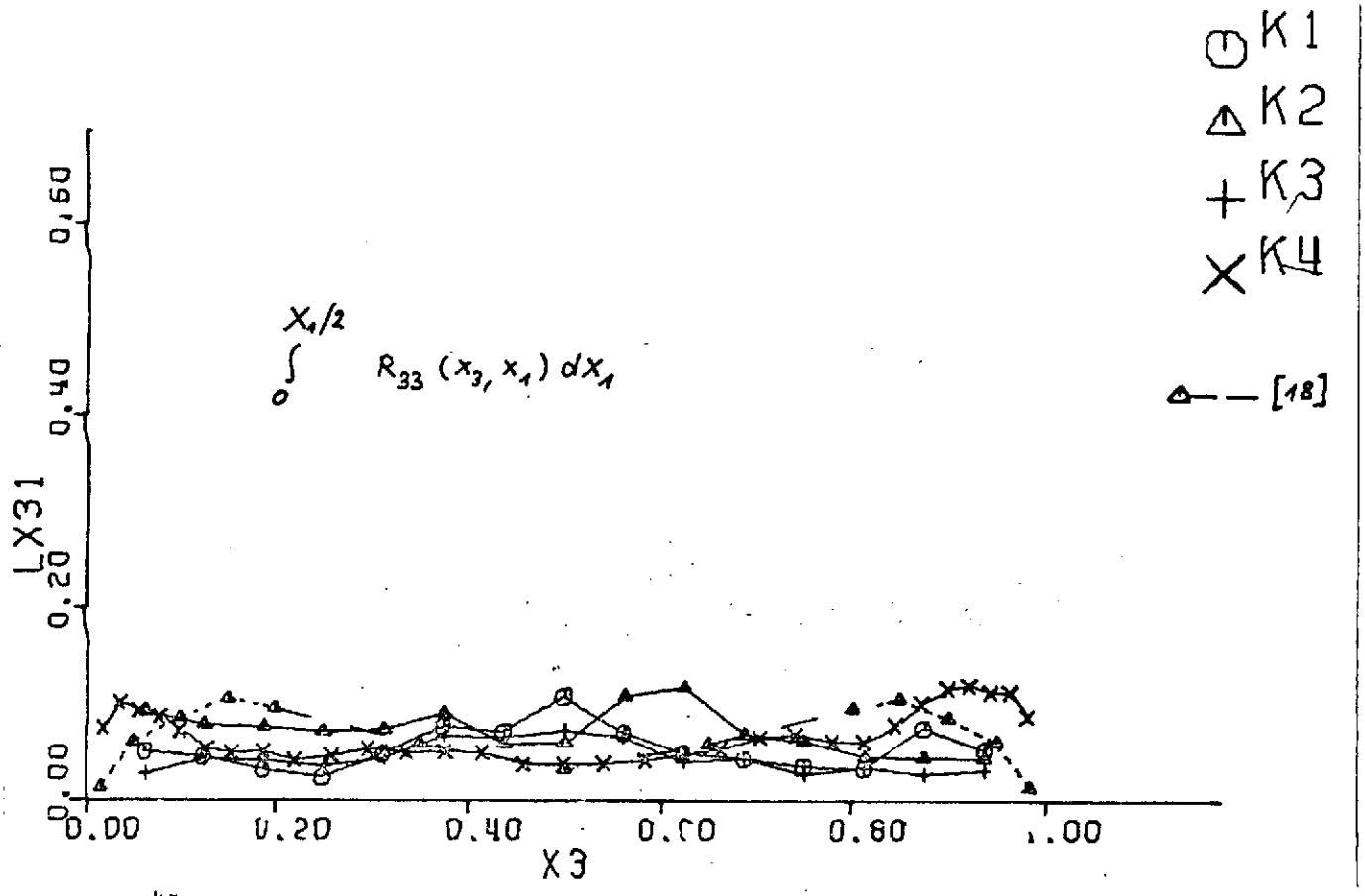
К1
К2
К3
К4
[18]
$\int_0^{X_1/2} R_{33}(x_3, x_1)\, dx_1$
LX31
0.00
0.20
0.40
0.60
0.00
0.20
0.40
0.60
1.00
X3

Figure 41.

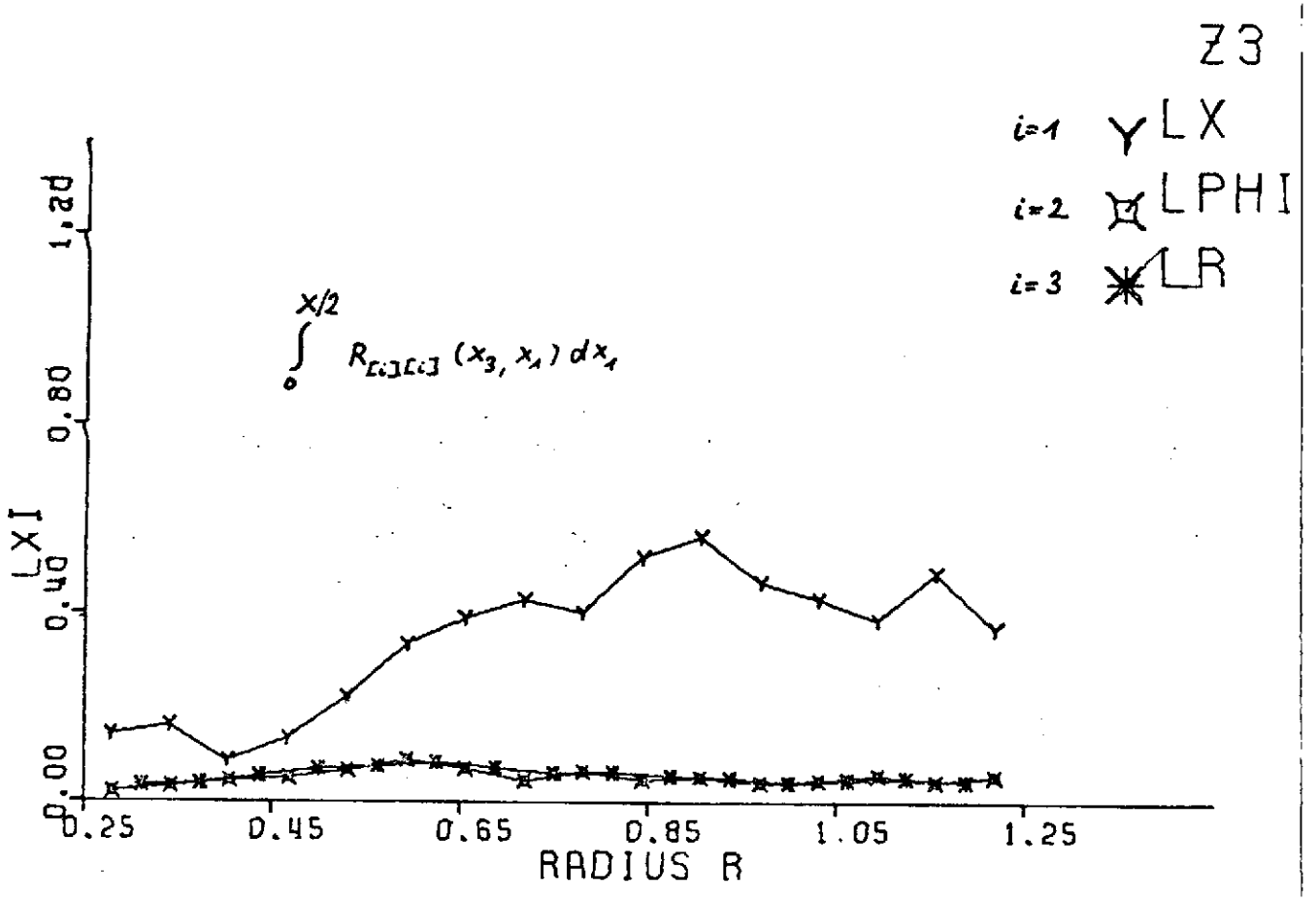
Z3
i=1 LX
i=2 LPHI
i=3 LR
$\int_0^{X/2} R_{[i][i]}(x_3, x_1)\, dx_1$
LXI
0.00
0.40
0.80
1.20
0.25
0.45
0.65
0.85
1.05
1.25
RADIUS R

Figure 42.

/236/

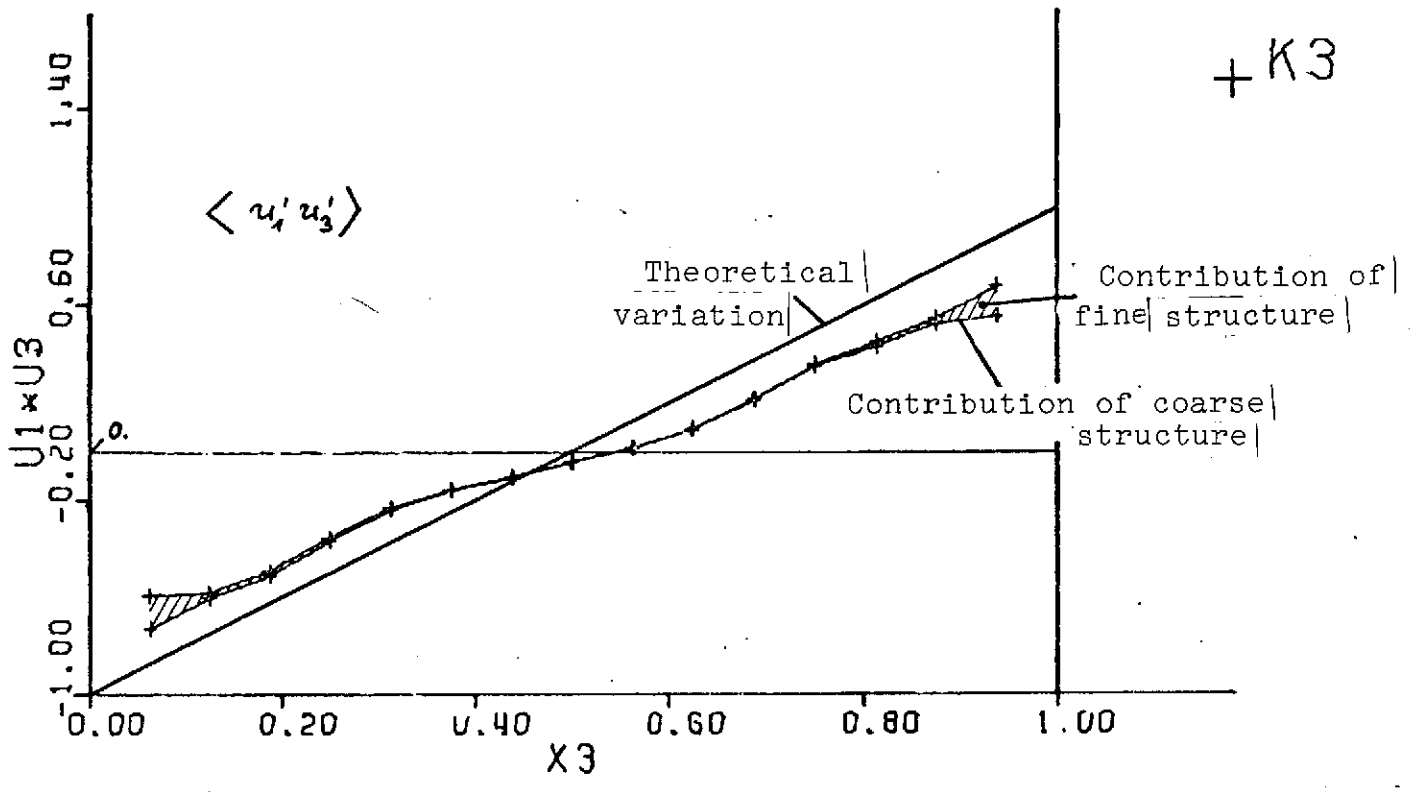

Figure 43.

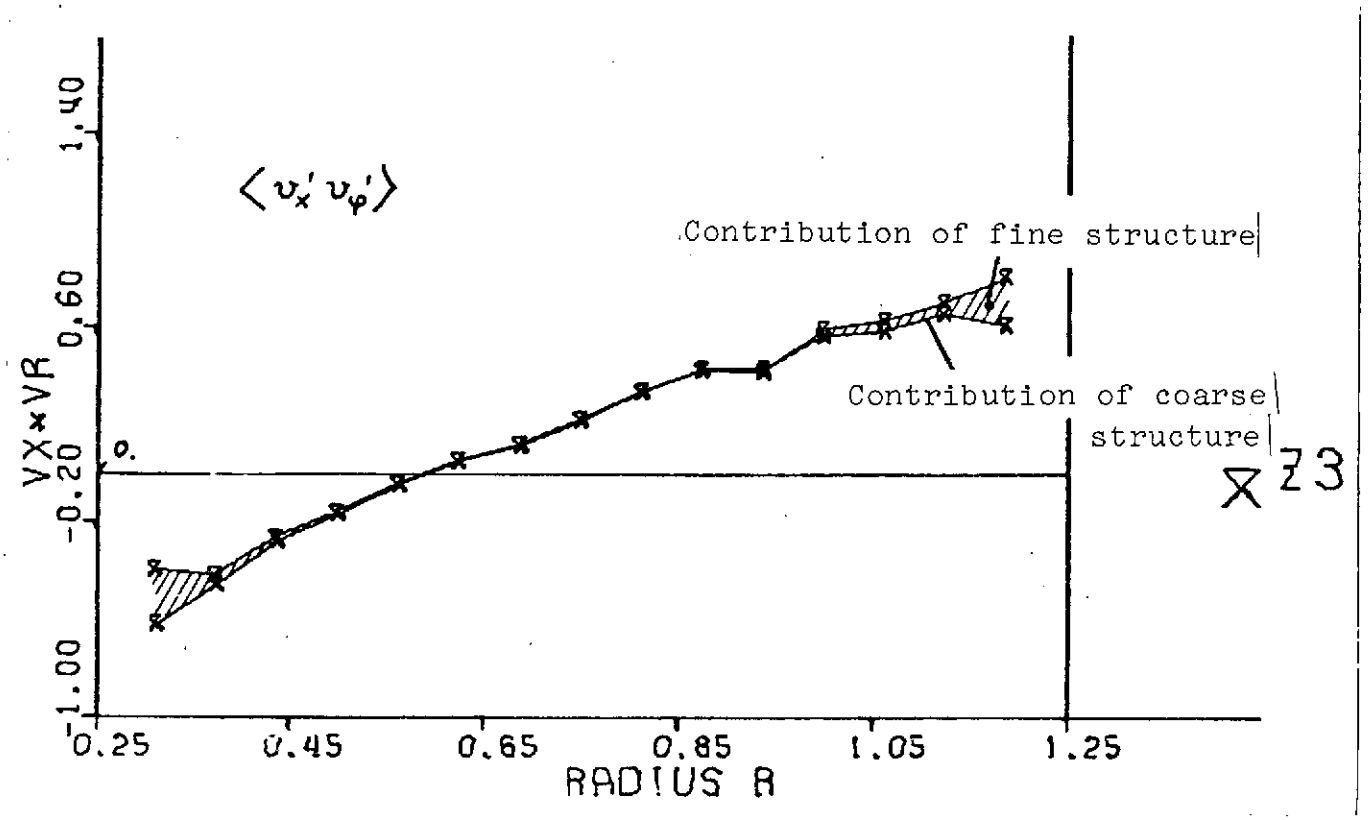
$\langle v_x' v_\varphi' \rangle$
Contribution of fine structure
Contribution of coarse structure
VX*VR
1.40
0.60
0.
-0.20
-1.00
0.25
0.45
0.65
0.85
1.05
1.25
RADIUS R
Z3

Figure 44.

/237

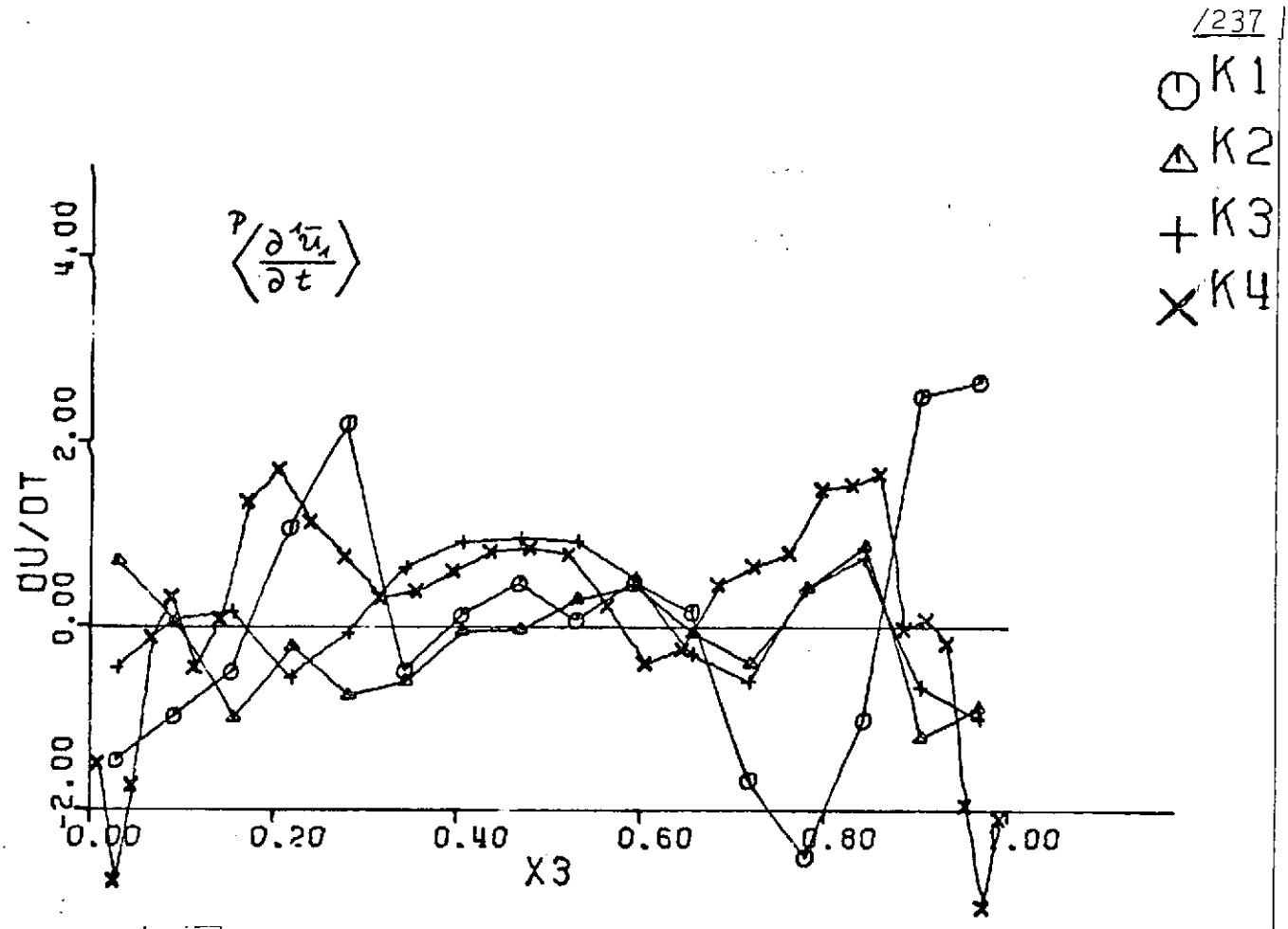

Figure 45.

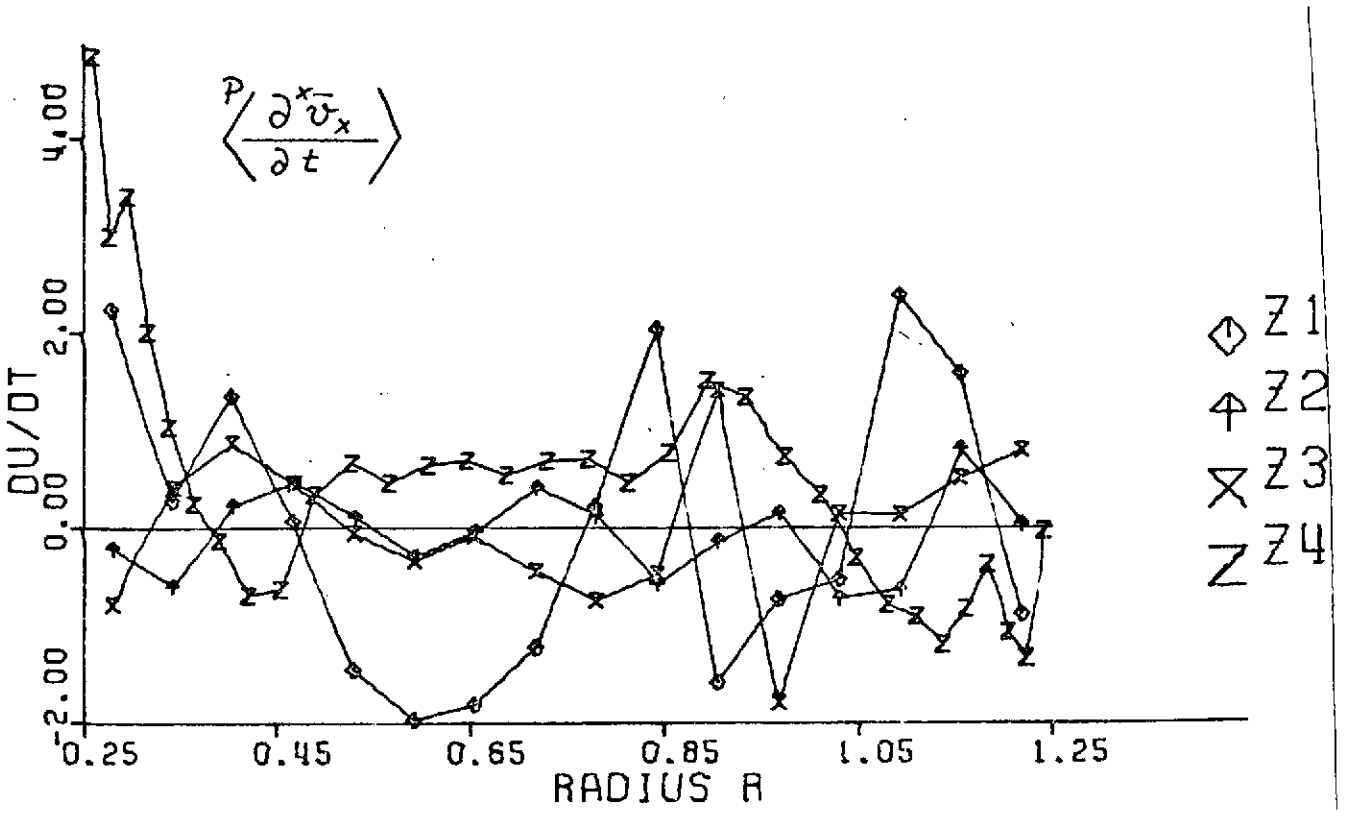
$\rho\left\langle \frac{\partial^x \bar{v}_x}{\partial t} \right\rangle$
4.00
2.00
0.00
-2.00
DU/DT
0.25
0.45
0.65
0.85
1.05
1.25
RADIUS R
Z1
Z2
Z3
Z4

Figure 46.

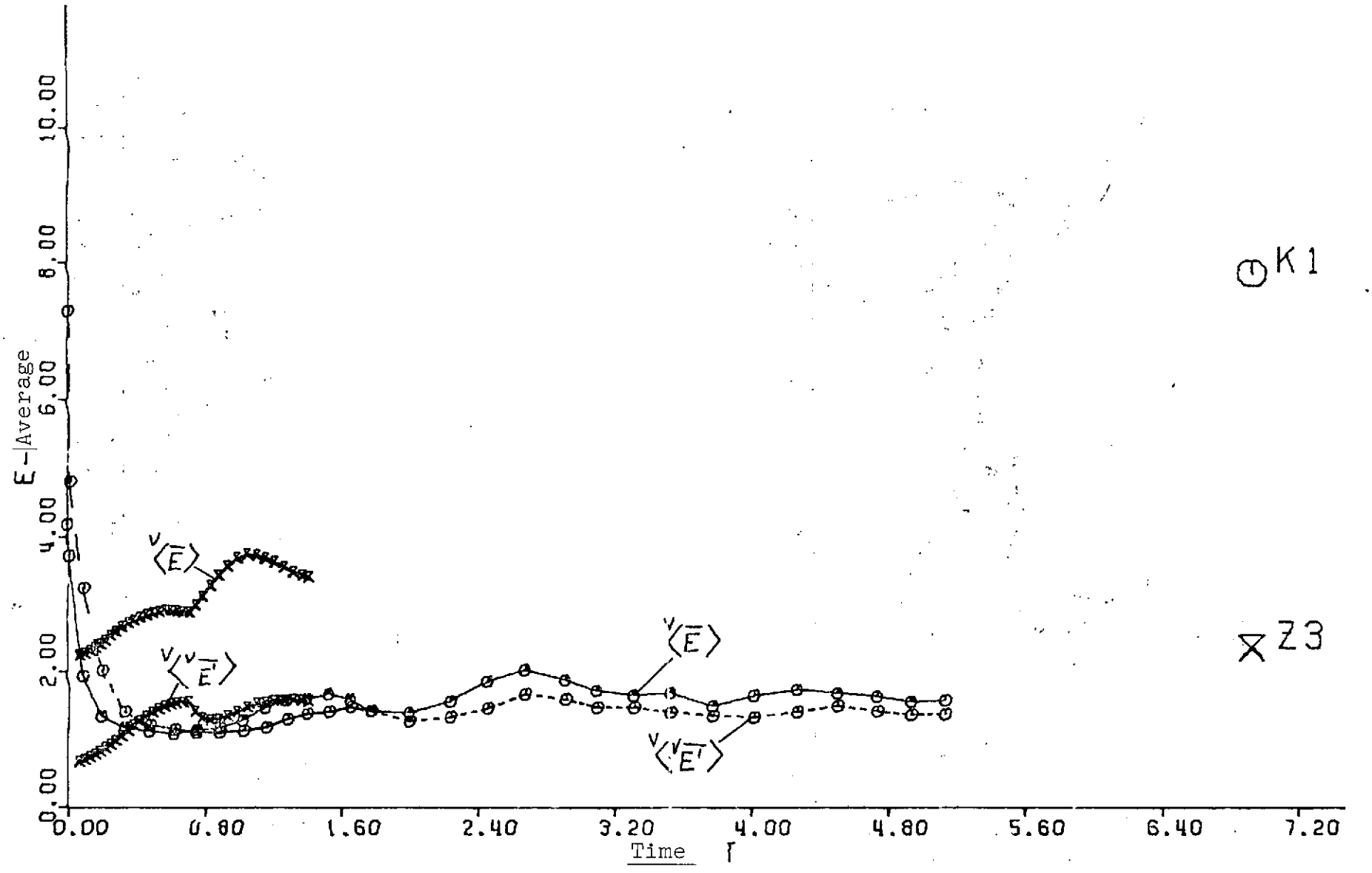
E-|Average
10.00
8.00
6.00
4.00
2.00
0.00
0.00
0.80
1.60
2.40
3.20
4.00
4.80
5.60
6.40
7.20
Time T
K1
Z3

Figure 47.

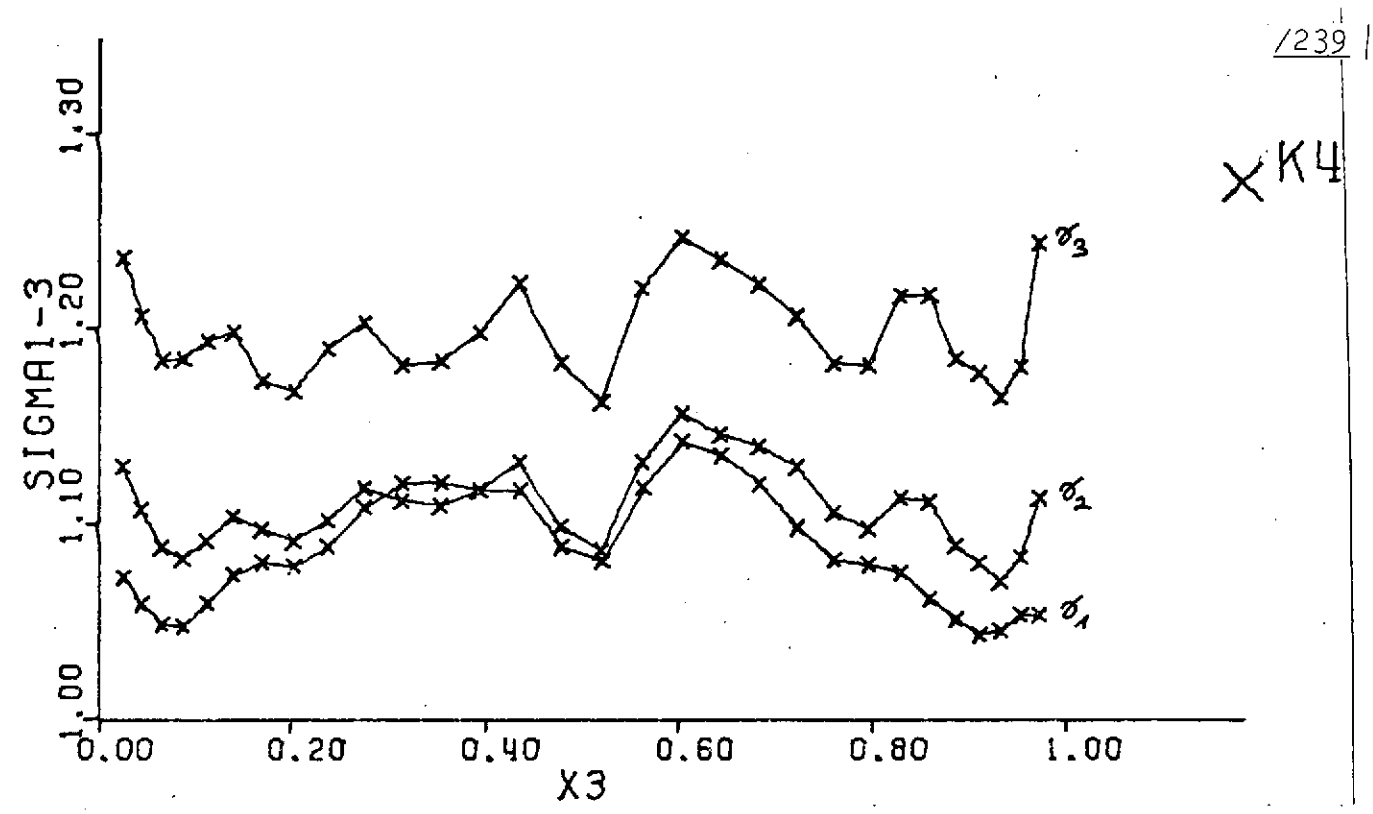
/239
K4
SIGMA1-3
1.00
1.10
1.20
1.30
0.00
0.20
0.40
0.60
0.80
1.00
X3
σ3
σ2
σ1

Figure 48.

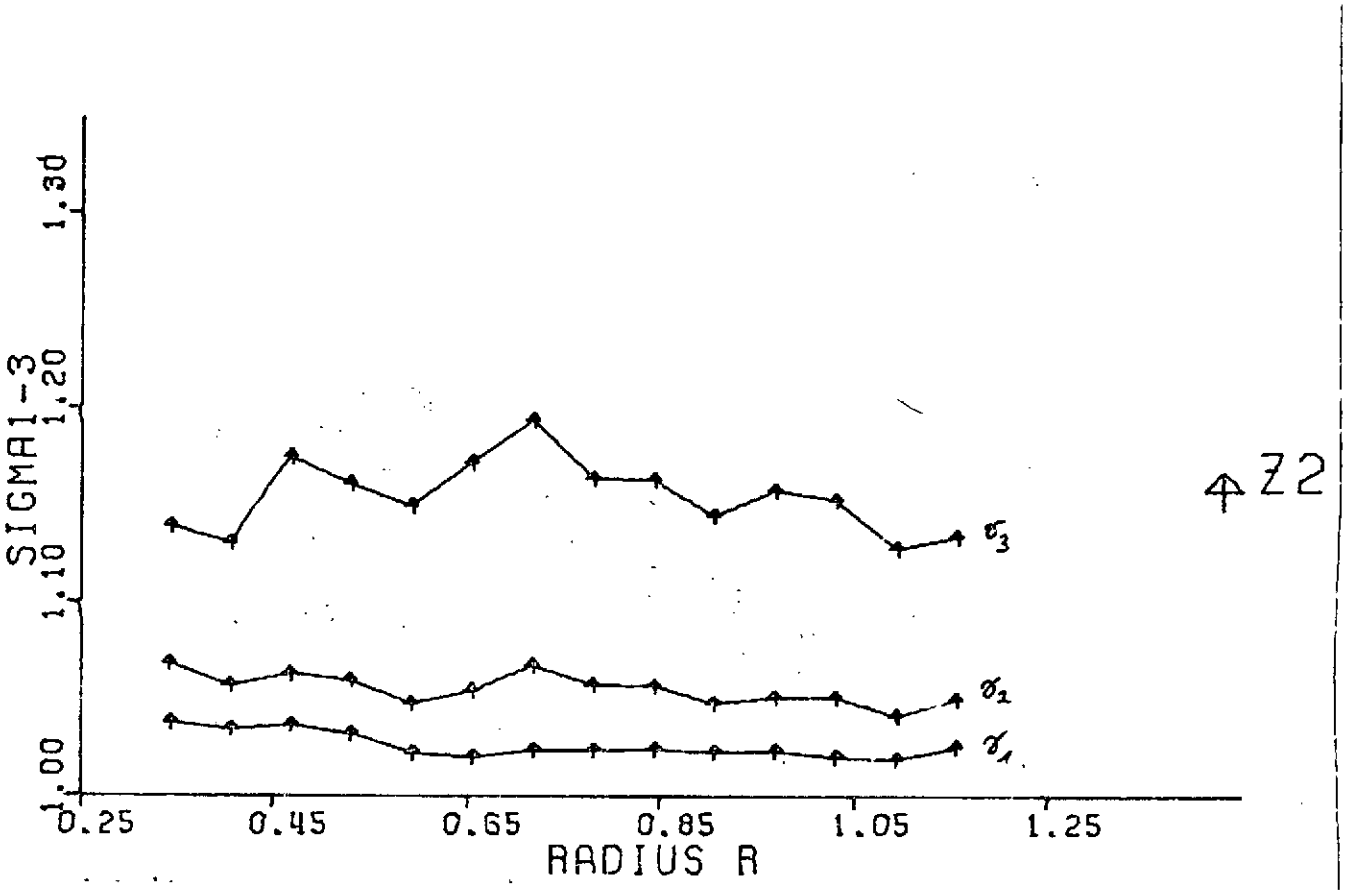
SIGMA1-3
1.00
1.10
1.20
1.30
0.25
0.45
0.65
0.85
1.05
1.25
RADIUS R
σ_3
σ_2
σ_1
Z2

Figure 49.

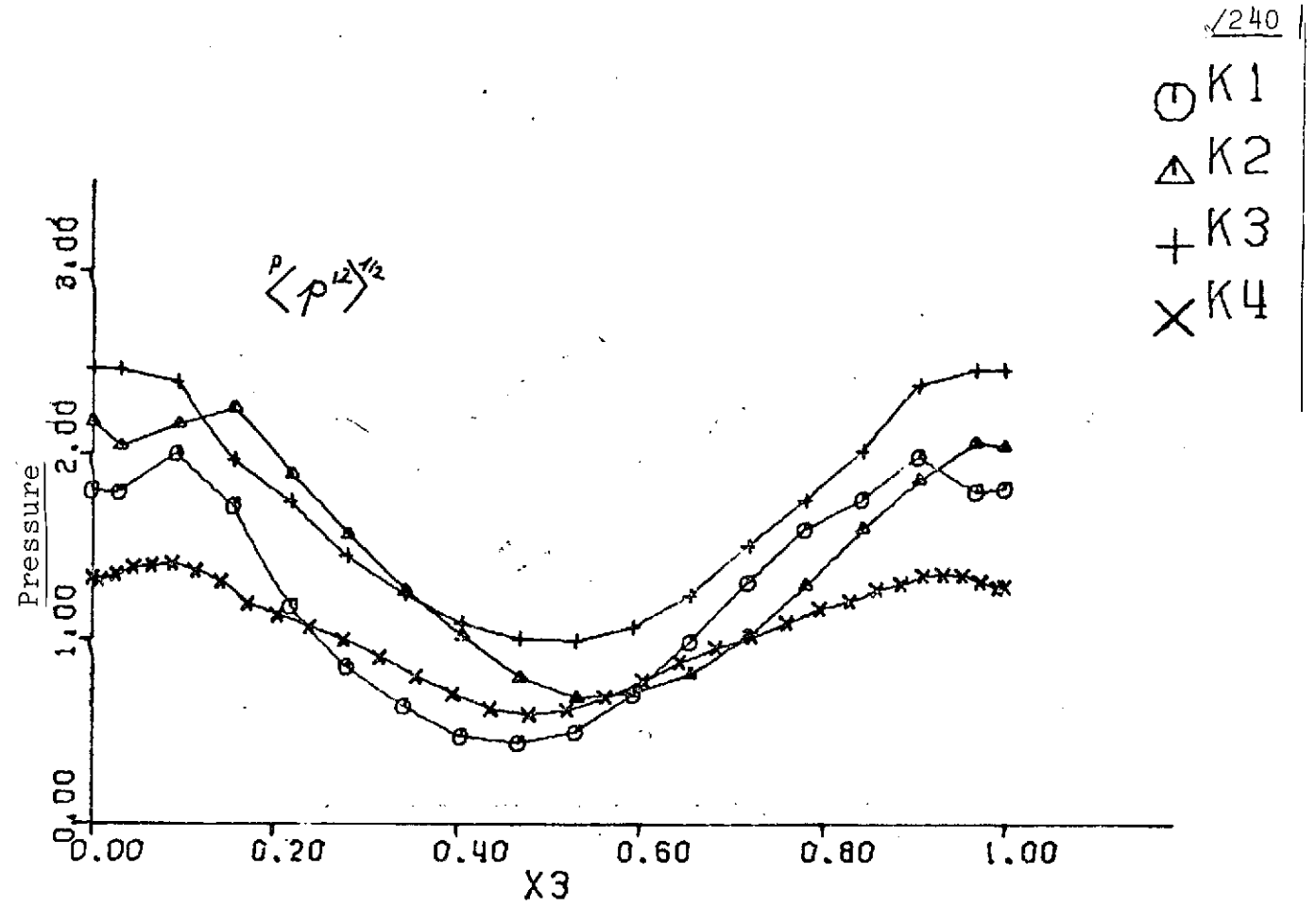
K1
K2
K3
K4
$\langle p^{12} \rangle^{1/2}$
Pressure
3.00
2.00
1.00
0.00
0.00
0.20
0.40
0.60
0.80
1.00
X3

Figure 50.

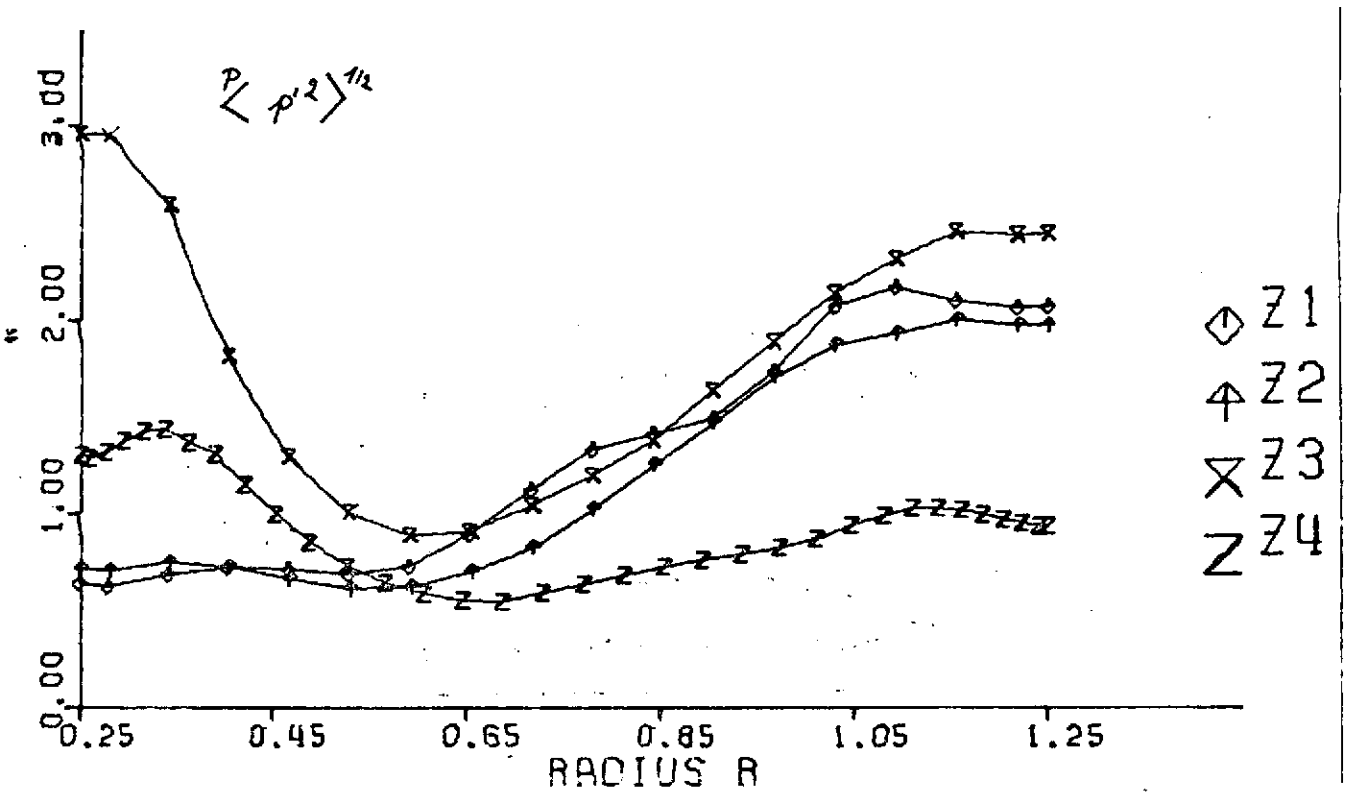
$\rho\langle p'^2\rangle^{1/2}$
3.00
2.00
1.00
0.00
0.25
0.45
0.65
0.85
1.05
1.25
RADIUS R
Z1
Z2
Z3
Z4

Figure 51.

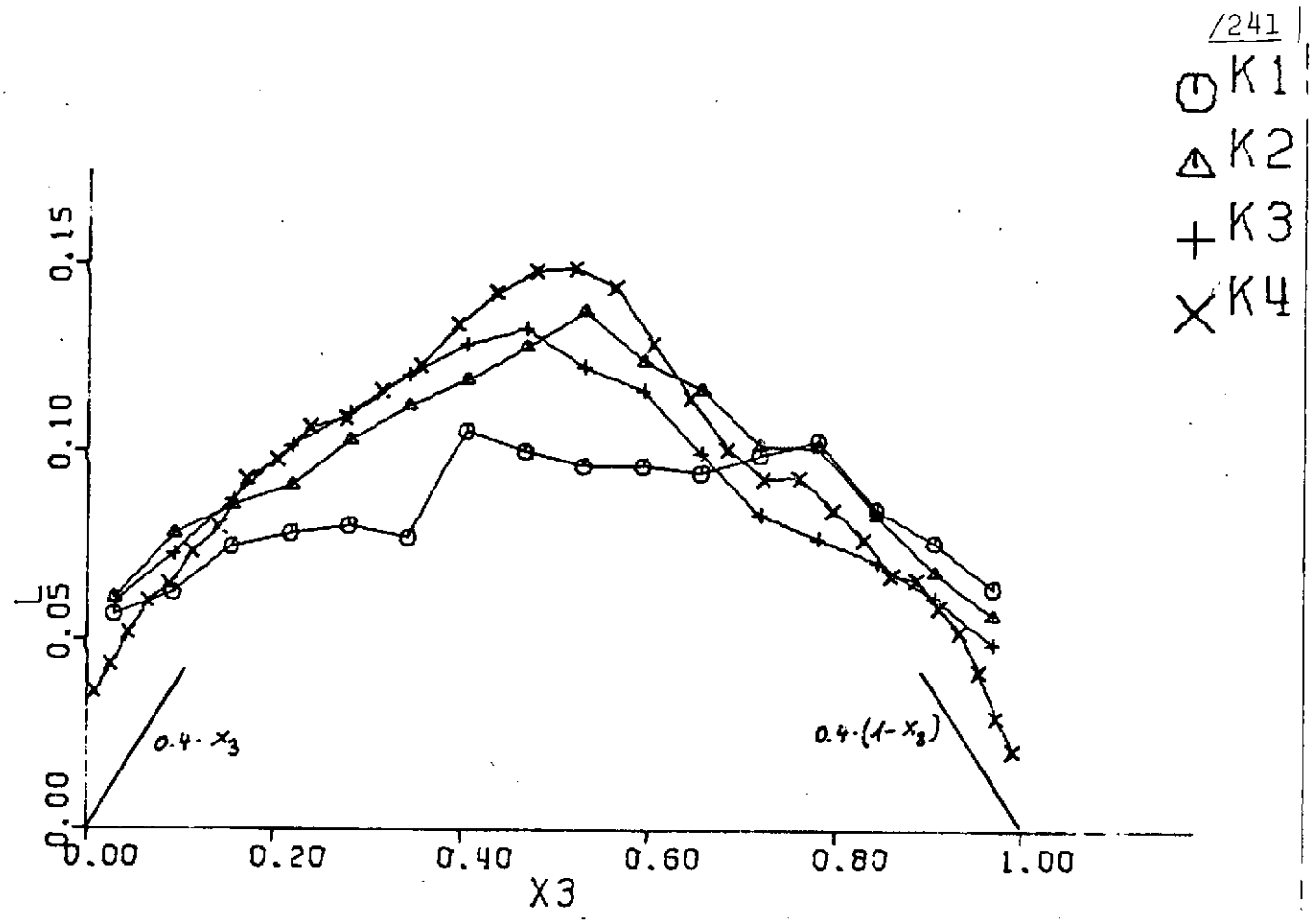
/241
K1
K2
K3
K4
L
0.00
0.05
0.10
0.15
0.4·x3
0.4·(1-x3)
0.00
0.20
0.40
0.60
0.80
1.00
X3

Figure 52.

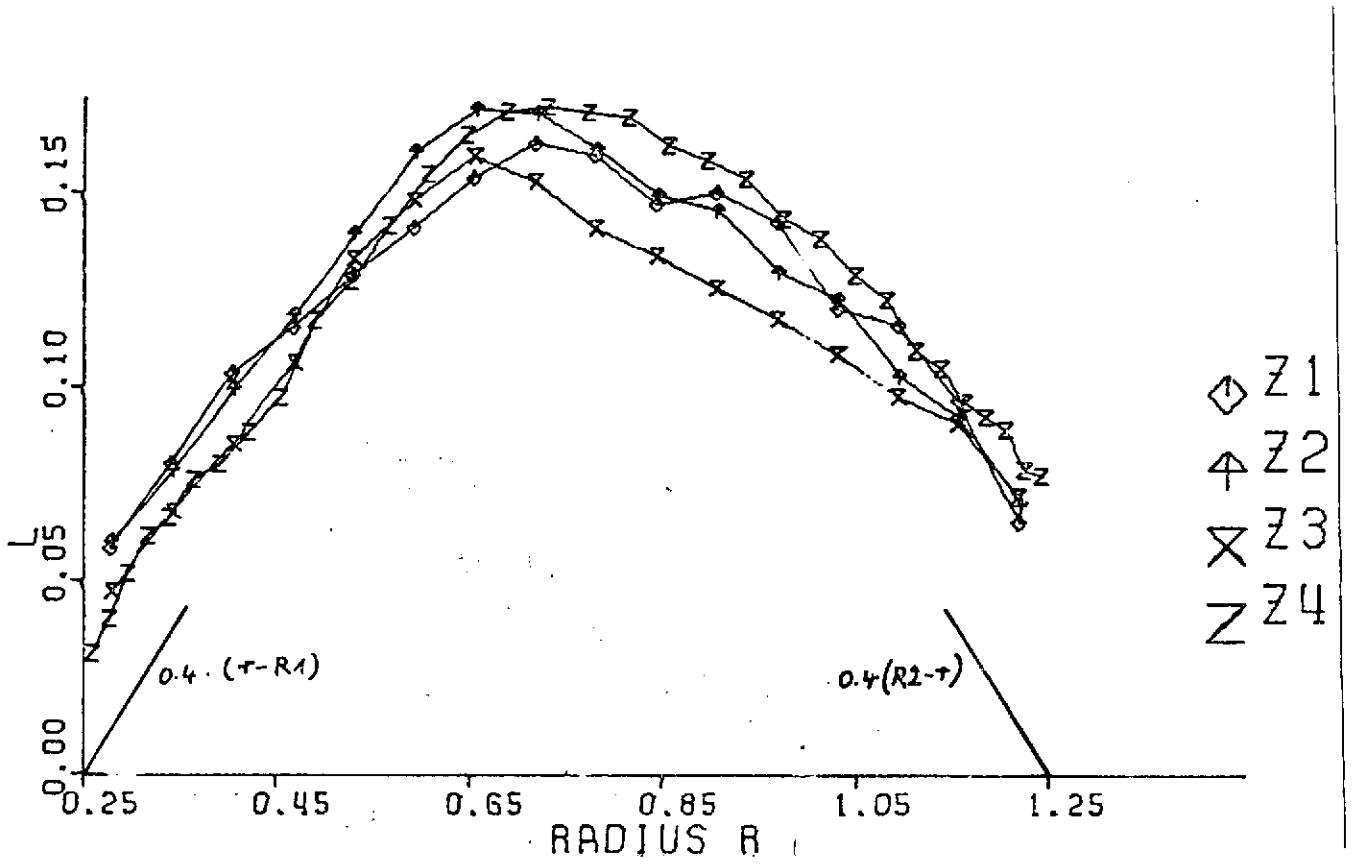
L
0.00
0.05
0.10
0.15
0.25
0.45
0.65
0.85
1.05
1.25
RADIUS R
0.4 . (r-R1)
0.4(R2-r)
Z1
Z2
Z3
Z4

Figure 53.

/242

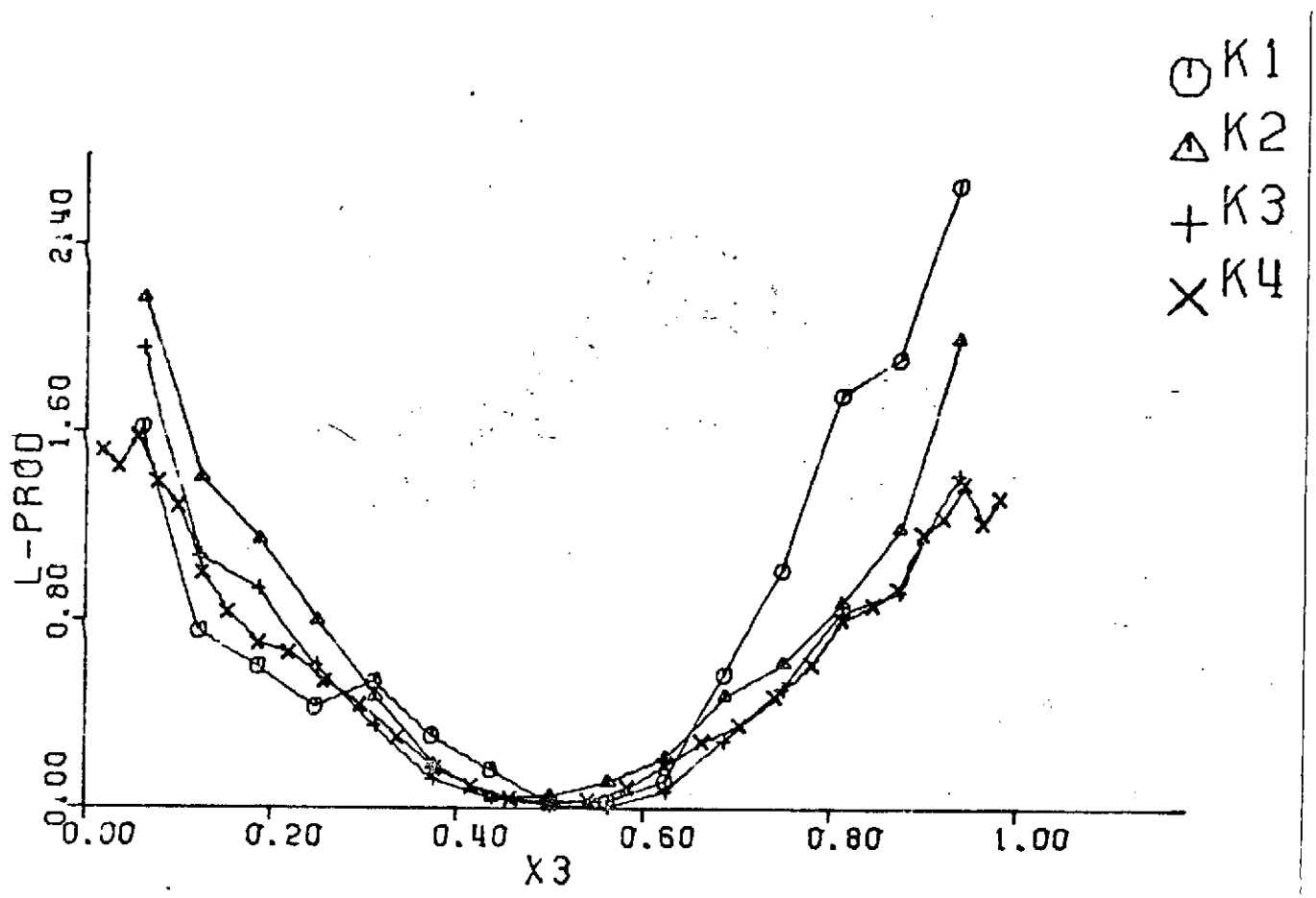

Figure 54.

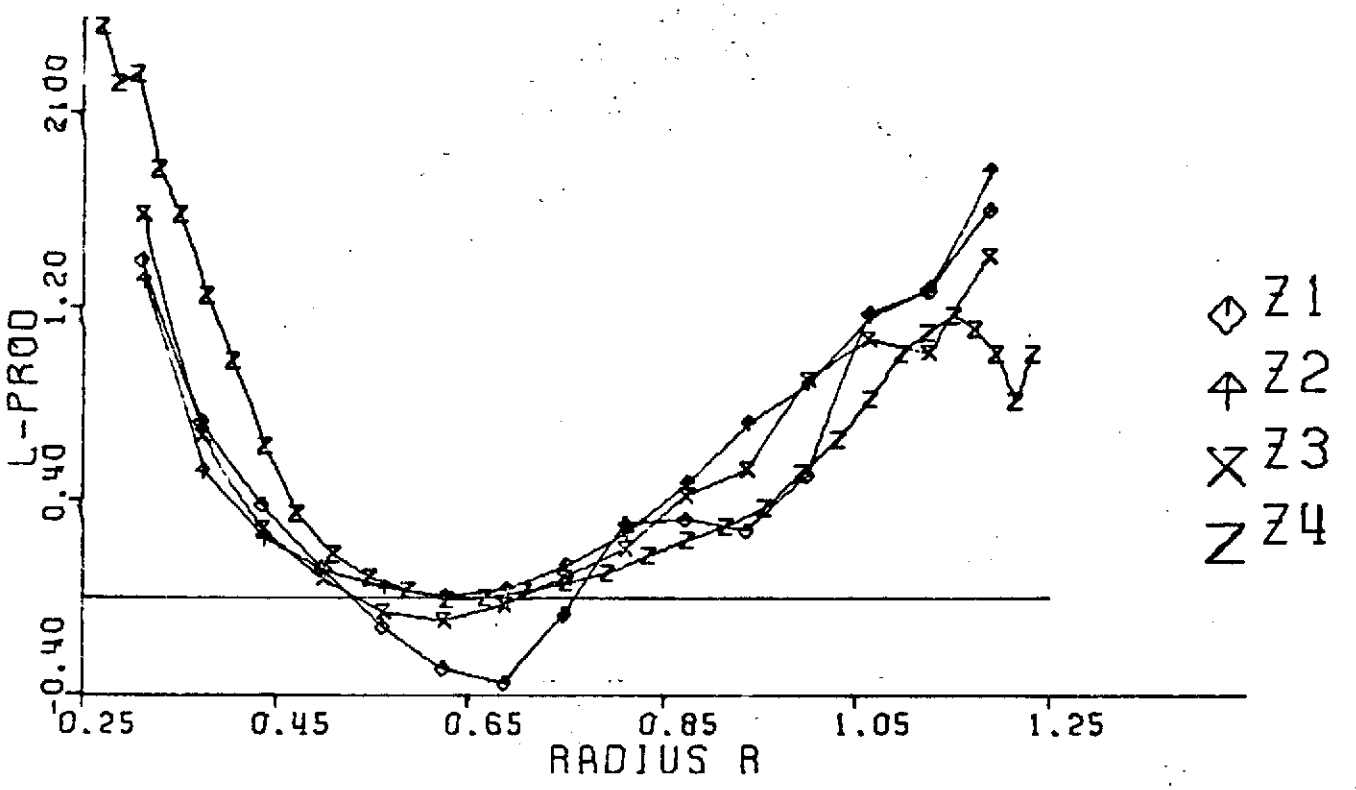
L-PROD
2.00
1.20
0.40
-0.40
0.25
0.45
0.65
0.85
1.05
1.25
RADIUS R
Z1
Z2
Z3
Z4

Figure 55.

/243

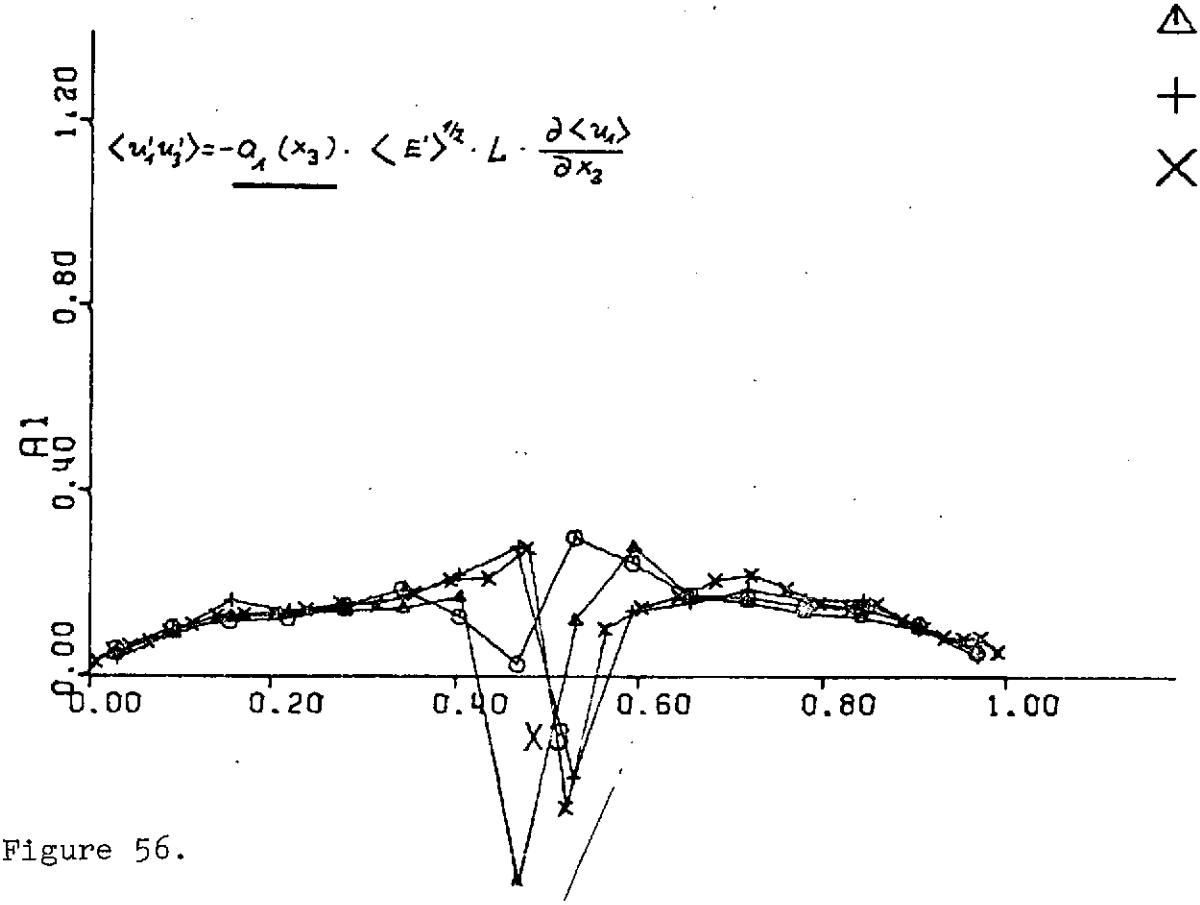

Figure 56.

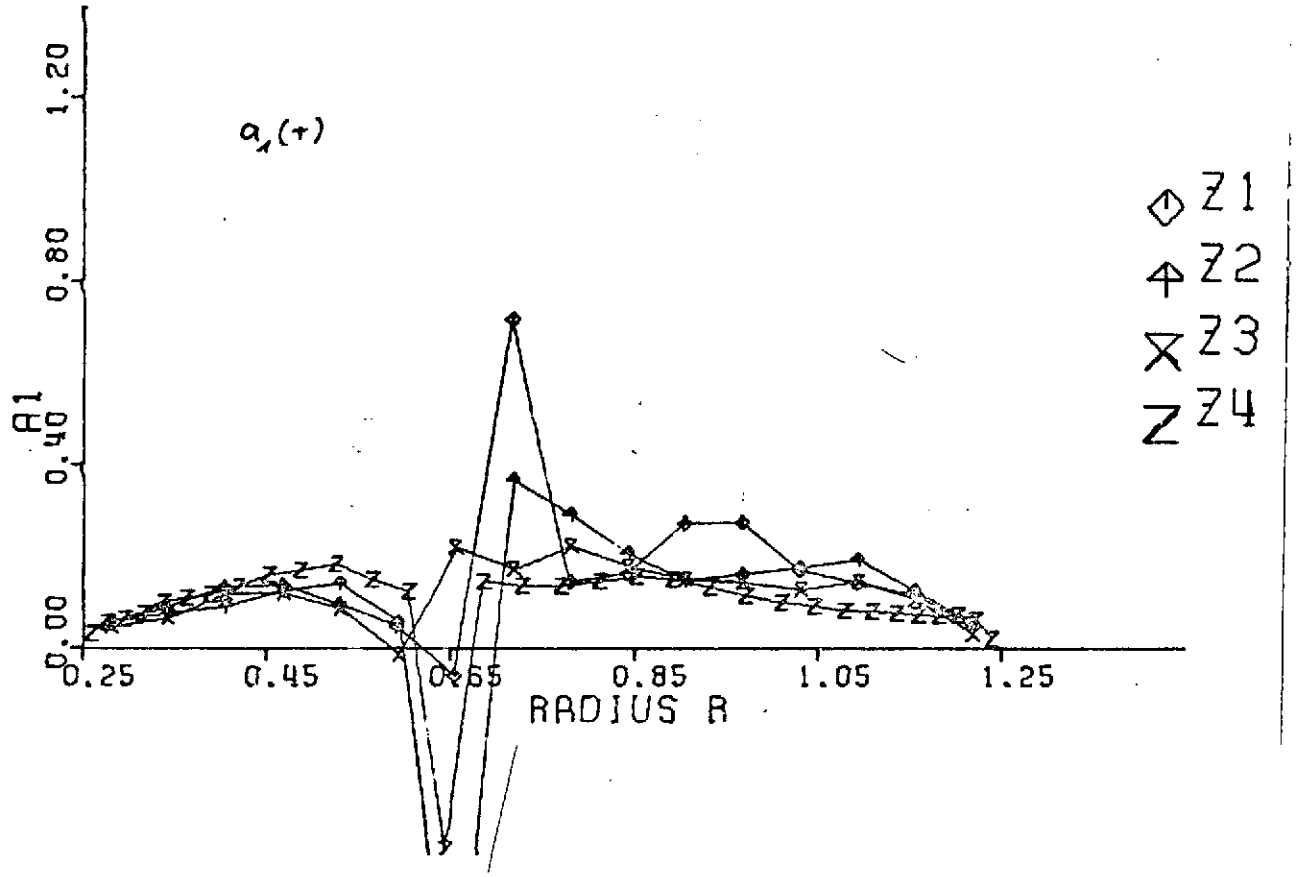
$a_1(\tau)$
A1
1.20
0.80
0.40
0.00
0.25
0.45
0.65
0.85
1.05
1.25
RADIUS R
Z1
Z2
Z3
Z4

Figure 57.

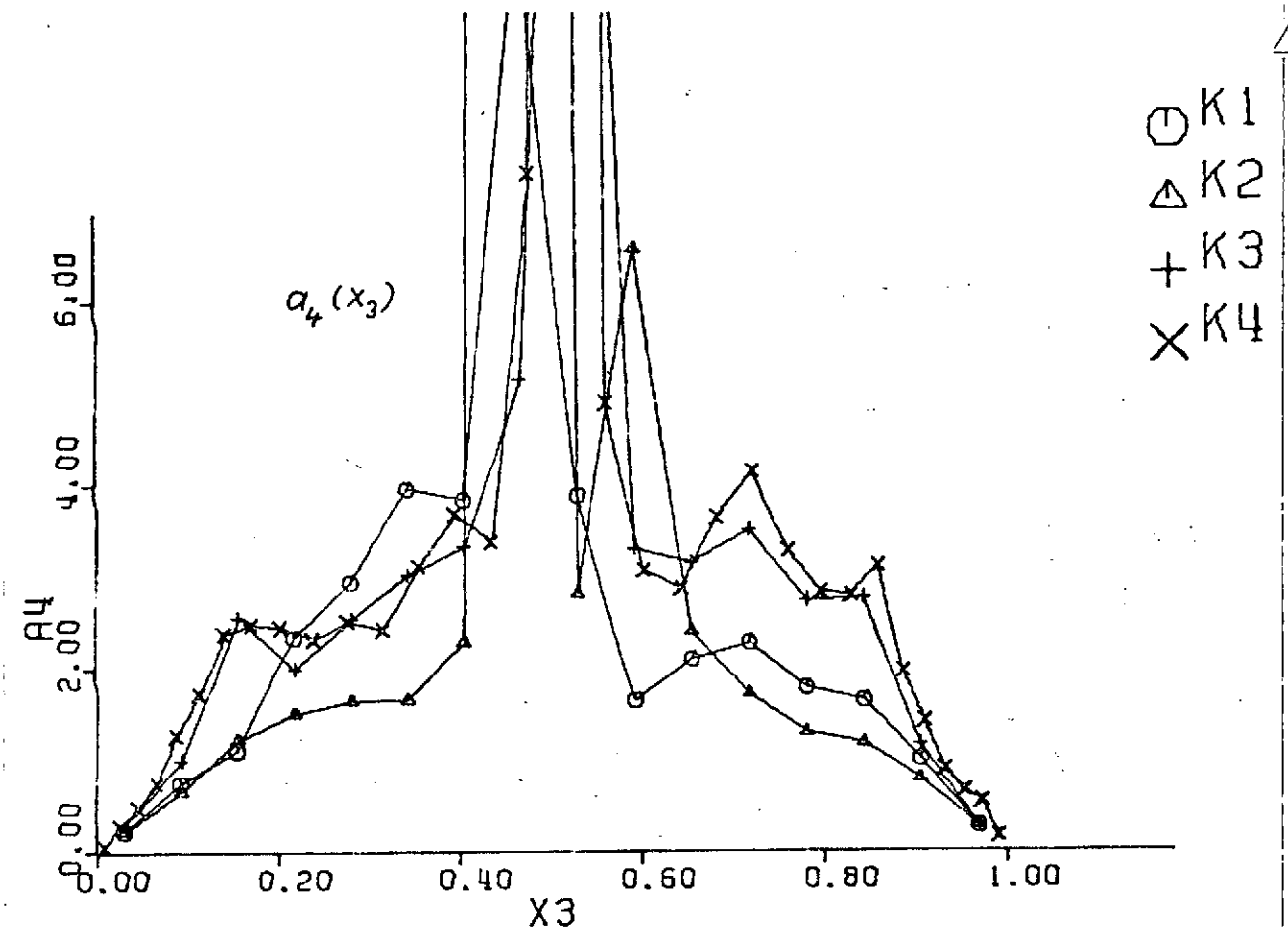

Figure 58.

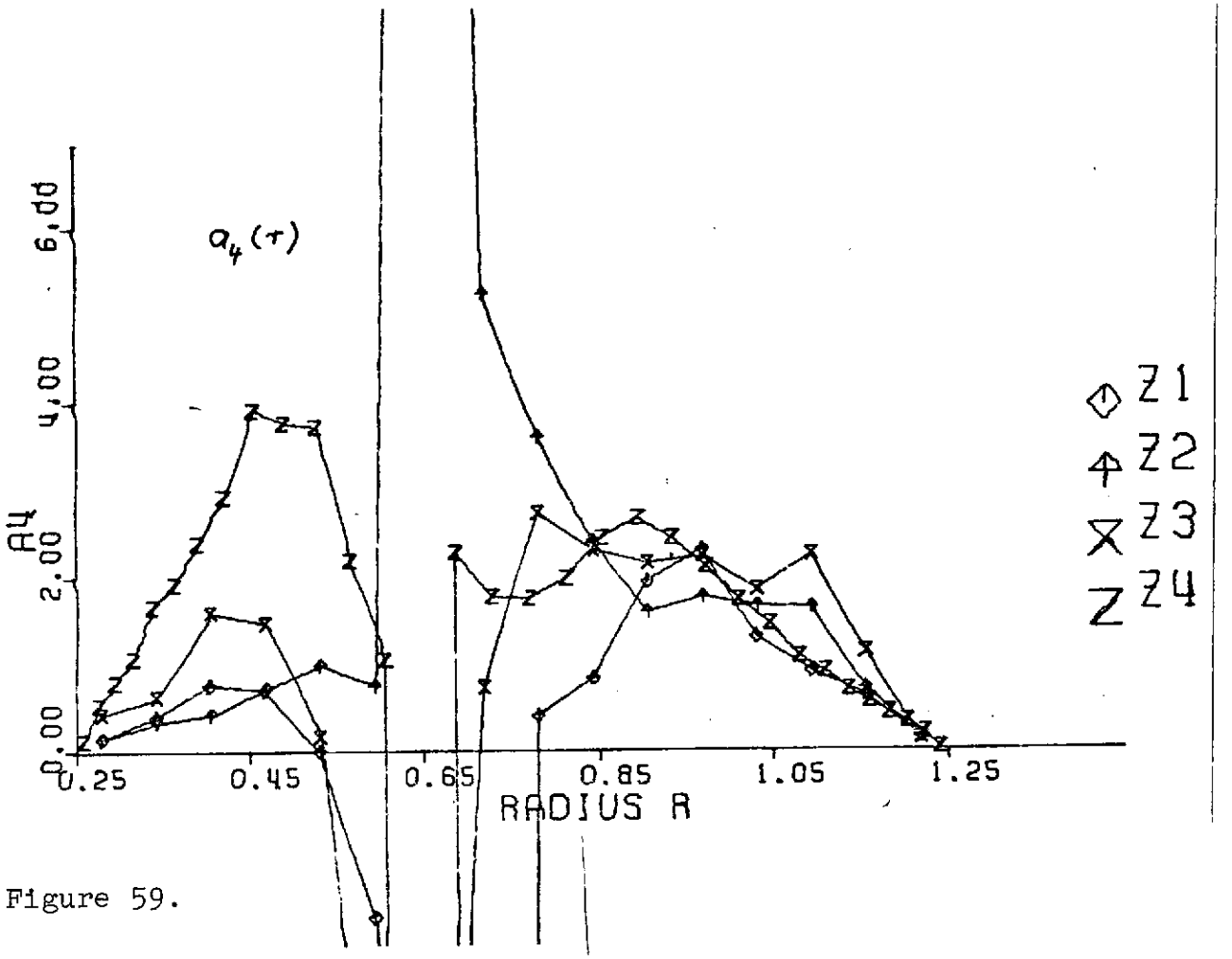
$a_4(r)$
6,00
4,00
2,00
0,00
A4
0.25
0.45
0.65
0.85
1.05
1.25
RADIUS R
Z1
Z2
Z3
Z4

Figure 59.

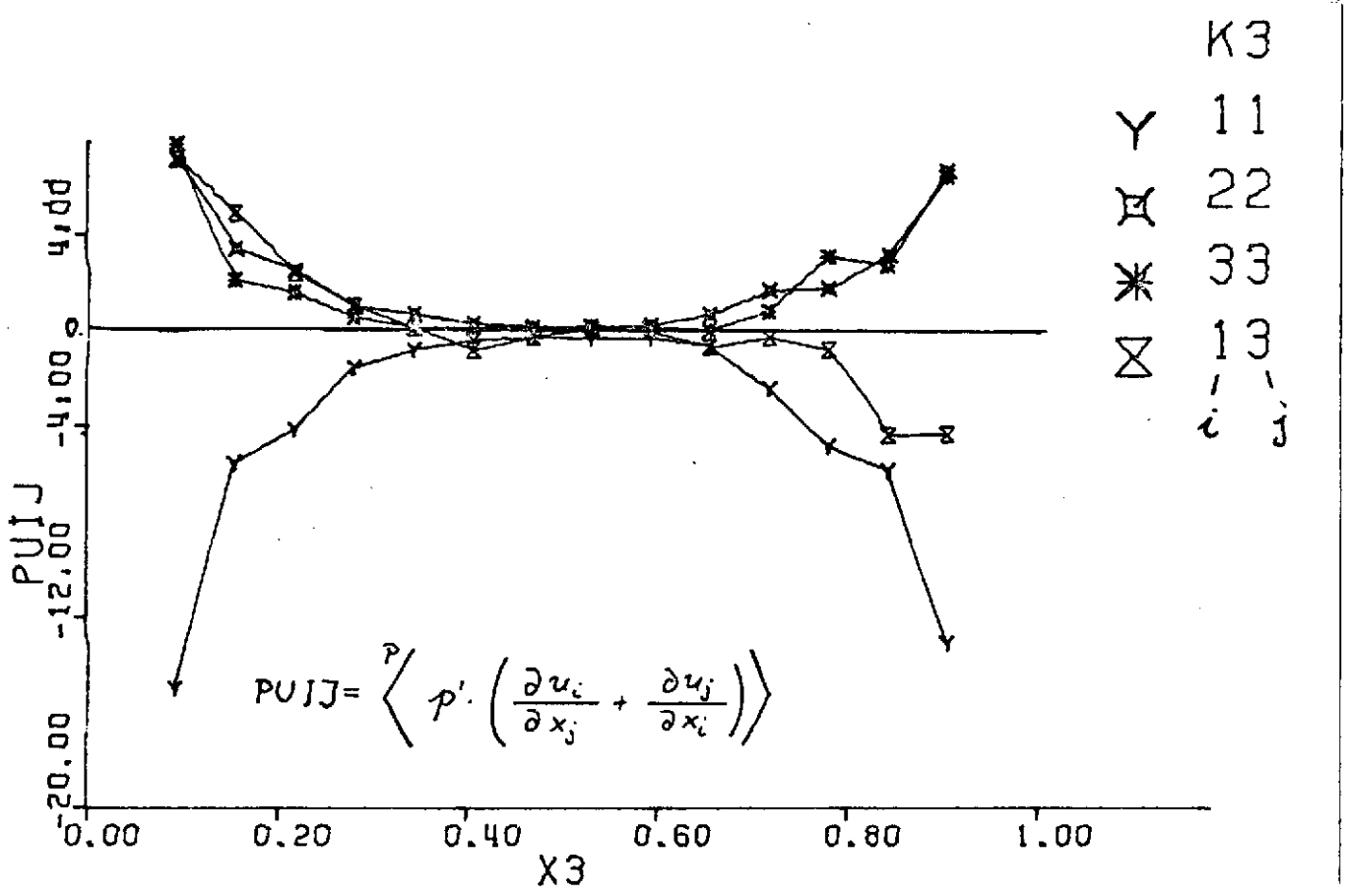
K3
Y 11
22
33
13
i j
4,00
0.
-4,00
-12,00
-20,00
PUIJ
PUJJ= ⟨ p' · (∂u_i/∂x_j + ∂u_j/∂x_i) ⟩
0.00
0.20
0.40
0.60
0.80
1.00
X3

Figure 60.

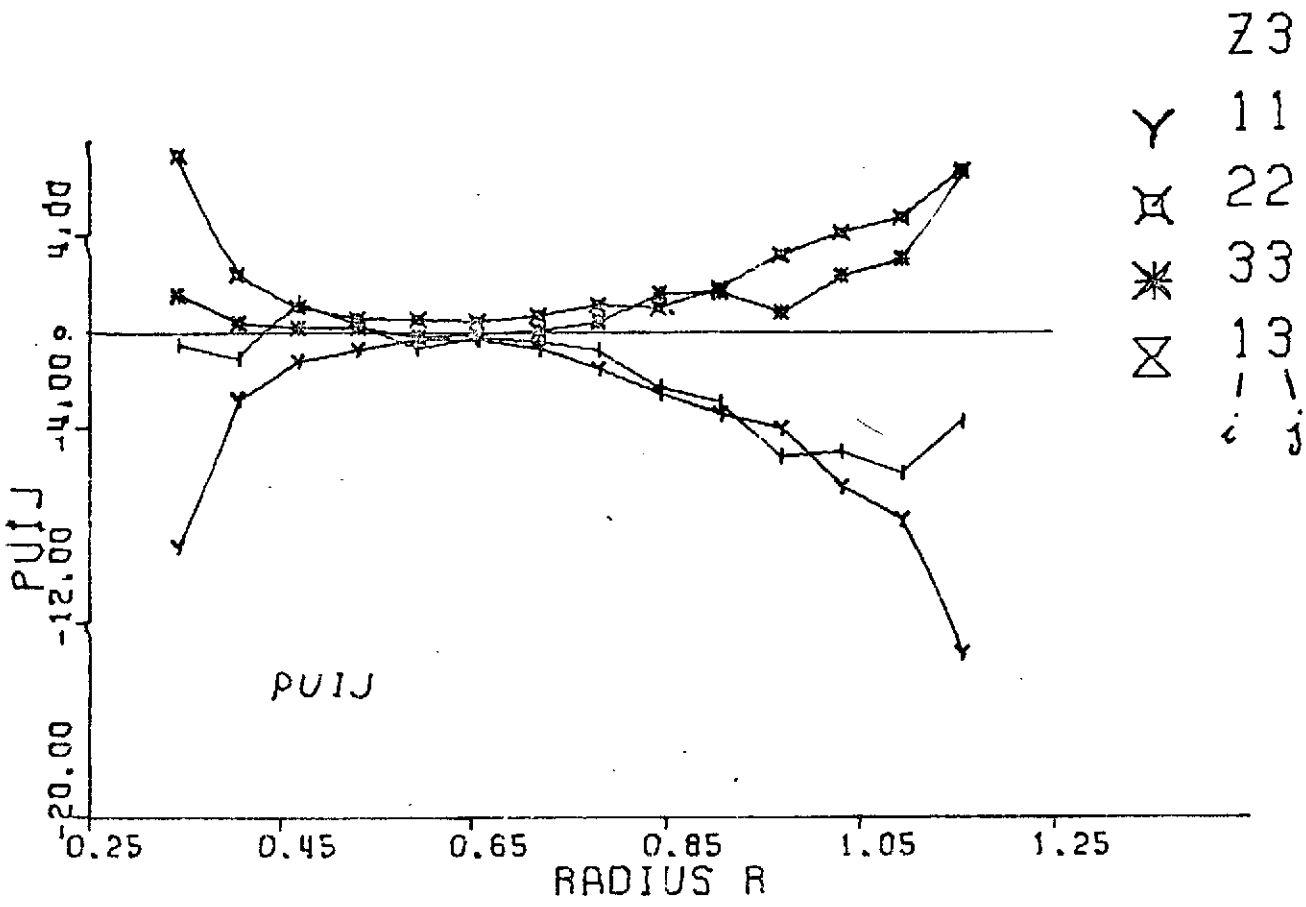
Z 3
11
22
33
13
i j
4.00
-4.00
-12.00
-20.00
PUIJ
PUIJ
0.25
0.45
0.65
0.85
1.05
1.25
RADIUS R

Figure 61.

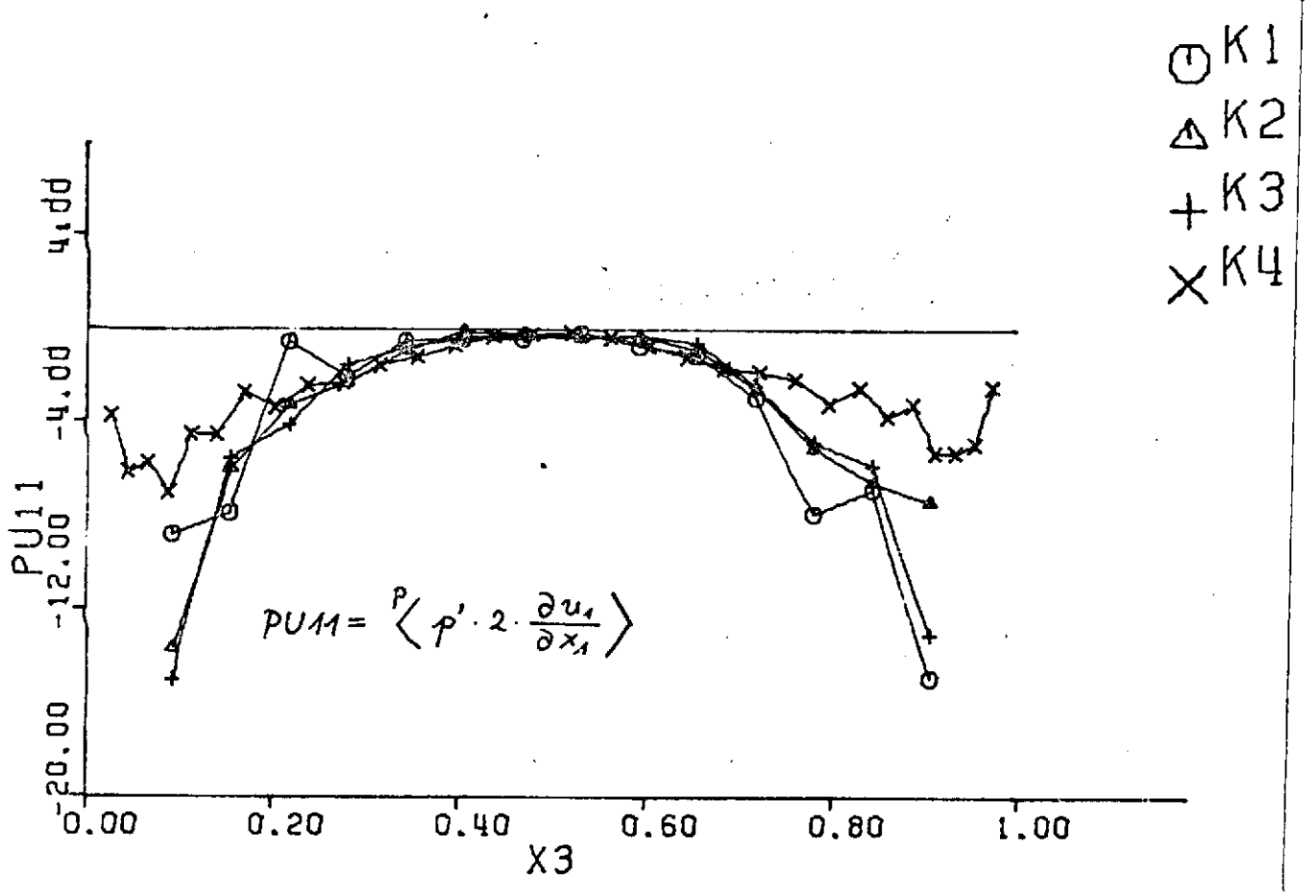
K1
K2
K3
K4
4.00
-4.00
-12.00
-20.00
PU11
$PU11 = {}^{P}\langle p' \cdot 2 \cdot \frac{\partial u_1}{\partial x_1} \rangle$
0.00
0.20
0.40
0.60
0.80
1.00
X3

Figure 62.

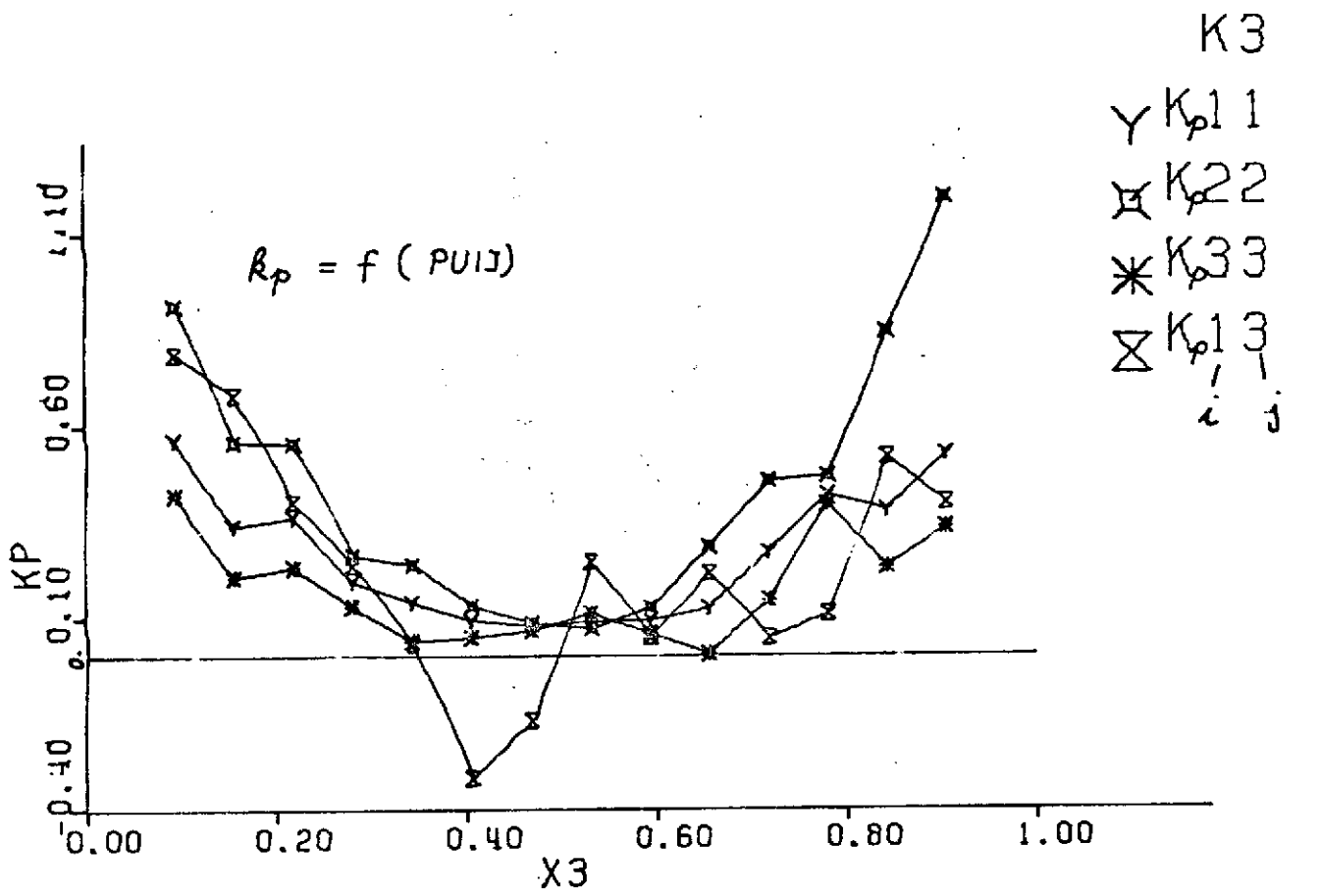
K3
Kp11
Kp22
Kp33
Kp13
i j
Kp = f (PUIJ)
KP
1.10
0.60
0.10
-0.40
0.00
0.20
0.40
0.60
0.80
1.00
X3

Figure 63.

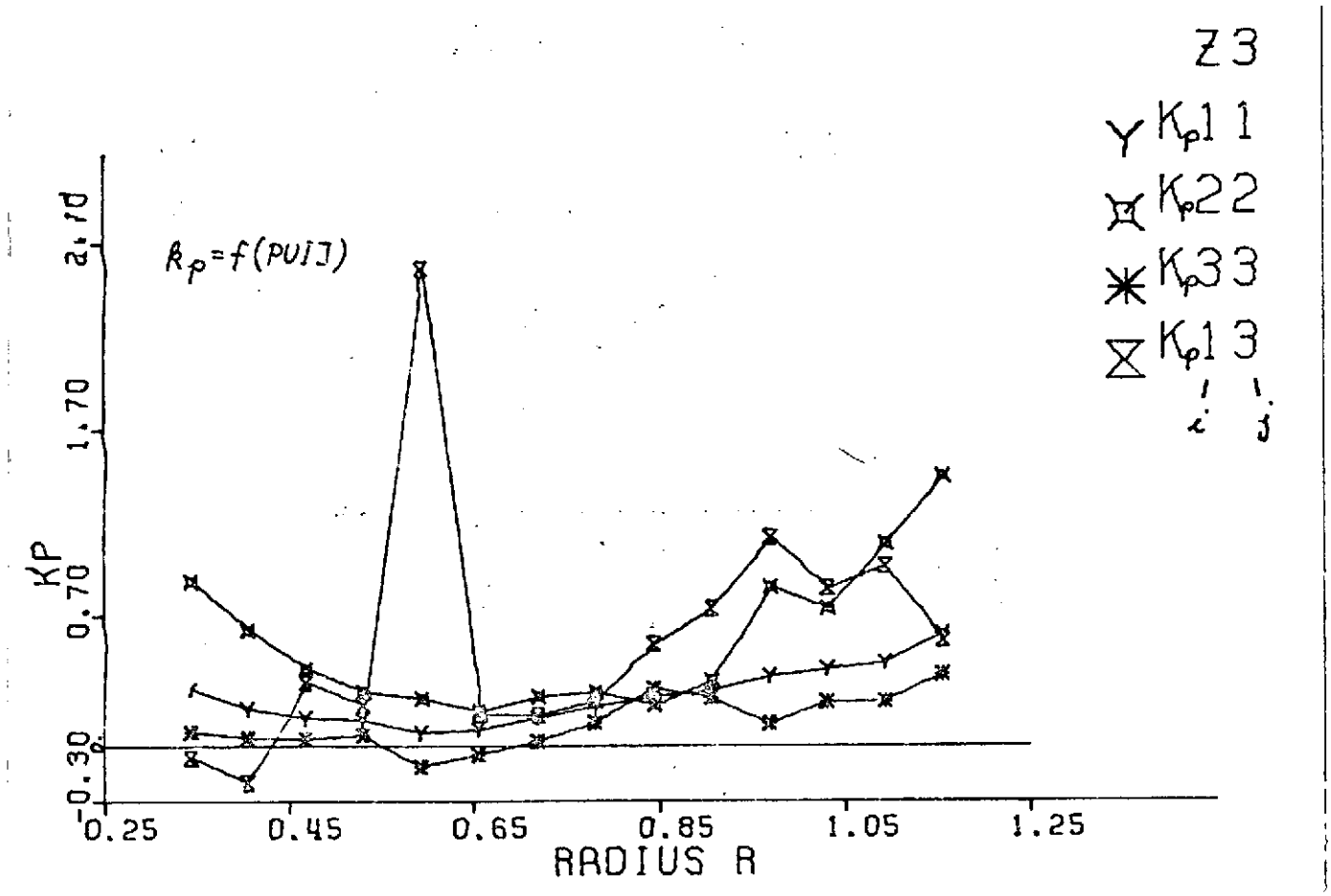
Z 3
Kp11
Kp22
Kp33
Kp13
i j
Kp=f(PUIJ)
KP
2.10
1.70
0.70
-0.30
0.25
0.45
0.65
0.85
1.05
1.25
RADIUS R

Figure 64.

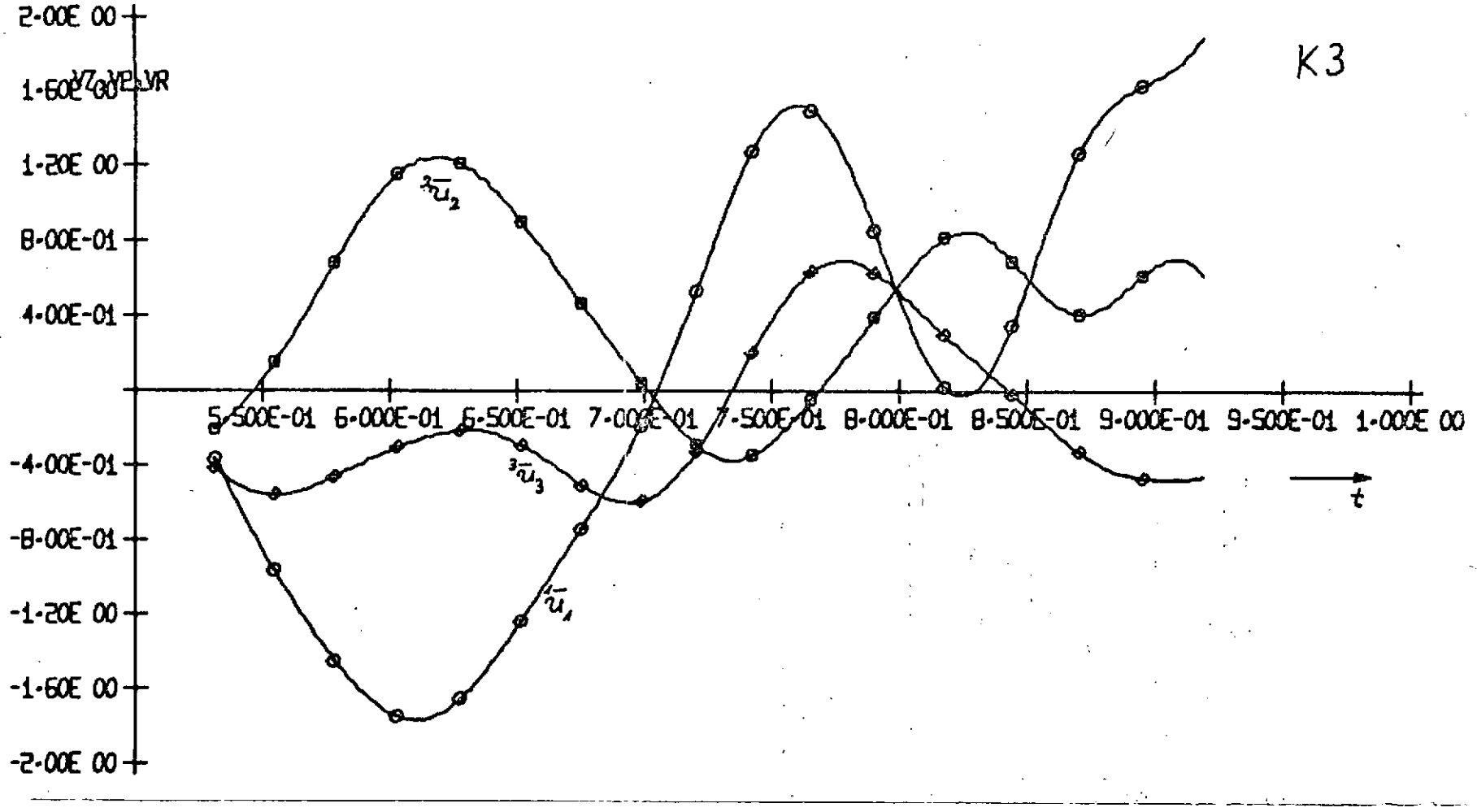

Figure 65. Velocity fluctuations of the coarse structure as a function of time t at a location x_3=0.6 for plate flow, case K3

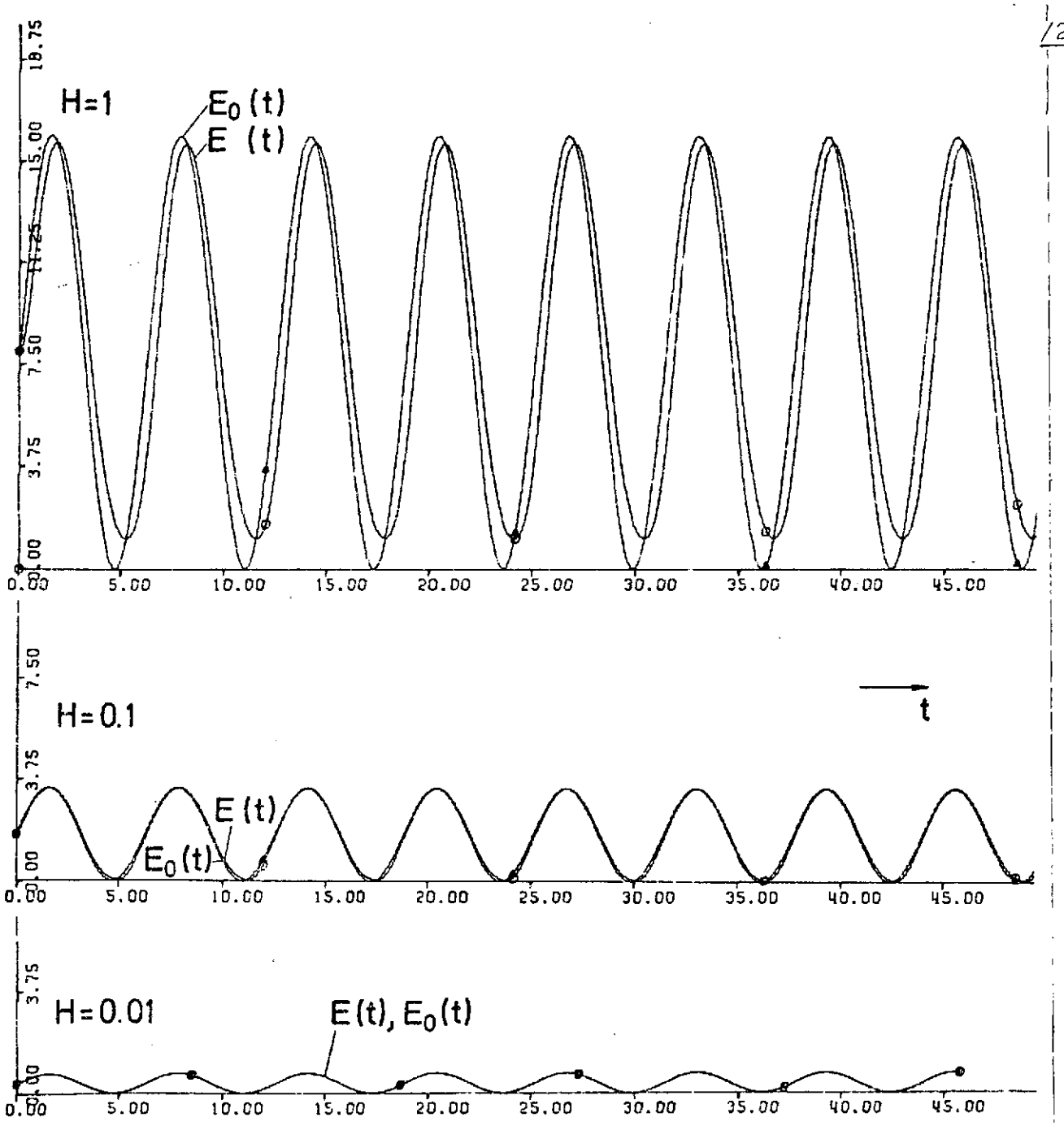

Figure 66. Kinetic energy of fine structure as a function of time t for periodic source at various mesh sizes H; E(t) is the solution of the model differential equation, $E_0(t)$ is the quasi-stationary approximation

Translated for National Aeronautics and Space Administration under contract no. NASw 2483, by SCITRAN, P.O. Box 5456, Santa Barbara, California, 93108